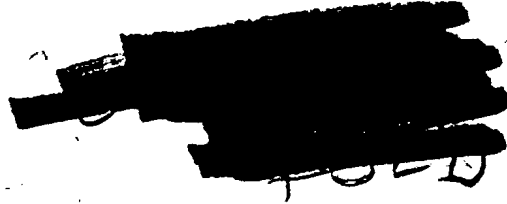


*Russian Original Vol. 32, No. 1, January, 1972*

Translation published July, 1972



# SOVIET ATOMIC ENERGY

АТОМНАЯ ЭНЕРГИЯ  
(АТОМНАЯ ЭНЕРГИЯ)

TRANSLATED FROM RUSSIAN



CONSULTANTS BUREAU, NEW YORK

# SOVIET ATOMIC ENERGY

*Soviet Atomic Energy* is a cover-to-cover translation of *Atomnaya Energiya*, a publication of the Academy of Sciences of the USSR.

An arrangement with Mezhdunarodnaya Kniga, the Soviet book export agency, makes available both advance copies of the Russian journal and original glossy photographs and artwork. This serves to decrease the necessary time lag between publication of the original and publication of the translation and helps to improve the quality of the latter. The translation began with the first issue of the Russian journal.

### Editorial Board of *Atomnaya Energiya*:

**Editor:** M. D. Millionshchikov

Deputy Director  
I. V. Kurchatov Institute of Atomic Energy  
Academy of Sciences of the USSR  
Moscow, USSR

**Associate Editors:** N. A. Kolokol'tsov  
N. A. Vlasov

A. I. Alikhanov

V. V. Matveev

A. A. Bochvar

M. G. Meshcheryakov

N. A. Dollezhal'

P. N. Palei

V. S. Fursov

V. B. Shevchenko

I. N. Golovin

D. L. Simonenko

V. F. Kalinin

V. I. Smirnov

A. K. Krasin

A. P. Vinogradov

A. I. Leipunskii

A. P. Zefirov

Copyright © 1972 Consultants Bureau, New York, a division of Plenum Publishing Corporation, 227 West 17th Street, New York, N. Y. 10011. All rights reserved. No article contained herein may be reproduced for any purpose whatsoever without permission of the publishers.

Consultants Bureau journals appear about six months after the publication of the original Russian issue. For bibliographic accuracy, the English issue published by Consultants Bureau carries the same number and date as the original Russian from which it was translated. For example, a Russian issue published in December will appear in a Consultants Bureau English translation about the following June, but the translation issue will carry the December date. When ordering any volume or particular issue of a Consultants Bureau journal, please specify the date and, where applicable, the volume and issue numbers of the original Russian. The material you will receive will be a translation of that Russian volume or issue.

### Subscription

\$67.50 per volume (6 issues)

Single Issue: \$30

2 volumes per year

Single Article: \$15

(Add \$5 for orders outside the United States and Canada.)

### CONSULTANTS BUREAU, NEW YORK AND LONDON



227 West 17th Street  
New York, New York 10011

Davis House  
8 Scrubs Lane  
Harlesden, NW10 6SE  
England

Published monthly. Second-class postage paid at Jamaica, New York 11431.

# SOVIET ATOMIC ENERGY

A translation of *Atomnaya Énergiya*

Translation published July, 1972

Volume 32, Number 1

January, 1972

## CONTENTS

	Engl./Russ.	
On the Stability of the Cans of Cylindrical Fuel Elements with an Initial Ellipticity – Yu. I. Likhachev and V. V. Popov .....	1	3
Diffusional and Thermodynamic Properties of the $\gamma$ -Phase of the System Uranium – Niobium – G. B. Fedorov, E. A. Smirnov, and V. N. Gusev .....	8	11
Deposition of Corrosion Products on the Surface of Zirconium Alloys – V. V. Gerasimov, A. I. Gromova, I. K. Morozova, V. N. Belous, A. S. Ilyukhin, G. A. Shchapov, L. G. Varnacheva, and G. P. Saenko .....	12	15
Mechanism of Reduction of Uranium Hexafluoride by Hydrogen – Yu. N. Tumanov and N. P. Galkin .....	17	21
Calculation of Regular Systems of Neutron Absorbers – Ya. V. Shevelev and I. L. Chikhladze .....	23	27
Thermalization of Neutrons in $H_{20}$ at 318 and 77°K – S. N. Ishmaev, I. P. Sadikov, and A. A. Chernyshov .....	29	33
Determination of Lithium in Solid Materials from the Reaction $Li^6(n, \alpha)H^3$ – B. P. Zverev, Yu. F. Simakhin, and A. G. Dutov .....	35	39
Thermonuclear Combustion in a Bounded Region – A. F. Nastoyashchii .....	39	43
Radiative Widths of $U^{238}$ Neutron Resonances – Kh. Malétski, L. B. Pikel'ner, I. M. Salamatin, and É. I. Sharapov .....	45	49

### ABSTRACTS

Variational Composite Methods of Calculating Neutron Distribution in Nuclear Reactors – I. S. Slesarev, A. M. Sirotkin, and V. V. Khromov .....	48	53
Radioactivity of Metamict Zircons – I. M. Lipova and G. A. Kuznetsova .....	49	53
Monte Carlo Calculations of Characteristics of Secondary Electrons Knocked Out from Various Materials by $\gamma$ -Radiation – V. V. Smirnov and A. V. Malyshenkov .....	50	54
The Kaon Factory – a Two-Stage ( $\approx 3.7$ GeV) Isochronous Cyclotron – L. A. Sarkisyan ...	50	55
Thermal Stability of Anhydrous Uranium Trichloride – V. V. Rachev, L. A. Tarasova, and A. I. Pavlova-Verevkina .....	52	56

### LETTERS TO THE EDITOR

Adjoint Reactor Kinetics Equations: Delayed Neutrons Case – V. V. Orlov .....	53	57
A New Procedure for Measuring Thermal Coefficient of Reactivity and Worth of Control Shim Rods in the IGR Reactor – V. D. Lavrenikov .....	56	58
Redesign of the IRT-TM Reactor Dry Experimental Channels – O. F. Gusarov, V. V. Karnaukhov, and V. K. Leus .....	59	60
Critical Thermal Fluxes in the Boiling of a Eutectic Sodium–Potassium Alloy under Conditions of Free Convection – V. I. Subbotin, D. N. Sorokin, A. P. Kudryavtsev, V. I. Brigutsa, and R. I. Zhirova .....	61	62
Measurement of Integrated Characteristics of Slow-Neutron Spectrum of VVR-M Critical Assembly – A. V. Nikonov and V. B. Klimentov .....	64	64

**CONTENTS**

(continued)

Engl./Russ.

Possibility of Measuring the Spectral Characteristics of a Neutron Flux using Direct-Charge Detectors – V. S. Kirsanov, M. G. Mitel'man, N. D. Rozenblyum, E. N. Babulevich, V. A. Zagadkin, and Yu. M. Shipovskikh.....	66	65
Spectrometry of Low-Energy Ions by Surface-Barrier Silicon Detectors – G. F. Bogdanov and B. P. Maksimenko .....	68	66
Measurement of Neutron Spectra with Threshold Detectors – K. K. Koshaeva, S. N. Kraitor, and L. B. Pikel'ner .....	70	68
The Effect of Neutron Irradiation on the Operation of Surface Barrier Fission Fragment Detectors – E. A. Seregina, N. N. Semenova, and B. D. Kuz'minov.....	73	70
The Effect of the Angular Dimensions of a Detector on the Error in the Determination of Certain Kinematic Characteristics – G. N. Potetyunko.....	76	72
Visualization of Spatial Dose Distribution in a Fast Electron Beam – Yu. P. Vagin, G. L. Kabanov, Yu. A. Medvedev, and B. M. Stepanov.....	78	73
Spectra of Electrons Ejected in the Passage of Co <sup>60</sup> Gamma Rays through a Two-Component Medium – L. V. Popova and L. B. Chegodaeva .....	80	75
Angular Distributions of Bremsstrahlung from 12-22 MeV Electrons as a Function of Target Thickness – V. P. Kovalev, V. P. Kharin, and V. V. Gordeev.....	83	77
Matching of Accelerating Channels in a High Energy Proton Linear Accelerator – B. I. Bondarev and L. Yu. Solov'ev.....	86	79
Effect on Nonlinear Resonances on Beam Dimensions in the 70-GeV Accelerator – V. I. Gridasov, K. P. Myznikov, and V. N. Chepegin.....	89	81
Value of $\bar{\nu}$ from Energy Balance in U <sup>233</sup> and Pu <sup>239</sup> Fission – N. P. Kolosov, B. D. Kuz'minov, A. I. Sergachev, and V. M. Surin .....	92	83
Absolute Measurements of the Quantity $\alpha$ for U <sup>235</sup> and Pu <sup>239</sup> in the Neutron Energy Region of 10 keV-1 MeV – V. N. Kononov, E. D. Poletaev, Yu. S. Prokopets, A. A. Metlev, and Yu. Ya. Stavisskii.....	95	85
Chill-Casting Method of Bituminizing Natural Sorbents for Ir <sup>192</sup> – Kh. Daiev, G. Delchev, G. Gradev, S. Simov, and V. Zhelyazkov.....	98	87
<b>INFORMATION</b>		
All-Union Izotop Agency Serving the National Economy Exhibit at Exposition of Achievements of the National Economy – V. A. Dolinin.....	101	91
Seminars and Conferences at V/O Izotop.....	104	93
<b>CONFERENCES</b>		
Sixth All-Union Conference on Synthesis, Production, and Applications of Scintillators – L. Ya. Zhil'tsova, E. N. Matveeva, and I. M. Stoletova .....	106	94
Fourth Conference of the International Nuclear Data Committee – M. F. Troyanov.....	108	95
International Conference on Elementary Particles – I. A. Savin.....	110	96
Fourth International Conference on Plasma Physics and Controlled Nuclear Fusion – B. B. Kadomtsev and V. D. Shafranov.....	113	98
<b>BRIEF COMMUNICATIONS.....</b>	<b>118</b>	<b>101</b>

The Russian press date (podpisano k pechati) of this issue was 12/17/1971. Publication therefore did not occur prior to this date, but must be assumed to have taken place reasonably soon thereafter.

## ON THE STABILITY OF THE CANS OF CYLINDRICAL FUEL ELEMENTS WITH AN INITIAL ELLIPTICITY

Yu. I. Likhachev and V. V. Popov

UDC 621.039.54

The fuel-element cans of gas-cooled and water-cooled reactors are subjected to a fairly high external pressure due to the coolant (sometimes exceeding 100 atm). The cans are thus in danger of losing stability, possibly leading to the collapse of the compensation volume or to the formation of a longitudinal corrugation in the parts of the can resting on the heat-emitting core.

The stability of the cans of cylindrical fuel elements was studied earlier [1-4]; however, no allowance was made for either the initial ellipticity of the can or the creep of the material of which it was composed.

The creep of cylindrical cans with an initial ellipticity was considered (with various simplifying assumptions) in [5-7], but without allowing for the influence of the thermal flux, the swelling of the steel, and the changes taking place in the temperature and pressure during deformation, which are important factors in the cans of fuel elements.

Let us consider the creep of a cylindrical fuel-element can having an initial ellipticity  $w_1 = w_0 \cos 2\theta$  subjected to a time-varying excess external pressure  $q(t)$  and a thermal (temperature) field  $T(t, z)$ , where  $w_0(\theta)$  is the radial deviation of the middle of the surface of the can from the ideal circular form and  $z$  is the distance from the middle of the surface.

The process of can deformation develops as time progresses in a series of short stages [8]. Let us suppose that at the  $n$ -th stage of deformation  $\Delta_n t = t_n - t_{n-1}$  the stresses, strains, and displacements have received increments  $\Delta_n \sigma$ ,  $\Delta_n \varepsilon$ ,  $\Delta_n w$ ,  $\Delta_n \nu$ . The increments in the stresses should satisfy the following equilibrium equations

$$\pi R \Delta_n q = -4 \int_0^{\pi/2} \int_{-\delta/2}^{\delta/2} \Delta_n \sigma_x dz d\theta; \quad (1)$$

$$R \Delta_n q = - \int_{-\delta/2}^{\delta/2} \Delta_n \sigma_\theta dz; \quad (2)$$

$$\Delta_n M = - \int_{-\delta/2}^{\delta/2} \Delta_n \sigma_\theta z dz, \quad (3)$$

where  $\Delta_n M = \Delta_n M_c + R w_{n-1} \Delta_n q + R q_n \Delta_n w$  is the increment in the bending moment;  $\Delta_n q = q_n - q_{n-1}$  is the increment in the constant component of the bending moment;  $q_{n-1}$  and  $q_n$  are the pressures at the beginning and end of the deformation stage.

In accordance with the "rigid-normal" hypothesis (Levi-Kirchhoff) and the assumption of plane deformation, we have [9] the following for the strain increments

$$\begin{aligned} \Delta_n \varepsilon_\theta &= \Delta_n \varepsilon_\theta^0 + z \Delta_n \kappa; \\ \Delta_n \varepsilon_x &= \Delta_n \varepsilon_x^0 = \text{const}, \end{aligned} \quad (4)$$

where  $\Delta_n \varepsilon_\theta^0$ ,  $\Delta_n \kappa$  are the increments in the circumferential deformation and the curvature of the middle of the surface:

$$\begin{aligned} \Delta_n \varepsilon_\theta^0 &= \frac{1}{R} \left[ \frac{d(\Delta_n \nu)}{d\theta} - \Delta_n w \right]; \\ \Delta_n \kappa &= \frac{d^2}{d\theta^2} (\Delta_n w) + \frac{1}{R^2} (\Delta_n w). \end{aligned} \quad (5)$$

Translated from *Atomnaya Energiya*, Vol. 32, No. 1, pp. 3-9, January, 1972. Original article submitted December 8, 1970.

© 1972 Consultants Bureau, a division of Plenum Publishing Corporation, 227 West 17th Street, New York, N. Y. 10011. All rights reserved. This article cannot be reproduced for any purpose whatsoever without permission of the publisher. A copy of this article is available from the publisher for \$15.00.

Let us write down the physical relationships between the stresses and strains in the form [8]:

$$\begin{aligned}\Delta_n \varepsilon_0 &= \frac{1}{E} \Delta_n \sigma_0 - \frac{\mu}{E} \Delta_n \sigma_x + \frac{1}{3} \Delta_n S + \alpha \Delta_n T + \langle \xi_0^c(n) \rangle \Delta_n t; \\ \Delta_n \varepsilon_x &= \frac{1}{E} \Delta_n \sigma_x - \frac{\mu}{E} \Delta_n \sigma_0 + \frac{1}{3} \Delta_n S + \alpha \Delta_n T + \langle \xi_x^c(n) \rangle \Delta_n t.\end{aligned}\quad (6)$$

The elastic modulus  $E$ , the Poisson coefficient  $\mu$ , and the thermal expansion coefficient  $\alpha$  are taken as constants (defined for a certain mean temperature); this may be justified from the following considerations. During the operation of the reactor at normal load the can temperature usually varies little, so that the average values of the characteristics in question may be used for practical calculations. In considering transient processes (when the reactor is just coming up to power) the deformation of the fuel-element can be calculated in short time stages, starting from a temperature  $T_n$  (characteristic of the particular can material) at which creep deformation becomes appreciable (for example, in 1Kh18N9T steel, from  $T_n \approx 500^\circ\text{C}$ ). In the temperature range  $T_n - T_{\max}$  it is permissible to average the quantities  $E$ ,  $\mu$ , and  $\alpha$  (for 1Kh18N9T steel the working temperature  $T_{\max} \leq 650^\circ\text{C}$ ). The quantity  $\Delta_n S$  determines the swelling of the can material during the  $n$ -th stage of loading:

$$\Delta_n S = S_n(z) - S_{n-1}(z).$$

The swelling of the steel is determined [10-12] by the integrated neutron flux  $\Phi$  (neutron energy  $E > 0.1$  MeV) and the temperature level:

$$S = A_3 \Phi^* L(T),$$

the temperature dependence may be written

$$L(T) = e^{-\frac{Q_3}{RT}} - B_3 e^{-\frac{Q_3^*}{RT}}.$$

The creep deformations are determined by the expressions

$$\begin{aligned}\xi_0^c &= \frac{1}{2} (2\sigma_0 - \sigma_x) \Phi_c; \\ \xi_x^c &= \frac{1}{2} (2\sigma_x - \sigma_0) \Phi_c.\end{aligned}\quad (7)$$

For the theory of strengthening [13]

$$\Phi_c(\sigma_i, T, \varepsilon_i^c) = A_3 e^{-\frac{Q_3}{RT}} e^{-H(\varepsilon_i^c) \sigma_i^{m_3(T)-1}}, \quad (8)$$

where

$$H(\varepsilon_i^c) = \begin{cases} \frac{\varepsilon_i^c}{\varepsilon_0^c} H(T) & \text{for the stage of transient creep,} \\ H(T) & \text{for the stage of steady creep;} \end{cases}$$

$\varepsilon_0^c = A_4 e^{-\frac{Q_4}{RT}} \sigma_i^{m_4(T)}$  is the deformation at the beginning of the stage of steady creep;  $A_3$  and  $A_4$  are experimental coefficients;  $Q_3$  and  $Q_4$  are the activation energies of the creep process;  $m_3(T)$ ,  $m_4(T)$ ,  $H(T)$  are certain functions of temperature,  $\varepsilon_i^c = \int_0^i \frac{d\varepsilon_i^c}{dt} dt$  is the accumulated creep deformation;  $d\varepsilon_i^c = (\sqrt{2}/3) \sqrt{(d\varepsilon_0^c - d\varepsilon_x^c)^2 + \sqrt{(d\varepsilon_x^c - d\varepsilon_r^c)^2 + (d\varepsilon_r^c - d\varepsilon_0^c)^2}}$  is the intensity of the differentials of creep deformation;  $\sigma_i = \sqrt{\sigma_x^2 + \sigma_0^2 - \sigma_x \sigma_0}$  is the intensity of the stresses. From the condition of the elastic change in volume

$$d\varepsilon_r^c = -d\varepsilon_0^c - d\varepsilon_x^c. \quad (9)$$

The increment in temperature in the range  $t_n$  to  $t_{n-1}$  may be found from the expression

$$\Delta_n T(z) = T(t_n, z) - T(t_{n-1}, z); \quad (10)$$

$\langle \xi_{(n)}^c \rangle$  is a certain mean value of the function  $\xi_{(n)}^c$  in the temperature range in question, refined by the method of successive approximations. In the first approximation, the function  $\xi_{(n)}^c$  is determined from the stresses in the previous  $(n-1)$ -th stage of loading  $\langle \xi_{(n)}^c \rangle = \xi_{(n-1)}^c$ . Then the stress increments and the value of the function  $[\xi_{(n)}^c]$  at the end of the stage of deformation are determined.

In the second and subsequent approximations we take

$$\langle \xi_{(n)}^c \rangle = \frac{1}{2} (\xi_{(n-1)}^c + \xi_{(n)}^c), \quad (11)$$

the calculation being continued until the values of the function  $\langle \xi^c_{(n)} \rangle$  obtained in the previous and following stages are sufficiently close.

The symmetry conditions should also be satisfied:

$$\left. \begin{aligned} \frac{d\Delta_n w}{d\theta} \Big|_{\theta=0} = 0; \quad \frac{d\Delta_n w}{d\theta} \Big|_{\theta=\frac{\pi}{2}} = 0; \\ \Delta_n v \Big|_{\theta=0} = 0; \quad \Delta_n v \Big|_{\theta=\frac{\pi}{2}} = 0 \end{aligned} \right\} \quad (12)$$

and also the initial conditions for the stresses:

$$\sigma_j(\theta, z) = \sigma_{j0}(\theta, z) \quad (j = x, 0), \quad (12a)$$

where  $\sigma_{j0}(\theta, z)$  are the stresses in the can at the onset of the deformation process. Solving the system of Eqs. (1)-(12):

$$\left. \begin{aligned} \Delta_n \sigma_x &= \frac{E}{1-\mu^2} \left[ \mu \Delta_n \varepsilon_\theta^0 + \mu \Delta_n \kappa z + \Delta_n \varepsilon_x^0 - (1+\mu) \alpha \Delta_n T - (1+\mu) \frac{\Delta_n S}{3} - \mu \Delta_n \varepsilon_\theta^c - \Delta_n \varepsilon_x^c \right]; \\ \Delta_n \sigma_0 &= \frac{E}{1-\mu^2} \left[ \Delta_n \varepsilon_\theta^0 + \mu \Delta_n \varepsilon_x^0 + \Delta_n \kappa z - (1+\mu) \alpha \Delta_n T - (1+\mu) \frac{\Delta_n S}{3} - \mu \Delta_n \varepsilon_x^c - \Delta_n \varepsilon_\theta^c \right], \end{aligned} \right\} \quad (13)$$

where  $\Delta_n \varepsilon^c$ ,  $\Delta_n \varepsilon_x^c$  are the increments in the creep deformations:

$$\Delta_n \varepsilon_\theta^c = \langle \xi_{\theta(n)}^c \rangle \Delta_n t; \quad \Delta_n \varepsilon_x^c = \langle \xi_{x(n)}^c \rangle \Delta_n t; \quad (13a)$$

$$\left. \begin{aligned} \Delta_n \varepsilon_x^0 &= \frac{2}{\pi \delta} \int_0^{\pi/2} \int_{-\delta/2}^{\delta/2} \Delta_n \varepsilon_x^c d\theta dz - \frac{1-2\mu}{2E} \frac{R}{\delta} \Delta_n q + \frac{\alpha}{\delta} \int_{-\delta/2}^{\delta/2} \Delta_n T dz + \frac{1}{3\delta} \int_{-\delta/2}^{\delta/2} \Delta_n S dz; \\ \Delta_n \varepsilon_\theta^0 &= \frac{1}{\delta} \int_{-\delta/2}^{\delta/2} \Delta_n \varepsilon_\theta^c dz + \frac{\mu}{\delta} \int_{-\delta/2}^{\delta/2} \Delta_n \varepsilon_x^c dz - \frac{2\mu}{\pi \delta} \int_0^{\pi/2} \int_{-\delta/2}^{\delta/2} \Delta_n \varepsilon_x^c d\theta dz - \frac{2-2\mu}{2E} \frac{R}{\delta} \Delta_n q + \frac{\alpha}{\delta} \int_{-\delta/2}^{\delta/2} \Delta_n T dz + \frac{1}{3\delta} \int_{-\delta/2}^{\delta/2} \Delta_n S dz; \end{aligned} \right\} \quad (14)$$

$$\Delta_n \kappa = \frac{12}{\delta^3} \int_{-\delta/2}^{\delta/2} \Delta_n \varepsilon_{\theta z}^c dz + \frac{12\mu}{\delta^3} \int_{-\delta/2}^{\delta/2} \Delta_n \varepsilon_{xz}^c dz + \frac{12\alpha(1+\mu)}{\delta^3} \int_{-\delta/2}^{\delta/2} \Delta_n T z dz + \frac{4(1+\mu)}{\delta^3} \int_{-\delta/2}^{\delta/2} \Delta_n S z dz - \frac{3\Delta_n M}{q_e R^3}; \quad (15)$$

$$\Delta_n M_c = \frac{Rq_e}{3} \left[ b_0/2 + \frac{C_0 R A^2}{2} + \frac{4(1+\mu) R^2}{\delta^3} \int_{-\delta/2}^{\delta/2} \Delta_n S z dz + \frac{12\alpha(1+\mu) R^2}{\delta^3} \int_{-\delta/2}^{\delta/2} \Delta_n T z dz \right]; \quad (16)$$

$$\Delta_n w = \sum_{j=1}^{\infty} b_j \cos 2j\theta - \frac{C_0 R}{2}; \quad (17)$$

$$\left. \begin{aligned} b_j &= \frac{12\pi}{4j^2 - A^2} \int_0^{\pi/2} F(\theta) \cos 2j\theta d\theta; \\ C_0 &= \frac{4}{\pi} \int_0^{\pi/2} \Delta_n \varepsilon_\theta^0; \quad b_0 = \frac{4}{\pi} \int_0^{\pi/2} F(\theta) d\theta; \end{aligned} \right\} \quad (17a)$$

$$\left. \begin{aligned} A^2 &= \left( 1 + \frac{3q_n}{q_e} \right); \quad F(\theta) = \frac{\mu_{n-1}}{q_e} \Delta_n q \\ &- 4 \frac{R^2}{\delta^3} \left( \int_{-\delta/2}^{\delta/2} \Delta_n \varepsilon_{\theta z}^c dz + \mu \int_{-\delta/2}^{\delta/2} \Delta_n \varepsilon_{xz}^c dz \right). \end{aligned} \right\}$$

Relations (13)-(17) enable us to calculate the increments in the stresses at each n-th step in time if we know the stresses at the end of the (n-1)-th step, the functions  $\xi^c_{(n)}$  being refined by the method of successive approximations. In considering the process in which the reactor is coming up to power, the stresses in the can are determined from the following relationships for the initial stage of deformation ( $t = t_0$ ):

$$\left. \begin{aligned} \sigma_{\theta 0}(\theta, z) &= -\frac{R}{\delta} q(t_0) - \frac{12M_0}{\delta^3} z + \\ &+ \frac{\alpha E(T_n)}{1-\mu} [T_n - T(t, z)]; \\ \sigma_{x 0}(\theta, z) &= -\frac{Rq(t_0)}{2\delta} - \mu \frac{12M_0}{\delta^3} z + \\ &+ \frac{\alpha E(T_n)}{1-\mu} [T_n - T(t, z)]. \end{aligned} \right\} \quad (18)$$

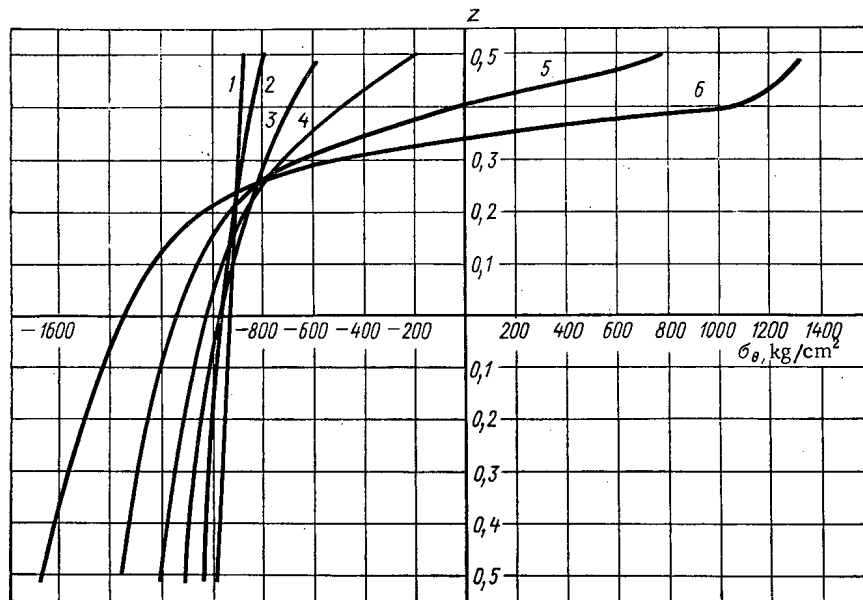


Fig. 1. Stress distribution over the thickness of the can for various periods of operation of the fuel element: 1)  $t = 0$ ; 2)  $t = 60$  h; 3)  $t = 120$  h; 4)  $t = 180$  h; 5)  $t = 240$  h; 6)  $t = 300$  h.

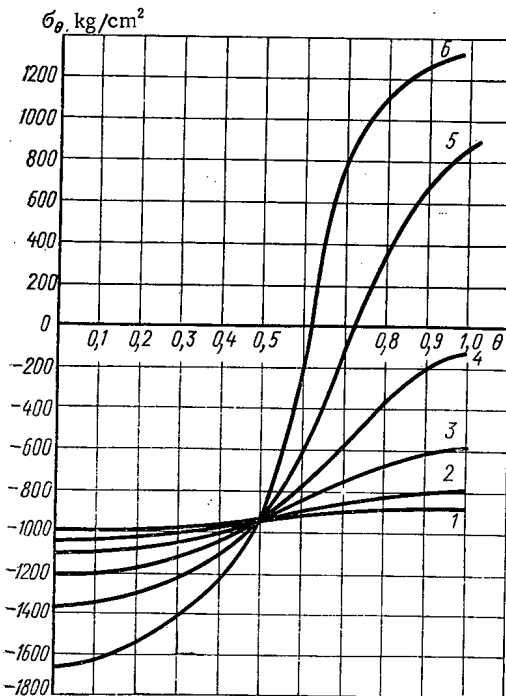


Fig. 2. Stress distribution over the circumference of the fuel element for various periods of operation of the fuel element: 1)  $t = 0$ ; 2)  $t = 60$  h; 3)  $t = 120$  h; 4)  $t = 180$  h; 5)  $t = 240$  h; 6)  $t = 300$  h.

where  $M_0(\theta) = q(t_0)R(w_2 + w_1)$  is the bending moment in the cross sections of the can with an initial ellipticity  $w_1(\theta)$ , which, as a result of the application of the pressure  $q(t_0)$ , acquires the additional curvatures [14]:

$$w_2(\theta) = \frac{w_0}{q_e q(t_0) - 1} \cos 2\theta, \quad (19)$$

where  $q_e = [E(T_n)/4(1 - \mu^2)](\delta/R)^3$  is the critical pressure for an ideally circular tube;  $t_0$  is the time within which the average temperature of the can becomes equal to the characteristic temperature corresponding to the appearance of creep  $T_n$ . A dangerous state of the can may occur for the following reasons.

1. For ductile material, the creep-engendered increase in the sag and the bending moments has the effect that the intensity of the stresses in most stressed cross section of the can reaches the yield stress:

$$\sigma_i(t, \theta, \pm \delta/2) = \sigma_T(T, \eta), \quad (20)$$

which may be regarded as the onset of the loss of stability (owing to the small thickness of the can). Here we allow for the change in the yield stress of the can material arising from changes in temperature and the effects of irradiation, the quantity  $\eta(t)$  determining the radiation damage accumulated during the operation of the can (for example, this quantity may be given by the dose of radiation  $\Phi$  or by the number of displaced atoms in the can material [15]).

2. For an ideally elastic material, at a certain critical time  $t_k$  the sagging of the can increases sharply and a loss of stability sets in.

3. The can material accumulates damage arising from the prolonged action of stresses at high temperatures, which may cause the appearance of cracks and break the air-tightness of the fuel element before the can loses stability. In this case the working efficiency is determined by the criteria of long-term strength or long-term ductility.



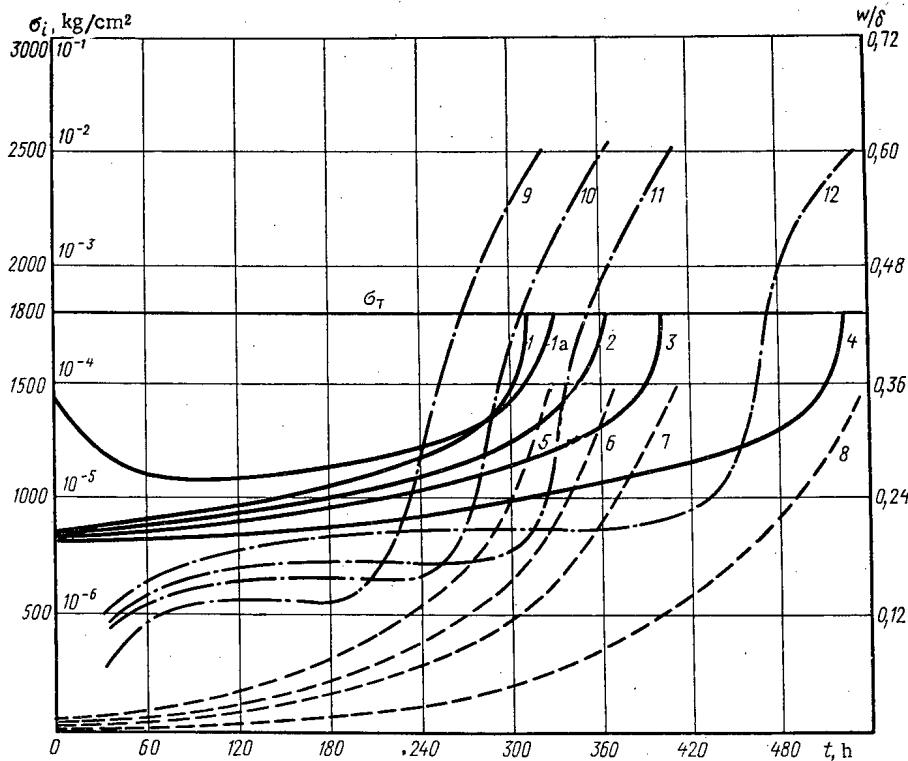


Fig. 3. Time changes in the intensity of the stresses (curves 1-4), the maximum sags (curves 5-8), and the total damage to the can material (curves 9-12) in the most-stressed parts of the can for different values of the original ellipticity: 1, 5, 9)  $w_0/\delta = 0.01$ ; 2, 6, 10)  $w_0/\delta = 0.007$ ; 3, 7, 11)  $w_0/\delta = 0.005$ ; 4, 8, 12)  $w_0/\delta = 0.002$ .

4. If, as a result of the increase in ellipticity, the can closes the gap and rests on the fuel core, there may be an irreversible increase in the length of the can in the course of heat exchange (thermomechanical ratchet) [16]. The time  $t_x$  required for the onset of this mechanism may be determined from the condition

$$R - r(t_x) = \frac{1}{2} w(0, t_x),$$

where  $r(t)$  is the change in the radius of the core due to swelling.

We used the foregoing theory in conjunction with an electronic computer (the M-20) in order to calculate the stability of austenitic steel fuel-element cans for a gas-cooled fast reactor.

Figures 1 and 2 show the thickness and circumferential stress distributions in a can with dimensions of  $\delta/R = 0.14$  and an initial ellipticity of  $w_0/\delta = 0.01$  for various periods of operation of the fuel elements, the can being subjected to a pressure of  $q = 130$  atm at  $670^\circ\text{C}$  (the temperature drop along the wall is taken as zero). The changes in the maximum sags, the damage to the can material, and the stress intensities at the most stressed points are shown in Fig. 3 as functions of time for the same temperature and pressure and for various values of the initial ellipticity ( $w_0/\delta = 0.01 - 0.002$ ). The dangerous state of the can for all  $w_0/\delta$  was determined by the appearance of plastic deformations ( $\sigma_i = \sigma_T$ ); on reducing  $w_0/\delta$  (from 0.01 to 0.002) the time to the onset of the loss of stability  $t_x$  increased (from 323 to 535 h).

For all values of the initial ellipticity considered, the maximum sag at the instant of reaching the dangerous state equals  $w_0/\delta \approx 0.36$ , while the damage factor  $a \approx 1.4 \cdot 10^{-2}$ . Curve 1a in Fig. 3 shows the time variation in the stress intensity for the case in which the temperature drop along the wall equals  $\Delta = 30^\circ\text{C}$ . The initial fall in the curve is due to the relaxation of the thermal stresses arising from the drop  $\Delta$ . The time of operation of the can before reaching the dangerous state was greater in the presence of a temperature drop than in the  $\Delta = 0$  case. Figure 4 shows the effect of a reduction in the excess external pressure, resulting from the accumulation of gaseous fission products under the can, on the loss of can stability ( $w_0/\delta = 0.01$ ,  $T = 670^\circ\text{C}$ ). The time to the onset of can stability loss increases from 323 h (for

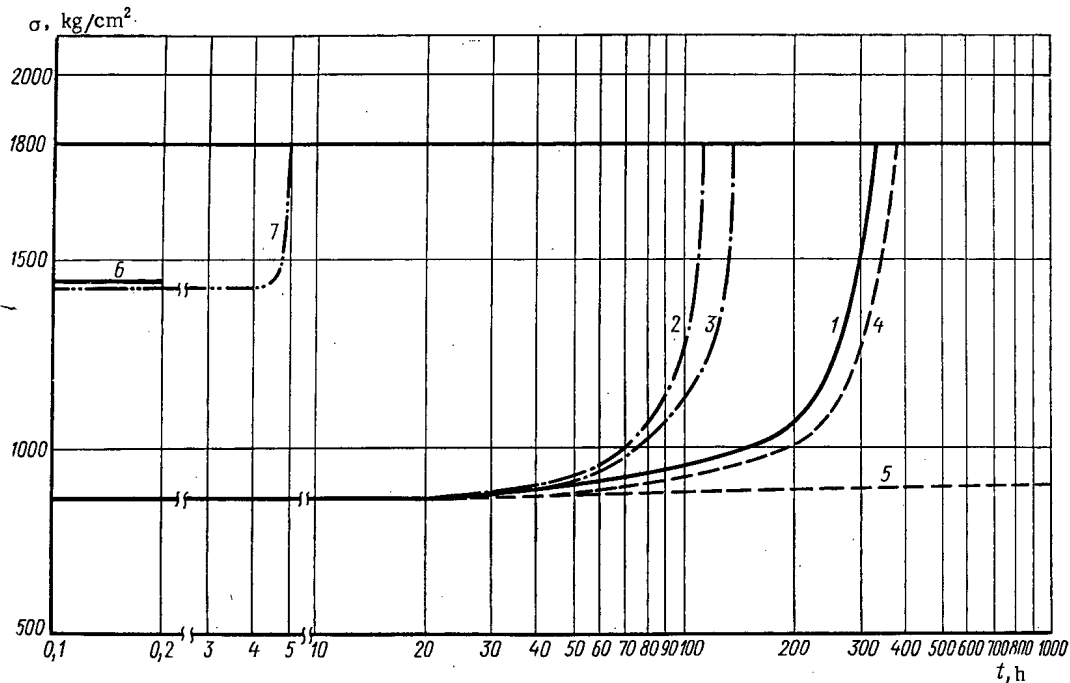


Fig. 4. Effect of changes in temperature (curves 2, 3) and pressure (curves 4, 5) on the loss of can stability: 1)  $q = \text{const}$ ,  $T = \text{const}$ ; 2) temperature increases by  $0.3^\circ\text{C}$  in 1 h; 3) temperature increases by  $0.2^\circ\text{C}$  in 1 h; 4) pressure falls from 130 to 0 atm in  $10^4$  h; 5) pressure falls from 130 to 0 atm in  $10^3$  h; 6, 7) system passes to nominal power in 0.2 and 5 h respectively.

a constant pressure of  $q = 130$  atm) to 356 h if the pressure falls linearly from 130 to 0 atm in  $10^4$  h. The can does not lose stability at all if the pressure falls from 130 atm to zero in  $10^3$  h. The same figure illustrates the effect of a change in the temperature of the can ( $w_0/\delta = 0.01$ ,  $q = 130$  atm) while the reactor is working at nominal power on the loss of stability. If the temperature rises linearly by  $20^\circ\text{C}$  in 100 h, the time to the onset of stability loss falls from 323 to 132 h; for a temperature rise of  $30^\circ\text{C}$  in 100 h the time falls to 107 h.

The change in the stress intensity for two transient modes (reactor passing to nominal power in 0.2 and 5 h with a constant external pressure of  $q = 130$  atm and  $w_0/\delta = 0.01$ ) is illustrated in Fig. 4. In the case of the rapid transient mode, creep is unable to develop, the sagging is slight, and the can fails to reach the dangerous state. For the slow passage to nominal power creep does occur, leading to substantial sagging, and the dangerous state correspondingly arises ( $\sigma_i = \sigma_T$ ).

We may thus draw the following conclusions.

1. We have found a solution to the problem of the stability of a cylindrical fuel-element can in the creep stage, allowing for the initial ellipticity and also accounting for changes in the pressure (due to gaseous fission products) and temperature during service.
2. The use of the theory of strengthening and the solution of the problem in terms of increments enable us to discuss the stability of the can in the transient modes of reactor operation.
3. In the solution we allow for the effect of the nonuniform swelling of the steel, such as may occur for large integrated fluxes in fast reactors, on the loss of stability of the can.
4. The results of our calculations show that the time to the onset of can stability loss is considerably affected by the initial ellipticity of the can, by any fall in excess external pressure, and by any change of temperature.

#### LITERATURE CITED

1. E. Clükler and E. Passig, Nucl. Eng. and Design, 7, No. 3, 236 (1969).
2. D. Howl, J. Brit. Nucl. Energy Soc., 4, No. 4, 337 (1965).

3. K. Ward, J. Brit. Nucl. Energy Soc., 4, No. 4, 354 (1965).
4. D. Howl, J. Brit. Nucl. Energy Soc., No. 2, 103 (1969).
5. N. Hoff, IASS, No. 26, 663 (1959).
6. B. Sandstrom, Trans. Roy. Inst. Technol., Stockholm, No. 115 (1957).
7. T. Wam, J. Franklin Inst., 272, No. 1, 138 (1961).
8. I. A. Birger, Izv. Akad. Nauk SSSR, Mekhanika, No. 2, 113 (1965).
9. I. A. Birger, Circular Plates and Shells of Rotation [in Russian], Oborongiz, Moscow (1961).
10. S. D. Harkness and Che-Yu-Li, Symposium on Radiation Damage in Reactor Materials, Vienna Tuns (1969), Sm-120/F-4.
11. S. Oldberg and D. Sandusky, Trans. ANS, 12, 588 (1969).
12. U. Wolf and A. Withop, Trans. ANS, 12, 114 (1969).
13. B. F. Shopp, in: Strength and Deformation in Nonuniform Temperature Fields [Russian translation], Gosatomizdat, Moscow (1962).
14. S. P. Timoshenko, Stability of Elastic Systems [Russian translation], Gostekhteorizdat, Moscow (1955).
15. W. Sheely, Nucl. Sci. and Engn., 29, No. 2, 174 (1967).
16. E. Duncombe and I. Goldberg, Nucl. Applications and Technol., 9, No. 1 (1970).

DIFFUSIONAL AND THERMODYNAMIC PROPERTIES OF THE  $\gamma$ -PHASE  
OF THE SYSTEM URANIUM - NIOBIUM

G. B. Fedorov, E. A. Smirnov,  
and V. N. Gusev

UDC 539.219.3:669.822

Alloying of uranium with refractory metals having a bcc lattice improves the mechanical and corrosion resistance properties of the uranium, and is one of the principal ways of coping with radiation swelling.

The effect of the alloying elements on resistance to swelling can be estimated with the aid of data on self-diffusion of the components in alloys of uranium with refractory bcc metals. A decrease in the self-diffusion coefficients of  $\gamma$ -uranium as molybdenum, zirconium, and niobium are added had been reported earlier [1]. But later on it was demonstrated that alloying with zirconium actually increases the self-diffusion coefficients of uranium, and only combined alloying of uranium with both zirconium and niobium (in a ratio of 1:1 at. %) results in an appreciable loss of mobility on the part of the uranium atoms.

Bulk diffusion coefficients of uranium and niobium in uranium alloys with niobium contents of 5, 10, 20, 35, 50, 65, 80, and 90 at. % were determined in this work. These investigations were carried out over

the temperature range from 930° to 1900° C, using the radioactive isotopes  $U^{235}$  and  $Nb^{95}$  and the method of stripping off layers and measuring the integrated radioactivity of the remainder of the specimens. The alloys were prepared by arc remelting from electron-beam niobium and electrolytic uranium.

The specimens, as remelted, were subjected to phase recrystallization followed by a homogenization anneal, with the purpose of eliminating the cast structure.

The procedure followed in measuring the bulk diffusion coefficients of uranium and niobium has been described in an earlier article [2]. The temperature dependences of the diffusion coefficients of uranium and niobium are cited in Fig. 1, and the values of the diffusion parameters of the components appear in Table 1. Alloying of uranium with niobium brings about a considerable fall-off in the self-diffusion coefficients of the components. For example, when uranium is alloyed with niobium in amounts from 5 to 20 at. %, a decline in the self-diffusion coefficients of uranium is observed in the range of investigated temperatures, to the extent of 15 times and 50 times respectively, and this is found to be in excellent agreement with the earlier reported findings [1]. Alloying of the uranium has practically no effect on the energy of activation of self-diffusion when the niobium content is as high as 20 at. %. But any further increase in the alloying element (to 35 at. % Nb, say, or higher) brings about a significant rise in the energy of activation of diffusion on the uranium and the niobium.

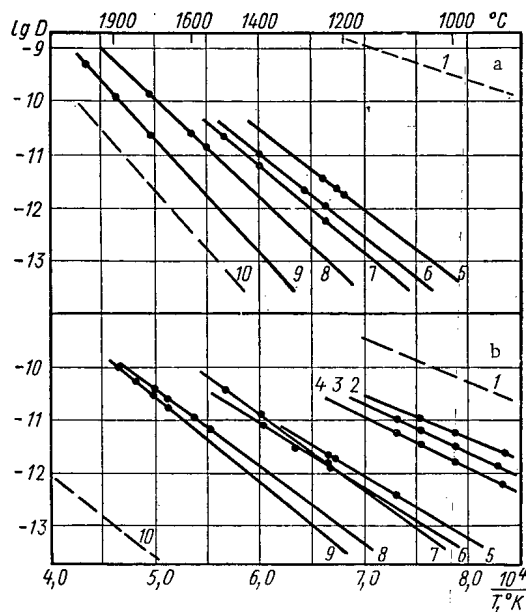


Fig. 1. Temperature dependences of the diffusion coefficients of  $Nb^{95}$  (a) and  $U^{235}$  (b) in uranium-niobium alloys: 1) pure uranium; 2) 5 at. % Nb; 3) 10 at. % Nb; 4) 20 at. % Nb; 5) 35 at. % Nb; 6) 50 at. % Nb; 7) 65 at. % Nb; 8) 80 at. % Nb; 9) 90 at. % Nb; 10) pure niobium.

Translated from *Atomnaya Energiya*, Vol. 32, No. 1, pp. 11-14, January, 1972. Original article submitted November 23, 1970; final revision submitted April 12, 1971.

© 1972 Consultants Bureau, a division of Plenum Publishing Corporation, 227 West 17th Street, New York, N. Y. 10011. All rights reserved. This article cannot be reproduced for any purpose whatsoever without permission of the publisher. A copy of this article is available from the publisher for \$15.00.

TABLE 1. Diffusion Parameters of Components in  $\gamma$ -Phase of System Uranium–Niobium

Diffusion parameters	Niobium content, at. %										
	0	5	10	20	35	50	65	80	90	100	
$U^{235}$	Q, kcal/g atom	36,0 [5]	34	35,2	39,6	53,2	57,2	65,6	67,0	73,0	76,7 [6]
	$D_0$ , cm <sup>2</sup> /sec	$1,1 \cdot 10^{-4}$ [5]	$3,2 \cdot 10^{-6}$	$3,5 \cdot 10^{-6}$	$10^{-5}$	$1,25 \cdot 10^{-4}$	$2,5 \cdot 10^{-4}$	$4,0 \cdot 10^{-3}$	$6,3 \cdot 10^{-4}$	$2,5 \cdot 10^{-3}$	$6,5 \cdot 10^{-6}$ [6]
$Nb^{95}$	Q, kcal/g atom	28,5 [2]	—	—	—	68,8	72,7	77,5	91,5	100,6	100,6 [7]
	$D_0$ , cm <sup>2</sup> /sec	$1,2 \cdot 10^{-5}$ [2]	—	—	—	$3,1 \cdot 10^{-2}$	$3,1 \cdot 10^{-2}$	$7,6 \cdot 10^{-2}$	1,1	5,2	0,91 [7]

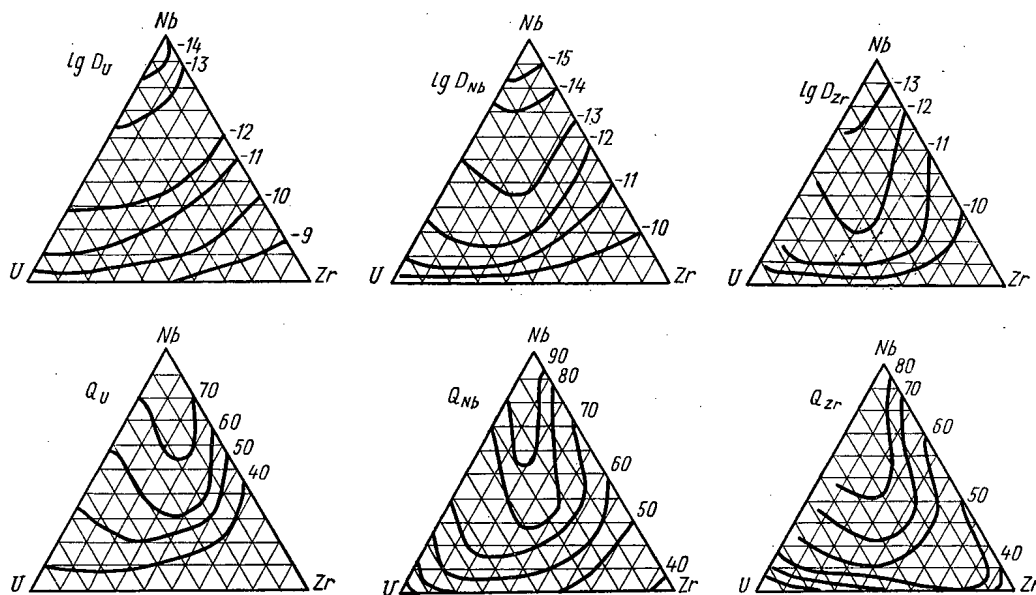


Fig. 2. Isolines of coefficients and of energies of activation of diffusion of components in the system U–Nb–Zr at 1100°C.

A familiar procedure [4] was enlisted to provide a comparison in studying the effect of niobium alloying on self-diffusion of uranium in the  $\alpha$ -phase at temperatures in the range 550–630°C. Introduction of as little as 2 at.% niobium lowers the bulk self-diffusion coefficient of  $\alpha$ -uranium by about three times.

It must be borne in mind that self-diffusion in pure uranium takes place in the supersaturated vacancies of the matrix [5, 8, 9]. This makes it perfectly clear that the self-diffusion parameters of uranium and the diffusion parameters of the vacancies are closely similar. The decline in the self-diffusion coefficients of the components as uranium is alloyed with niobium unquestionably improves resistance to swelling, inasmuch as the basic transport process at work in the volume-diffusion mechanism of the motion of voids is the movement of vacancies from one position on the surface of the void to another through the surrounding host matrix [10].

On the basis of the results obtained and findings published earlier [2–4, 11], isolines of the diffusion coefficients and energies of activation were constructed at 1100°C in the case of the system uranium–niobium–zirconium (Fig. 2). The concentration dependences of the diffusion characteristics in the uranium–niobium part of the ternary diagram show satisfactory agreement with diagrams of the solidus temperature [12] and with hardness and creep diagrams [13] of alloys belonging to the system uranium–niobium–zirconium in the  $\gamma$ -state, which provides experimental proof of the existence of some correlation between the diffusion characteristics of the components and refractory behavior.

This lends added interest to investigations of interdiffusion in the system uranium–niobium, since the interdiffusion parameters characterize to an even greater extent the refractory properties of the alloys [4]. The interdiffusion coefficients were calculated on the basis of Darken's formula [14]:

$$\tilde{D} = (D_1^* x_2 + D_2^* x_1) \left( 1 + \frac{\partial \lg f_1}{\partial \lg x_1} \right), \quad (1)$$

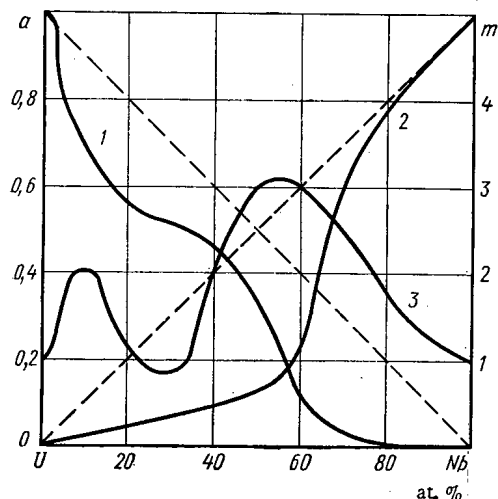


Fig. 3. Thermodynamic properties of the system U-Nb at 1000°C: 1) uranium activity; 2) niobium activity; 3) thermodynamic multiplicative factor.

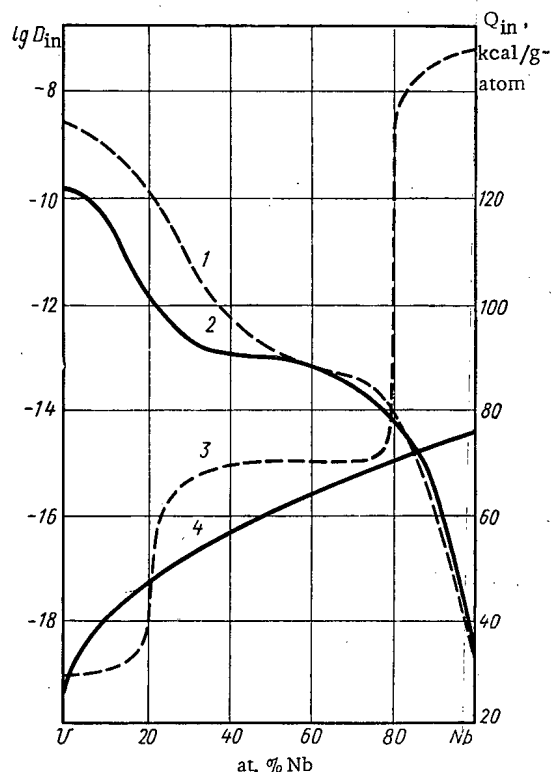
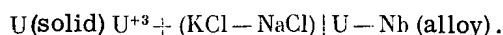


Fig. 4. Concentration dependences of coefficients and of energies of activation of interdiffusion in the system U-Nb at 1000°C: 1)  $\bar{D}$  [15]; 2)  $\tilde{D}$  [present article]; 3)  $\tilde{Q}$  [15]; 4)  $\bar{Q}$  [present article].

The interdiffusion coefficients in the system uranium-niobium were determined by other authors [15] using the Matano method. Concentration dependences of the energies of activation  $Q$  and of the interdiffusion coefficients  $D$  converted to 1000°C values are plotted in Fig. 4. The predicted and experimentally determined interdiffusion coefficients in the range of niobium concentrations 50-100 at.% Nb are clearly

where  $D_i^*$  is the diffusion coefficient of the  $i$ -th component, measured with the aid of radioactive isotopes;  $x_i$  is the concentration of the  $i$ -th component;  $f_i$  is the coefficient of thermodynamic activity coefficient.

The thermodynamic properties of the system were studied by the method of measuring the electromotive forces (emf) of the concentration cells [3] over the temperature range from 750° to 900°C using, as one of the electrodes, uranium alloys with contents of 5, 11.7, 20, 32, 47, 72, and 87 at.% Nb. Temperature dependences of the emf of a concentration cell of the type



were obtained. The potential-building process in the cell is uranium transport. The thermodynamic activities of uranium were found from the formula

$$\lg a_U = -\frac{Z_U E F}{2.3 R T} = -15,120 \frac{E}{T}, \quad (2)$$

where  $Z_U$  is the valence of the uranium;  $F$  is the Faraday number;  $E$  is the cell emf.

As earlier [3], the valence of uranium was assigned the value three. The activity of the niobium was calculated by graphical integration of the Gibbs-Duhem equation:

$$\lg a_{Nb} = -\int_0^{x_U} \frac{\lg a_U}{x_{Nb}^2} dx_U - \frac{x_U}{x_{Nb}} \lg a_U. \quad (3)$$

Results of the calculations are plotted in Fig. 3.

Recalling that  $f_U = a_U/x_U$ , we calculated the values of the thermodynamic multiplicative factor in Eq. (1) from the concentration dependence of the emf:

$$m = 1 + \frac{\partial \lg f_U}{\partial \lg x_U} = -\frac{15,120}{T} \cdot \frac{\partial E}{\partial \lg x_U}. \quad (4)$$

The concentration dependence of the thermodynamic multiplicative factor is also plotted in Fig. 3, for 1000°C.

The negative deviations of the thermodynamic activity of the components from ideal behavior is evidence, as an examination of the thermodynamic properties of the system uranium-niobium clearly argues, for strengthening of the interatomic bond in the  $\gamma$ -solid solution.

On the basis of Darken's equation (1), the interdiffusion coefficients  $D$  were determined for 1000°C (Fig. 4). The concentration dependence of the energy of activation of interdiffusion  $Q$  was calculated under the assumption that the temperature dependence of  $D$  is of the form

$$\tilde{D} = \bar{D}_0 \exp\left(-\frac{\tilde{Q}}{RT}\right). \quad (5)$$

satisfactory agreement in Fig. 4. A slight discrepancy in the interdiffusion coefficients in the uranium-rich region might be due to anomalies in the uranium diffusion characteristics stemming, in our opinion, from supersaturation of the matrix with vacancies [5, 8, 9].

The resulting concentration dependences of the energy of activation of interdiffusion are in satisfactory agreement with published data [15], except for the 80-100 at.% Nb region, where the published values of the energies of activation are seen to be much higher.

Consequently, the rise in the energy of activation and the lowering of the interdiffusion coefficients accompanying alloying of uranium with niobium provide evidence on increased refractory strength which, as stated earlier, must have the effect of also enhancing the resistance of the alloys to gas swelling.

#### LITERATURE CITED

1. Y. Adda and A. Kirianenko, *J. Nucl. Materials*, 6, 135 (1962).
2. G. B. Fedorov, E. A. Smirnov, and V. N. Gusev, *At. Énerg.*, 27, 149 (1969).
3. G. B. Fedorov and E. A. Smirnov, *At. Énerg.*, 21, 189 (1966).
4. G. B. Fedorov, E. A. Smirnov, and F. I. Zhomov, in: *Physical Metallurgy and General Metallurgy of Pure Metals*, No. 7 [in Russian], Atomizdat, Moscow (1968), p. 166.
5. G. B. Fedorov and E. A. Smirnov, in: *Physical Metallurgy and General Metallurgy of Pure Metals*, No. 6 [in Russian], Atomizdat, Moscow (1967), p. 181.
6. G. B. Fedorov et al., *At. Énerg.*, 31, 516 (1971).
7. G. B. Fedorov, F. I. Zhomov, and E. A. Smirnov, in: *Physical Metallurgy and General Metallurgy of Pure Metals*, No. 8 [in Russian], Atomizdat, Moscow (1969), p. 145.
8. G. B. Fedorov, E. A. Smirnov, and F. I. Zhomov, in: *Physical Metallurgy and General Metallurgy of Pure Metals*, No. 5 [in Russian], Atomizdat, Moscow (1966), p. 92.
9. G. B. Fedorov, E. A. Smirnov, and S. S. Moiseenko, in: *Physical Metallurgy and General Metallurgy of Pure Metals*, No. 7 [in Russian], Atomizdat, Moscow (1968), p. 124.
10. P. Shewmon, *Trans. Met. Soc. AIME*, 230, 1134 (1964).
11. G. B. Fedorov, E. A. Smirnov, and S. M. Novikov, in: *Physical Metallurgy and General Metallurgy of Pure Metals*, No. 8 [in Russian], Atomizdat, Moscow (1969), p. 41.
12. E. M. Tararaeva et al., *Theoretical and Experimental Methods for Investigating Phase Diagrams of Metallic Systems* [in Russian], Nauka, Moscow (1968), p. 266.
13. V. A. Bugrov and O. S. Ivanov, *Physical Chemistry of Thorium-Uranium Alloys and Refractory Compounds* [in Russian], Nauka, Moscow (1968), p. 86 and 92.
14. L. Darken, *Trans. AIME*, 175, 184 (1948).
15. N. Peterson and R. Ogilvie, *Trans. AIME*, 227, 1083 (1963).

## DEPOSITION OF CORROSION PRODUCTS ON THE SURFACE OF ZIRCONIUM ALLOYS

V. V. Gerasimov, A. I. Gromova,  
I. K. Morozova, V. N. Belous,  
A. S. Ilyukhin, G. A. Shchapov,  
L. G. Varnacheva, and G. P. Saenko

UDC 620.197.1

The purpose of this work was to obtain experimental results and to generalize the literature data on the amount of deposits on the surface of zirconium alloys as a function of the composition of the medium, time of exposure, and temperature of irradiation.

For the investigation we used plate samples of zirconium alloys [1] with 1% niobium; 2) with 2.5% niobium; 3) system Zr-Sn-Fe; 4) system Zr-Ni-Fe; 5) system Zr-Nb-Cu] with dimensions  $50 \times 20 \times 1$  mm. For each time exposure we tested three to five parallel samples. The tests were conducted under static and dynamic conditions. After the experiments iron was washed off the samples with a hot solution of hydrochloric acid (1:1) and analyzed by a chemicoanalytical method. The details of the method of conducting the tests were described earlier [1].

The experimental data in the literature on the deposition of corrosion products on the surface of construction materials are extremely scanty. The available indications pertain to general considerations of

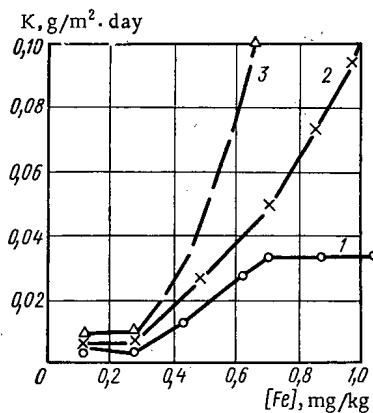


Fig. 1

Fig. 1. Rate of deposition of corrosion products  $K$  of steels on construction materials under static conditions in water at  $300^\circ\text{C}$  (in 100 h of tests): 1) on a zirconium alloy with 2.5% niobium; 2) on a nickel alloy (N-1); 3) on a titanium alloy (VT-1-2).

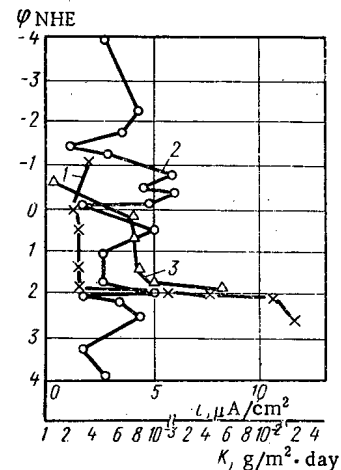


Fig. 2

Fig. 2. Rate of deposition of corrosion products of steels on construction materials in water at  $300^\circ\text{C}$ : 1) on zirconium alloy; 2) on titanium alloy; 3) anodic polarization on alloy of zirconium with 2.5% niobium.

Translated from *Atomnaya Énergiya*, Vol. 32, No. 1, pp. 15-19, January, 1972. Original article submitted December 14, 1970; revision submitted February 14, 1971.

© 1972 Consultants Bureau, a division of Plenum Publishing Corporation, 227 West 17th Street, New York, N. Y. 10011. All rights reserved. This article cannot be reproduced for any purpose whatsoever without permission of the publisher. A copy of this article is available from the publisher for \$15.00.



the possible pathways of accumulation of corrosion products in the system and their subsequent deposition on the surface of the materials. In [2, 3], in particular, a predominant deposition of corrosion products on stainless steel in comparison with zirconium alloys is mentioned. The authors of [4] note that the corrosion products of the circuit are more firmly retained on stainless steel than on zirconium alloys, attributing this phenomenon to different models of growth of the oxide film – inward and outward.

It was shown in [1] that the absolute value of the deposition of corrosion products on a zirconium alloy (under static conditions in water at 300°C in the absence of a heat flow) is lower than on alloys of titanium and nickel. It was reported in the same work that the value of the deposits on the surface of the materials was 0.01–0.1 g/m<sup>2</sup>·day, depending on the concentration of the corrosion products in the system. The rate of deposition of corrosion products of iron on a zirconium alloy with 2.5% niobium has a concentration dependence similar to that of the corrosion products in water (pH = 7) under static conditions (Fig. 1). In water with an iron concentration of 0.1–0.3 mg/kg, the rate of deposition on a zirconium alloy does not exceed  $5 \cdot 10^{-3}$ – $7 \cdot 10^{-3}$  g/cm<sup>2</sup>·day (see Fig. 1). Increasing the iron concentration in the water from 0.3 to 0.7 mg/liter leads to a substantial increase in the rate of deposition on all three materials.

TABLE 1. Rate of Deposition of Corrosion Products of Steels on Alloys of Zirconium, Titanium, and Nickel

Medium	Iron content in solution, mg/liter	Rate of deposition · 10 <sup>3</sup> g/m <sup>2</sup> ·day		
		alloy of zirconium with 2.5% niobium	on nickel alloy	on titanium alloy
Distilled water pH ≈ 6.6, [O <sub>2</sub> ] ≤ 0.025 mg/liter	0.12	6	8.4	6.0
	0.27	3.6	8.48	6.0
	0.72	32.4	116	42.2
	1.0	32.0	—	102
Distilled water, pH = 10 (NH <sub>4</sub> OH), [O <sub>2</sub> ] ≤ 0.025 mg/liter	0.5	7.8	16	14
Distilled water, pH = 3 (HNO <sub>3</sub> ), [O <sub>2</sub> ] ≤ 0.025 mg/liter	0.12	8	25	29
	0.24	23.5	11.3	12.8
Distilled water, pH ≈ 6.6, [O <sub>2</sub> ] ≈ 2–3 mg/liter	0.12	6.32	9.74	6.57

The change in the composition of water may be the cause of the change in the rate of deposition. It is known [5, 6] that the oxygen concentration in water and the pH value may influence not only the concentration of the corrosion products in the system, but also their dispersed composition [1], and, consequently, the amount of deposits of the corrosion products on the surface of the materials. When the pH value is increased from 6.6 to 10 (at comparatively close values of the concentration of corrosion products under static conditions), the rate of deposition on the zirconium alloy with 2.5% niobium decreases, while it increases with increasing pH up to 3 (Table 1). Increasing the oxygen concentration in the medium from 0.02 to 3 mg/kg practically does not influence the rate of deposition of corrosion products on the zirconium alloy at the same concentration of corrosion products in water (see Table 1). The rate of deposition on the zirconium alloy depends substantially on the time: with increasing time of exposure the rate of deposition drops, both under static conditions

TABLE 2. Dependence of the Rate of Deposition of Corrosion Products on a Zirconium Alloy with 2.5% Niobium on the Time

Static conditions			Dynamic conditions		
medium	time of testing, h	rate of deposition · 10 <sup>-3</sup> g/m <sup>2</sup> ·day	medium	time of testing, h	rate of deposition · 10 <sup>-3</sup> g/m <sup>2</sup> ·day
Desalted deaerated water, pH = 10 (NH <sub>4</sub> OH), t = 300°C	100	25.1	Steam—water mixture, pH ≈ 8.5–9, [O <sub>2</sub> ] = 0.02 mg/liter (in water), [Fe] = 0.02 mg/liter, * t = 285°C, rate of flow v ≈ 4 m/sec	2600	1.3
	300	1.58		9300	1.8
Desalted deaerated water, pH ≈ 6.6, t = 300°C	100	7.8	Moist steam, pH ≈ 8.8–9.8, rate of flow v = 20 m/sec	1500	1.7
	300	1.6		3000	0.46
	500	0.6		6700	0.13

\*The iron concentration in the water of the circuit increased to ~2 mg/kg during the testing.

TABLE 3. Influence of Irradiation on the Rate of Deposition of Corrosion Products of Iron on Zirconium Alloys

Alloy No.	Medium				Rate of movement of coolant, m/sec	Time of testing, h	Intensity of neutron flux, neutrons/sec	Rate of deposition, $10^{-3}$ g/m <sup>2</sup> · day	Color of film
	t, °C	pH	[O <sub>2</sub> ], mg/kg	[Fe], mg/kg					
2	220-240	~ 6,5	0,1-0,5	~ 0,1	up to 1	3500	~ 10 <sup>13</sup>	0,33	Black
3	280	~ 6,5	~ 0,5	up to 0,1	—	3450	—	0,139	"
							3 · 10 <sup>13</sup>	0,765	Dark gray
4	280	~ 6,5	~ 0,5	up to 0,1	—	3450	—	0,486	Black
							3 · 10 <sup>13</sup>	1,25	Light gray
1	330	9-10	0,02	0,05	4	5500	—	0,56	Black
							10 <sup>13</sup>	0,52	"

TABLE 4. Deposition of Corrosion Products on Zircalloy Jackets of Fuel Cells in the Loop of the NRX Reactor, Cooled with a Steam - Water Mixture [6] (t = 285° C)

Concentration of corrosion products in coolant, mg/kg	Thermal flux on surface, W/cm <sup>2</sup>	Temperature of jacket, °C	Time of testing, days	Deposition, mg/cm <sup>2</sup>	Rate of deposition, $10^{-3}$ g/m <sup>2</sup> · day
0,035	100	295	16	200	125
0,006	70	295	65	150	23
0,005	68	550	5	4	8
0,005	66	295	5	5	10
0,003	62	290	32	5	1,56
0,003	58	400	32	4	1,25

and under dynamic conditions (Table 2). The increase in the rate of deposition of corrosion products on the zirconium alloy in 9300 h of testing (in comparison with the rate of deposition in 2600 h) is explained by an increased concentration of iron in the system during the testing period (up to ~ 2 mg/kg).

Irradiation in the reactor spectrum with intensity  $10^{12}$ - $10^{13}$  neutrons/cm<sup>2</sup> · sec in the absence of a thermal flux practically does not intensify the rate of deposition of corrosion products on a zirconium alloy possessing a dense black oxide film (Table 3, alloy 1). Irradiation increases the rate of deposition of corrosion products on the zirconium alloy only in the case when the color of the film formed on the alloy changes from black to a lighter color, and, consequently, its density changes (see Table

3, alloys 3 and 4). As is evidenced by the literature data, the rate of deposition of corrosion products on the jackets of fuel cells, made of zircalloy, is somewhat higher under conditions of irradiation (Table 4) than the results obtained on samples in the absence of a thermal flux (see Table 3). Regardless of the duration of the testing, despite the fact that the concentration of corrosion products in the coolant in experiments with fuel cells was significantly lower (0.006-0.04 mg/kg, see Table 4), in comparison with the iron concentration in the system (0.05-0.1 mg/kg, see Table 3), the rate of deposition on the fuel cells proved higher than on samples without a thermal flux. As is evidenced by the results of Table 4, as well as [7], the rate of deposition of corrosion products on the zirconium alloy depends on the values of the thermal flux (the authors do not characterize the oxide film formed on the jackets). In [8] it was indicated that although ionizing irradiation somewhat increases the rate of deposition, it is a function of the amount of dissolved and colloidal iron in the system. In the opinion of the authors of this work, the influence of irradiation on the rate of deposition of corrosion products of iron on zirconium alloys must be related to the oxide films formed on the alloy itself. Thus, thin dense oxide films can adsorb substantially less iron oxides and other corrosion products than thick loose and more porous oxide films. If this assumption is correct, then the amount of deposited iron should depend on the color of the oxide film and its thickness, i.e., ultimately on the weight gain. Data on the dependence of the rate of deposition on the color of the film on alloy 1 under conditions of irradiation with a thermal neutron flux with intensity  $3.0 \cdot 10^{13}$  neutrons/cm<sup>2</sup> · sec (t = 280° C, time of testing 3450 h), are presented below:

Color of film	Rate of deposition · 10 <sup>-3</sup> , g/m <sup>2</sup> · day
Black	1.04
Dark gray	2.16
Light gray	3.48

TABLE 5. Dependence of the Rate of Deposition on the Weight Gain of Samples with Oxide Films of the Same Color

Color of film	Alloy No.	Rate of deposition $\cdot 10^{-4}$ g/m <sup>2</sup> · day	Weight gain, mg /cm <sup>2</sup>	
Black (obtained with irradiation)	3	1,39	8	
		1,39	30	
		2,78	20	
	4	1,39	17	
		2,08	25	
		2,78	12	
		2,78	17	
		2,78	24	
		4,86	11	
	4,86	13		
Dark gray (obtained with irradiation)		3	7,65	165
		1	27,8	176
	2	21,6	53	
Light gray (obtained with irradiation)	4	27,8	610	
		12,5	550	

As is evidenced by the data cited, the rate of deposition depends on the color of the film (the lighter the film, and, consequently, the looser it is, the higher the rate of deposition of corrosion products). Under conditions of irradiation on samples of a zirconium alloy possessing black, dark gray, and gray films, the amounts of deposits increase correspondingly. Thus, the amount of deposits on the surface is a function of the properties of the oxide films formed on zirconium alloys. Under conditions of irradiation without a thermal flux, when, as a rule, a lighter oxide film is formed on the samples, there is two to six times as much deposition as without irradiation.

A change in the weight gain that is not accompanied by a change in the color of the film does not lead to any significant change in the value of the deposition (Table 5). It may be assumed that the deposition of corrosion products on the surface of construction materials is of an electrochemical nature. The rate of deposition should depend on the potential of the zirconium alloy and the presence of contact of the alloy with other materials.

However, experiments conducted in an electrochemical autoclave on an alloy of zirconium with 2.5% niobium and on an alloy of titanium at the temperature 300°C did not confirm this hypothesis.

A sample of a zirconium or titanium alloy with area 50 cm<sup>2</sup>, to which a definite potential, maintained potentiostatically for 100 h, was communicated, was placed in an electrochemical autoclave.

In the range of potentials from -4 to +4 V (normal hydrogen electrode), the rate of deposition of corrosion products of steel varied in the range 0.005-0.02 g/m<sup>2</sup> · day (Fig. 2). The observable fluctuations, as can be seen from Fig. 2, are not a function of the potential communicated to the electrode, but are explained by a difference in the concentrations of the corrosion products in the medium (0.02-0.15 mg/kg).

Thus, on a titanium alloy in the potential interval from -4 to +4 V (normal hydrogen electrode)\* and a stress in water at the temperature 300°C, a uniform dark phase film is formed. An analogous dependence is observed on the zirconium alloy in the potential interval from -1 to +1.9 V (i.e., in the case of formation of a dark oxide film on the surface, corresponding to the passive region of the anodic polarization curve), but then, as the potential is increased to +2 to 2.5 V, a white oxide film is formed (corresponding to the region of superpassivation of the anodic polarization curve), and the rate of deposition of corrosion products at the potentials in this region increases significantly (curve 1, Fig. 2).

Probably the increased rate of deposition of corrosion products on the zirconium alloy in this case should be explained by a change in the sorption properties of the film formed on the surface of the alloy, and not by the value of the set potential. The process of deposition of corrosion products on the surface of construction materials is not of an electrochemical nature.

Thus, evidently the rate of deposition of corrosion products (iron oxides) on zirconium alloys is a function chiefly of three components: the iron concentration in the coolant, the thermal flux, and the properties of the films formed on the alloy. Thus, the dependence of the rate of deposition of corrosion products of iron on an alloy of zirconium with 2.5% niobium on the concentration of corrosion products in the medium found in this work convincingly shows that the iron concentration in the water of operating nuclear installations, from the standpoint of the formation of possible deposits on the surface of construction materials, should be less than 0.5 mg/kg.

The results obtained permit us to assume that the deposits of corrosion products should be negligible when the water system is observed. The authors of [9], who investigated the deposition on fuel cells, arrived at an analogous conclusion.

\*A potential of -4 V was communicated to one of the samples in the autoclave, and a potential of +4 V to the other.

Thus, the rate of deposition of corrosion products of iron on zirconium alloys under static and dynamic conditions in water at 300°C, including conditions of irradiation, was evaluated.

On the basis of the aforementioned we can draw the following conclusions.

1. If the zirconium alloy is corrosion-resistant and a uniform black oxide film is formed on its surface, then:

1) with increasing iron concentration in the system (more than 0.5 mg/kg) the rate of deposition of corrosion products of iron on the alloy increases significantly;

2) the rate of deposition of corrosion products of iron on zirconium alloys decreases with time and when the pH is raised from 7 to 10;

3) increasing the oxygen concentration in the medium and irradiation in the reactor spectrum with intensity up to  $10^3$  neutrons/cm<sup>2</sup>·sec practically does not increase the rate of deposition of corrosion products of iron on a zirconium alloy in the absence of a thermal flux;

4) the rate of deposition of corrosion products of iron on the zirconium alloys does not depend on the potential in the passive region.

2. The rate of deposition of corrosion products of iron depends substantially on the quality of the oxide film formed on the zirconium alloy. Thus, the rate of deposition of corrosion products on samples with a dense black oxide film is lower than on samples possessing a loose light colored oxide film.

#### LITERATURE CITED

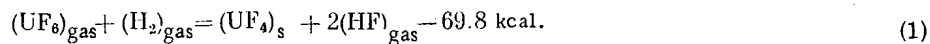
1. A. I. Gromova et al., *Teploenergetika*, No. 6, 54 (1970).
2. H. Hami et al., *NSI-Tr-61* (1966).
3. W. Pearl, M. Fitzsimmons, and M. Siegler, *Trans. Amer. Nucl. Soc.*, 4, No. 2, 349 (1961).
4. J. Wanklyn and P. Fones, *J. Nucl. Mater.*, 6, No. 3, 291 (1962).
5. I. K. Morozova et al., *Teploenergetika*, No. 10, 72 (1970).
6. *Gariigliano Nuclear Power Plant Operation Report for 2nd Quarter of 1967 (TID-24131)*.
7. A. B. Andreeva et al., in: *Transactions of the Symposium of the Council of Economic Mutual Aid, "State and prospects of the development of atomic electric power plants with water-moderated water-cooled reactors"* (Moscow, 1968) [in Russian], Vol. 2, IAE, Moscow (1968), p. 357.
8. J. Simon et al., *WAPD-CDA(AD)-446* (1959).
9. L. Joseph, *Nucleonics*, 24, No. 3, 51 (1966).

MECHANISM OF REDUCTION OF URANIUM HEXAFLUORIDE  
BY HYDROGEN

Yu. N. Tumanov and N. P. Galkin

UDC 546.6:541.121

The reduction of uranium hexafluoride by hydrogen is usually represented [1-5] by the equation of the exothermic reaction

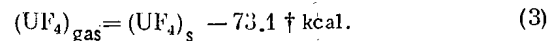
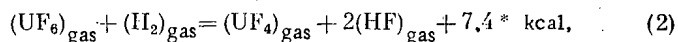


Although the thermodynamic characteristics of this reaction indicate that the thermodynamics do not limit the reduction of uranium hexafluoride by hydrogen [6], in practice this process begins only at 498-523°K, and is slow and incomplete even at 873°K [7].

The difficulty of reducing  $\text{UF}_6$  by hydrogen is usually attributed [1-7] to the high activation energy; to reduce this, one usually employs atomic hydrogen, generated by a gas-plasma reaction of hydrogen with fluorine, by an electric discharge [8], or by dissociation of ammonia [1].

The experimental activation energy of reaction (1) is 8.15 kcal/mole [5]. Since the activation energies of the elementary stages may differ markedly from that of the overall reaction, the relatively low activation energy of reaction (1) indicates a complex and stagewise reduction mechanism and the presence of a limiting state. Our paper deals with these aspects.

Reaction (1) may be represented to a first approximation as consisting of two stages:



Although the first stage (2) is endothermic, it is not limited by thermodynamics (Table 1).

The high exoeffect of condensation of  $\text{UF}_4$  is responsible for the overall exothermic effect of reaction (1).

The fact that when  $\text{UF}_6$  is reduced by hydrogen under fairly mild conditions both the tetrafluoride and pentafluoride are present, may be some indication† of the stagewise reduction mechanism of  $\text{UF}_6$ , according to which reaction (2) takes place in two stages:

\*We took the following value of the heats of formation of gaseous fluorides at  $T = 298^\circ\text{K}$  and  $p = 1 \text{ atm}$ :  $\Delta H_{\text{UF}_6}^\circ = -510, 77 \pm 0.45 \text{ kcal/mole}$  [9],  $\Delta H_{\text{UF}_5}^\circ = -449 \pm 5 \text{ kcal/mole}$  [7, 10],  $\Delta H_{\text{UF}_4}^\circ = -374.9 \pm 5 \text{ kcal/mole}$  [11, 12],  $\Delta H_{\text{HF}}^\circ = -64.2 \pm 0.3 \text{ kcal/mole}$  [13].

†The heat of sublimation of  $\text{UF}_4$  was assessed from data of Akishin et al. [12].

‡ $\text{UF}_5$  may be obtained by the reaction  $\text{UF}_4 + \text{UF}_6 \rightarrow 2 \text{UF}_5$ .

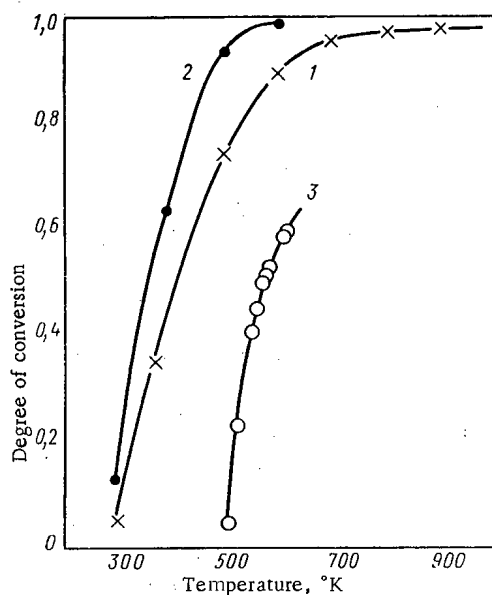


Fig. 1. Degree of hydrogen reduction of  $\text{UF}_6$  versus absolute temperature: 1) calculated curve at a molar ratio  $\text{UF}_6 : \text{H}_2 = 1 : 1$ ; 2) calculated curve at a molar ratio  $\text{UF}_6 : \text{H}_2 = 1 : 5$ ; 3) experimental curve [2] at a molar ratio  $\text{UF}_6 : \text{H}_2 = 1 : 5$ , contact time 30 min.

Translated from *Atomnaya Energiya*, Vol. 32, No. 1, pp. 21-25, January, 1972. Original article submitted January 6, 1971.

© 1972 Consultants Bureau, a division of Plenum Publishing Corporation, 227 West 17th Street, New York, N. Y. 10011. All rights reserved. This article cannot be reproduced for any purpose whatsoever without permission of the publisher. A copy of this article is available from the publisher for \$15.00.

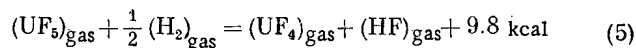
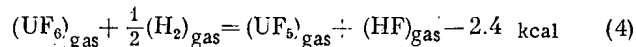
TABLE 1. Results of Calculation of the Equilibrium of Reaction (2)

Temperature, °K	298	400	600	1000	1400	1800	2200	2600
Equilibrium constant $K_e$ , atm	$1,26 \cdot 10^4$	$2,95 \cdot 10^5$	$6,46 \cdot 10^6$	$7,17 \cdot 10^7$	$7,24 \cdot 10^7$	$7,41 \cdot 10^7$	$7,58 \cdot 10^7$	$7,76 \cdot 10^7$
Degree of conversion of $UF_6$	0,988	0,998	~ 1	~ 1	~ 1	~ 1	~ 1	~ 1

\* The thermodynamic properties of uranium fluorides are given in [14].

TABLE 2. Results of Calculation of the Equilibrium of Stagemwise Reaction of Reduction of  $UF_6$  by Hydrogen

$T$ , °K	Reaction (4)		Reaction (5)	
	$K_e$ , atm <sup>1/2</sup>	x - degree of conversion of $UF_6$	$K_e$ , atm <sup>1/2</sup>	x - degree of conversion of $UF_5$
298	$4,17 \cdot 10^6$	~ 1	$3,02 \cdot 10^{-3}$	0,05
400	$1,26 \cdot 10^8$	~ 1	$2,34 \cdot 10^{-1}$	0,345
500	$5,89 \cdot 10^9$	~ 1	$3,98 \cdot 10^0$	0,745
600	$3,32 \cdot 10^5$	~ 1	$1,95 \cdot 10^1$	0,895
1000	$9,12 \cdot 10^4$	~ 1	$4,58 \cdot 10^2$	0,98
1400	$6,46 \cdot 10^4$	~ 1	$1,02 \cdot 10^3$	0,99
1800	$2,89 \cdot 10^4$	~ 1	$2,63 \cdot 10^3$	0,995
2200	$2,0 \cdot 10^4$	~ 1	$3,8 \cdot 10^3$	0,999
2600	$1,55 \cdot 10^4$	~ 1	$5 \cdot 10^3$	~ 1
3000	$1,26 \cdot 10^4$	~ 1	$6,46 \cdot 10^3$	~ 1

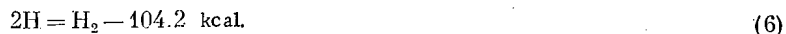


The reduction of  $UF_6$  to the pentafluoride is not limited by thermodynamics, but if we disregard condensation of  $UF_4$ , reduction of the pentafluoride to the tetrafluoride takes place quantitatively only above 1000°K (Table 2). Therefore if condensation of  $UF_4$  in the reaction zone is retarded in some way, we cannot assert that the equilibrium of the reduction of  $UF_6$  by hydrogen to  $UF_4$  is wholly displaced to the right.

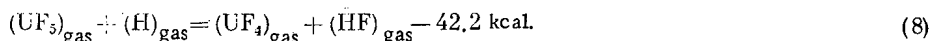
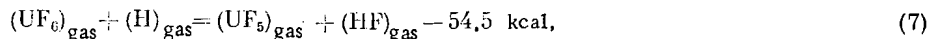
Although the assumption of stagewise reduction of  $UF_6$  agrees qualitatively with the experimental data, Eqs. (4) and (5) do not reveal enough about the mechanism of

(1). Furthermore, the experimental curve of the reduction of  $UF_6$  to  $UF_4$  versus temperature [6] lies far below the calculated data (Fig. 1), which is hardly possible under the conditions of continuous displacement of equilibrium of  $UF_4$  condensation.

Since all practical methods of hydrogen reduction of  $UF_6$  involve the appearance of atomic hydrogen in some way or another, we must examine the ways in which hydrogen atoms are generated in the system  $UF_6 - H_2$ . The role of atomic hydrogen is usually reduced [1-4] to evolution of the heat of recombination in the reaction zone by the reaction



However, markedly exothermic reactions of direct reduction of  $UF_6$  are just as possible:

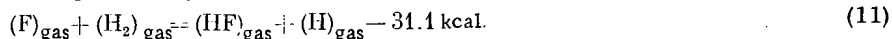
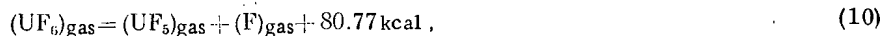


How can hydrogen atoms be generated during reduction of  $UF_6$  in a reactor with a "hot wall"? Three schemes of hydrogen atom generation in the system  $UF_6 - H_2$  may be visualized.

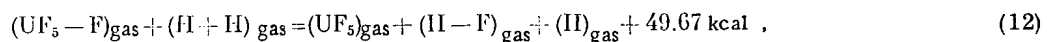
Scheme 1 - via dissociation of  $H_2$  molecules:



Scheme 2 - via dissociation of  $UF_6$  molecules:



Scheme 3 - via formation of monoradicals during bimolecular collision by the Semenov scheme [15]:



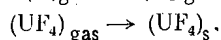
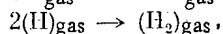
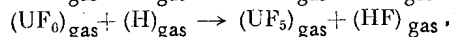
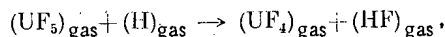
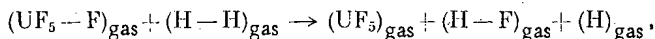
where  $UF_5$ , fluorine, and hydrogen are monoradicals.

All the schemes include markedly endothermic stages, but scheme 3 is thermodynamically more advantageous than schemes (1) and (2) (Table 3).

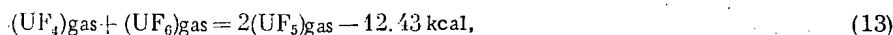
TABLE 3. Thermodynamic Characteristics of Reactions Leading to the Appearance of Hydrogen Atoms in the System  $UF_6-H_2$ 

T, °K	Scheme		Scheme				Scheme	
	$K_{e_9}$ , atm	$\alpha$ -degree of dissociation of $H_2$	$K_{e_{10}}$ , atm	$\alpha$ -degree of dissociation of $UF_6$	$K_{e_{11}}$ , atm	$\alpha$ -degree of conversion of $H_2$	$K_{e_{12}}$ , atm	$\alpha$ -degree of conversion of $UF_6$
298	$5.92 \cdot 10^{-72}$	$1.22 \cdot 10^{-36}$	$10^{-52}$	$10^{-26}$	—	—	$7.98 \cdot 10^{-30}$	$2.95 \cdot 10^{-10}$
600	$2.12 \cdot 10^{-33}$	$2.3 \cdot 10^{-17}$	$10^{-23}$	$3.17 \cdot 10^{-12}$	$8.52 \cdot 10^{11}$	$\sim 1$	$8.92 \cdot 10^{-12}$	$2.6 \cdot 10^{-4}$
1000	$5.1 \cdot 10^{-18}$	$1.13 \cdot 10^{-9}$	$3.02 \cdot 10^{-11}$	$5.62 \cdot 10^{-6}$	$2.34 \cdot 10^6$	$\sim 1$	$1.92 \cdot 10^{-4}$	$6.5 \cdot 10^{-2}$
1400	$2.34 \cdot 10^{-11}$	$2.42 \cdot 10^{-6}$	$3.16 \cdot 10^{-6}$	$1.78 \cdot 10^{-3}$	$2.57 \cdot 10^4$	$\sim 1$	$1.44 \cdot 10^{-1}$	$4.4 \cdot 10^{-1}$
1800	$1.27 \cdot 10^{-7}$	$1.78 \cdot 10^{-4}$	$1.855 \cdot 10^{-3}$	$5 \cdot 10^{-2}$	$2.09 \cdot 10^3$	$\sim 1$	4.82	$7.9 \cdot 10^{-1}$
2200	$3.14 \cdot 10^{-5}$	$2.8 \cdot 10^{-3}$	$1.01 \cdot 10^{-1}$	$3.1 \cdot 10^{-1}$	$4.28 \cdot 10^2$	$\sim 1$	$5.2 \cdot 10^1$	$9.35 \cdot 10^{-1}$
2600	$1.46 \cdot 10^{-3}$	$1.91 \cdot 10^{-2}$	1,596	$7.7 \cdot 10^{-1}$	$1.37 \cdot 10^2$	$\sim 1$	$2.69 \cdot 10^2$	$9.77 \cdot 10^{-1}$
3000	$2.47 \cdot 10^{-2}$	$7.83 \cdot 10^{-2}$	$1.23 \cdot 10^1$	$9.6 \cdot 10^{-1}$	$6.02 \cdot 10^1$	0,988	$8.92 \cdot 10^2$	$9.87 \cdot 10^{-1}$

Therefore the following mechanism of reduction of  $UF_6$  by hydrogen may be presented



Furthermore, a certain part is also played by the reactions:



etc.

An attempt must be made to assess the kinetic constants of the elementary stages included in schemes 1-3.

Let us first assess the rates of establishment of dissociation equilibria of  $UF_6$  and  $H_2$ , because they are the limiting values in schemes 1 and 2. If we take as the rate the value  $1/\tau$  ( $\text{sec}^{-1}$ ), where  $\tau$  is the time required for the partial pressures of hydrogen and fluorine to reach half the equilibrium values [1], then for bimolecular reaction (9), which must be written as



at a pressure  $p_{H_2}^0 = p_{UF_6}^0 = 0.5 \text{ atm}$ , we get

$$\frac{1}{\tau_H} = 4p_M k'_{16} \sqrt{K_{e_9} p_{H_2}} = \frac{2.23 \cdot 10^{12}}{T^2} (K_{e_9})^{1/2}. \quad (17)$$

To assess the value of  $1/\tau_F$  we must find the velocity constant of reaction (10). This was calculated from the two independent equations:

$$k_{10} = \lambda_0 \exp\left(-\frac{E_0}{RT}\right) \sum_{f=1}^{f-1} \left(\frac{E_0}{RT}\right)^{f-1} \frac{1}{(f-1)!}; \quad (18)$$

$$k_{10} = \frac{kT}{h} \exp\left(\frac{\Delta S^*}{R}\right) \exp\left(-\frac{E_0 - RT}{RT}\right), \quad (19)$$

where  $\lambda_0$  is the velocity constant of monomolecular decomposition of excited  $UF_6$  molecules;  $f$  is the number of oscillators involved in the reaction;  $E_0$  is the activation energy of the elementary stage;  $R$ ,  $k$ , and  $h$  are respectively the gas constant, the Boltzmann constant, and the Planck constant; and  $\Delta S^*$  is the change in entropy.

The results of calculations by Eqs. (18) and (19) agree closely (Fig. 2) if we put  $f = 3$ ,  $\Delta S^* = S_{UF_5} - S_{UF_6}$ ,  $E_0 = E_{UF_5-F} = 80.72 \text{ kcal}$  [14].

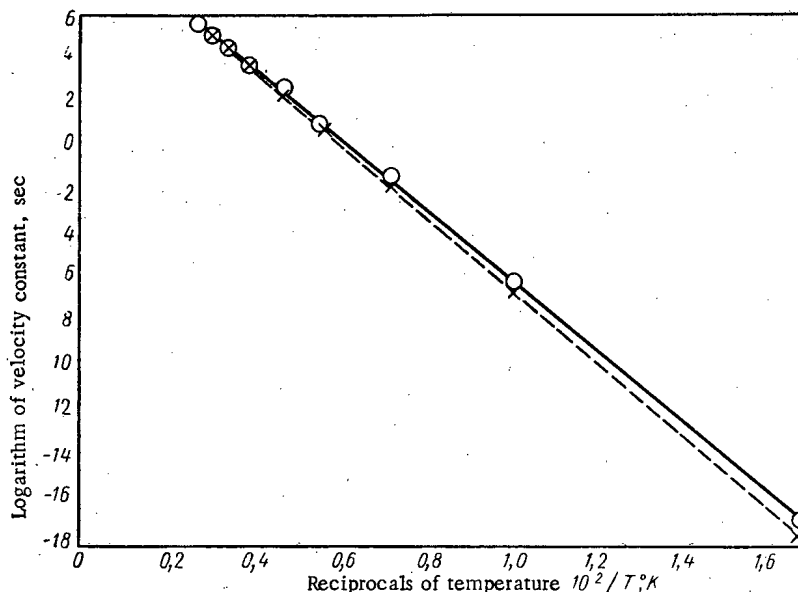


Fig. 2. Logarithm of velocity constant of the reaction  $\text{UF}_6 \rightarrow \text{UF}_5 + \text{F}$  versus the reciprocals of temperature.  $\circ$ ) 18;  $\times$ ) 19.

For the value of  $1/\tau_F$  we obtained the expression

$$\frac{1}{\tau_F} = 2k'_{10} (K_{e_{10}})^{1/2}. \quad (20)$$

The results of the calculation (Table 4) show that dissociation equilibrium of  $\text{UF}_6$  is reached in the range 1800-600°K more rapidly than for  $\text{H}_2$  by a factor of 0.5-4. The velocity constant of reaction (11) in the range 1000-4000°K may be assessed by the equation [16]

$$k_{11} = 7.76 \cdot 10^7 T^{0.69} \exp\left(-\frac{2500}{RT}\right). \quad (21)$$

Beginning at  $T \approx 1800^\circ\text{K}$  the role of dissociation of  $\text{UF}_6$  during its conversion to the tetrafluoride becomes appreciable and, with a further increase in temperature, scheme 2 becomes predominant. However, at temperatures in the range  $\sim 1000$ -1500°K, reduction of  $\text{UF}_6$  apparently proceeds via scheme 3.

The activation energy of reaction (12) may be assessed by the equation [15]

$$E_{\text{act}} = E_{\text{UF}_6} + E_{\text{H-H}} - E_{\text{H-F}}; \quad (22)$$

it is 49.67 kcal. For reactions of saturated molecules of type (12), the preexponential factor is equal (with high probability) to the value  $10^{13} \text{ cm}^3 \cdot \text{mole}^{-1} \cdot \text{sec}^{-1}$  [15], so that

$$k_{12} = 10^{13} \exp\left(-\frac{49600}{RT}\right) \text{ cm}^3 \cdot \text{mole}^{-1} \cdot \text{sec}^{-1} \quad (23)$$

To calculate the velocity constants of reactions (7) and (8), we may propose the equation

$$k_{7-8} = 10^{13} \exp\left(-\frac{0.28E_{\text{UF}_6} - F}{RT}\right) \text{ cm}^3 \cdot \text{mole}^{-1} \cdot \text{sec}^{-1} \quad (24)$$

An equation of this type was used for calculating the kinetic constants of the analogous reduction of sulfur hexafluoride:



Calculations by the equations

$$k_{25} = 2 \cdot 10^{15} \exp\left(-\frac{30000 \pm 5000}{RT}\right), \quad [16]$$

$$k_{25} = 10^{13} \exp\left(-\frac{27000}{RT}\right)$$



TABLE 4. Rate of Establishment of Dissociation Equilibria of Hydrogen and Uranium Hexafluoride

T, °K	H <sub>2</sub> ⇌ 2H		UF <sub>6</sub> ⇌ UF <sub>5</sub> +F	
	K <sub>e</sub> , atm	1/τ <sub>H</sub> , sec <sup>-1</sup>	K <sub>e</sub> , atm	1/τ <sub>F</sub> , sec <sup>-1</sup>
600	2,12·10 <sup>-33</sup>	2,85·10 <sup>-10</sup>	10 <sup>-23</sup>	1,18·10 <sup>-6</sup>
1000	5,1·10 <sup>-18</sup>	5,04·10 <sup>-3</sup>	3,02·10 <sup>-11</sup>	1,43·10 <sup>-1</sup>
1400	2,34·10 <sup>-11</sup>	5,51·10 <sup>0</sup>	3,16·10 <sup>-6</sup>	2,4·10 <sup>1</sup>
1800	1,27·10 <sup>-7</sup>	2,54·10 <sup>2</sup>	1,855·10 <sup>-3</sup>	4,0·10 <sup>2</sup>

give results displaying satisfactory mutual agreement. Therefore

$$k_8 = 10^{13} \exp\left(-\frac{22\,600}{RT}\right) \text{ cm}^3 \cdot \text{mole}^{-1} \cdot \text{sec}^{-1}, \quad (26)$$

$$k_7 = 10^{13} \exp\left(-\frac{26\,400}{RT}\right) \text{ cm}^3 \cdot \text{mole}^{-1} \cdot \text{sec}^{-1}, \quad (27)$$

The value of  $k_6$  for the reaction  $2\text{H} + \text{H}_2 \rightarrow \text{H}_2 + \text{H}_2$  in the range 290–7000°K may be calculated by the equation [16]

$$k_6 = 6.03 \cdot 10^{18} T^{-1.09} \text{ cm}^6 \cdot \text{mole}^{-2} \cdot \text{sec}^{-1}. \quad (28)$$

In accordance with the Frenkel' equation [17], the rate of removal of supersaturation of uranium tetrafluoride by formation of nuclei of the condensed phase in UF<sub>4</sub> vapor has the form:

$$J_{\text{UF}_4} = \exp\left(\frac{-7.2 \cdot 10^3 \sigma^3}{T^3 \left(\lg \frac{p}{p_\infty}\right)^2}\right) \frac{1.13 \cdot 10^2 \sigma^2 p}{T^{5/2} \left(\lg \frac{p}{p_\infty}\right)^{3/2}} \left(\frac{g^*}{m}\right)^{1/2} \text{ sec}^{-1}, \quad (29)$$

where  $\sigma$  is the surface tension;  $p$  and  $p_\infty$  are respectively the vapor pressure and the equilibrium pressure; and  $g^*$  and  $m$  are respectively the critical size of the nucleus and its mass.

For the velocity constant of  $k_{13}$ , by analogy with  $k_7$  and  $k_8$  we may write the equation

$$k_{13} = 10^{13} \exp\left(-\frac{0.28E_{\text{UF}_5-\text{F}}}{RT}\right) = 10^{13} \exp\left(-\frac{22\,600}{RT}\right) \text{ cm}^3 \cdot \text{mole}^{-1} \cdot \text{sec}^{-1}. \quad (30)$$

The role of reactions (14) and (15) cannot be determined, but it is apparently fairly great after the appearance of condensed uranium tetrafluoride in the system.

The results may be summarized as follows.

1. Reduction of uranium hexafluoride by hydrogen to the tetrafluoride is an endothermic reaction; the exothermic effect of overall reaction (1) is due to condensation of UF<sub>4</sub> and it cannot always be used for activation of UF<sub>6</sub> reduction.
2. The appearance of hydrogen atoms in the system UF<sub>6</sub>-H<sub>2</sub> activates reduction not only by recombination of hydrogen molecules, but also as a result of markedly endothermic reduction of UF<sub>6</sub> and UF<sub>5</sub> molecules by atomic hydrogen.
3. Owing to the high thermodynamic stability of H<sub>2</sub> and UF<sub>6</sub> molecules, at least up to 1400°K, the primary stage of reduction of UF<sub>6</sub> is the endothermic reaction of formation of monoradicals of hydrogen and UF<sub>5</sub>, accompanied by exothermic reduction of UF<sub>5</sub> and UF<sub>6</sub> by atomic hydrogen.
4. Above 1400°K an important part is played by dissociation of UF<sub>6</sub> molecules, accompanied by the exothermic reaction of atomic fluorine with hydrogen molecules to form atomic hydrogen.
5. The concentration of UF<sub>4</sub> molecules in the gas phase decreases continuously to the equilibrium concentration owing to formation of nuclei of a condensed phase, which at  $\sigma = 5 \cdot 10^3 \text{ erg} \cdot \text{cm}^{-2}$  include from 4 to 67 UF<sub>4</sub> molecules in the range 400–1200°K. Under these conditions the rate of condensation of UF<sub>4</sub> is  $10^4 \text{ sec}^{-1}$ . Condensation of UF<sub>4</sub> molecules may be accompanied by decomposition of UF<sub>6</sub> molecules, giving two UF<sub>5</sub> molecules.
6. The appearance of condensed tetrafluoride in the system UF<sub>6</sub>-H<sub>2</sub> may accelerate decomposition of UF<sub>6</sub> with formation of UF<sub>5</sub> and "intermediate" uranium fluorides.

7. The experimental activation energy of hydrogen reduction of  $UF_6$ , 8.15 kcal/mole, is not the true activation energy. The activation energy of the limiting stage of reduction of  $UF_6$  is  $\sim 49.67$  kcal/mole. The appearance of condensed uranium pentafluoride, atomic hydrogen, and condensed tetrafluoride reduces the activation energy of reduction of the hexafluoride.

## LITERATURE CITED

1. C. Harrington and A. Ruele, Technology of Uranium Manufacture [Russian translation], Gosatomizdat, Moscow (1961), p. 108.
2. Chemistry and Technology of Uranium Fluorides (N. P. Galkin, editor) [in Russian], Atomizdat, Moscow (1961), p. 226.
3. Ya. M. Sterlin, Metallurgy of Uranium [in Russian], Gosatomizdat, Moscow (1962), p. 402.
4. Technology of Uranium (N. P. Galkin and B. N. Sudarikov, editors) [in Russian], Atomizdat, Moscow (1964), p. 327.
5. N. B. Sudarikov and E. G. Rakov, Processes and Equipment of Uranium Manufacture [in Russian], Mashinostroenie, Moscow (1969), p. 164.
6. J. Dawson, D. Ingram, and L. Bireumshao, J. Chem. Soc., 1421 (1950).
7. J. Katz and E. Rabinovich, Chemistry of Uranium, Vol. 1 [Russian translation], IL, Moscow (1954), p. 355.
8. W. Sham, R. Spenceley, and F. Feetzel, US Patent cl. 23-14.5, N 2, 898, 187 (1959).
9. J. Settle, H. Feder, and W. Hubbard, J. Phys. Chem., 67, 1892 (1963).
10. A. Wolf, J. Posey, and K. Rapp, Inorg. Chem., 4, 751 (1965).
11. Yu. V. Gagarinskii and L. A. Khripin, Uranium Tetrafluoride [in Russian], Atomizdat, Moscow (1966), p. 90.
12. P. A. Akishin and Yu. S. Khodeev, Zh. Fiz. Khim., 35, 1169 (1961).
13. Thermodynamic Properties of Individual Substances ( $\bar{V}$ . P. Glushko, editor) [in Russian], Izd-vo AN SSSR, Moscow (1962).
14. N. P. Galkin, Yu. N. Tumanov, and Yu. P. Butylkin, Thermodynamic Properties of Inorganic Fluorides [in Russian], Atomizdat, Moscow (1972).
15. V. N. Kondrat'ev, Kinetics of Chemical Gaseous Reactions [in Russian], Izd-vo AN SSSR, Moscow (1958).
16. V. N. Kondrat'ev, Velocity Constants of Gas-Phase Reactions [in Russian], Nauka, Moscow (1970).
17. Ya. I. Frenkel', Selected Works, Vol. 3 [in Russian], Izd-vo AN SSSR, Moscow-Leningrad (1959).

## CALCULATION OF REGULAR SYSTEMS OF NEUTRON ABSORBERS

Ya. V. Shevelev and I. L. Chikhladze

UDC 621.039.51

The most frequently used method of calculating systems of absorbers is based on a solution of the criticality equations [1-3]. It is not easy to calculate the effect of absorbers by this method, however, since the neutron distribution must be investigated simultaneously both over the reactor as a whole and close to each individual absorber. The difficulties are increased if several energy groups are taken into account.

We propose a two or three stage procedure for calculating systems of absorbers occupying a small fraction of the reactor volume. First the actual reactor is replaced by an equivalent reactor in which the neutron distribution over the region occupied by the absorbers is a smooth function of coordinates, possibly having discontinuities in magnitude and slope at some boundary. At large distances from this region the neutron distribution coincides with the true distribution. The equivalent reactor is critical when the actual reactor is critical. The criticality condition for the equivalent reactor and the smooth neutron distribution in it are then found. If necessary the true neutron distribution over the region occupied by the absorbers is calculated. The calculation as a whole is greatly simplified, and the last stage is not always necessary.

Statement of the Problem. Let us consider the simplest problem of this class. Suppose a plane strip of material which is a weak neutron absorber contains cylindrical rods which absorb thermal neutrons only (an unessential restriction). The strip is placed in the reactor core or reflector and is periodic in the  $y$  direction (Fig. 1). A cell contains  $n$  rods positioned arbitrarily at the points  $r_i$ , where  $i = 1, 2, \dots, n$ : the rods are numbered in order of increasing  $x_i$ . The coordinates of the remaining rods are given by

$$r_{im} = r_i + ma, \text{ where } m = -\infty, \dots, -1, 0, 1, \dots, \infty. \quad (1)$$

It is assumed that  $\rho_i/L \ll 1$ , where  $\rho_i$  is the radius of a rod and  $L$  is the diffusion length. However this is not a limitation in principle.

The thermal neutron flux  $\Phi(x, y)$  fluctuates in the strip and close to it; i. e., there is a complex microstructure. Since these fluctuations are rapidly damped out with distance from the strip it is appropriate to consider the smoothed out fluxes above and below the strip

$$\Phi_+(x) = \frac{1}{a} \int_0^a \Phi(x, y) dy, \quad x > x_n; \quad (2)$$

$$\Phi_-(x) = \frac{1}{a} \int_0^a \Phi(x, y) dy, \quad x < x_1.$$

The true flux  $\Phi$  outside the absorbers is given by

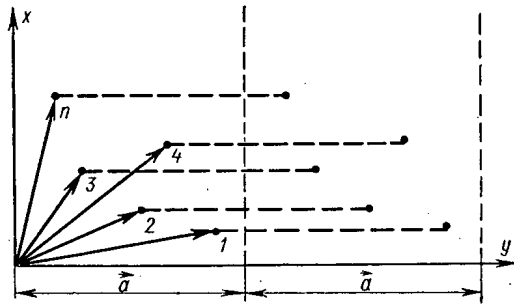
$$-\nabla^2 \Phi + \frac{1}{L^2} \Phi = \frac{q}{L^2 \Sigma}, \quad (3)$$

where  $q$  is the density of thermal neutron sources. We assume the strip is so thin that  $q$  is the same on its lower and upper surfaces. For  $\Phi_{\mp}(x)$  we obtain the equation

$$-\frac{d^2 \Phi_{\mp}}{dx^2} + \frac{\Phi_{\mp}}{L^2} = \frac{q}{D}. \quad (4)$$

Translated from *Atomnaya Energiya*, Vol. 32, No. 1, pp. 27-32, January, 1972. Original article submitted February 16, 1971.

© 1972 Consultants Bureau, a division of Plenum Publishing Corporation, 227 West 17th Street, New York, N. Y. 10011. All rights reserved. This article cannot be reproduced for any purpose whatsoever without permission of the publisher. A copy of this article is available from the publisher for \$15.00.

Fig. 1. Cell with  $n$  rods spaced with pitch  $a$ .

The problem can be solved by assuming that  $q$  varies or that the properties of the media and the source strengths inside the strip and on opposite sides of it are different, but we limit ourselves to the simplest case when

$$D = D_+ = D_-; \quad q = q_- = q_+; \quad L_+ = L_-.$$

At large distances from the strip  $\Phi$  coincides either with  $\Phi_+$  (above) or with  $\Phi_-$  (for  $x < 0$ ). We extrapolate the functions  $\Phi_+$  and  $\Phi_-$  by Eq. (4) inside the strip to some arbitrary boundary separating the regions, e.g., to the line  $x = 0$ . We obtain the values of the functions  $\Phi_{+0}$  and  $\Phi_{-0}$  and their derivatives  $d\Phi_{+0}/dx$  and  $d\Phi_{-0}/dx$  on this boundary;

the values of  $\Phi_{+0}$  and  $\Phi_{-0}$  may differ, and the values of the derivatives will also differ. The specific properties of the strip must appear in a definite relation among the four quantities mentioned and also possibly  $q/\Sigma$  which appears in Eq. (3). Since the equations are linear and Eq. (3) is second order, these relations can be written in the form

$$\begin{aligned} M_+^{(1)}\Phi_{+0} + M_-^{(1)}\Phi_{-0} + N_+^{(1)}a \frac{d\Phi_{+0}}{dx} + N_-^{(1)}a \frac{d\Phi_{-0}}{dx} + K^{(1)} \frac{q}{\Sigma} &= 0; \\ M_+^{(2)}\Phi_{+0} + M_-^{(2)}\Phi_{-0} + N_+^{(2)}a \frac{d\Phi_{+0}}{dx} + N_-^{(2)}a \frac{d\Phi_{-0}}{dx} + K^{(2)} \frac{q}{\Sigma} &= 0. \end{aligned} \quad (5)$$

By using Eqs. (4) and (5) the solution of Eq. (3) in the lower part can be related to the solution above the strip. Thus the dimensionless coefficients  $M_{\pm}^{1,2}$ ,  $N_{\pm}^{1,2}$ , and  $K^{1,2}$  completely determine those properties of the strip which affect the thermal neutron flux far from it. In solving the criticality problem these equations are used instead of the standard joining equations for thermal neutrons. In a similar way equations of the type of (5) are obtained for neutrons undergoing moderation. After the criticality condition has been found it is possible to return to the equations determining the actual rather than the smoothed out fluxes, and to construct them.

We determine the coefficients  $M$ ,  $N$ , and  $K$ .

Solution of the Problem for Constant Neutron Flux at the Surface of the Absorber. The problem is simpler to solve when the absorbers are rather widely separated ( $\rho_i/a \ll 1$ ).

We write the solution of Eq. (3) as the sum of a regular part  $\Phi_{\text{reg}}$  and singular solutions symmetric with respect to each rod

$$\Phi(r) = \Phi_{\text{reg}}(x) + \sum_{i=1}^n C_i \sum_{m=-\infty}^{\infty} K_0 \left( \frac{|r - r_{im}|}{L} \right). \quad (6)$$

The function  $\Phi_{\text{reg}}(x)$  satisfies Eq. (3) over the whole volume. The singular terms satisfy Eq. (3) without the right hand side. Since Eq. (3) does not hold close to the surface of an absorber, effective boundary conditions are set [4]:

$$\left. \frac{\partial \Phi}{\partial \rho_j} \right|_{|r - r_j| = \rho_j} = \frac{\Phi(|r_j + \rho_j|)}{\lambda_t \gamma_j}; \quad \gamma_j = \gamma \left( \frac{\rho_j}{\lambda_t} \right). \quad (7)$$

By substituting (6) into (7) we obtain the equation for the coefficients  $C_i$ :

$$C_j v_j + \sum_{i \neq j} C_i v_{ij} + \Phi_{\text{reg}}(x_j) + \frac{\pi L}{a} \sum_i C_i = 0, \quad (8)$$

where

$$v_{ij} = v \left( \frac{r_i - r_j}{a}; \frac{a}{L} \right) = \left[ \sum_{m=-\infty}^{\infty} K_0 \left( \frac{|r_i - r_j + ma|}{L} \right) \right] - \frac{\pi L}{a}; \quad (9)$$

$$v_j = \gamma_j \frac{\lambda_t}{\rho_j} \frac{\rho_j}{L} K_1 \left( \frac{\rho_j}{L} \right) + v \left( \frac{\rho_j}{a}; \frac{a}{L} \right). \quad (10)$$

The term  $\pi L/a$  in Eqs. (8) and (9) is separated out because, as is shown in the Appendix, if  $a/L \rightarrow 0$  the quantities  $v_{ij}$  remain finite. The coefficients  $v_{ij}$  are calculated in the Appendix. By using (8) the  $C_i$  can be expressed in terms of  $\Phi_{\text{reg}}$  which by Eq. (3) is given by

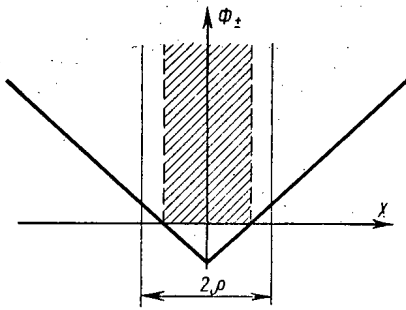


Fig. 2. Smoothed out extrapolated neutron flux for  $v_1 < 0$ ; absorbers are placed in the plane of symmetry. The shaded region is "displaced."

$$\Phi_{\text{reg } 0}(x) = \Phi_{\text{reg } 0} \text{ch} \frac{x}{L} + L \frac{d\Phi_{\text{reg } 0}}{dx} \text{sh} \frac{x}{L} + \frac{q}{\Sigma} \left(1 - \text{ch} \frac{x}{L}\right), \quad (11)$$

where  $\Phi_{\text{reg } 0}$  and  $d\Phi_{\text{reg } 0}/dx$  are the values of this function and its derivative on the arbitrary boundary  $x = 0$ . Thus the values of the  $C_i$  are expressed linearly in terms of  $q/\Sigma$  and the two so far undetermined constants  $\Phi_{\text{reg } 0}$  and  $d\Phi_{\text{reg } 0}/dx$ .

Let us calculate the functions  $\Phi_{\pm}(x)$ . We first average the sum in (6)

$$\int_0^1 \sum_{m=-\infty}^{\infty} K_0 \left( \frac{|r - r_{im} - a\xi|}{L} \right) d\xi = \sum_{m=-\infty}^{\infty} \int_0^1 K_0 \left( \frac{|x + y - r_i - (m + \xi)a|}{L} \right) d\xi.$$

After the change of variable  $m + \xi = t$  we obtain

$$\sum_{m=-\infty}^{\infty} \int_m^{m+1} K_0 \left( \frac{|x + y - r_i - at|}{L} \right) dt = \int_{-\infty}^{\infty} K_0 \left( \sqrt{\frac{(x-x_i)^2}{L^2} + \frac{(y-y_i-at)^2}{L^2}} \right) dt.$$

It is known [5], that

$$\int_{-\infty}^{\infty} K_0 \left( \sqrt{p^2 + q^2} \right) dq = \pi e^{-|p|} \quad (12)$$

and therefore

$$\int_0^1 \sum_{m=-\infty}^{\infty} K_0 \left( \frac{|r - r_i - ma - a\xi|}{L} \right) d\xi = \frac{\pi L}{a} e^{-|x-x_i|/L}. \quad (13)$$

Thus according to (3) and (13)

$$\Phi_{\mp} = \Phi_{\text{reg}} + \delta\Phi_{\mp}, \quad (14)$$

where

$$\delta\Phi_{+} = \sum_i C_i \frac{\pi L}{a} e^{-\frac{x-x_i}{L}}; \quad \delta\Phi_{-} = \sum_i C_i \frac{\pi L}{a} e^{\frac{x_i-x}{L}}. \quad (15)$$

Each of the functions  $\delta\Phi_{\mp}$  satisfies Eq. (14) without the right hand side and  $\Phi_{\text{reg}}$  satisfies it with the right hand side. Therefore the extrapolations of the functions  $\Phi_{\mp}$  are obvious.

$$\begin{aligned} \Phi_{-0} &= \Phi_{\text{reg } 0} + \frac{\pi L}{a} \sum_i C_i e^{x_i/L}; & \frac{d\Phi_{+0}}{dx} &= \frac{d\Phi_{\text{reg } 0}}{dx} - \frac{\pi}{a} \sum_i C_i e^{x_i/L}; \\ \Phi_{-0} &= \Phi_{\text{reg } 0} + \frac{\pi L}{a} \sum_i C_i e^{-x_i/L}; & \frac{d\Phi_{-0}}{dx} &= \frac{d\Phi_{\text{reg } 0}}{dx} + \frac{\pi}{a} \sum_i C_i e^{-x_i/L}. \end{aligned} \quad (16)$$

We rewrite Eq. (8) by using (11):

$$C_j v_j + \sum_{i \neq j} C_i v_{ij} + \frac{\pi L}{a} \sum_i C_i + \Phi_{\text{reg } 0} \text{ch} \frac{x_j}{L} + L \frac{d\Phi_{\text{reg } 0}}{dx} \text{sh} \frac{x_j}{L} + \frac{q}{\Sigma} \left(1 - \text{ch} \frac{x_j}{L}\right) = 0. \quad (17)$$

The unknowns  $C_i$ ,  $\Phi_{\text{reg } 0}$ , and  $d\Phi_{\text{reg } 0}/dx$  can be eliminated from (16) and (17) to yield two equations in  $\Phi_{\mp 0}$ ,  $d\Phi_{\mp 0}/dx$ , and  $q/\Sigma$  since the number of equations in these systems is  $n + 4$  and the number of unknowns eliminated is  $n + 2$ . Therefore Eqs. (16) and (17) lead to relations of the type of (5), i. e., to explicit expressions for the required coefficients.



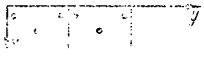
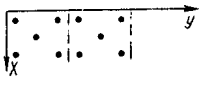
**Specific Types of Lattices and Analysis of Results.** Arbitrary regular lattices can be analyzed by using Eqs. (16) and (17) and formulas (A.6), (A.7), and (A.10). In the simplest case when  $n = 1$  it is convenient to set the arbitrary boundary along the line of centers of the absorbers. Then according to (16)

$$\left. \begin{aligned} \Phi_{+0} &= \Phi_{-0} = \Phi_{\text{reg } 0} + \frac{\pi L}{a} C_1; \\ -\frac{d\Phi_{+0}}{dx} - \frac{d\Phi_{\text{reg } 0}}{dx} &= \frac{d\Phi_{\text{reg } 0}}{dx} - \frac{d\Phi_{+0}}{dx} = -C_1 \end{aligned} \right\} \quad (18)$$

and from (17)

$$C_1 \left( v_1 + \frac{\pi L}{a} \right) + \Phi_{\text{reg } 0} = 0. \quad (19)$$

TABLE 1. Types of Absorber Lattices Considered and Results of Two-Group Calculations of Reflector Savings. The Core and Reflector Parameters Correspond to the IGR Reactor [6]

Lattice structure	$\frac{d}{a}=0,1$	$\frac{d}{a}=0,14$	$\frac{d}{a}=0,2$	$\gamma^*$
	23,4 27,0 29,0	20,3 21,9 23,7	17,1 17,7 18,9	$\gamma_1$ $\gamma_2$ $\gamma_3$
	17,9 20,5 22,5	15,7 16,8 18,0	13,8 14,2 14,9	$\gamma_1$ $\gamma_2$ $\gamma_3$
	15,0 17,1 18,7	13,3 14,1 15,0	11,9 12,2 13,9	$\gamma_1$ $\gamma_2$ $\gamma_3$
	13,5 14,9 16,1	12,4 13,0 13,6 †	11,4 11,6 12,6	$\gamma_1$ $\gamma_2$ $\gamma_3$

\*  $\gamma_2 = 1.3$ ;  $\gamma_3 = 1.616$  corresponds to IGR rods. In all three cases  $a = 14$  mm.

† Data for lattice used in IGR

By eliminating the unknowns  $C_i$ ,  $\Phi_{\text{reg}0}$ , and  $d\Phi_{\text{reg}0}/dx$  from (18) and (19) we obtain the two equations

$$\left. \begin{aligned} \Phi_{+0} &= \Phi_{-0}; \\ a \frac{d\Phi_{+0}}{dx} &= a \frac{d\Phi_{-0}}{dx} + \frac{2\pi}{v_1} \Phi_{+0}. \end{aligned} \right\} \quad (20)$$

By comparing (20) and (5) we find

$$\begin{aligned} M_{+}^{(1)} &= M_{-}^{(1)}; \quad N_{+}^{(1)} = N_{-}^{(1)} = K^{(1)} = 0; \\ N_{-}^{(2)} &= -N_{+}^{(2)}; \quad M_{+}^{(2)} = -\frac{\pi}{v_1} N_{+}^{(2)}; \\ M_{-}^{(2)} &= -\frac{\pi}{v_1} N_{+}^{(2)}; \quad K^{(2)} = 0. \end{aligned}$$

Equations (20) are similar to the boundary conditions which describe absorption in a thin foil [4]. Thus an array of cylinders can be regarded as equivalent to an absorbing layer for which the product of the thickness  $\Delta$  and the macroscopic absorption cross section  $\Sigma_c$  is

$$(\Delta \Sigma_c)_{\text{equ}} = \frac{2\pi \lambda_t}{3v_1 a} \approx \frac{2\pi}{3} \frac{\frac{\rho}{a}}{\gamma + \frac{\rho}{\lambda_t} \ln \frac{a}{2\pi\rho}}; \quad \frac{\rho}{\lambda} \ll 1. \quad (21)$$

However the analogy with a thin absorber does not completely represent the situation. The quantity  $v_1$  can be negative for  $a/(2\rho) < \pi$  as is confirmed by more accurate calculations. If a zero value of  $v_1$  in Eq. (20) can be interpreted as the blackness of the equivalent absorbing layer becoming infinite\* then a negative value of  $v_1$  can only be interpreted as the result of the displacement of the medium by absorbers of finite thickness (Fig. 2). It is clear that the width of the displacement region must not exceed the diameter of the cylinders. Fortunately this physical requirement is satisfied even in the crude approximation considered.

By using Eqs. (16) and (17) in the two-group approximation and taking the usual continuity conditions at boundaries for neutrons undergoing moderation, reflector savings were calculated for various lattices of absorbers placed close to the core in the reflector of the IGR reactor [6]. The results of the calculations are shown in Table 1 and in the corresponding graphs of Figs. 3 and 4. These calculations permitted the selection of a five-rod absorber lattice for the lower reflector of the IGR reactor. The calculated results are in satisfactory agreement with experiment.

\*Actually it is well known that the flux  $\Phi$  is not zero even on the boundary of an absolutely black absorber.

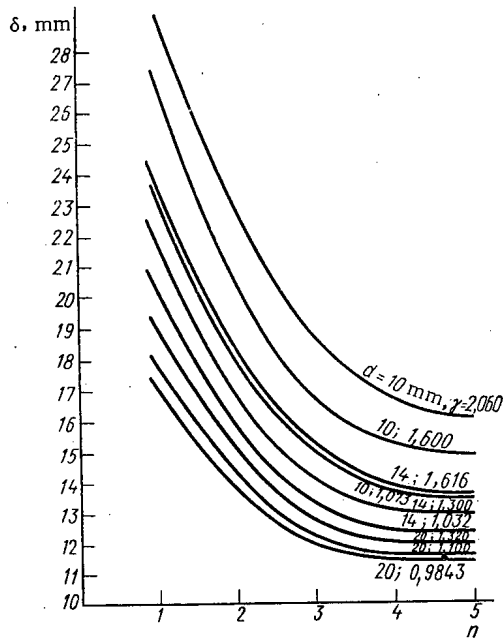


Fig. 3

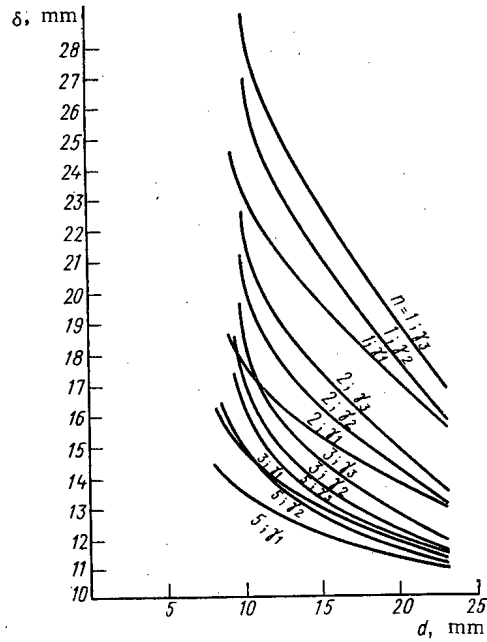


Fig. 4

Fig. 3. Reflector savings  $\delta$  as a function of the number of absorbing rods  $n$  in a cell for rods of various diameters and various values of  $\gamma$ .

Fig. 4. Reflector savings  $\delta$  as a function of the diameter of an absorbing rod  $d$  for various numbers of absorbing rods  $n$  in a cell and various values of  $\gamma$ . Values of  $\gamma_{1,2,3}$  are listed in Table 1.

APPENDIX

Calculation of coefficients  $v_{ij}$ ,  $v_j$ , and  $v$ . According to (9)

$$v_{ij} = v \left( \frac{r_i - r_j}{a}; \frac{a}{L} \right); \quad v = \left( \frac{x+y}{a}; \frac{a}{L} \right) = \left[ \sum_{m=-\infty}^{\infty} K_0 \left( \frac{\sqrt{x^2 + (y+ma)^2}}{L} \right) \right] - \frac{\pi L}{a} \tag{A.1}$$

Following [4] the Poisson summation formula is used:

$$\sum_{m=-\infty}^{\infty} \varphi(2\pi m) = \frac{1}{2\pi} \sum_{v=-\infty}^{\infty} \int_{-\infty}^{\infty} \varphi(K) e^{-ivk} dK. \tag{A.2}$$

Using (A.2) and (A.1) we obtain

$$\frac{\pi L}{a} + v \left( \frac{x+y}{a}; \frac{a}{L} \right) = \frac{1}{2\pi} \sum_{v=-\infty}^{\infty} \int_{-\infty}^{\infty} e^{-ivk} K_0 \left( \frac{\sqrt{x^2 + \left(y + \frac{ak}{2\pi}\right)^2}}{L} \right) dk.$$

Making the change of variable  $t = (y + ak/2\pi)/L$  and using the formula [5]

$$K_0 \left( \sqrt{p^2 + t^2} \right) = \int_0^{\infty} e^{-u} \frac{p^2 + t^2}{4u} \frac{du}{2u}, \tag{A.3}$$

we obtain

$$\frac{\pi L}{a} + v = \frac{L}{a} \sum_{v=-\infty}^{\infty} e^{iv2\pi \frac{y}{a}} \int_0^{\infty} e^{-u} \frac{x^2}{4L^2 u} \frac{du}{u} \int_{-\infty}^{\infty} e^{-i2\pi v \frac{L}{a} t - \frac{t^2}{4u}} dt, \tag{A.4}$$

where

$$\int_{-\infty}^{\infty} e^{-i2\pi v \frac{L}{a} t - \frac{t^2}{4u}} dt = 2 \sqrt{u} \int_{-\infty}^{\infty} e^{-s^2 - i2\pi v \frac{L}{a} 2 \sqrt{u} s} ds = 2 \sqrt{\pi u} e^{-4\pi^2 v^2 \frac{L^2}{a^2} u}.$$

Thus

$$\frac{\pi L}{a} + \nu = \frac{L}{a} \sum_{\nu=-\infty}^{\infty} e^{i\nu 2\pi \frac{y}{a}} \int_0^{\infty} \sqrt{\frac{\pi}{a}} e^{-u \left( \nu + 4\pi^2 \nu^2 \frac{L^2}{a^2} \right) - \frac{x^2}{4L^2 u^2}} du$$

or

$$\frac{\pi L}{a} + \nu = \frac{L}{a} \sum_{\nu=-\infty}^{\infty} \frac{e^{i\nu 2\pi \frac{y}{a}}}{\sqrt{1 + 4\pi^2 \nu^2 \frac{L^2}{a^2}}} 2\sqrt{\frac{\pi}{a}} \int_0^{\infty} e^{-t^2 - \frac{(1 + 4\pi^2 \nu^2 \frac{L^2}{a^2}) \frac{x^2}{L^2}}{4t^2}} dt$$

and further

$$\frac{\pi L}{a} + \nu = \frac{\pi L}{a} \sum_{\nu=-\infty}^{\infty} \frac{e^{i2\pi \nu \frac{y}{a}}}{\sqrt{1 + (2\pi \nu \frac{L}{a})^2}} e^{-\frac{|x|}{L} \sqrt{1 + (2\pi \nu \frac{L}{a})^2}} \quad (\text{A.5})$$

Separating out the term with  $\nu = 0$  we obtain

$$\nu \left( \frac{x+y}{a}; \frac{a}{L} \right) = \frac{\pi L}{a} (e^{-\frac{|x|}{L}} - 1) + \text{Re} \sum_{\nu=1}^{\infty} \frac{e^{i\nu 2\pi \frac{y}{a}}}{\sqrt{1 + (2\pi \nu \frac{L}{a})^2}} \frac{1}{\nu} e^{-\frac{2\pi \nu |x|}{a} \sqrt{1 + (2\pi \nu \frac{L}{a})^2}} \quad (\text{A.6})$$

Equation (A.6) is the working formula and has the obvious limit as  $a/L \rightarrow 0$ :

$$\begin{aligned} \nu \left( \frac{x+y}{a}; \frac{a}{L} \right) &= -\frac{\pi |x|}{a} + \text{Re} \sum_{\nu=1}^{\infty} \frac{1}{\nu} e^{-2\pi \nu \frac{|x|-iy}{a}} = -\frac{\pi |x|}{a} - \frac{1}{2} \ln \left[ 1 - e^{-2\pi \frac{|x|}{a}} \cos 2\pi \frac{y}{a} \right]^2 \\ &+ (e^{-2\pi \frac{|x|}{a}} \text{sh } 2\pi \frac{y}{a})^2 = -\frac{1}{2} \ln \left[ 2 \left( \text{ch } \frac{2\pi x}{a} - \cos \frac{2\pi y}{a} \right) \right]. \end{aligned} \quad (\text{A.7})$$

As  $\nu$  increases the terms of series (A.6) converge rapidly to the corresponding terms of the series (A.7). In view of this the obvious relation

$$\nu_{L \neq \infty} \approx \nu_{L=\infty} + (S_{\nu} - S_{\nu}|_{L=\infty}), \quad (\text{A.8})$$

can be used where the  $S_{\nu}$  are the partial sums of the corresponding series. In particular it follows from (A.7) that if  $\sqrt{x^2 + y^2} = \rho$ , then for  $\rho \ll a$

$$\nu \left( \frac{\rho}{a} \right) = \ln \frac{a}{2\pi\rho} \quad (\text{A.9})$$

and therefore from (10)

$$\nu_j = \gamma_j \frac{\lambda_j}{\rho_j} + \ln \frac{a}{2\pi\rho_j} \quad (\text{A.10})$$

#### LITERATURE CITED

1. G. V. Sinyutyun and V. G. Semenov, Second Geneva Conference [in Russian], Vol. II, Atomizdat, Moscow (1958).
2. V. I. Nosov, Atomnaya Énergiya, 9, 262 (1960); 10, 269 (1961); 21, 410 (1966); 23, 25 (1967).
3. I. Chermak, Calculation of the Effectiveness of Partially Inserted Rods [in Russian], 1616, Prague (1966).
4. A. D. Galanin, Theory of Thermal Neutron Reactors [in Russian], Atomizdat, Moscow (1959).
5. I. S. Gradshtein and I. M. Ryzhik, Tables of Integrals, Sums, Series, and Products [in Russian], Fizmatgiz, Moscow (1962).
6. I. V. Kurchatov et al., Paper No. 322a [in Russian], Third Geneva Conference (1964).



THERMALIZATION OF NEUTRONS IN H<sub>2</sub>O AT 318 AND 77° K

S. N. Ishmaev, I. P. Sadikov,  
and A. A. Chernyshov

UDC 539.125.523.5

An analysis of the time evolution of the neutron spectrum in a moderator after the arrival of a pulse from the source constitutes one of the most effective methods of studying the thermalization of neutrons. Experiments of this kind provide excellent information as to the effect of the chemical bond and the thermal motion of the atoms in the moderator on the rate of establishment of equilibrium between the neutrons and the medium, and may serve as a reliable base for the verification of the methods commonly employed in calculating neutron spectra and extracting data relating to the scattering laws of the moderator. In addition to this, such investigations are essential in order to find ways of creating efficient pulsed sources of thermal and cold neutrons in accelerators and pulse reactors. So far, measurements and calculations have only been carried out for the nonstationary neutron spectra of beryllium [1, 2], graphite [1, 3, 4], heavy water [5, 6], zirconium hydride [7, 8], and ice at a low temperature [8]. Compared with the other moderators, light water is a difficult subject for experimental study, since the thermalization of the neutrons takes place very rapidly, thus making extreme demands on the time resolution of the system. Although the author's first measurements of nonstationary neutron spectra in water [7, 9] were carried out with a fairly high resolution (3.5  $\mu$ sec), the results disagreed seriously with theory [10, 11]. The reasons for this disagreement lay in the perturbations arising in the experimental work as a result of the introduction of a channel for extracting the neutron beam from the water moderator [12].

In this paper we shall describe the results of subsequent experiments relating to the time thermalization of neutrons in water at 318 and in ice at 77° K.

Conditions of the Experiments. As a pulsed source of fast neutrons with a short (0.6  $\mu$ sec) rise time we used the linear electron accelerator of the I. V. Kurchatov Institute of Atomic Energy. Near the lead target of the accelerator we placed a cryostat containing a flat aluminum vessel (8  $\times$  25  $\times$  29 cm in size) holding the moderator (water or ice). The ice was cooled to 77° K with liquid nitrogen. The neutron beam was extracted from the surface of the moderator. In contrast to the earlier measurements of nonstationary neutron spectra, which used a mechanical interrupter [1, 9], in this case we used a new experimental method constituting a combination of a crystal spectrometer with the time-of-flight method. Using time-of-flight discrimination ( $L \approx 6$  m) in a multichannel analyzer, we directly and simultaneously measured the time dependence of the flux of monochromatic neutrons  $\Phi_E(t)$  for seven fixed energies corresponding to different orders of neutron reflections from an iron single crystal ( $d_{110} = 2.023$  Å). The time resolution  $\Delta t$  depended on the energy; in the range 0.005–0.250 eV it varied from 6.3 to 1.5  $\mu$ sec. In order to obtain a resolution of this kind, we had to secure a highly-monochromatic beam ( $\Delta E/E \approx 2 \cdot 10^{-3}$ ); this we achieved by reflecting the neutrons from the crystal in almost exactly the backward direction ( $\theta_{\text{Bragg}} = 83^\circ 52'$ ,  $\Delta\theta \leq 20'$ ). The measuring method and the method of data analysis were described in full detail earlier [12].

Results. The time dependence of the neutron flux in H<sub>2</sub>O measured for various energies is shown in Fig. 1. The results obtained for water and ice are referred to the same intensity of the fast neutron source, allowance being made for the efficiency of the detector and the reflecting power of the crystal.

For the case of short periods ( $t < 1.0$   $\mu$ sec), when the average energy of the neutron spectrum is large compared with  $kT$ , the difference in chemical bond between the liquid and solid states of H<sub>2</sub>O has hardly any effect on the initial stage in the thermalization of the neutrons. The difference which appears later between

---

Translated from *Atomnaya Énergiya*, Vol. 32, No. 1, pp. 33–38, January, 1972. Original article submitted December 7, 1970.

© 1972 Consultants Bureau, a division of Plenum Publishing Corporation, 227 West 17th Street, New York, N. Y. 10011. All rights reserved. This article cannot be reproduced for any purpose whatsoever without permission of the publisher. A copy of this article is available from the publisher for \$15.00.

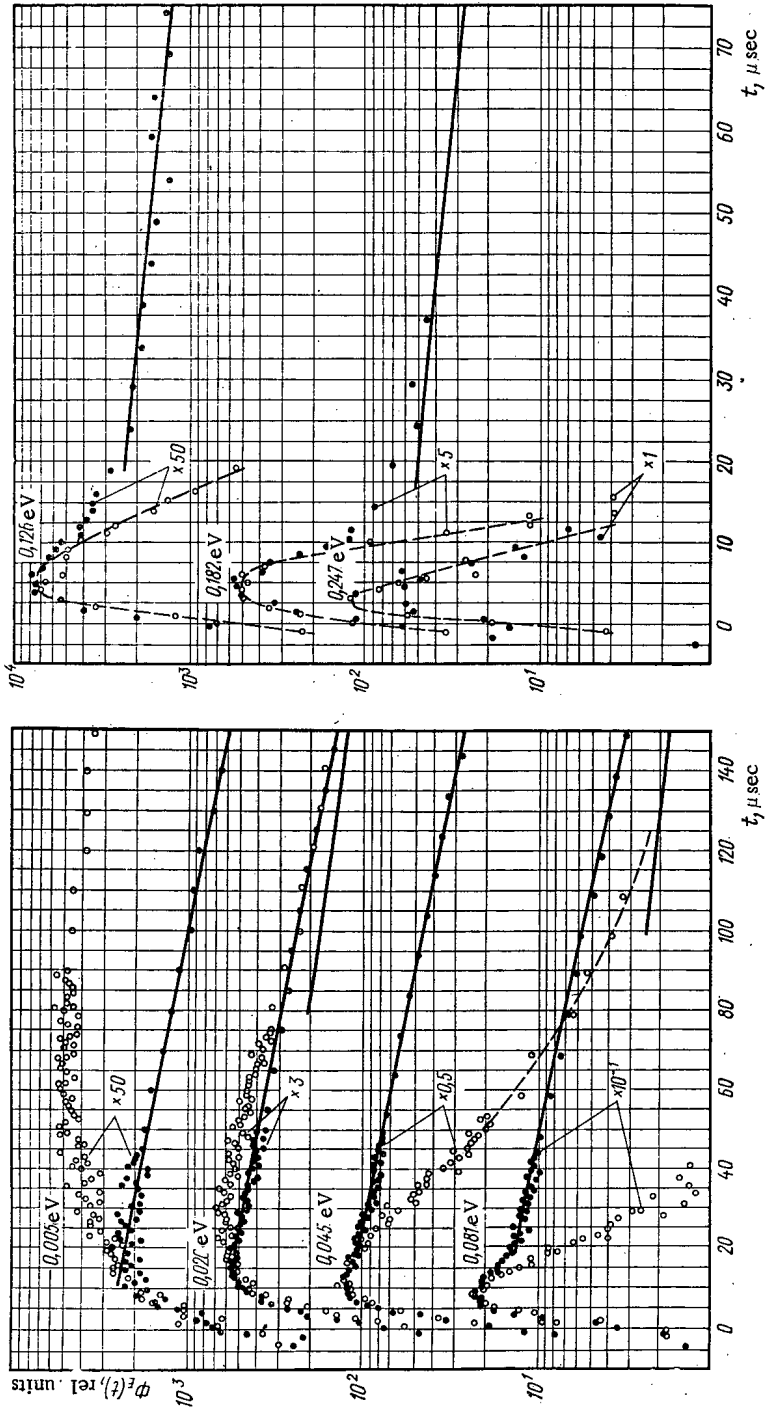


Fig. 1. Neutron fluxes of different energies in relation to time in water (● - 318°K) and ice (○ - 77°K).

TABLE 1. Neutron Thermalization Time for Water and Ice

$T, ^\circ\text{K}$	Water 318°K Geometrical parameter $B^2=0,161 \text{ cm}^{-2}$ )					Ice, 77°K	
	$E, \text{eV}$	0,005	0,020	0,045	0,081	0,126	0,005
$A_0(E), \text{rel units}$	$56,0 \pm 5,3$	$200 \pm 8$	$261 \pm 5$	$166 \pm 6$	$58,5 \pm 5,5$	$194 \pm 43$	$123 \pm 39$
$\alpha_0, \text{sec}^{-1}$	$10\,646 \pm 671$	$10\,589 \pm 275$	$10\,938 \pm 227$	$11\,248 \pm 390$	$11\,279 \pm 991$	$6\,287 \pm 1468$	$6\,570 \pm 1234$
	$10\,870 \pm 119$ ( $10\,650 \pm 32$ [13]) *					$6\,453 \pm 139$ ( $6219 \pm 418$ [14]) *	
$A_1(E)/A_0(E)$	-1,30	-1,58	—	+3,99	+5,45	-1,01	+2,30
$\tau_{th}, \mu\text{sec}$	$6,48 \pm 2,64$	$5,99 \pm 0,56$	—	$5,46 \pm 0,56$	$6,11 \pm 0,83$	$53,8 \pm 1,6$	$56,8 \pm 1,4$
	$5,8 \pm 0,6$					$55,5 \pm 1,5$	

\* Calculation:  $\alpha_0 = \langle \Sigma_a v \rangle_\infty + \langle Dv \rangle_\infty B^2 - C \cdot B^4$ .

the behavior of the neutron flux in water and ice respectively is mainly due to the sharp reduction in the temperature of the medium and the corresponding change in the proportion of neutrons of a specified energy in the asymptotic equilibrium spectrum. The asymptotic behavior of the  $\Phi_E(t)$  relationship is indicated in Fig. 1 by the continuous lines, which are obtained by analyzing the experimental results over long periods by the method of least squares. Close to equilibrium, the neutron flux may be expressed in the form of a superposition of the fundamental and first energy harmonic only:

$$\Phi_E(t) = A_0(E) e^{-\alpha_0 t} + A_1(E) e^{-\alpha_1 t} + \dots, \quad (1)$$

where  $A_0(E)$  and  $A_1(E)$  are the eigenfunctions of the scattering operator in the nonstationary kinetic Boltzmann equation describing the thermalization of the neutrons, while  $\alpha_0$  and  $\alpha_1$  are the corresponding eigenvalues. Equation (1) is only valid if  $\alpha_0$  and  $\alpha_1$  lie in the discrete part of the spectrum of eigenvalues, while the contribution of the higher energy harmonics may be neglected. The values of the amplitude  $A_0(E)$  and the decay constant  $\alpha_0$  of the fundamental harmonic are shown in Table 1. We see that the values of  $\alpha_0$  determined for various energies coincide, within the limits of experimental error. This means that an equilibrium neutron spectrum has been established in the system in question. The temperature of the medium has a considerable effect on the time required to establish equilibrium, and also on the lifetime of the thermal neutrons. Whereas in water the same exponential fall in neutron flux appears for all energies after approximately 30  $\mu\text{sec}$  in the case of ice at 77°K thermalization requires at least 200  $\mu\text{sec}$ . The lifetime of the neutrons  $1/\alpha_0$  in a particular block of ice is 1.7 times longer than in the corresponding water. The weighted mean values of  $\alpha_0$  are close to those calculated on the basis of the diffusion parameters of water and ice measured by the pulse method [13, 14].

By analyzing the  $\Phi_E(t)$  relationships measured for seven energy values, we may reconstruct the approximate form of the energy spectrum of the neutrons in water at various instants of time. In Fig. 2 these spectra are compared with the results of a numerical solution of the kinetic equation in the diffusion approximation based on the Nelkin model for water [11]. The results agree quite reasonably with one another. A certain difference which appears at  $t = 4 \mu\text{sec}$  may be due to a distortion of the experimental curve arising from inadequate resolution, and also to differences in the spatial distribution of the source considered in the calculations and experiments respectively.

The results of these experiments enable us to analyze the question as to the existence of such a parameter as the "thermalization time" for  $\text{H}_2\text{O}$ . By using Eq. (1), in fact, we obtain

$$\left| \frac{\Phi_E(t) e^{-\alpha_0 t}}{A_0(E)} - 1 \right| = \left| \frac{A_1(E)}{A_0(E)} \right| e^{-(\alpha_1 - \alpha_0)t}, \quad (2)$$

from which we may find the thermalization time  $\tau_{th} = 1/(\alpha_1 - \alpha_0)$ , which characterizes the rate at which the neutrons approach thermal equilibrium with the medium. Figure 3 illustrates the relation of Eq. (2)

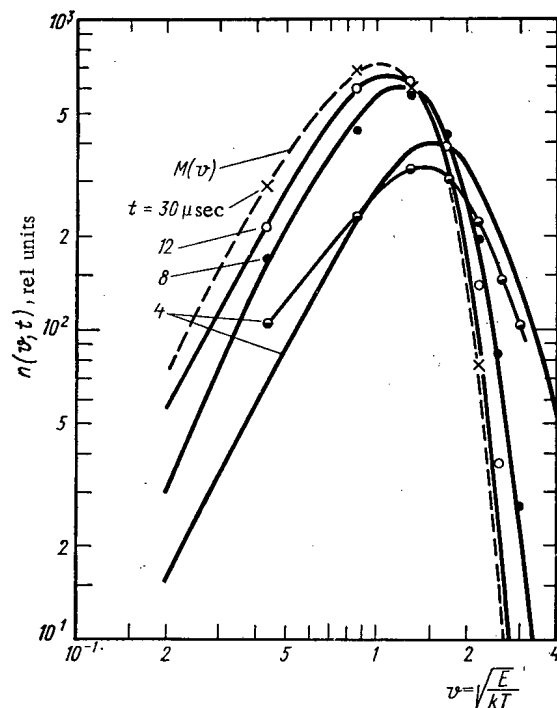


Fig. 2. Nonstationary neutron spectra in water: —) calculation based on the Nelkin model for an infinite medium with uniformly-distributed sources [11]; the points correspond to the sections  $t = \text{const}$  of the experimental  $\Phi_E(t)e^{\alpha_0 t/\lambda_{tr}(E)}$ ;  $M(v)$  is the Maxwell spectrum.

for water and ice on a semilogarithmic scale. The errors these indicated are simply those associated with the statistical accuracy of the measurements, not with any errors committed in the determination of  $\alpha_0$  and  $A_0(E)$ ; the finite time resolution is also not taken into account. Since the eigenfunction  $A_1(E)$  is a sign-varying quantity, the eigenvalue  $\alpha_1$  can only be reliably determined for those energies at which  $A_1(E)$  differs substantially from zero.

In water, after about  $10 \mu\text{sec}$  the form of relation (2) is almost exactly the same (expressed as a function of time) for all neutron energies. The results obtained on analyzing these data by the method of least squares are presented in Table 1. Since the values of  $\tau_{th}$  determined for various energy groups agree within the limits of experimental error, we may conclude that a discrete eigenvalue  $\alpha_1$  really exists for water, and that the parameter  $\tau_{th}$  has a physical meaning. The weighted-mean thermalization time based on data relating to various energies is shown in Table 1.

The thermalization constant was also determined in [15], in which the time dependence of the rate of neutron absorption in a large water system was analyzed after introducing resonance absorbers (cadmium and gadolinium) into it. Here a slightly lower value was obtained:  $\tau_{th} = 4.1 \pm 0.4 \mu\text{sec}$ . The authors of [16] gave a numerical solution for the nonstationary diffusion equation, using the Nelkin model for  $\text{H}_2\text{O}$ , and obtained the spectrum of eigenvalues as a function of  $B^2$ . These results indicated that for  $B^2 = 0.161 \text{ cm}^{-2}$   $\tau_{th} = 5.53 \mu\text{sec}$ , in good agreement with our own experimental thermalization time. The value of  $\tau_{th}$  for ice can only be determined from the measurements at the two lowest energies. The relationship of Eq. (2) was analyzed for  $t > 30 \mu\text{sec}$ . We see from Table 1 that the values of  $\tau_{th}$  obtained for these energies are quite close together. The weighted-mean thermalization time for the neutrons in ice at  $77^\circ\text{K}$  is much smaller than the time found in [8] from the time dependence of the average energy of the neutron spectrum ( $77 \pm 7 \mu\text{sec}$ ) and from the transmission of neutrons through an indium absorber ( $67 \pm 10 \mu\text{sec}$ ). It should be remembered that the results of these measurements [8] may have erred as a consequence of perturbations arising from the experimental channel introduced in order to extract the neutron beam.

The rate of establishment of the equilibrium neutron spectrum in ice cooled to  $77^\circ\text{K}$  is approximately a factor of ten lower than that obtained for water. It is an interesting fact that the value obtained in [17] for ice at  $268^\circ\text{K}$  is  $\tau_{th} = 4.8 \pm 0.5 \mu\text{sec}$ , almost the same as the thermalization time in water. This indicated that the differences in the scattering powers due to the liquid and solid states of  $\text{H}_2\text{O}$  are not very great, the principal cause of the reduction in the rate of establishment of the equilibrium neutron spectrum being the severe reduction in the temperature of the medium.

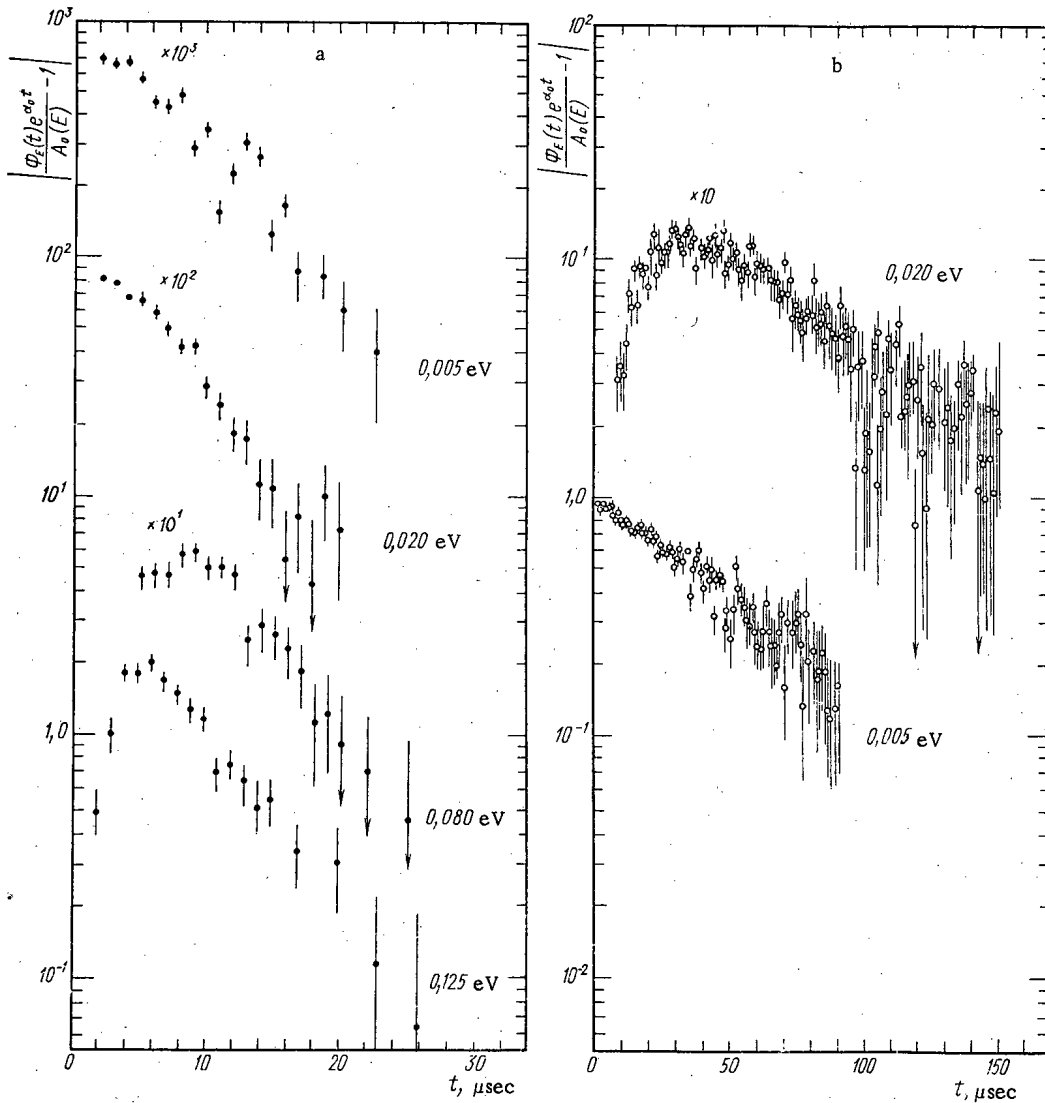


Fig. 3. Time fall-off of the first energy harmonic for water and ice: a) 318°K; b) 77°K.

In conclusion, we should note one further fact, which is of particular importance in creating an efficient pulsed source of slow neutrons. We see from Fig. 1 that, when the neutron energy  $E \gg kT$ , the flux of monochromatic neutrons has a sharp maximum, and its extent is determined by the time of retardation to the specified energy. For neutrons with  $E \lesssim kT$ , the thermal motion constitutes the factor preventing the achievement of the maximum possible flux value, since a considerable proportion of the neutrons are scattered into a higher energy range, with the acquisition of energy. Furthermore, the length of the pulse is very considerable in this case, being mainly determined by the lifetime of the neutrons in the equilibrium spectrum. The intensive cooling of the moderator to a temperature at which the condition  $kT \ll E$  is satisfied will clearly reduce the contribution of the diffusion component and constitute an effective means of obtaining strong fluxes of slow neutrons with a short pulse length.

The authors are grateful to V. I. Mostovoi and L. V. Mairov for valuable discussions regarding the method and the results of the measurements.

#### LITERATURE CITED

1. V. I. Mostovoi et al., "Pulsed neutron research," Proc. Symp., Karlsruhe, Vol. 1, IAEA, Vienna (1965), p. 623.
2. E. Gaertner et al., PNR, 1, 483 (1965).

3. E. Barnard et al., Nucl. Sci. and Engng., 17, 513 (1963).
4. K. Nicholson and M. Poole, AERE-R, 4842 (1965).
5. M. Poole and P. Wydler, PNR, 1, 535 (1965).
6. R. Kryter et al., PNR, 1, 465 (1965).
7. S. N. Ishmaev et al., PNR, 1, 643 (1965).
8. J. Kallfelz and W. Reichardt, PNR, 1, 545 (1965).
9. S. N. Ishmaev et al., "Neutron thermalization and reactor spectra," Proc. Symp., Ann Arbor, Vol. 2, IAEA, Vienna (1968), p. 439.
10. L. V. Maiorov, V. F. Turchin, and M. S. Yudkevich, Paper No. R/360 presented by the USSR to the Third International Conference on the Peaceful Use of Atomic Energy [in Russian], Geneva (1964).
11. A. Ghatak and T. Krieger, Nucl. Sci. and Engng., 21, 304 (1965).
12. S. N. Ishmaev, I. P. Sadikov, and A. A. Chernyshov, Preprint IAE-1954 [in Russian] (1970).
13. E. Arai and M. Kuchle, Nukleonik, 7, 416 (1965).
14. A. V. Antonov et al., "Inelastic scattering of neutrons in solids and liquids," Proc. Symp., IAEA, Vienna (1961), p. 377.
15. E. Möller and N. Sjöstrand, Arkiv Fys., 27, 150 (1965).
16. A. Ghatak and H. Honeck, Nucl. Sci. and Engng., 21, 227 (1965).
17. E. Möller, "Pulsed neutron research," Proc. Symp., Karlsruhe, Vol. 1, IAEA, Vienna (1965), p. 155.

DETERMINATION OF LITHIUM IN SOLID MATERIALS FROM  
THE REACTION  $\text{Li}^6(n, \alpha)\text{H}^3$

B. P. Zverev, Yu. F. Simakhin,  
and A. G. Dutov

UDC 543.53

Many papers have been written on the determination of lithium in various materials by the neutron-activation method. Some of these have employed the  $\text{Li}^6(n, \alpha)\text{H}^3$  reaction with thermal neutrons. In one case [1] the  $\beta$  particles of radioactive tritium were recorded in order to determine lithium. The energy of the  $\beta$  particles was 18.6 keV, and there were accordingly great difficulties in using the detector. In another case [2] a secondary reaction was used, the delayed neutrons of the  $\text{N}^{17}$  isotope being recorded. In another case [3] the secondary reaction  $\text{O}^{16}(t, n)\text{F}^{18}$  was employed, the lithium content being determined from the  $\text{F}^{18}$  activity. In certain experiments the charged particles formed in the  $\text{Li}^6(n, \alpha)\text{H}^3$  reaction were directly recorded. In determining the isotopic composition of lithium in [4] by irradiation with a Po-Be neutron source, the particles were recorded with a ZnS scintillator.

In the  $\text{Li}^7$  isotope the  $\text{Li}^7(n, \gamma)\text{Li}^8$  reaction takes place with a cross section of 36 mb, forming the  $\text{Li}^8$  isotope with a half life of 0.85 sec. In this case  $\beta$  particles with  $E_\beta = 13$  MeV may be recorded with a Cerenkov counter [5]. Such methods either have a low sensitivity, or require the destruction of the sample, or alternatively the use of standard specimens made of the same material as that being studied, although this is not always possible. In this paper we shall set out a method of determining the lithium content of solids without destroying the sample, using standard specimens of any convenient material.

Method. The reaction  $\text{Li}^6(n, \alpha)\text{H}^3$ , involving thermal neutrons and having a cross section of 945 b, is exothermic. The energy evolved ( $Q = 4.78$  MeV) is divided between the  $\alpha$  particle and the tritium nucleus in inverse proportion to their masses ( $E_\alpha = 2.05$  MeV,  $E_t = 2.73$  MeV). The tritium nuclei and the  $\alpha$  particles have specific ranges; only particles formed in a thin surface layer will escape in the direction of the detector (the range of the  $\alpha$  particles is a few microns, that of the tritons a few tens of microns). Owing to the absorption of energy from the particles as these move in the sample material, the energy spectrum of the escaping particles will be continuous. Since the range of the  $\alpha$  particles with  $E_\alpha = 2.05$  MeV is an order of magnitude smaller than that of the tritons with  $E_t = 2.73$  MeV, while the probability of the formation of both particles in unit volume is the same, it will be impossible to distinguish the  $\alpha$  particles against the overwhelming background of tritons in the spectrum as recorded by an external detector.

On irradiation with thermal neutrons, only a number of tritons given by the expression

$$N_t = N_{\text{Li}} f \sigma \Phi \quad (1)$$

will be formed per unit time in unit volume of a sample containing lithium, where  $N_{\text{Li}}$  is the lithium concentration in  $\text{cm}^{-3}$ ;  $f$  is the abundance of the  $\text{Li}^6$  isotope in a natural mixture;  $\sigma$  is the cross section of the  $\text{Li}^6(n, \alpha)\text{H}^3$  reaction in  $\text{cm}^2$ ;  $\Phi$  is the flux of thermal neutrons in neutrons/ $\text{cm}^2 \cdot \text{sec}$ .

In practice, the thickness of the sample is greater than the range of the tritons with  $E_t = 2.73$  MeV (thick sample), so that only some of the particles escape from the sample. It may be shown that

$$n_t = \frac{N_t}{4} (R - R_n),$$

Translated from *Atomnaya Energiya*, Vol. 32, No. 1, pp. 39-42, January, 1972. Original article submitted December 14, 1970

© 1972 Consultants Bureau, a division of Plenum Publishing Corporation, 227 West 17th Street, New York, N. Y. 10011. All rights reserved. This article cannot be reproduced for any purpose whatsoever without permission of the publisher. A copy of this article is available from the publisher for \$15.00.

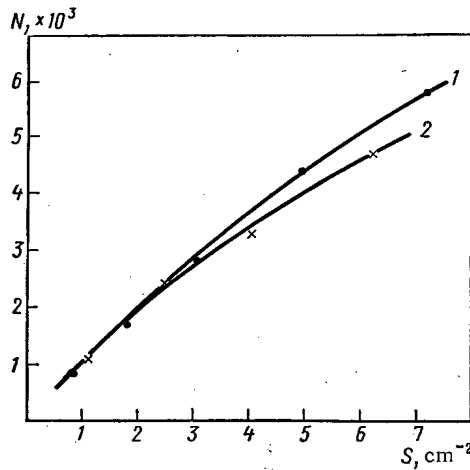


Fig. 1

Fig. 1. Dependence of the count on the area of the standard specimens for a constant lithium concentration and a constant specimen shape.

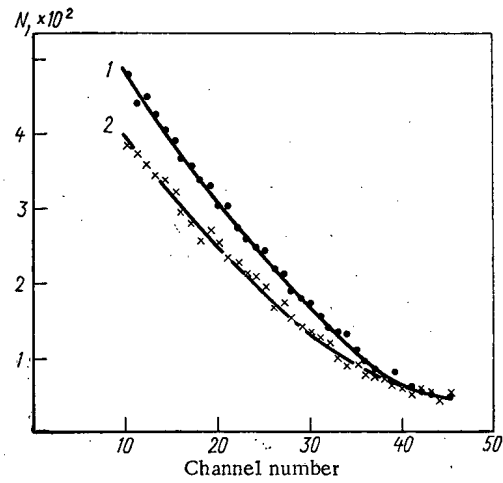


Fig. 2

Fig. 2. Mixed spectrum (1) and background spectrum (2) from a quartz plate.

particles escape through a unit surface of a flat, thick sample in unit time into the solid angle  $2\pi$ , where  $R$  is the range of particles with  $E_t = 2.73$  MeV in cm;  $R_n$  is the range of particles having an energy equal to the discrimination level in the sample material.

Let us substitute the value of  $N_t$  from (1):

$$n_t = \frac{N_{Li}}{4} f \sigma \Phi (R - R_n) \gamma. \quad (2)$$

In Eq. (2) we have introduced a coefficient  $\gamma$  allowing for the geometry of the sample-detector system. In addition to this,  $\gamma$  depends on the area of the sample and the topography of the neutron beam. Equation (2) is difficult to use in calculating the lithium content, since it is a very tedious matter to allow for the geometrical positioning of the sample and detector as well as the topography of the neutron beam. Furthermore the calculation of the product  $\sigma\Phi$  is very indeterminate. In order to obviate these difficulties it is essential to use standard specimens with a reasonably accurately known lithium content.

Let there be a standard specimen with a lithium concentration  $N_{Li_0}$ ; then

$$n_{t_0} = \frac{N_{Li_0}}{4} f \sigma \Phi (R_0 - R_{n_0}) \gamma. \quad (3)$$

The coefficient  $\gamma$  calculated from Eq. (3) gives the following on being substituted into (2)

$$n_t = \frac{N_{Li} - n_{t_0} (R - R_n)}{N_{Li_0} (R_0 - R_{n_0})}.$$

Whence

$$N_{Li} = \frac{n_t (R_0 - R_{n_0})}{n_{t_0} (R - R_n)} N_{Li_0}, \quad (4)$$

where the quantities with the zero index relate to the standard specimen. The ranges  $R$  for the tritons are calculated from the formula

$$R(E) = 2.993 R_p \left( \frac{E}{2.993} \right) \approx 3 R_p \left( \frac{E}{3} \right),$$

where  $R_p$  is the range of a proton. Knowing the mean atomic weight of the sample and standard, we may find  $R_p$  from tabulated data [6]. Equation (4) enables us to find the lithium concentration in the sample to an accuracy only restricted by the statistical error in determining the quantity  $n_t$ .



TABLE 1. Lithium Content of Certain Quartz Samples

Number of sample	Area, cm <sup>2</sup>	Concentration, cm <sup>-3</sup>	Content, wt. %	Error, %
1	1,43	0,92·10 <sup>19</sup>	4,0·10 <sup>-3</sup>	12
2	2,10	4,5·10 <sup>18</sup>	1,9·10 <sup>-3</sup>	20
3	3,54	7,1·10 <sup>18</sup>	3,1·10 <sup>-3</sup>	11
4	3,59	1,1·10 <sup>19</sup>	4,6·10 <sup>-3</sup>	7
5	3,35	0,98·10 <sup>19</sup>	4,2·10 <sup>-3</sup>	8

Experimental Part. As a detector of tritons we used a thin CsI(Tl) crystal placed (together with the sample) in a vacuum chamber in order to eliminate the absorption of energy from the tritons in the air. The pressure in the chamber was reduced to about 10<sup>-2</sup> mm Hg. Inside the chamber was a device for interchanging samples, so that five of these could be studied without breaking the vacuum. The CsI(Tl) crystal constituted a disc 30 mm in diameter and 20-30 μm thick, optically coupled with an FEU-13 photomultiplier. The plane of the sample was inclined to the plane of the detector at an angle of 30°.

In addition to thermal neutrons, resonance and fast neutrons (about 10% of the total) as well as γ quanta appeared in the beam emerging from the horizontal channel of the VVR-S reactor in which the measurements were carried out. In recording the tritons, a considerable background due to γ radiation, β particles, and protons is therefore to be expected. The latter arise from the elastic scattering of fast neutrons in the hydrogen of organic contaminants occupying the sample surface and parts surrounding the detector. Protons also arise as a result of an (n, p) reaction taking place in aluminum, nitrogen, and other elements.

The small thickness of the CsI(Tl) crystal (20-30 μm) enabled us to exclude the β - γ background and bring the detector closer to the sample (38 mm), thus increasing the geometrical efficiency of triton recording. The background from the protons was reduced by careful siting of the sample, detector, and shielding screens.

For low lithium contents, the background pulse count rate may be much greater than the triton count rate; the spectrum of the latter can only be distinguished by subtracting the background from the mixed spectrum. Since tritons are only formed under the action of thermal neutrons, the mixed spectrum may be recorded by allowing the whole beam from the channel to fall on the sample, and the background spectrum by excluding the thermal neutrons from the beam. If over the whole measuring period we first record the mixed spectrum, then cover the thermal neutron beam and record the background spectrum, any slight fluctuations in the power of the reactor will introduce a considerable error into the determination of the number of tritons. In order to eliminate this kind of error, we modulated the thermal neutron beam. The essence of the method employed lay in the fact that the beam of thermal neutrons was divided into pulses of equal length by means of an interrupter, the rest of the radiation from the channel remaining practically constant [7]. The mechanism of the interrupter was coupled to the analyzer through an electronic circuit: on passing the thermal-neutron beam the analyzer recorded the mixed spectrum; and when the beam in question was cut off, the background spectrum was subtracted. The modulation frequency could always be chosen in such a way that changes in the reactor power during one period of oscillation could be neglected.

In the present investigation we used an AI-100-1 analyzer, the memory of this being divided into two parts of 50 channels each on the principle proposed in [8], but with certain slight changes. With the beam of thermal neutrons uncovered, the signals only fall on the main analyzer input and are entered into the first 50 channels. With the thermal-neutron beam covered, in addition to the signal applied to the main input a pulse also passes to the memory-dividing circuit, and the second 50 channels are operated. The modulation frequency is 50 Hz. At this frequency, any nonuniformity in the operation of the reactor may be neglected. The modulation circuit proposed in [7] has the disadvantage that the spectra are still added when the beam of thermal neutrons is incompletely covered. In this case a proportion of the useful pulses, equal to the ratio of the time during which the beam is intersected by the cadmium boundary to the duration of the modulation half period, is recorded in the background spectrum. In the earlier experiments [7], for example, with a beam width of 0.3 cm, this proportion of the pulses amounts to more than 10% of the total number. In our own modulation system, this disadvantage is eliminated, since no pulses are counted while the beam is intersected by the cadmium boundary.

The standard specimens were prepared in the following way. Epoxy resin ED-6 and glycerin with LiCl · H<sub>2</sub>O dissolved in it were mixed until a homogeneous mass was obtained, after which a hardener was added (polyethylene polyamine). The mixture was poured onto an even glass surface and held for several days at room temperature. The weight of the mixture remained constant after hardening, so that the exact lithium content was known. From the resultant plates we cut standard specimens of various shapes and sizes.

**Results.** It is clear from the derivation of Eq. (4) that the standard specimen and test sample should have the same shape and size. We therefore plotted the relation between the number of tritons recorded and the area of the standard specimens for a constant lithium concentration and a constant specimen shape. In Fig. 1 curve 1 represents the relationship for circular samples and curve 2 for square samples. Each sample was irradiated in a thermal neutron flux of  $\Phi = 10^8$  neutrons/cm<sup>2</sup> · sec for 5 min. The lithium concentration was  $N_{Li_0} = 2.1 \cdot 10^{19}$  atoms/cm<sup>3</sup>.

We determined the lithium content in quartz plates. Figure 2 shows the mixed spectrum and the background obtained from a quartz plate irradiated for 12 min. The calculated lithium content  $N_{Li} = 1.13 \cdot 10^{19}$  atoms/cm<sup>3</sup> ( $4.9 \cdot 10^{-3}$  wt. %).

The discrimination threshold was established at the 1.5-MeV triton energy level. This level corresponds to an  $\alpha$  particle energy of 2 MeV, since the light yield of the CsI(Tl) crystal on excitation by  $\alpha$  particles is smaller than on excitation by tritons.

Table 1 shows the results of a determination of lithium content in relation to area and concentration. The error in the measurements is mainly due to the statistical error in determining the value of  $n_t$ . The error diminishes on increasing the measuring time and the area of the samples.

The method in question enables us to determine the lithium content of solids without breaking the sample, the sensitivity being  $10^{-4}$ - $5 \cdot 10^{-5}$  wt. %, depending on the density. Since the tritons recorded are formed in a thin surface layer, the lithium content may be determined layer-by-layer, which is useful when studying certain properties of solids.

#### LITERATURE CITED

1. L. Kaplan and K. Wilzbach, *Analyt. Chem.*, 26, No. 11, 1797 (1954).
2. S. Amil and J. Welwart, *Analyt. Chem.*, 35, No. 4, 566 (1963).
3. E. M. Lobanov et al., *Izv. Akad. Nauk Uz̄bekSSR, Ser. Fiz.-Matem. Nauk*, No. 6, 76 (1966).
4. I. N. Plaksin et al., *Radiokhimiya*, 11, No. 4, 501 (1967).
5. H. Lukens, *J. Radioanalyt. Chem.*, 1, No. 4, 349 (1968).
6. S. V. Starodubtsev and A. N. Romanov, *Passage of Charged Particles through Matter* [in Russian], Izd. AN Uz̄SSR, Tashkent (1962).
7. T. Isenhour and G. Morison, *Analyt. Chem.*, 38, No. 2, 162 (1966).
8. R. B. Begzhanov and D. A. Gladyshev, in: *Electromagnetic Transitions in Nuclei* [in Russian], Fanlar, Tashkent (1966), p. 214.

## THERMONUCLEAR COMBUSTION IN A BOUNDED REGION

A. F. Nastoyashchii

UDC 533.9.08

In this paper we will discuss the possibility of thermonuclear combustion in a hot plasma having a density near that characteristic of a solid. Such a plasma could be produced, e.g., by heating a thermonuclear substance by a pulsed laser or an electron beam. Huge fields – of the order of a megagauss and higher, and which cannot at present be produced – would be required for magnetic confinement of a plasma having such parameters. Attempts might be made, however, to prevent the rapid escape of the plasma by surrounding it with a massive shell.

In this case the thermal contact between the plasma and the surrounding walls will give rise to heat leakage as a result of the thermal conductivity (and bremsstrahlung). On the other hand, a fusion reaction is occurring in the plasma. The corresponding reaction heat evolved will tend to offset the heat loss. Accordingly, it is completely pertinent to ask whether a thermal equilibrium of a plasma with walls is possible and if so under what conditions. This state of thermal equilibrium would have a quite long "confinement time," required for nearly complete reaction of the thermonuclear substance.

Without taking up the practical questions associated with the technical feasibility of the corresponding experimental apparatus, we will study the necessary conditions under which steady states of a hot plasma can in principle exist. For this purpose we consider the three simplest plasma configurations: an infinite plane layer, an infinitely long cylinder, and a sphere.

In these three cases the steady-state temperature field is described by the heat-conduction equation

$$\frac{1}{x^{s-1}} \frac{\partial}{\partial x} \left( x^{s-1} \kappa \frac{\partial T}{\partial x} \right) = -Q \quad (1)$$

$$(Q = FQ_F - Q_T),$$

where  $S$  takes on the values 1-3 for the plane layer, long cylinder, and sphere, respectively;  $Q_F$  is the rate of heat evolution per unit volume;  $Q_T$  is the bremsstrahlung heat loss; and  $\kappa$  is the thermal conductivity of the plasma:

$$Q_F = bn^2 \left( \frac{\Delta}{T} \right)^{2/3} e^{-\left( \frac{\Delta}{T} \right)^{1/3}}; \quad (2)$$

$$Q_T = cn^2 (T)^{1/2}; \quad (3)$$

$$\kappa = \beta T^{5/2}, \quad (4)$$

Here  $n$  is the plasma density;  $T$  is the temperature; and  $b$ ,  $c$ , and  $\Delta$  are constants which can be found in, e.g., [1]. The numerical value of the constant  $\beta$  here is 1.8 times that given in [1].

In the heat source we will take into account only that part of the heat which is evolved during the deceleration of charged particles (reaction products), and we will neglect the neutron contribution. In this case for the fusion reaction in an equal-percentage mixture of deuterium and tritium we have  $b = 1.1 \cdot 10^{-20}$  erg · cm<sup>3</sup>/sec.

The function  $F = F(xL_Q^{-1})$  takes into account the circumstance that only some of the evolved energy goes into plasma heating for the case of characteristic plasma dimensions small in comparison with the range of  $\alpha$ 's ( $d < l_\alpha$ ).

Translated from *Atomnaya Énergiya*, Vol. 32, No. 1, pp. 43-47, January, 1972. Original article submitted November 16, 1970.

© 1972 Consultants Bureau, a division of Plenum Publishing Corporation, 227 West 17th Street, New York, N. Y. 10011. All rights reserved. This article cannot be reproduced for any purpose whatsoever without permission of the publisher. A copy of this article is available from the publisher for \$15.00.

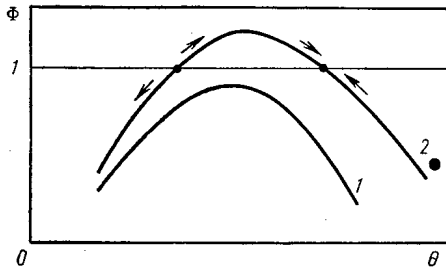


Fig. 1. Characteristic temperature dependence of the function  $\Phi = \Phi(\theta_0)$ :  
 1)  $n_0 d = (n_0 d)_{cr}$ ; 2)  $n_0 d > (n_0 d)_{cr}$ .

TABLE 1. The  $d_{cr}$  Values (in centimeters)

	$s=1$	$s=2$	$s=3$
$\kappa = \kappa_e$	0,60	0,75	0,85
$\kappa = \kappa_i$	0,25	0,30	0,35
$\kappa = 0$	0,17	0,17	0,17

The  $\alpha$ 's lose energy primarily due to "cooling" in collisions with electrons. Here the  $\alpha$  range depends on the electron density  $n$  and temperature  $T$ :

$$l_\alpha = a \frac{T^{3/2}}{n}, \tag{5}$$

where we are to set  $a = 3.8 \cdot 10^{10} \text{ cm}^4/\text{deg}^{3/2}$ .

At an electron density of  $n = 4 \cdot 10^{22} \text{ cm}^{-3}$  and temperature of  $T = 10^8 \text{ K}$ , the  $\alpha$  range is  $l_\alpha = 0.95 \text{ cm}$ .

We will assume that the shell has an infinite heat capacity, so we can assume zero temperature on the surface bounding the plasma. At the center of the plasma layer symmetry requires that gradients vanish. Accordingly, the boundary conditions on Eq. (1) can be written

$$T'|_{x=0} = T'|_{x=d} = 0. \tag{6}$$

Converting to the dimensionless variables  $\xi = xd^{-1}$ ,  $\theta = T\Delta^{-1}$  and assuming a power-law temperature dependence for the thermal conductivity,  $\kappa = \beta T^k$ , we can convert Eq. (1) with boundary conditions (6) to

$$\frac{1}{\xi^{s-1}} \frac{\partial}{\partial \xi} \xi^{s-1} \frac{\partial}{\partial \xi} \theta^{k+1} = -q(n_0 d, \theta); \tag{7}$$

$$\theta|_{\xi=0} = \theta|_{\xi=1} = 0. \tag{8}$$

Examination of the structure of Eqs. (1)-(3) shows that the right side of Eq. (7) will depend on the electron density and the plasma dimensions only through the combination  $n_0 d$ :

$$q = \frac{(k+1)(n_0 d)^2}{\beta \Delta^{k+1}} [F(\xi n_0 d) q_F - q_T] \tag{9}$$

$$(q_F = Q_F n^{-2}, \quad q_T = Q_T n^{-2}),$$

where  $q_F$  and  $q_T$  are functions of the dimensionless temperature  $\theta$ ;  $n_0 = n|_{\xi=0}$  is the plasma density at the center of the layer; and  $d$  is the half-width of the layer.

This problem is apparently quite similar to the familiar problem of a "thermal explosion" in chemical kinetics. In fact, there are significant differences, due to nonlinear thermal conductivity (4), which differs from the Arrhenius conductivity by heat-evolution law (2) and the existence of volume energy loss due to radiation. As a result of the combined effects of these factors, a thermal explosion in its usual sense [2] does not occur during thermonuclear combustion.

The steady-state temperature distribution satisfying Eq. (7) and boundary conditions (8) must be of the form

$$\theta = \theta(\xi, n_0 d),$$

i. e., it must depend on  $n_0 d$  as a parameter. There are no other parameters in this problem.

In order for there to be a steady-state solution, certain conditions must be satisfied. These conditions must take the form of some dependence of the parameter  $n_0 d$  on the temperature  $\theta_0 = \theta|_{\xi=0}$ :

$$n_0 d = f(\theta_0). \tag{10}$$

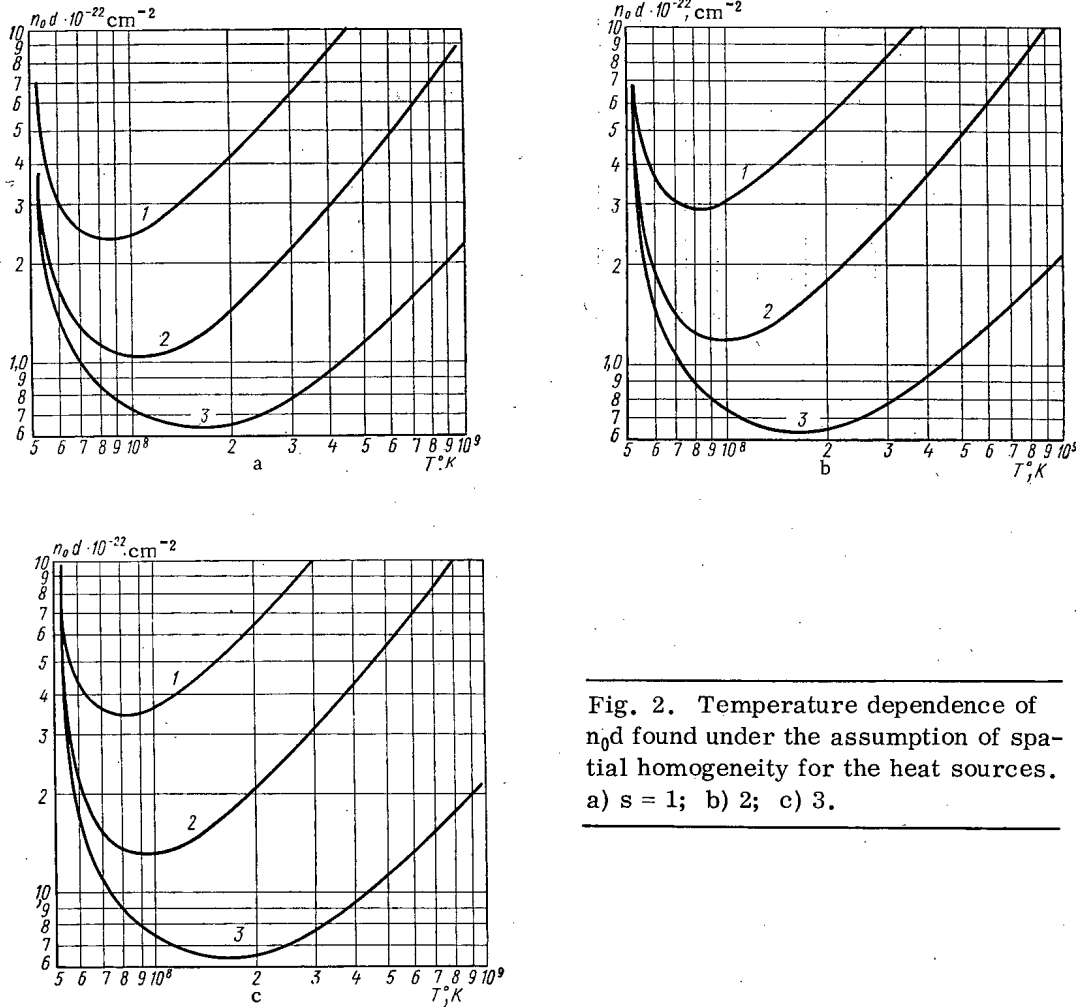


Fig. 2. Temperature dependence of  $n_0 d$  found under the assumption of spatial homogeneity for the heat sources. a)  $s = 1$ ; b) 2; c) 3.

It is shown below that the function  $f(\theta_0)$  reaches a minimum at some temperature  $\theta_*$  corresponding to the minimum possible value  $(n_0 d)_{CR}$ ; with  $n_0 d < (n_0 d)_{CR}$  a steady state is not possible.

The dimensions  $d_{CR}$  calculated for the normal density of solid deuterium turn out to be comparable to the  $\alpha$  range. We will accordingly consider two limiting cases.

1. In the first case of  $d \ll l_{QR}$ , we can assume that the heat evolved is distributed uniformly throughout the volume occupied by the plasma. Moreover, since the bremsstrahlung depends rather weakly on the temperature, we can replace  $q_T$  in Eq. (9) by some average  $\bar{q}_T$ . The resulting error is quite low, since the temperature changes little over most of the plasma because of the nonlinear thermal conductivity and falls off sharply only in the immediate vicinity of the walls.

Replacing  $q(\theta)$  by  $\bar{q}$  on the right side of Eq. (7) and integrating this equation through the use of boundary conditions (8), we find a temperature field

$$\theta^{k+1} = \theta_0^{k+1} - \frac{\bar{q}}{2s} \xi^2. \tag{11}$$

Assuming  $\theta = 0$  at  $\xi = 1$  in this last expression, we find the necessary condition for the existence of steady-state solutions:

$$\frac{1}{2s} \frac{\bar{q}}{\theta_0^{k+1}} = 1. \tag{12}$$

Using Eq. (9) for  $q$ , we can transform this condition to the form

$$\Phi(n_0 d, \theta_0) = \frac{F q_F}{q_T + q_x} = 1, \tag{13}$$

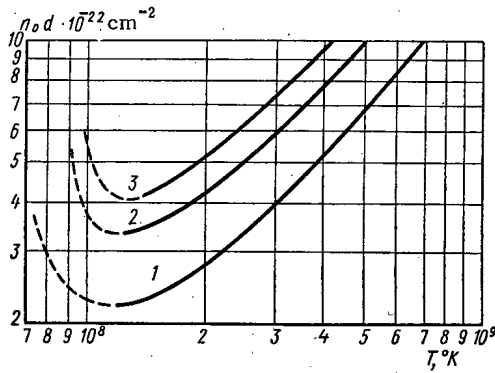


Fig. 3. Temperature dependences of  $n_0 d$  ( $l\alpha \ll d$ ). 1)  $s = 1$ ; 2) 2; 3) 3.

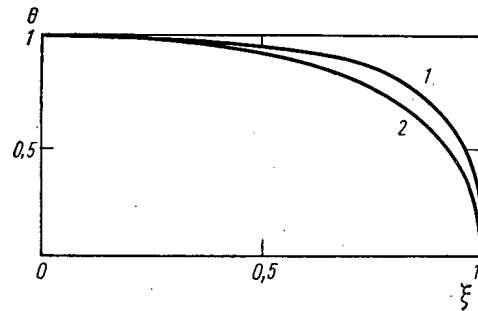


Fig. 4. Spatial distribution of the plasma temperature in the range  $T_0 \gg 10^8$  K. 1)  $s = 1$ ; 2) 3.

where

$$q_{\chi} = \beta \frac{2s}{k+1} \frac{T_0^{k+1}}{(n_0 d)^2} \tag{14}$$

The quantity  $Q_{\chi} = n_0^2 q_{\chi}$  represents the rate of heat loss per unit volume due to conduction. This loss depends on the exponent  $k$  in the expression for  $\kappa$  as well as on the configuration of the plasma volume ( $s$ ).

Figure 1 shows a typical  $\Phi = \Phi(\theta_0)$  dependence for a fixed  $n_0 d$  value. The intersections of the  $\Phi(\theta_0)$  curve with the line  $\Phi = 1$  correspond to steady states; if the curve maximum lies below the line, no steady state is possible.

With  $n_0 d > (n_0 d)_{CR}$  there are two possible states of thermal equilibrium. Here the equilibrium corresponding to the left-hand intersection is unstable. In fact, because of the positive derivative of the function  $\Phi(\theta_0)$ , which represents the ratio of the volume heat evolution to energy loss from the plasma, the slightest overheating of the plasma will result in self-heating. As a result the system should enter a new equilibrium state, corresponding to the right-hand intersection.

The characteristic transition time is

$$\tau_r \sim \frac{F Q_F}{n T} \tag{15}$$

At a plasma density of  $n = 4 \cdot 10^{22} \text{ cm}^{-3}$  and a temperature of  $T = 10^8$  K, this time is  $\tau \approx 5 \cdot 10^{-9}$  sec. By way of comparison, we note that the total "burn-up" time of the mixture under these conditions is  $\tau_F \sim 10^{-6}$  sec.

A thermal equilibrium cannot be reached with  $n_0 d < (nd)_{CR}$ , and the plasma quickly cools. The corresponding cooling time\* is  $\tau_{\chi} \sim d^2 n / \kappa \sim 10^{-8}$  sec with  $d \sim 1$  cm.

According to the theory for a thermal explosion [2] with  $d < d_{CR}$ , on the other hand, a steady state is reached, and with  $d > d_{CR}$  the temperature of the reacting mixture increases without limit (a thermal explosion). This discrepancy arises because in the thermal-explosion problem the corresponding function  $\Phi(\theta_0)$ , if plotted on the basis of the Semenov diagram, would have a minimum at some point  $\theta_{min}$  (in contrast with the case under consideration here).

Figure 2 shows temperature dependences of  $n_0 d$  found under the assumption of a spatially homogenous heat source  $q_k$ . The function  $F$  is assumed given by

$$F = 1 - e^{-\frac{d}{l\alpha}} \tag{16}$$

We consider three different cases corresponding to the different curve labels in Fig. 2: 1) the heat is transferred by electrons, and we have  $\kappa = \kappa_e$ ; 2) heat is transferred by ions (the electrons are magnetized), and we have  $\kappa = \kappa_i$ ; 3) the thermal conductivity is formally set equal to zero (there is no thermal

\*Here and below, all the calculations correspond to the normal density of solid deuterium, with  $n = 4 \cdot 10^{22} \text{ cm}^{-3}$  and  $T = 10^8$  K.

contact between the plasma and walls), and we have  $\kappa = 0$ . Here the second case corresponds to the application of a magnetic field of  $3 \cdot 10^5 \text{ G} < B < 2 \cdot 10^6 \text{ G}$ . The third case should be treated as purely hypothetical.

2. In the other limiting case of large plasma dimensions ( $l_\alpha \ll d$ ), the heat evolution can be assumed local and dependent on the local temperature. The corresponding problem is solved numerically; Fig. 3 shows temperature dependences obtained for  $n_0 d$ .

In the transition region ( $d \sim l_\alpha$ ) the results of the numerical calculations are in satisfactory agreement with results of the preceding model and with the results of [3], obtained by reducing to the problem to the thermal-explosion model [2].

Figure 4 shows characteristic temperature distributions which arise in the stable plasma state. The temperature is seen to change relatively slowly over most of the gap and to fall off rapidly to zero as  $\xi \rightarrow 1$ .

At a low-temperature thermal equilibrium we observe oscillations in the temperature distribution. These oscillations are damped as the average plasma temperature is raised. The oscillations are expressed most clearly in the spherical and cylindrical cases. The oscillations arise because in this temperature range the heat-source function may change sign.

Table 1 shows  $d_{\text{CR}}$  values for the normal density of solid deuterium:  $n = 4 \cdot 10^{22} \text{ cm}^{-3}$ . With  $\kappa = \kappa_i$  and  $\kappa = 0$ , we can assume  $d_{\text{CR}} \ll l_\alpha$ . At  $\kappa = \kappa_e$ , we have  $d_{\text{CR}} \approx l_\alpha$ , so Table 1 shows  $d_{\text{CR}}$  values obtained through the use of function F.

In the absence of a magnetic field, therefore, and at densities nearly equal to those characteristic of solids, a thermonuclear plasma may reach thermal equilibrium if the volume it occupies is greater than about  $3 \text{ cm}^3$ .

The minimum energy required to initiate (or ignite) a self-sustained fusion reaction in a sphere is

$$W = 4\pi T \frac{(n_0 d)_{\text{CR}}^3}{n_0^2} \equiv W_S (n_S) / \sigma^2,$$

where  $\sigma = n_0 / n_N$  is the degree of compression (with respect to the normal density  $n_N$  of the solid deuterium-tritium mixture). With  $\kappa = \kappa_i$  and  $\sigma \approx 3-4$  the compressional energy is  $W \approx 100 \text{ kJ}$ .

In superintense fields ( $B > B_* \approx 2 \text{ MG}$ ), in which the curvature of  $\alpha$  trajectories by the magnetic field becomes significant, the critical dimension  $d_{\text{CR}}$  is proportional to the Larmor radius, so the ignition energy should fall off according to a  $W = W_* (B_* / B)^3$  law.

We can draw the following conclusions from this discussion.

1. A thermonuclear plasma with confining walls can reach thermal equilibrium only under the condition  $(n_0 d) \geq (n_0 d)_{\text{CR}}$ ; otherwise the plasma cools rapidly.
2. With  $(n_0 d) \geq (n_0 d)_{\text{CR}}$ , two thermal-equilibrium states of the plasma are possible – at low and high temperatures. That at low temperatures is unstable: the slightest overheating of the plasma leads to its subsequent self-heating.
3. The energy required to ignite the thermonuclear reaction can be reduced by increasing the density of the thermonuclear material and by imposing a sufficiently strong magnetic field.

Note Added in Proof. After this paper had been submitted, the author learned of [4], which deals with the thermal equilibrium of a gaseous cylinder of a thermonuclear plasma (with  $n \approx 10^{14}-10^{17} \text{ cm}^{-3}$ ) under the assumption of an  $\alpha$  range small in comparison with the system's dimensions.

The principal difference between our results and those of [4] is due to the account of the finite  $\alpha$  range, which results in solutions of different nature. In particular, in our case solutions of the oscillatory type disappear; two states of thermal equilibrium at different temperatures are possible; etc. These differences are particularly important when a magnetic field is imposed (for at  $\kappa = 0$  the critical dimension remains finite).

In a comparison of our results obtained for the cylindrical case under the assumption  $l_\alpha = 0$  (curve 2 in Fig. 3), it should be taken into account that at our plasma parameters ( $n \approx 10^{23} \text{ cm}^{-3}$ ), the Coulomb logarithm is roughly half that in [4].

The possibility of a thermal equilibrium in a thermonuclear plasma with confining walls was also discussed in [5], in which the radiation losses, however, were not taken into account.

#### LITERATURE CITED

1. L. A. Artsimovich, Controlled Thermonuclear Reactions [in Russian], Fizmatgiz, Moscow (1961).
2. D. A. Frank-Kamenetskii, Diffusion and Heat Transfer in Chemical Kinetics [in Russian], Nauka, Moscow (1967).
3. A. A. Vedenov, B. Ya. Lyubimov, and A. F. Nastoyashchii, Report to the International Conference on Laser Plasmas, Moscow (1970).
4. S. Alikhanov, I. Konkashbaev, and V. Chebotaev, Nuclear Fusion, 10, No. 2, 13 (1970).
5. H. Alfvén and E. Smars, Nature, 188, 801 (1960).



RADIATIVE WIDTHS OF  $U^{238}$  NEUTRON RESONANCES

Kh. Malétski, L. B. Pikel'ner,  
I. M. Salamatin, and É. I. Sharapov

UDC 621.039.512.26

$U^{238}$  neutron resonances have been studied in a number of laboratories [1-3]. This nucleus is of interest because it enables one to obtain a strength function and the distributions of reduced neutron widths and level spacings.  $S$  neutrons excite a system of spin  $1/2$  levels in  $U^{238}$  with a mean spacing of  $D \sim 18$  eV, which is convenient for observation. In addition the value of uranium in reactor engineering must be taken into account.

Interest in  $U^{238}$  was renewed with the appearance of [4] devoted mainly to the radiative widths  $\Gamma_\gamma$  of  $U^{238}$  resonances. Values of  $\Gamma_\gamma$  for individual levels reported earlier [5, 6] did not, as a rule, differ from the average of  $\sim 24$  MeV by more than the experimental error. Measurements made during a subterranean nuclear explosion in the United States and reported by Glass et al. [4] gave values of  $\Gamma_\gamma$  for a large number of levels in the energy range up to 2 keV which are significantly different from those reported earlier.

Figure 1 shows the data of [4] in the energy range up to 1.4 keV. The values of  $\Gamma_\gamma$  vary periodically with energy from 12 to 33 MeV in this energy range as shown by the broken curve in the figure. Glass et al. class this behavior of  $\Gamma_\gamma$  with other known facts as a manifestation of intermediate structure in the effective cross sections. These results raised a doubt as to the validity of the statistical approach to the total radiative widths of levels of compound nuclei.

Because of the importance of the question we measured the transmission and radiative capture of neutrons in  $U^{238}$ .

The measurements were made at the IBR pulsed reactor with a linear electron accelerator as injector. For a flight path of 500 m the resolution was 6 nsec/m. The samples were discs of natural uranium metal having diameters of 160 mm (radiative capture) and 190 mm (transmission). The transmission was measured in three samples 1.4 and 12 mm thick, and radiative capture was measured with a sample 1 mm thick ( $n = 4.8 \cdot 10^{21}$  nuclei/cm<sup>2</sup>). A sectional liquid scintillation detector of about 250 liters volume having a cylindrical channel along the axis of the neutron beam was employed as a radiative capture detector. The sensitive volume of the detector consists of six symmetrically placed sections with the lateral planes parallel to the axis of the beam. The detector electronics permits sorting of pulses from each section lying above a specified threshold, recording of the composite pulse from all sections, or counting double or triple coincidences involving any sections.

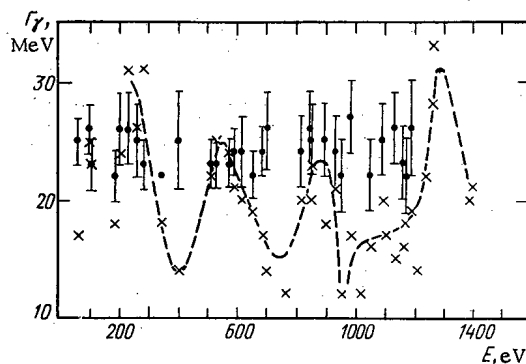


Fig. 1. Radiative widths of  $U^{238}$  resonances as a function of neutron energy:  $\times$ ) data from [4]; broken curve drawn by Glass et al. [4] for convenience of discussion;  $\bullet$ ) results of present work.

An important problem in the measurement of radiative capture is the accurate determination of the product of the neutron flux  $P(E)$  and the efficiency of the detector in counting neutron captures  $\varepsilon_\gamma$  which appears in the expression

$$\sum N_i = P(E) \varepsilon_\gamma \frac{\Gamma_\gamma}{\Gamma} A. \quad (1)$$

Translated from *Atomnaya Energiya*, Vol. 32, No. 1, pp. 49-51, January, 1972. Original article submitted March 3, 1971.

© 1972 Consultants Bureau, a division of Plenum Publishing Corporation, 227 West 17th Street, New York, N. Y. 10011. All rights reserved. This article cannot be reproduced for any purpose whatsoever without permission of the publisher. A copy of this article is available from the publisher for \$15.00.

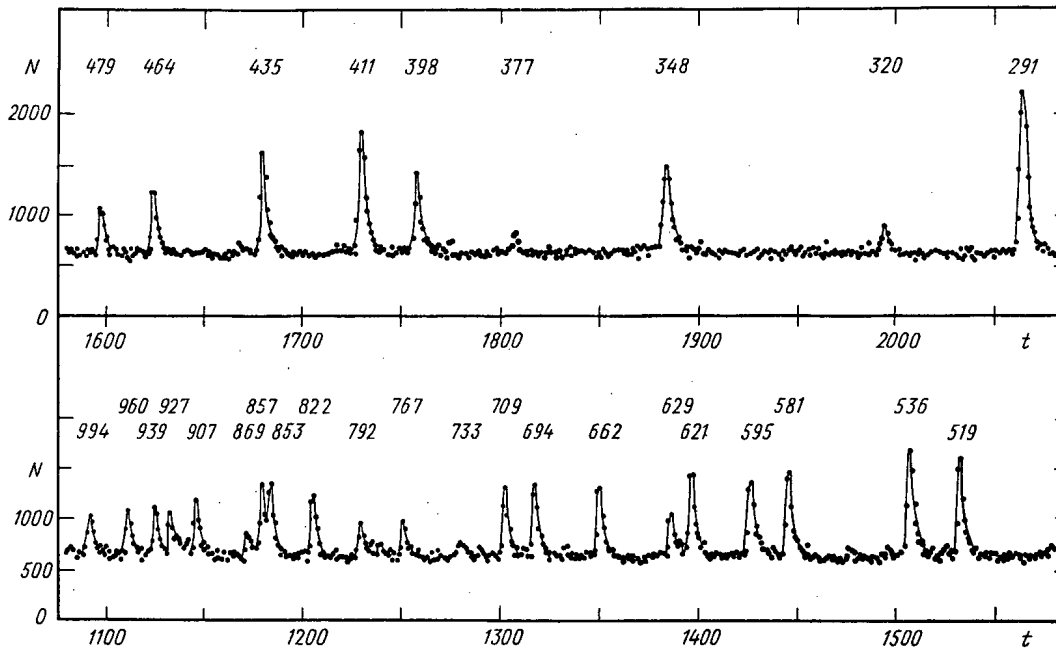


Fig. 2. A portion of the spectrogram of radiative capture of neutrons obtained with a uranium sample 1 mm thick. The numbers above the resonances are the energies in electron volts.

Here  $\Sigma N_i$  is the sum of the detector counts over a resonance, corrected for background;  $\Gamma_\gamma$  and  $\Gamma$  are the radiative and total widths of the resonance; and  $A$  is the area of the resonance dip in the transmission curve. In our case we had to be sure that  $\epsilon_\gamma$  did not vary from resonance to resonance. To test this we made measurements under all the conditions mentioned above and compared the ratios of the areas of the resonances in the various cases. Since the softening of the spectrum, i. e., the increase in the multiplicity of gamma photons in cascade, leads to an increase in the efficiency of counting captures in the coincidences mode with a low threshold, while the counting efficiency in individual sections with a high threshold (3 MeV) is lowered, the ratio of the areas of the resonances under such conditions is a sensitive indicator of the change in character of the spectrum. In our measurements these ratios remained constant from resonance to resonance within the limits of statistical error ( $\sim 5\%$ ) so we can say that the detector efficiency is constant.

Figure 2 shows a portion of the  $U^{238}$  spectrogram obtained with an  $(n,\gamma)$  detector in a double coincidence arrangement. The level between resonances is due mainly to the intrinsic background of the detector and to the gamma activity of the sample. The energy dependence of the flux was obtained from measurements with a thin boron counter, and the absolute calibration of  $P(E)\epsilon_\gamma$  was accomplished by determining the quantity  $A$  from the transmission for resonances with  $\Gamma_n \ll \Gamma_\gamma$ , for which the ratio  $\Gamma_\gamma/\Gamma$  in Eq. (1) is almost independent of the assumed values of  $\Gamma_n$  and  $\Gamma_\gamma$ . For calibration we used those resonances for which the values of  $\Gamma_n$  in the literature are in good agreement with one another and with our data from measurements of the total cross section.

The transmission was measured with the same detector but the uranium sample in the detector was replaced by a set of samples having large capture cross sections alternating with thin layers of moderator. Cadmium, rhenium, tantalum, and rare earth elements were used as capturing samples.

The transmission curves were processed by using the area method and taking account of the interference of resonance and potential scattering. The resonance parameters obtained by combining the data on transmission and radiative capture are listed in Table 1. For resonances in which  $\Gamma_n > \Gamma_\gamma$  the main source of information on  $\Gamma_\gamma$  is the measurement of radiative capture, as was shown in [7]. When necessary a correction was introduced for the capture of neutrons after scattering.

Table 1 shows that the radiative widths are nearly the same for neutron energies up to 1200 eV. The mean value  $\bar{\Gamma}_\gamma = 24$  MeV and the deviations from the mean barely exceed the experimental error which is about 10% for most resonances. An increase in the accuracy of the measurements might possibly show

TABLE 1. Parameters of  $U^{238}$  Neutron Resonances

$E_0$ , eV	$\Gamma_n$ , MeV	$\Gamma_\gamma$ , MeV	$E_0$ , eV	$\Gamma_n$ , MeV	$\Gamma_\gamma$ , MeV
66±0.1	24±1.5	25±2	621±0.9	33±10	24±3
80.7±0.1	2.2±0.2		629±0.9	7±1	
102.4±0.1	70±3	26±2	662±1	150±20	22±2
116.9±0.1	22±3	23±2	694±1	40±10	24±2
145.8±0.1	0.84±0.06		709±1	20±5	26±3
165.4±0.1	3±0.3		733±1.1	3.5±0.6	
189.5±0.2	164±5	22±2	767±1.2	7±1	
208.4±0.2	48±2	26±3	792±1.2	6±1	
237.6±0.2	27±3	26±3	822±1.3	66±16	24±3
273.9±0.25	22±3	25±3	853±1.4		26±3
291.2±0.25	16.4±2	23±2	857±1.4		25±3
311.7±0.3	0.9±0.1		869±1.4	5±2	
348.1±0.35	78±10	22±2	907±1.5	40±10	25±3
377±0.4	0.9±0.15		939±1.6	120±20	24±3
398.1±0.45	4.7±0.5		960±1.6	130±20	22±3
410.7±0.45	20±3	25±4	994±1.7		27±3
434.6±0.5	8±1		1 026±2	8±2	
464.1±0.55	5±0.5		1 057±2	90±30	22±3
479.4±0.6	3.5±0.5		1 100±2		25±3
519±0.7	42±6	23±2	1 142±2		26±3
536.2±0.7	55±15	23±2	1 170±2		23±3
580.7±0.8	36±6	23±2	1 179±2		22±3
594.8±0.8	93±10	24±2	1 197±2		26±4

small fluctuations in  $\bar{\Gamma}_\gamma$ , but in any case Fig. 1 shows that the fluctuations reported in [4] are clearly not real. The mean value  $\bar{\Gamma}_\gamma = 19$  MeV obtained in [4] is also a considerable underestimate.

We previously reported the main results on the radiative widths of  $U^{238}$  [8], and the data of the Belgian group [9] published at the same time are in good agreement with ours.

In conclusion the authors thank T. S. Afanas'ev and N. T. Khot'ko for help in performing the measurements.

## LITERATURE CITED

1. L. Bollinger et al., Phys. Rev., 105, 661 (1957).
2. F. Firk, J. Lynn, and M. Moxon, Nucl. Phys., 41, 614 (1963).
3. J. Garg et al., Phys. Rev., 134, B985 (1964).
4. N. Glass et al., Proc. II Conf. on Neutron Cross Sections and Technology (D. Goldman, editor) (1968), p. 573.
5. J. Rosen, Phys. Rev., 118, 687 (1960).
6. M. Asghar, C. Chaffey, and M. Moxon, Nucl. Phys., 85, 305 (1966).
7. Kh. Malétski et al., Yadernaya Fizika, 9, 1119 (1969).
8. Kh. Malétski et al., Soviet-French Seminar on Nuclear Data [in Russian], Dubna (1970).
9. G. Rohr, H. Weigmann, and J. Winter, Proc. II Intern. Conf. on Nucl. Data for Reactors, Vol. 1, CN 26/18, IAEA, Vienna (1970).

## ABSTRACTS

VARIATIONAL COMPOSITE METHODS OF CALCULATING NEUTRON  
DISTRIBUTION IN NUCLEAR REACTORSI. S. Slesarev, A. M. Sirotkin,  
and V. V. Khromov

UDC 621.039.5/6

The variational approach has broad possibilities for the creation of composite methods which, in calculations of physical systems, allow the simultaneous use of approximations of different orders within the scope of one method or the application of several different methods at once in an arbitrary combination of their approximations.

The variational formulation of the problem usually consists of the construction of a functional for which the equation under examination is a Euler-Lagrange equation.

A one-velocity kinetic equation in plane-parallel geometry was used in the study, and the functional  $F_0$ , stationary for the solutions of the initial equation and equal to the quantity  $k_{\text{eff}}$ , was examined. The fact that  $F_0$  allows the use of discontinuous trial functions is significant.

A sufficiently general approximate representation of the desired solution in the geometry examined is

$$\Psi_{ik}(x, \mu) \approx \sum_{n=0}^{N(i)} Q_n^i(\mu) a_n^{ik}(x), \quad (1)$$

where  $ik$  is the number of the phase space region for the variables  $x$  and  $\mu$ ;  $Q_n^i$  is some known polynomial;  $a_n^{ik}$  is the desired function;  $N$  is the number of members in the series, which depends on the number  $i$  of the physical zone.

Many approximation methods may be obtained through the variational method, if trial functions are used which are a particular case of (1) and satisfy the restriction that  $F_0$  be stationary.

It is shown that the functional examined is suitable for the derivation of the equations for  $DP_n$ ,  $S_n$  and of other methods.

Since  $F_0$  allows the use of all kinds of trial functions, having the form of (1) in different zones of the reactor or of another physical system, all "matching" conditions for equations for a broad class of approximation methods are obtained from a single principle - the need for the functional  $F_0$  to be stationary.

The extraction of matching conditions at the boundaries of zones where the change of method or number of approximations takes place is the important step in the derivation of the composite methods equations. Matching conditions of a general type, which are suitable for combinations of many existing methods, were formulated in the study.

Equations and matching conditions of certain variational composite methods -  $DP_n$ - $DP_m$ ,  $DP_n$ - $S_m$ ,  $S_n$ - $S_m$  (the indices  $n$  and  $m$  indicate the possibility of using different approximations in neighboring zones of the system) - were presented as concrete examples.

The  $DP_n$ - $DP_m$  method was verified in calculated investigations of the quantity  $k_{\text{eff}}$  and of the neutron distribution in a multiregion heterogeneous multiplying system. The results of the calculations, which are presented, demonstrate the flexibility of the method and its high degree of accuracy, together with a significant decrease in the extent of the computations. This decrease is due to the reduction in the order of the approximations for the  $DP_n$  method in those zones where this is warranted a priori from physical considerations.

Translated from *Atomnaya Energiya*, Vol. 32, No. 1, p. 53, January, 1972. Original article submitted September 22, 1970.

© 1972 Consultants Bureau, a division of Plenum Publishing Corporation, 227 West 17th Street, New York, N. Y. 10011. All rights reserved. This article cannot be reproduced for any purpose whatsoever without permission of the publisher. A copy of this article is available from the publisher for \$15.00.

## RADIOACTIVITY OF METAMICT ZIRCONS

I. M. Lipova and G. A. Kuznetsova

UDC 553.494:539.16

Interpretation of the nature of the metamict state in minerals is one of the urgent problems in current mineralogy. The most popular relevant viewpoint on metamict minerals sees them as primary crystalline substances converted to an amorphous form under the influence of radioactive radiations emitted by uranium and thorium incorporated in the minerals.

Zircon is a most abundant accessory mineral, and an important industrial source of zirconium, and is known in nature in both crystalline and metamict states. The role played by radioactive radiation in metamict decay of a mineral was studied in tests run on a series of zircon specimens (incorporating zircon per se, cyrtolite, malacon, alvite, naegite, etc., comprising a continuous series from crystalline to complete x-ray amorphous differences). The way the uranium and thorium contents, the  $\alpha$ -activity, the total  $\alpha$ -exposure dose vary, the forms of occurrence of uranium and thorium, and the distribution of uranium and thorium in the minerals, were studied.

Specimens of zircons from various types of geological formations existing in the USSR and in foreign countries were investigated. The entire series of zircons was arbitrarily broken down into three groups on the basis of the number of reflections on the Debye powder diagrams: crystalline, semimetamict, and metamict.

The uranium content was determined by the luminescent method, and the thorium content was determined colorimetrically, using arsenazo-III reagent. The  $\alpha$ -activity was measured in a thin layer of the specimen applied to the substrate, with a scintillation counter and a PS-10,000 scaler used in the measurements. The total  $\alpha$ -exposure dose was calculated by multiplication of the  $\alpha$ -activity by the absolute age of the mineral.

The uranium content and thorium content in the zircons increase from the crystalline differences (hundreds of a percent of uranium and thorium) to metamict differences (whole percents of uranium and thorium). But no exact quantitative relationship linking the degree of x-ray amorphousness of zircon and the content of the radioactive elements (uranium and thorium separately, or their sum) was observed.

The thorium/uranium ratio is determined by the genesis of the rocks. As a rule,  $\text{Th}/\text{U} > 1$  in zircons from pegmatites of alkaline granites, alkaline syenites, nephelin syenites, greisens, albitites bound with alkaline rocks, and hydrothermalites of alkaline composition, and usually the ratio  $\text{Th}/\text{U} < 1$  in zircons from granites, granitic pegmatites, and apogranites.

The degree of x-ray amorphousness of zircon tends to increase with increasing total dose of uranium and thorium  $\alpha$ -emission: in the case of crystalline zircons  $n 10^{14}$   $\alpha/\text{mg}$ , in the case of semimetamict zircons  $n 10^{15}$   $\alpha/\text{mg}$ , and metamict zircons  $n 10^{16-17}$   $\alpha/\text{mg}$ .

Uranium and thorium are represented as both by the scattered or dispersed form and by microinclusions of radioactive minerals. The latter are syngenetic in rare instances, but more often epigenetic with respect to the zircon. When the content of inclusions of uranium and thorium minerals is high, the direct relationship between the degree of x-ray amorphousness and the  $\alpha$ -radiation dose breaks down.

Dispersed uranium is unevenly distributed throughout the volume of the mineral (microradiography). Portions with a higher density of  $\alpha$ -tracks correspond to the optically isotropic phase, and portions having a lower track density correspond to the anisotropic phase of the mineral. These data are confirmed by the microprobe method.

The maximum uranium content in the specimens investigated was detected in Japanese naegite (6.66%  $\text{U}_3\text{O}_8$  in the transparent fraction of the mineral containing no microinclusions when viewed in 497-fold magnification). All of the uranium seems to be included isomorphically in the structure of  $\text{ZrSiO}_4$  (4 mole % uranium). Naegite is the most deeply metamict of the whole series of zircons investigated.

---

Translated from *Atomnaya Énergiya*, Vol. 32, No. 1, pp. 53-54, January, 1972. Original article submitted March 23, 1971.

MONTE CARLO CALCULATIONS OF CHARACTERISTICS OF  
SECONDARY ELECTRONS KNOCKED OUT FROM VARIOUS  
MATERIALS BY  $\gamma$ -RADIATION\*

V. V. Smirnov and A. V. Malyshev

UDC 539.124.17

Energy spectra, angular distributions, and quantum yields of secondary electrons knocked out by  $\gamma$ -radiation from aluminum and copper targets of different thicknesses were calculated by the Monte Carlo method. In the region of energies of interest (0.4 to 1.3 MeV), production of electrons in the irradiated material was due solely to Compton scattering and to photoelectric absorption of the  $\gamma$ -emission. Values of the energies and directions of escape of the Compton electrons were calculated on the basis of the Klein-Nishima formula. The pattern of angular distributions of the photoelectrons was obtained on the basis of tabular data compiled by Haltberg. The target-depth distribution of the electrons formed was assumed uniform.

In dealing with the motion of an electron through the material, the entire path traversed by the electron from the point of origin to the target boundary was broken up into discrete segments within which the electron energy losses were determined according to Bethe-Bloch theory, and the angular distributions were estimated in conformity with Mollier theory.

As a result of these calculations, the energy spectra, angular distributions, and quantum yields of secondary electrons knocked out by the  $\gamma$ -radiation of the radioisotope isotopes of  $\text{Co}^{60}$ ,  $\text{Cs}^{137}$ , and  $\text{Au}^{198}$  from aluminum targets 0.1  $R_0$  and 0.6  $R_0$  in thickness were determined ( $R_0$  is the total range of the electron having the highest energy). The quantum yields of the secondary electrons knocked out of an aluminum target of equilibrium thickness (0.6  $R_0$ ) by  $\gamma$ -radiation emitted by  $\text{Co}^{60}$ ,  $\text{Cs}^{137}$ , and  $\text{Au}^{198}$ , in the forward direction (0-90°), was, respectively, 8.0, 3.0, and 1.1 in units of  $10^{-3}$  electron photon, and respectively 0.25, 0.20, and 0.06 in the same units in the backward direction (90-180°). Comparison of the calculated energy spectra, angular distributions, and quantum yields of secondary electrons knocked out in the forward direction and available experimental data indicated agreement within 10%.

The calculations of quantum yields of secondary electrons for targets of various thicknesses (aluminum and copper targets) indicated that the relative yield of electrons for a given thickness expressed in terms of a fraction of  $R_0$ , and the atomic number of the target, is independent of the energy of the incident  $\gamma$ -photons. The relative yields of secondary electrons in the case of aluminum and copper targets of different thicknesses were approximated by empirical formulas which were in agreement with the experimental data to within 5%.

THE KAON FACTORY - A TWO-STAGE (~ 3.7 GeV) ISOCRONOUS  
CYCLOTRON†

L. A. Sarkisyan

UDC 621.384.633.5

Many research centers are carrying out investigations into the creation of "kaon factories," that is, accelerators aimed at producing 3-7 GeV protons with an average beam current of the order of 100  $\mu\text{A}$ . Tables 1 and 2 indicate possible parameters for three versions of a cascade-type isochronous cyclotron proposed by the author in 1970 [1, 2].

\*Translated from *Atomnaya Énergiya*, Vol. 32, No. 1, p. 54, January, 1972. Original article submitted June 23, 1971.

†Translated from *Atomnaya Énergiya*, Vol. 32, No. 1, pp. 55-56, January, 1972. Original article submitted May 3, 1971; revision submitted August 2, 1971.

TABLE 1. Parameters of ~ 2.7 GeV Three-Stage Cyclotron System

Stages of cyclotron system	$H_0$ , Oe	$N$	$\lambda$ , cm	$Q_z$	$Q_r$	$r_\infty$ , cm	$r_{II}$ , cm	$r_R$ , cm	$\epsilon_R$	$WK$ , GeV	$eV$ , MeV/rev
First	6000	8	8	0,2	$\sim 1 \leq Q_r \leq 2$	521	$\sim 0$	415	0,281	0,8	1
Second	3000	12	14,1	0,65	$\sim 1,86 \leq Q_r \leq 3$	1042	900	980	0,67	1,7	2,5
Third	2000	16	33	0,65	$\sim 2,86 \leq Q_r \leq 4$	1563	1474	1511	1,3	2,7	4,5

Note: Notation same as in reference [2].

TABLE 2. Parameters of Second Stage of Cascade, ~ 2.7 GeV and ~ 3.7 GeV

Stages of cyclotron system	$H_0$ , Oe	$N$	$\lambda$ , cm	$Q_z$	$Q_r$	$r_\infty$ , cm	$r_{II}$ , cm	$r_R$ , cm	$\epsilon_R$	$WK$ , GeV	$eV$ , MeV/rev
Second	2000	16	33	0,65	$\sim 1,86 \leq Q_r \leq 4$	1563	1320	1510	1,3	2,7	6
"	1300	20	36,5	0,65	$\sim 1,86 \leq Q_r \leq 5$	2405,6	2024	2354	1,39	3,7	8

The present article studies transit through linear resonances in a cascade cyclotron. The increase in the amplitude of radial oscillations after dynamic transit through the most dangerous integral resonance was calculated on the basis of the equation

$$\rho = \frac{rH_s}{SH} \left[ \cos S\varphi \int_0^\varphi \cos \left( \frac{\chi_r}{2} - \varphi_1^2 \right) d\varphi_1 + \sin S\varphi \int_0^\varphi \sin \left( \frac{\chi_r}{2} - \varphi_1^2 \right) d\varphi_1 \right],$$

where  $H_s$  and  $S$  are the amplitude and number of the lowest harmonic of the field;  $H$  is the average field;  $r$  is the orbit radius;  $\varphi_1$  is the variable phase;  $\chi_r = dQ_r/d\varphi|_{\varphi=0} \approx eV/2\pi E_0$ .

Assuming that the peak increase in amplitude following transit of the integral resonance is 2 cm, the tolerance for the lowest harmonic of the vertical field component in the second cyclotron, in the case of a three-stage cyclotron system, is  $H_2 = 0.55$  Oe, while the  $H_3 = 0.45$  Oe in a three-cyclotron system. Tolerances on the field harmonics in the second cyclotron of a two-stage cyclotron system with cyclotron energies 2.7 GeV and 3.7 GeV are respectively:  $H_2 = 0.19$  Oe,  $H_3 = 0.53$  Oe, and  $H_2 = 0.13$  Oe,  $H_3 = 0.26$  Oe,  $H_4 = 0.44$  Oe. In the case of an uncompensated field harmonic  $\sim 0.15$  Oe, the total increase in the amplitude of the radial oscillations in the three-stage cyclotron is  $\sim 1.3$  cm, in the two-stage cyclotron  $\sim 2.5$  cm and  $\sim 4$  cm, which is acceptable.

The indicated tolerances on the lower harmonics of the field in zones of integral resonance can be achieved in two stages. The harmonic can be corrected to within 1 Oe or less [3] during the magnetic measurements by using a harmonic coil and independently adjusting the amplitude and phase of the harmonic. Later on, the results of measurements taken with profilometers of the radial shape of the beam before and after the transit through resonance (in pulsed mode) can be used during the starting and adjustment of the cyclotron, and the harmonic field can be corrected to a permissible value with the aid of the harmonic coil.

Tolerances on the first harmonic of the vertical component of the field in the zone of an integral resonance ( $Q_r \approx 1$ ,  $r \approx 200$  cm) in the Vancouver 500 MeV  $H^-$ -meson factory was assigned the value  $H_1 = 0.12$  Oe [4] as the amplitude of the radial oscillations increased by 0.4 cm and  $eV = 400$  keV/revolution. The tolerance on the first harmonic of the radial field component in the zone of the integral resonance ( $Q_z = 1$ ,  $r \approx 450$  cm) is 0.7 Oe in the case of the Zürich 590 MeV meson factory, as the amplitude of the axial oscillations is increased by 0.5 cm and  $eV = 2.4$  MeV [5].

#### LITERATURE CITED

1. L. A. Sarkisyan, Second All-Union Conference on Charged-Particle Accelerators [in Russian], Moscow (November, 1970).
2. L. A. Sarkisyan, *At. Énerg.*, **30**, 466 (1971).
3. R. Allas et al., *Nucl. Instrum. and Methods*, **64**, 333 (1968).
4. M. Graddock and J. Richardson, *IEEE Trans. Nucl. Sci.*, **NS-16**, 415 (1969).
5. W. Joho, SIN-Report TM-11-8 (1970).

## THERMAL STABILITY OF ANHYDROUS URANIUM TRICHLORIDE

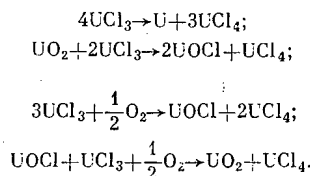
V. V. Rachev, L. A. Tarasova,  
and A. I. Pavlova-Verevkina

UDC 543.226:546.791

Views differ on the thermal stability of  $UCl_3$  [1-3]. With the object of securing more precise information on the behavior of  $UCl_3$  under vacuum heating conditions, and the reasons for the formation of  $UCl_4$ , x-ray structural analysis was applied to the study of the phase composition of all the sublimation products of  $UCl_3$  and of the nonsublimating residue over the temperature range 750-950°C and vacuum range  $10^{-6}$  to  $10^{-5}$  torr. The design of the equipment was such as to eliminate any possibility of contact between the degassed parts of the evaporator assembly, the initial and final sublimation products, with components of the air. The initial  $UCl_3$  preparations contained 96-98.5% of the base material and impurities of either 4%  $UO_2$  or 1.5%  $UOCl$ .

The volatile fractions were unambiguously identified as  $UCl_3$  and  $UCl_4$ . The following were detected in the residues after sublimation:  $\alpha$ -phase of metallic uranium; alloy  $\gamma$ -U-Mo with cubic lattice constant  $a = 3.412 \pm 0.06 \text{ \AA}$ ; monooxychloride of trivalent uranium ( $UOCl$ ) with the tetragonal unit cell parameters  $a = 4.036 \text{ \AA}$ ,  $c = 6.882 \text{ \AA}$ ; uranium dioxide ( $UO_2$ ) with the cubic cell parameter  $a = 5.470 \text{ \AA}$ ; an unknown phase with the cubic cell parameter  $a = 4.95 \text{ \AA}$ . This phase is assumed to be the solid solution  $U(O_{1-x-y}N_xC_y)$ .

Over 50% of the  $UCl_3$  present sublimes in unaltered form, no matter what the experimental conditions. Formation of  $UCl_4$  in the sublimation process is determined by side processes whose chemical mechanism can be represented by the parallel competing reactions:



The presence of  $U(O_{1-x-y}N_xC_y)$  is probably due to interaction of the metallic uranium formed in disproportionation with the residual gases in the system, with the uranium performing the role of getter. An important practical consequence on the confirmed preferential sublimation of  $UCl_3$  in unaltered form as it is heated in vacuum is the possibility of using vacuum sublimation in the preparation of  $UCl_3$  of special purity. The decisive factor here is careful protection of the original product and arrangement from contact with constituents of the air, oxygen in particular.

## LITERATURE CITED

1. L. Brewer et al., TJD-5290, Book 1, Paper No. 33 (1958).
2. S. A. Shukarev, I. V. Vasil'kova, and A. I. Efimov, Zh. Neorgan. Khim., 1, No. 12, 2652 (1956).
3. J. Katz and E. Rabinowitch, The Chemistry of Uranium [Russian translation], IL, Moscow (1954), p. 367 and p. 415.

---

Translated from Atomnaya Energiya, Vol. 32, No. 1, p. 56, January, 1972. Original article submitted May 20, 1970; abstract submitted October 18, 1971.



## LETTERS TO THE EDITOR

## ADJOINT REACTOR KINETICS EQUATIONS: DELAYED NEUTRON CASE

V. V. Orlov

UDC 621.039.512

The extension of the theory of neutron worth to nonstationary and nonhomogeneous problems [1, 2] was attempted without taking delayed neutrons into account. But they can be taken into account only if we introduce, in addition to the neutron worth  $F^+(\bar{r}, \bar{v}, t)$ , the worth of the fragments acting as sources of the  $i$ -th group of delayed neutrons  $C_i^+(\bar{r}, t)$  with respect to some functional:

$$J_p = \int d\bar{r} d\bar{v} dt F(\bar{r}, \bar{v}, t) P(\bar{r}, \bar{v}, t).$$

Then  $C_i^+(\bar{r}, t)$  will be equal to  $J_p$  if one fragment of the  $i$ -th kind is introduced at point  $\bar{r}$  at time  $t$ . Taking the physical meaning of  $C_i^+$  as point of departure, we can then find the equation for that function.

Let  $N$  fragments of the  $i$ -th kind be placed at point  $r$  at time  $t$ . Then their total worth will be  $NC_i^+(\bar{r}, t) = J_p$ . If we now select out a small time interval  $\Delta t$  after  $t$ , we can state that  $J_p$  is equal to the worth of neutrons generated from fragments in the time  $\Delta t$ , plus the worth of the fragments remaining by the time  $t + \Delta t$ :

$$NC_i^+(\bar{r}, t) = N\lambda_i \Delta t \frac{1}{4\pi} \int d\bar{v} \lambda_i(v) F^+(\bar{r}, \bar{v}, t) + N(1 - \lambda_i \Delta t) C_i^+(\bar{r}, t + \Delta t).$$

Expanding this into a series in  $\Delta t$  and retaining first-order terms, we can obtain equations for  $C_i^+(r, t)$ .

In addition, delayed neutrons have to be taken into account in the equation for  $F^+(\bar{r}, \bar{v}, t)$ . Continuing the discussion in [2], we find that they produce  $Nv\Delta t\nu\Sigma_f\beta_i$  fragments of the  $i$ -th kind in a time  $\Delta t$  after  $N$  neutrons arrive at point  $r$  with velocity  $v$ , and the worth of each of them is  $C_i^+(\bar{r}, t)$ .

As a result we obtain the following system of equations for the worths  $F^+$ ,  $C_i^+$  which becomes, in the usual notation,

$$\begin{aligned} -\frac{1}{v} \cdot \frac{\partial F^+}{\partial t} + \hat{L}^+ F^+ + \frac{\nu\Sigma_f}{4\pi} \sum_i \beta_i \int d\bar{v}' F^+ \lambda_i = \nu\Sigma_f \sum_i \beta_i C_i^+ + P(\bar{r}, \bar{v}, t); \\ -\frac{\partial C_i^+}{\partial t} = -\lambda_i C_i^+ + \frac{\lambda_i}{4\pi} \int d\bar{v}' F^+ \lambda_i. \end{aligned} \quad (1)$$

Treating this system as an equation for the "vector"  $F^+(F^+, C_1^+, C_2^+, \dots, C_n^+)$ ;  $\hat{\mathcal{L}}^+ F^+ = P$ , there is little difficulty in establishing its Hermitean conjugacy with respect to the basic system of equations of kinetics for the "vector"  $F(F, C_1, C_2, \dots, C_n)$  (here  $F$  is the neutron flux, and  $C_1, C_2, \dots, C_n$  are the concentrations of the sources of delayed neutrons):

$$\begin{aligned} \frac{1}{v} \cdot \frac{\partial F}{\partial t} + \hat{L}F + \frac{\sum_i \beta_i \lambda_i}{4\pi} \int d\bar{v}' F \nu \Sigma_f = \frac{1}{4\pi} \sum_i \lambda_i C_i \lambda_i(v) + Q(\bar{r}, \bar{v}, t); \\ \frac{\partial C_i}{\partial t} = -\lambda_i C_i + \beta_i \int d\bar{v}' F \nu \Sigma_f. \end{aligned} \quad (2)$$

Here  $\hat{L}$  is the operator of the stationary transport equation (and  $\hat{L}^+$  is the operator adjoint to it):

$$\hat{L}F = \frac{v}{v} \nabla F + F\Sigma - \int d\bar{v}' F \Sigma_s(\bar{v}' \rightarrow \bar{v}) - \frac{\chi(v)}{4\pi} \int d\bar{v}' F \nu \Sigma_f$$

Translated from *Atomnaya Énergiya*, Vol. 32, No. 1, pp. 57-58, January, 1972. Original article submitted February 15, 1971.

© 1972 Consultants Bureau, a division of Plenum Publishing Corporation, 227 West 17th Street, New York, N. Y. 10011. All rights reserved. This article cannot be reproduced for any purpose whatsoever without permission of the publisher. A copy of this article is available from the publisher for \$15.00.

and the fission-neutron spectrum

$$\chi(v) = (1-\beta)\chi_0(v) + \sum_i \beta_i \chi_i(v),$$

where  $\chi_0$  and  $\chi_i$  are the spectra of the prompt and delayed neutrons, respectively. Equations (1) can also be derived by a formal conjugation operation applied to the system of Eqs. (2).

Equations (1) and (2) can be solved by resorting to an eigenvalue series expansion. With the substitution into the homogeneous systems (1) and (2) of

$$\begin{aligned} F(\bar{r}, \bar{v}, t) &= \Phi_\alpha(\bar{r}, \bar{v}) e^{\alpha t}, \quad C_i(\bar{r}, t) = C_{i\alpha}(\bar{r}) e^{\alpha t}; \\ F^+(\bar{r}, \bar{v}, t) &= \Phi_{\alpha'}^+(\bar{r}, \bar{v}) e^{-\alpha' t} \quad \text{and} \quad C_i^+ = C_{i\alpha'}^+(\bar{r}) e^{-\alpha' t}, \end{aligned} \quad (3)$$

we find, for the eigenfunctions of the system of equations (cf. [3]):

$$\hat{L}\Phi_\alpha + \frac{\alpha}{v}\Phi_\alpha + \frac{\sum_i \beta_i \chi_i}{4\pi} \int d\bar{v}' \Phi_\alpha v \Sigma_f = \frac{1}{4\pi} \sum_i \lambda_i \chi_i C_{i\alpha}; \quad (4)$$

$$(\alpha + \lambda_i) C_{i\alpha} = \beta_i \int d\bar{v}' \Phi_\alpha v \Sigma_f;$$

$$\hat{L}^+ \Phi_{\alpha'}^+ + \frac{\alpha'}{v} \Phi_{\alpha'}^+ + \frac{v \Sigma_f}{4\pi} \sum_i \beta_i \int d\bar{v}' \Phi_{\alpha'}^+ \chi_i = v \Sigma_f \sum_i \beta_i C_{i\alpha'}^+; \quad (5)$$

$$(\alpha' + \lambda_i) C_{i\alpha'}^+ = \frac{\lambda_i}{4\pi} \int d\bar{v}' \Phi_{\alpha'}^+ \chi_i.$$

Eliminating  $C_{i\alpha}$  and  $C_{i\alpha'}^+$  in systems (4) and (5), we obtain the equations for the harmonics  $\Phi_\alpha$  and  $\Phi_{\alpha'}^+$ , directly:

$$\hat{L}\Phi_\alpha + \frac{\alpha}{v}\Phi_\alpha + \frac{\alpha}{4\pi} \sum_i \frac{\beta_i}{\alpha + \lambda_i} \chi_i \int d\bar{v}' \Phi_\alpha v \Sigma_f = 0; \quad (6)$$

$$\hat{L}^+ \Phi_{\alpha'}^+ + \frac{\alpha'}{v} \Phi_{\alpha'}^+ + \frac{\alpha' v \Sigma_f}{4\pi} \sum_i \frac{\beta_i}{\alpha' + \lambda_i} \int d\bar{v}' \Phi_{\alpha'}^+ \chi_i = 0.$$

It is readily seen that the functions  $\Phi_\alpha$  and  $\Phi_{\alpha'}^+$ , exhibit the orthogonality property. If we reconsider systems (4) and (5) as vector equations  $\hat{\mathcal{L}}\mathbf{F}_\alpha = 0$  and  $\hat{\mathcal{L}}^+\mathbf{F}_{\alpha'}^+ = 0$ , and multiply the first of them (as a scalar product) by  $\mathbf{F}_{\alpha'}^+(\Phi_{\alpha'}^+, C_{i\alpha'}^+)$ , and take the scalar product of the second by  $\mathbf{F}_\alpha(\Phi_\alpha, C_{i\alpha})$ , and subtract them (the scalar multiplication operation on the vectors includes summation with respect to the subscript  $i$ , with  $\Phi \equiv C_0$  assumed), we find that when  $\alpha \neq \alpha'$

$$\int d\bar{r} \left[ \int d\bar{v} \frac{\Phi_\alpha + \Phi_{\alpha'}^+}{v} + \sum_i C_{i\alpha} C_{i\alpha'}^+ \right] = 0,$$

i. e., the total worth of the neutrons and fragments of the  $\alpha$ -th harmonic with respect to the  $\alpha'$ -th harmonic is zero, and the harmonics are independent. The orthogonality condition for the harmonics of the neutron flux is found to be as follows:

$$\int d\bar{r} \int d\bar{v} \frac{\Phi_\alpha}{v} \left[ \Phi_{\alpha'}^+ + \frac{v \Sigma_f}{4\pi} \sum_i \frac{\lambda_i \beta_i}{(\alpha + \lambda_i)(\alpha' + \lambda_i)} \int d\bar{v}' \chi_i \Phi_{\alpha'}^+ \right] = 0. \quad (7)$$

For simplicity, we retain here only the real and simple eigenvalues. The analysis of the solutions and spectral properties of the equations may be found in [4].

Functions  $\Phi_{\alpha'}$ , which take into account both the discrete and the continuous portions of the spectrum, may provide what we would accept as a more natural basis for the solution of neutron kinetics problems by eigenfunction expansions than the "quasistationary" functions

$$\hat{L}\varphi_\alpha + \frac{\alpha}{v}\varphi_\alpha = 0, \quad (8)$$

resorted to by Pupko [5]. A certain artificiality noticeable in the selection of those functions for problems where delayed neutrons are taken into account cannot help but lead to a number of complications (interdependence of the harmonics, representation of time-exponential terms in other than finite form, in the form of series expansions in powers of the functions  $\varphi_{\alpha'}$ , and so forth).

The author acknowledges his indebtedness to V. Ya. Pupko, S. B. Shikhov, A. G. Shokod'ko, and G. Ya. Rumyantsev for most helpful counsel and discussion.

LITERATURE CITED

1. B. B. Kadomtsev, Dokl. Akad. Nauk SSSR, 113, No. 3 (1957).
2. G. I. Marchuk and V. V. Orlov, in: Neutron Physics [in Russian], Atomizdat, Moscow (1961).
3. T. Gozani, Nukleonik, B5, 55 (1963); A. Henry, Nucl. Sci. Engng., 20, 338 (1964).
4. S. B. Shikhov and A. A. Shkurpelov, in: Theoretical and Experimental Problems of Stationary Neutron Transport [in Russian], Atomizdat, Moscow (1971), p. 97.
5. V. Ya. Pupko, in: Theoretical and Experimental Problems of Stationary Neutron Transport [in Russian], Atomizdat, Moscow (1971), p. 166.

# A NEW PROCEDURE FOR MEASURING THERMAL COEFFICIENT OF REACTIVITY AND WORTH OF CONTROL SHIM RODS IN THE IGR REACTOR

V. D. Lavrenikov

UDC 621.039.522

The IGR reactor is a homogeneous uncooled uranium-graphite reactor [1]. Because of the absence of metallic structures, the core of this reactor can be heated to a rather elevated temperature ( $\sim 1400^\circ\text{K}$ ). The reactor is operated in two basic modes: a pulsed mode and a spiking mode. The spiking mode is an uncontrolled mode, the basic parameter being the initial reactivity. As a result of the introduction of excess reactivity generally in excess of the fraction of delayed neutrons, the reactor power level rises to some maximum value, and then decays as the core heats up (the reactor has a negative temperature coefficient of reactivity).

The pulsed mode is a controlled mode of reactor performance with a duration of 10 to 100 sec. The initial stage of this mode includes a specially selected spike with peak power slightly below the peak pulse power. A graph of the pulse shows a variety of pulse shapes: triangular, or various types of trapezoids. Near the top of the spike the shim rods are energized automatically, and these rods keep the power level subject to a prespecified law. Whatever the shape of the pulse these rods are constantly in motion, so that the negative reactivity appearing in response to heating of the reactor stacking is compensated.

The maximum temperature of the stacking is limited by the excess reactivity, so that the amount of heat generated in a pulse is likewise limited. Since dynamic measurements of the core temperature during the pulse are difficult to achieve, and the integrated current of the ionization chambers is proportional to the amount of heat released, we introduce the concept of the thermal coefficient of reactivity [2]:

$$\gamma(J) = \partial r / \partial J, \quad (1)$$

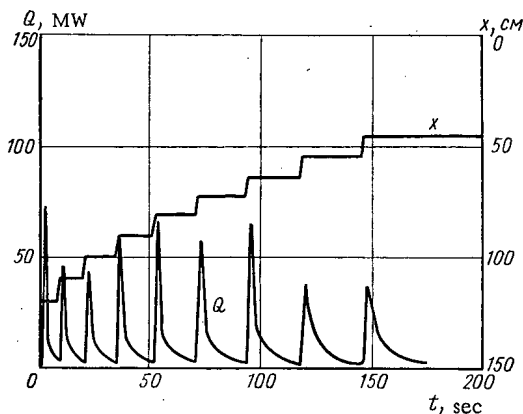


Fig. 1. Spike pulse.

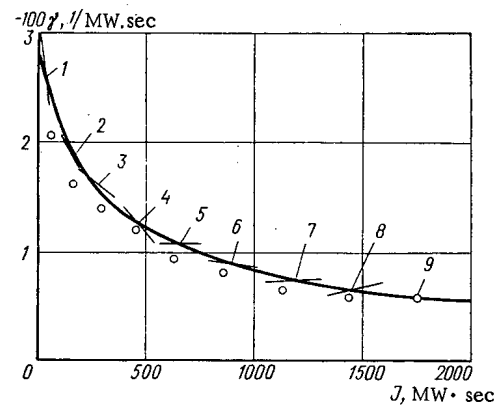


Fig. 2. Thermal coefficient of reactivity ( $\circ$  indicates operational measurement; 1-9 are spikes).

Translated from *Atomnaya Énergiya*, Vol. 32, No. 1, pp. 58-60, January, 1972. Original article submitted December 16, 1970.

© 1972 Consultants Bureau, a division of Plenum Publishing Corporation, 227 West 17th Street, New York, N. Y. 10011. All rights reserved. This article cannot be reproduced for any purpose whatsoever without permission of the publisher. A copy of this article is available from the publisher for \$15.00.

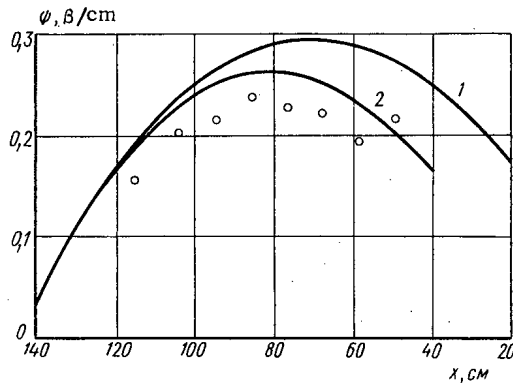


Fig. 3

Fig. 3. Worths of control rods in cold reactor [1] and during spike process [2] (O indicates operational measurement).

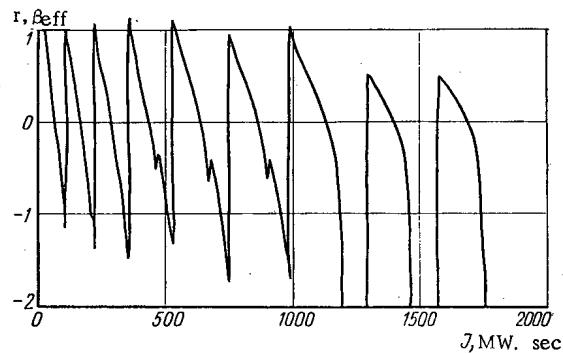


Fig. 4

Fig. 4. Operational measurement of thermal coefficient of reactivity and of worth of shim rods.

where  $r$  is the reactivity in fractions of  $\beta_{eff}$ ;  $J$  is the amount of heat released, in MW.sec. The worth of the shim rods

$$\psi(x) = \partial r / \partial x, \quad (2)$$

where  $x$  is the position of the rods in the core, in cm.

When investigating the dynamics of the IGR reactor, we have to know the parameters  $\gamma(J)$  and  $\psi(x)$  as accurately as possible, since the total reactivity is

$$r = r_0 + \int_0^J \gamma(J) dJ + \int_0^x \psi(x) dx, \quad (3)$$

where  $r_0$  is the initial reactivity in the spike. Equation (3) is valid in the case where the function  $J(x)$  is only slightly dependent upon the shape of the pulses, as observed in the IGR reactor for the pulse shapes actually in use.

Methods of measurement familiar in the current literature [3] are not applicable to the IGR reactor because of the way the parameters  $\gamma(J)$  and  $\psi(x)$  change during the pulse, on account of the intense heating of the reactor stacking. This paper presents an alternate procedure for independently measuring these two parameters throughout the range of heat generated.

The method involves basically separating out the reactivity components (3). The shim rods are withdrawn from the stacking stepwise each step being followed by a spike (Fig. 1). As the rods are being moved rapidly, the power varies insignificantly, and the reactivity (3) is determined by the component introduced by those rods [last term appearing in Eq. (3)]. When the rods are at rest, however, the reactivity (3) is dependent solely on the component related to the amount of heat released [next-to-last term in Eq. (3)].

The parameters of the spike and the number of spikes are selected such that the core will become heated to the peak temperature in about 5 min, so that dissipation of heat to the reflector will not have time to take effect. These parameters were determined beforehand on a test stand incorporating a model simulating the reactor and a real shim rod control servo system. A special device was also devised for use in the stepwise displacement of the shim rods.

The first spike develops after the first step is carried out. As soon as the power in the first spike falls to a preset level (20 to 2.6 MW in this case), the next step is carried out, followed in turn by the second spike. The reactor thus becomes a self-exciting spike generator. When a preset amount of heat has been generated the system shuts off.

The reactor power is recorded on a loop oscillograph as the train of spikes is being executed (ionization chambers provide data). The results are then processed. The processing includes compiling tables giving the time dependence of the power in this train of spikes. The amount of heat released  $J$  and the total

reactivity  $r$  are calculated from the tabular data on the basis of a special electronic digital computer program. The computer results are then sorted in order to isolate the dependence  $r(J)$  in the time intervals during which the shim rods are at rest. The dependence  $r(J)$  for each spike is approximated by second-order polynomials, on the basis of the method of least squares:

$$r(J) = a_0 + a_1J + a_2J^2, \quad (4)$$

where  $a_0$ ,  $a_1$ ,  $a_2$  are the coefficients of the approximating polynomial. Upon differentiating Eq. (4) with respect to  $J$ , we obtain

$$\gamma(J) = a_1 + 2a_2J. \quad (5)$$

Hence, the thermal coefficient of reactivity is approximated by segments of straight lines, for each spike (Fig. 2). The large error in the coefficient  $a_2$  in spikes 5, 7, 8 is explained by the fact that the shim rods execute slight displacements about their mean position in the intervals between steps, in response to the residual magnetization of the amplidyne. The continuous curve plotted in Fig. 2 shows the interpolation polynomial obtained via the method of least squares. The relative rms error in the measurement of  $\gamma(J)$  is roughly 5%.

The displacements of the shim rods were measured after each spike, with the object of measuring their worth. Moving-picture records were taken of the position indicators of the rods, on wide-format movie film. The recorded results, when processed, yield the rod displacement  $\Delta x$  in each step, and changes in the reactivity in each step  $\Delta r$  can be obtained from the results of computer processing of the power oscillograms. The worth of the shim rods in the  $k$ -th step is therefore

$$\bar{\psi}_k(\bar{x}_k) = \frac{\Delta r_k}{\Delta x_k}. \quad (6)$$

In order to improve the accuracy of calculations of the parameter  $\psi(x)$ , trapezoidal pulses were also used. The calculations relied on the use of the dependence  $\gamma(J)$  already based on Eq. (3). The results of those calculations were plotted as curve 2 in Fig. 3, while the worth of the shim rods in a cold reactor was plotted as curve 1.

Operational measurement of the parameters  $\gamma(J)$  and  $\psi(x)$  was carried out with the aid of a reactivity gage ("reactimeter") based on the MN-7 analog computer and an  $x$ - $y$  dataplotter, with voltage proportional to the amount of heat released  $J$  plotted on the  $x$ -axis and voltage proportional to the reactivity  $r$  plotted on the  $y$ -axis (Fig. 4). Processing of the recorded function  $r(J)$  yielded the parameters  $\gamma(J)$  and  $\psi(x)$  with the displacement of the shim rods in each step known. The error in the measurement of the parameters by that method is about 15%, the bulk of it being accounted for by the error in the electronic multiplier unit of the reactivity gage and the  $x$ - $y$  dataplotter.

The above procedure makes it possible to determine important parameters of pulsed reactors in a single pulse, to the desired accuracy, provided the experiment is prepared carefully. On-going operational measurements of these parameters call for the use of high-quality instrumentation.

The author is indebted to E. I. Krylatykh for invaluable assistance in carrying out the experiments.

#### LITERATURE CITED

1. I. V. Kurchatov et al., *At. Énerg.*, **17**, 463 (1964).
2. A. Ya. Kramerov and Ya. V. Shevelev, *Nuclear Reactor Engineering Calculations* [in Russian], Atomizdat, Moscow (1964).
3. J. R. Kipin, *Physical Fundamentals of Nuclear Reactor Kinetics* [Russian translation], Atomizdat, Moscow (1967).

# REDESIGN OF THE IRT-TM REACTOR DRY EXPERIMENTAL CHANNELS

O. F. Gusarov, V. V. Karnaukhov,  
and V. K. Leus

UDC 621.039.56

Irradiation of specimens in the vertical channels of IRT type reactors has been shown by experience to date to be associated with serious operating problems in the period of recharging through the channel plugs, in the first place, and to involve a lot of time spent in preparatory operations, in the second place, while the impossibility of charging and discharging specimens at power levels above 100 kW is the paramount problem overshadowing all the others.

Over a year and a half changes have been gradually introduced into the IRT-TM reactor design to convert to curved vertical channels having no plugs, and equipped with short top blind flanges. The curved channels permit charging and discharging of specimens at any reactor power level. We see clearly from Table 1 and Fig. 1 that the total background and the neutron background are both lower when curved vertical channels are used. Measurements were taken with official RUP-1 and Kran-1 dosimetric instruments. The optimum channel curvature which would eliminate direct streaming of neutrons out of the channel while being compatible with the necessary dimensions of the irradiation capsule were arrived at during the process of fabricating the channels. The arrangement of the channels in the reactor tank makes it possible to

TABLE 1. Background of Neutron Radiation and  $\gamma$ -Radiation on Top Face of IRT-TM Reactor

Measuring site (see Fig. 1)	Gamma-radiation, $\mu$ /sec		Thermal neutrons, neu- trons/cm $\cdot$ sec		Fast neu- trons, neu- trons/cm $^2 \cdot$ sec		Total dose, mrem/h	
	straight channels	curved channels	straight channels	curved channels	straight channels	curved channels	straight channels	curved channels
1	0,2 *	0,3 *	—	—	—	—	0,7	1
2	1,6 *	1,75 *	—	—	—	—	5,6	6,2
3	0,35 *	0,57	—	—	—	—	1,2	2
4	2,5 *	2,8 *	—	—	—	—	8,7	9,8
5	6 *	4,4 *	—	—	—	—	21	15,4
6	2,5 *	2,3 *	—	—	—	—	8,7	8
7	0,2 *	0,45 *	—	—	—	—	0,7	1,6
8	8,4	9	—	—	—	—	29,4	31,5
9	0,4 *	0,42 *	—	—	—	—	1,4	1,5
10	2,2 *	2,5 *	—	—	—	—	7,7	8,9
11	15	9,4	40	2,6	2	0-2	52,8	32,4
12	2 *	2,5 *	—	—	—	—	7	8,6
13	0,2 *	0,5 *	—	—	—	—	0,7	1,75
14	5	3,6	70	2,6	2	—	18	12,7
15	6	4	200	3,8	3	—	22,6	14
16	5	4,5	1200	2,8	4	—	22,5	15,7
17	4	3,5	50	5,2	2	—	14,5	12,3
18	4	3,6	70	5,4	2	—	14,5	12,6
19	3	3,6	470	2,7	2	—	12,5	12,6
20	0,7 *	1,2 *	—	2,3	—	—	2,4	4,2

\* Measurements taken at height of one meter from top face.

Translated from *Atomnaya Energiya*, Vol. 32, No. 1, pp. 60-62, January, 1972. Original article submitted December 14, 1970; revision submitted June 19, 1971.

© 1972 Consultants Bureau, a division of Plenum Publishing Corporation, 227 West 17th Street, New York, N. Y. 10011. All rights reserved. This article cannot be reproduced for any purpose whatsoever without permission of the publisher. A copy of this article is available from the publisher for \$15.00.

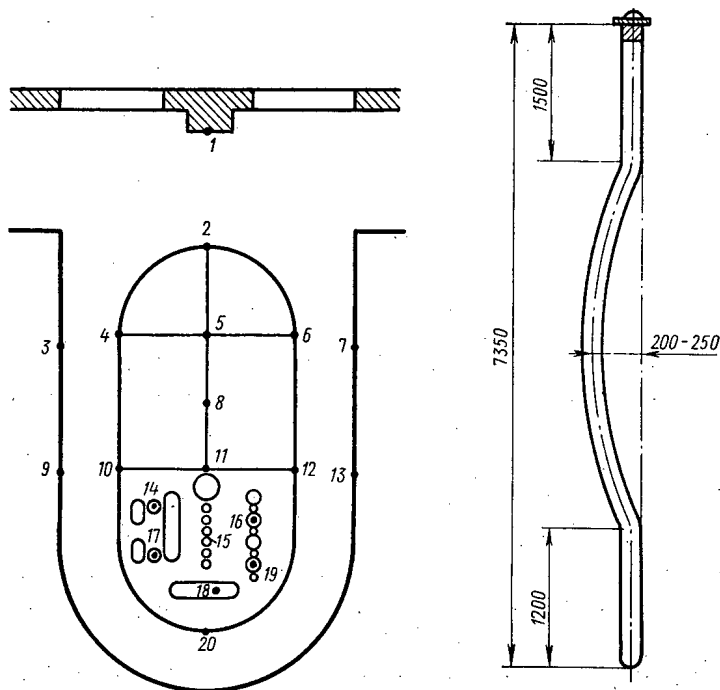


Fig. 1

Fig. 2

Fig. 1. Layout of top face of IRT-TM reactor (numerals indicate sites where dose rate measurements were taken).

Fig. 2. Diagram of curved channel with top blind flange.

carry out all of the in-core operations with freedom. A drawing of the channel with the top blind flange in place is shown in Fig. 2. The channel inner diameter was calibrated before the channel was installed in the core. This procedure facilitated optimization of the capsule dimensions for a tube of aluminum alloy AD 54 mm in diameter and 1.5 mm in wall thickness; the irradiation capsule is 46 mm in diameter and stands 200 mm high.

The following advantages of curved experimental channels were revealed in the course of operations:

1. Specimen charging and uncharging time was decreased tenfold in work with curved vertical channels, while irradiation exposure of attending personnel was reduced at the same time.
2. Background, both thermal and fast, on the top face was greatly reduced when direct streaming of radiation between the inner wall of the channel and the channel plug was eliminated.
3. The possibility of irradiating specimens in the experimental channels at any time and at any reactor power level came to light.

An insignificant increase in the total  $\gamma$ -emission background during the time the channels were being rebuilt was due to a buildup of induced activity in the structural materials and in the reactor tank water.



CRITICAL THERMAL FLUXES IN THE BOILING OF A EUTECTIC  
SODIUM - POTASSIUM ALLOY UNDER CONDITIONS OF FREE  
CONVECTION

V. I. Subbotin, D. N. Sorokin,  
A. P. Kudryavtsev, V. I. Brigutsa,  
and R. I. Zhirona

UDC 536.25:621.039.534.6

The critical thermal fluxes of sodium, cesium, and rubidium were studied in an earlier investigation, and the results were presented in [1]. For the fully-developed boiling of the alkali metals, the critical thermal fluxes measured in the range of reduced pressures in question ( $4 \cdot 10^{-5}$ - $3 \cdot 10^{-2}$ ) are given by the general relationship

$$q_{cr} = \left[ 1 + \frac{45}{Pr_{cr}} \left( \frac{p}{Pr_{cr}} \right)^{-0.4} \right] Br (g\gamma)^{1/2} [\sigma (\gamma - \gamma'')]^{1/4}. \quad (1)$$

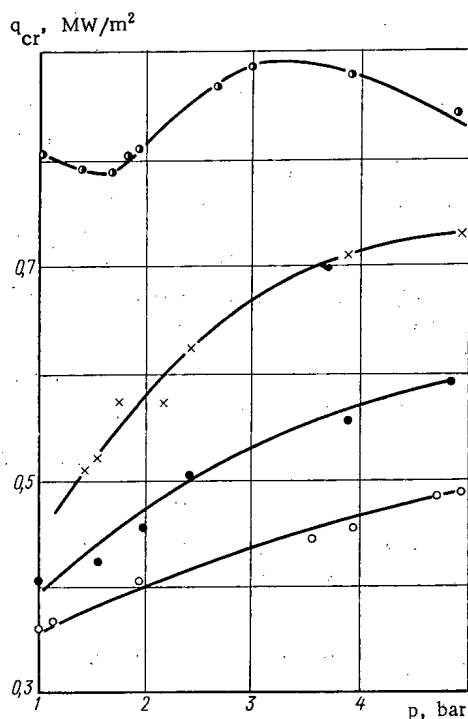


Fig. 1. Critical thermal fluxes for the boiling of organic binary mixtures under conditions of free convection [2]: (●) monoisopropylidiphenyl (MIPD)-benzene, concentration of low-boiling component 9%; (×) MIPD-benzene, concentration of low-boiling component 94%; (●) benzene; (○) MIPD.

Experimental investigations into the boiling of non-metallic binary mixtures [2-6] show that the critical fluxes and the pressure dependence of  $q_{cr}$  are considerably influenced by the concentrations of the components (Fig. 1). The critical thermal fluxes of binary mixtures are not accurately described by the generalized relationships holding for single-component nonmetallic liquids. It would appear just as unlikely that Eq. (1) could validly be used to calculate  $q_{cr}$  for the boiling of binary mixtures of alkali metals.

At the present time, the critical thermal flows associated with the boiling of binary mixtures of alkali metals can only be determined experimentally. However, the literature contains very little information on this question.

This paper is concerned with an experimental study of the critical thermal fluxes associated with the boiling of a eutectic sodium-potassium alloy (78% K and 22% Na by weight).

Boiling took place on a flat horizontal surface 38 mm in diameter, made of stainless steel. We used an alloy purified in a cold trap. The amount of oxygen in the sodium-potassium alloy before charging was  $10^{-3}$  wt.%. The experiments were carried out both under the pressure of the vapor itself and also under the pressure of an inert gas (argon), the argon pressure approximately corresponding to the saturation pressure,  $p_{gas} \leq p_{vap}$ . The method and apparatus were as described in [1].

Translated from *Atomnaya Energiya*, Vol. 32, No. 1, pp. 62-63, January, 1972. Original article submitted February 1, 1971.

© 1972 Consultants Bureau, a division of Plenum Publishing Corporation, 227 West 17th Street, New York, N. Y. 10011. All rights reserved. This article cannot be reproduced for any purpose whatsoever without permission of the publisher. A copy of this article is available from the publisher for \$15.00.

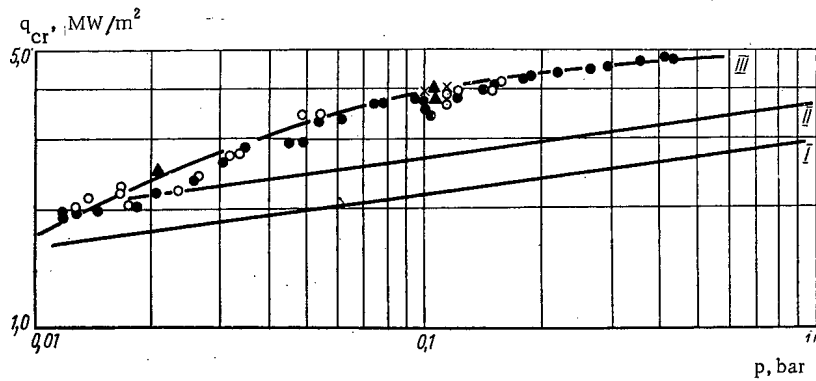


Fig. 2. Experimental data regarding the critical thermal fluxes in the boiling of a sodium-potassium alloy under conditions of free convection:  $\circ$ ,  $\bullet$ ) under the pressure of the vapor, first and second series of experiments respectively;  $\times$ ,  $\blacktriangle$ ) under the pressure of the argon, first and second series of experiments respectively; I) potassium, calculation from Eq. (1); II) sodium, calculation from Eq. (1); III) calculation from Eq. (2).

We made two series of experiments at pressures of approximately 0.012-0.45 and 0.013-0.17 kg/cm<sup>2</sup>. By a "series" we mean a set of experiments carried out on one particular working section, without cleaning the latter or changing the heat carrier. The results appear in Fig. 2. In one series of experiments the critical thermal fluxes were obtained at pressures of 0.02, 0.05, 0.1, and 0.42 kg/cm<sup>2</sup>, then the pressure was reduced to a minimum and the experiments were repeated. It follows from Fig. 2 that the reproducibility of the results was excellent. The saturation pressure was determined from the measured vapor pressure, using the pressure-temperature relationship on the saturation line given in [7]. Allowance was made for an "exposed column" correction, i. e., one associated with the height of the column of sodium-potassium alloy over the heat-transfer surface, this being particularly important at low pressures.

As in the case of sodium, potassium, and cesium [1], in the experiments with the sodium-potassium alloy we observed a variety of modes of heat transfer (for  $t_l \geq t_s$ ): convective heat transfer (even for very considerable temperature heads), with the subsequent outflow of heat by evaporation from the surface, heat transfer by unstable boiling, and heat transfer by fully-developed boiling. We also observed spontaneous transitions from one mode of heat transfer to another, the pressure and thermal flux remaining quite steady.

The critical thermal flux depends on the mode of heat transfer preceding the onset of the crisis [1]. Thus, in the sodium experiments, the critical thermal flux for developed boiling was much greater (roughly by a factor of two) than for unstable boiling.

In our experiments with the sodium-potassium alloy, the system only passed to the crisis in a state of developed boiling, so that the experimental results agreed closely together (Fig. 2).

In the sodium-potassium alloy, we were unable to detect influence of the inert gas (argon) on the stabilization of the boiling process such as appeared earlier in the case of sodium and potassium individually [1]. In the boiling of the sodium-potassium alloy under argon (the pressure of the gas being approximately equal to the saturation pressure) we noted a variety of modes of heat transfer, instability of boiling, and considerable pulsations in the wall temperature. The values of  $q_{cr}$  obtained for the boiling of the sodium-potassium alloy under argon pressure coincide with the values of  $q_{cr}$  corresponding to boiling under the ordinary vapor pressure (Fig. 2). For comparison, Fig. 2 shows the dependence of  $q_{cr}$  on pressure for sodium and potassium calculated from Eq. (1), which gives a fairly good representation of the experimental data relating to the developed boiling of these metals. We see that the nature of the relationship between  $q_{cr}$  and  $p_s$  for the sodium-potassium alloy is entirely different from that corresponding to sodium and potassium as such. The critical thermal fluxes for the Na-K alloy of eutectic composition are higher than those of the pure components.

The experimental data for the pressure range studied may be described by the empirical relation

$$q_{cr} = 5.8 \left( 1 - e^{-\frac{1}{1-p_s}} - e^{1-31p_s} \right) \cdot 10^6, \quad (2)$$

which in Fig. 2 corresponds to curve III. In Eq. (2)  $p_s$  is expressed in bars and  $q_{cr}$  in MW/m<sup>2</sup>.

Thus, for the sodium-potassium alloy, as for nonmetallic liquids, the pressure dependence of the critical thermal fluxes differs from that corresponding to the pure metals, while the values of  $q_{cr}$  may be much higher (Figs. 1 and 2).

In order to determine the influence of concentration on the critical thermal fluxes and on the character of the relationship between  $q_{cr}$  and  $p_s$  for various concentrations in binary mixtures of metals, further experiments will be needed, both for sodium-potassium and also for other alloys. In the boiling of metals, owing to their high thermal conductivity, the proportion of heat carried away from the heating surface by the vapor is smaller than in the case of nonmetallic liquids. We may therefore expect that in the case of metals the influence of concentration on the critical thermal fluxes will be less severe than in the case of nonmetallic liquids.

#### LITERATURE CITED

1. V. I. Subbotin et al., Heat Transfer in the Boiling of Metals under Conditions of Free Convection [in Russian], Nauka, Moscow (1969).
2. P. S. Sterman et al., Heat and Mass Transfer, Vol. 2 [in Russian], Nauka i Tekhnika, Minsk (1968).
3. V. G. Fastovskii et al., Teploénergetika, No. 8, 74 (1958).
4. G. I. Bobrovich et al., Prikl. Mekhan. i Teor. Fiz., No. 4, 137 (1962).
5. P. S. Sterman et al., Teploénergetika, No. 9, 59 (1967).
6. W. Van Wijk et al., Chem. Engng. Sci., 5, 68 (1956).
7. A. M. Belova, Dissertation [in Russian], Moscow (1969).

MEASUREMENT OF INTEGRATED CHARACTERISTICS OF  
SLOW-NEUTRON SPECTRUM OF VVR-M CRITICAL  
ASSEMBLY

A. V. Nikonov and V. B. Klimentov

UDC 621.039.512.44

The concept of effective neutron temperature is applied to highly thermalized spectra. It has been shown, however, that [1-3] despite the restrictions associated with assumptions of a Maxwellian predominantly thermal part of the spectrum and the  $1/E$  dependence of the epithermal component, the effective neutron temperature concept has proved applicable equally well to slightly enriched systems moderated by ordinary water. In some instances the neutron temperature has been estimated for highly enriched uranium-water lattices [4].

The integral method of determining effective neutron temperature [5] has been applied in investigations of the uranium-water lattice of the VVR-M critical assembly [6] with fuel elements 36% enriched, to check the validity of the method under those conditions. Lutecium, indium, and dysprosium indicators in the form of foils with respective effective thicknesses 0.07, 1.20, and 0.84 mg/cm<sup>2</sup> were employed. A control experiment revealed the virtual absence of any perturbation of the neutron field by those indicators.

The activation indicators were normalized with respect to the spectrum of a graphite column dimensioned 160 × 140 × 120 mm adjacent to the core of the critical assembly. With the close-to-Maxwellian spectrum taken into account, the indicators were placed in the thermal column at a distance of 70 cm from the edge of the core and 10 cm above the top edge of the core. The cadmium ratios measured with the aid of Dy<sup>164</sup> and In<sup>115</sup> indicators, with corrections for attenuation of the cadmium-moderated neutrons ( $F_{Cd}^{Dy} = 2.4$  [7] and  $F_{Cd}^{In} = 1.065$  [8]), were:

$$R_{Cd}^{Dy} = 536 \pm 25; R_{Cd}^{In} = 30 \pm 2.$$

The ratio  $r\sqrt{T_n/T_0}$ , characterizing the fraction of slowing-down neutrons in the spectrum, was not large:  $(1.81 \pm 0.16) \cdot 10^{-3}$ . It was determined from the cadmium ratio for indium:

$$r\sqrt{\frac{T_n}{T_0}} = \frac{1}{(R_{Cd}-1)\frac{S_0}{g} + R_{Cd}\left(\frac{1}{K}-W\right)}, \quad (1)$$

and the correction factors were assigned the values:  $K = 2.07$ ,  $W = 0.245$ ,  $S_0 = 18.8$  [9]. The value of  $g$  was determined by Westcott's method for the thermodynamic temperature of the thermal column  $t = 15^\circ\text{C}$  [ $g(15^\circ\text{C}) = 1.018$ ].

TABLE 1. Spectral Characteristics of the VVR-M Lattice

Measurement site	$U_x^{Lu}$	$U_x^{In}$	$r\sqrt{T_n/T_0}$	$T_n, ^\circ\text{C}$	$T_n(^{\circ}\text{K})/T_m(^{\circ}\text{K})$
Fuel element surface	$1.46 \pm 0.12$	$3.34 \pm 0.13$	0.1254	$138 \pm 22$	1.43
Water gap	$1.22 \pm 0.10$	$2.90 \pm 0.12$	0.1027	$56 \pm 11$	1.14
Water cavity	$1.14 \pm 0.10$	$1.96 \pm 0.09$	0.053	$36 \pm 7$	1.07

Translated from *Atomnaya Énergiya*, Vol. 32, No. 1, pp. 64-65, January, 1972. Original article submitted January 21, 1971.

© 1972 Consultants Bureau, a division of Plenum Publishing Corporation, 227 West 17th Street, New York, N. Y. 10011. All rights reserved. This article cannot be reproduced for any purpose whatsoever without permission of the publisher. A copy of this article is available from the publisher for \$15.00.

The quantity measured was the spectral ratio  $U_x$  defined as the ratio of  $\beta$ -activities of the spectrally sensitive indicator and of the type  $1/v$  indicator (in this case  $\text{Lu}^{176}$  and  $\text{Dy}^{164}$ ) normalized with respect to the spectrum of the thermal column:

$$U_x^{\text{Lu}} = \left( \frac{A^{\text{Lu}}}{A^{1/v}} \right)_x / \left( \frac{A^{\text{Lu}}}{A^{1/v}} \right)_{\text{tc}}$$

In Westcott's representation, this ratio becomes

$$U_x^{\text{Lu}} = \frac{(g+r\sqrt{T_n/T_0}S_0)_x}{(g+r\sqrt{T_n/T_0}S_0)_{\text{tc}}} \quad (2)$$

Using the experimental values of  $U_x^{\text{Lu}}$  and the tabulated values of  $g$  and  $S_0$  [9], we can determine the effective neutron temperature of the thermal spectrum under the condition that the characteristic  $r\sqrt{T_n/T_0}$  be known. This quantity can be determined from the spectral ratio for  $\text{In}^{115}$  and  $\text{Dy}^{164}$  ( $U_x^{\text{In}}$ ):

$$r\sqrt{\frac{T_n}{T_0}} = \frac{U_x^{\text{In}} X_{\text{tc}} - g^{\text{In}}}{S_0^{\text{In}} - U_x^{\text{In}} X_{\text{tc}} S_0^{1/v}}, \quad (3)$$

where

$$X_{\text{tc}} = \left[ \frac{g^{\text{In}} + r\sqrt{\frac{T_n}{T_0}} S_0^{\text{In}}}{1 + r\sqrt{\frac{T_n}{T_0}} S_0^{1/v}} \right]_{\text{tc}}$$

The system of equations (2) and (3) was solved by the method of iterations, and the values of  $g$  and  $S_0 = \sqrt{T_0/T_n}$  were determined from Westcott's tabular data [9].

Measurements were taken at three lattice points: on the surface of the fuel element, at the center of a water gap of thickness 3 mm, and at the center of the water cavity filled as a result of extraction of the hexagonal fuel element (width across flats 3.5 cm). Results of the measurements appear in Table 1.

The ratio of the measured neutron temperature  $T_n$  to the physical temperature of the moderator  $T_m$  proved to be beyond the range of validity of Westcott's spectral model ( $T_n/T_m < 1.07$ ) both for the fuel element surface and for the water gap. Clearly, the measured  $T_n$  values have no rigorously physical meaning under those conditions and can be used only as variables qualitatively illustrating changes in the slow-neutron spectrum in the reactor lattice. In contrast to the neutron temperature, the spectral ratios  $U_x$  are not related either to any models of the spectrum or to the accompanying restrictions. They are therefore treated as objective characteristics of the spectrum of the lattice under investigation.

The cited  $T_n$  values are in satisfactory agreement with published experimental data [4], where  $T_n = 123 \pm 21^\circ \text{C}$  was obtained for the surface of the highly enriched fuel element in the Melusine reactor.

#### LITERATURE CITED

1. S. Tassan, Nucl. Sci. Engng., 26, 271 (1966).
2. J. Volpe, Neutron Thermalization and Reactor Spectra, Vol. II, Vienna, IAEA (1968), p. 209.
3. N. Bauman et al., Neutron Thermalization and Reactor Spectra, Vol. II, IAEA, Vienna (1968), p. 177.
4. Neutron Fluence Measurements, 68-70, IAWA, Vienna (1970), STI/DOC/10/107.
5. C. Westcott et al., Proc. of the Second Intern. Conf. on the Peaceful Uses of Atomic Energy, Geneva (1958), P/202.
6. V. B. Klimentov et al., At. Énerg., 20, 63 (1966).
7. K. Beckurtz and K. Wirtz, Neutron Physics [Russian translation], Atomizdat, Moscow (1968).
8. G. A. Kopchinskii et al., At. Énerg., 24, 68 (1968).
9. C. Westcott, AECL-1101, CRRP-960 (1960).

POSSIBILITY OF MEASURING THE SPECTRAL CHARACTERISTICS  
OF A NEUTRON FLUX USING DIRECT-CHARGE DETECTORS

V. S. Kirsanov, M. G. Mitel'man,  
N. D. Rozenblyum, E. N. Babulevich,  
V. A. Zagadkin, and Yu. M. Shipovskikh

UDC 621.039.519

In connection with the use of various types of reactors it is of considerable interest to know the spectral characteristics of the neutron flux. As a first practical approximation the concept of the cadmium ratio is widely employed, this being based on the two-group representation of the neutron flux in which the latter is separated into thermal and superthermal parts [1]. At the present time the method of radioactive indicators is extensively employed in determining the cadmium ratio [1, 2].

The main disadvantage of the method is its laboriousness and the lack of operator control in the measurements.

Considering the fact that the direct-charge detector is metrologically identical with the method of radioactive indicators, it was earlier proposed [3, 4] to use a detector of this kind with a cadmium filter in order to determine the cadmium ratio. However, the use of a detector with a filter has considerable disadvantages:

- the rapid burn-up of the filter on continuously operating in strong thermal neutron fluxes;
- the greater size required for a detector with a filter;
- the fact that an absorbing filter introduces serious perturbations into the thermal-neutron flux close to the detector. The method of two detectors, analogous to the method of two foils [1, 2] overcomes these disadvantages.

Let there be two detectors with different emitter materials, then

$$\left. \begin{aligned} i_1 &= \varphi_1^T \Phi_T + \varphi_1^S \Phi_S; \\ i_2 &= \varphi_2^T \Phi_T + \varphi_2^S \Phi_S, \end{aligned} \right\} \quad (1)$$

where  $i_1, i_2$  are the currents of the detectors;  $\varphi_1^T, \varphi_2^T, \varphi_1^S, \varphi_2^S$  are the sensitivities of the detectors in the thermal and superthermal regions;  $\Phi_T, \Phi_S$  are the thermal- and superthermal-neutron fluxes. On the basis of the system of Eqs. (1) we may write the cadmium ratio in the form

$$R = \frac{i_1}{i_2} = \frac{\varphi_1^S / \varphi_1^T - \varphi_2^S / \varphi_2^T}{\varphi_1^S (1/\varphi_1^T - i_2/i_1 \cdot 1/\varphi_2^T)}, \quad (2)$$

where  $i_2$  is the current of the first detector due to the superthermal neutrons.

An experimental verification of the method of two detectors was carried out in the MR reactor of the I. V. Kurchatov Institute of Atomic Energy. Detectors were made with rhodium, vanadium, and

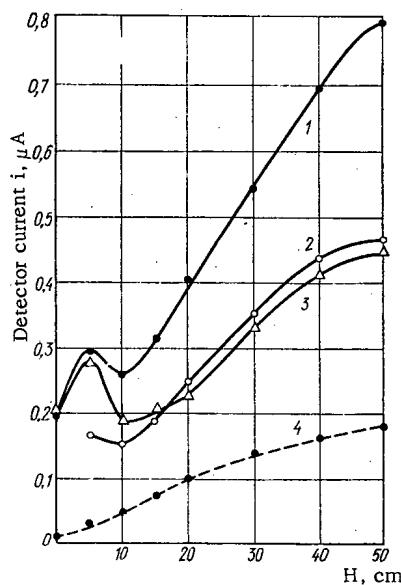


Fig. 1. Distribution of neutron flux over the height of the reactor channel plotted by means of various direct-charge detectors: 1) rhodium; 2) silver; 3) vanadium; 4) rhodium with a cadmium filter.

Translated from *Atomnaya Énergiya*, Vol. 32, No. 1, pp. 65-66, January, 1972. Original article submitted February 1, 1971.

© 1972 Consultants Bureau, a division of Plenum Publishing Corporation, 227 West 17th Street, New York, N. Y. 10011. All rights reserved. This article cannot be reproduced for any purpose whatsoever without permission of the publisher. A copy of this article is available from the publisher for \$15.00.

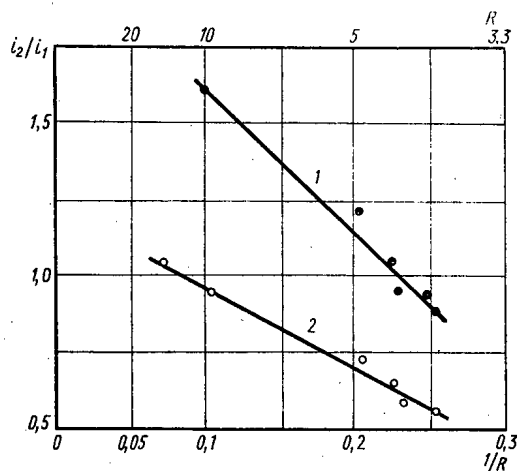


Fig. 2. Dependence of the current ratio of two detectors on the cadmium ratio with respect to rhodium:  $i_1$  corresponds to the current of a silver direct-charge detector for curve 1, and to that of a rhodium detector for curve 2;  $i_2$  corresponds to the current of a vanadium detector.

silver emitters and also one detector with a rhodium emitter and a cadmium filter. The length of the sensitive part (the emitter) was 25 mm in each detector.

We measured the distribution of the detector readings over the height of the active zone of the reactor. The results of the measurements for the upper half of the active zone are indicated in Fig. 1. Equation (2) may be expressed in the form

$$i_2/i_1 = -a \cdot 1/R + b, \quad (3)$$

where  $a$  and  $b$  are constant coefficients; Fig. 2 gives the current ratios  $i_V/i_{Ag}$  and  $i_V/i_{Rh}$  as functions of  $1/R_{Rh}$ , this being the reciprocal of the cadmium ratio with respect to the rhodium direct-charge detector and being calculated from the results of Fig. 1. It follows from Fig. 2 that with increasing current ratio the quantity  $1/R_{Rh}$  tends to diminish. We see furthermore that the relationship in question obeys a law corresponding to Eqs. (2) and (3).

We have thus shown that by using the two-detector method we may measure the cadmium ratio and thus secure data relating to the spectral characteristics of the neutron flux.

#### LITERATURE CITED

1. K. Bekurtz and K. Wirtz, Neutron Physics [Russian translation], Atomizdat, Moscow (1968).
2. E. I. Biryukov, P. N. Khrarov, and N. S. Shimanskaya, *At. Énerg.*, 28, 357 (1970).
3. N. D. Rozenblyum et al., Large-Dose Dosimetry [in Russian], FAN, Tashkent (1966), p. 135.
4. A. E. Alekseev, E. N. Babulevich, et al., *At. Énerg.*, 28, 139 (1970).

# SPECTROMETRY OF LOW-ENERGY IONS BY SURFACE-BARRIER SILICON DETECTORS

G. F. Bogdanov and B. P. Maksimenko

UDC 539.1.074

The present note reports investigations on the pulse height characteristics and the energy resolution of surface-barrier silicon detectors ( $t = 18^\circ\text{C}$ ) for the ions  $\text{H}_1^+$ ,  $\text{He}_4^{++}$ ,  $\text{Li}_7^+$ ,  $\text{C}_{12}^{++}$ ,  $\text{N}_{14}^{++}$ ,  $\text{O}_{16}^{++}$ ,  $\text{Ar}_{40}^{++}$  in the energy range 20-200 keV.

The detectors consist of n-type silicon of resistivity  $\sim 200\text{-}300 \Omega \cdot \text{cm}$ . The thickness of the gold entrance window (dead band) is  $\sim 40 \mu\text{g}/\text{cm}^2$ , corresponding to a sensitive area of  $7\text{-}10 \text{ mm}^2$ . At  $t = 18^\circ\text{C}$  the reverse current was not more than  $5 \cdot 10^{-8} \text{ A}$  at the working voltage of 50 V. The detectors were operated in conjunction with a vacuum-tube spectrometer arrangement, the intrinsic noise of which corresponded to the total width of the peak at half height (WPHH), equal to 3.5 keV. The detectors were tested on a magnetic

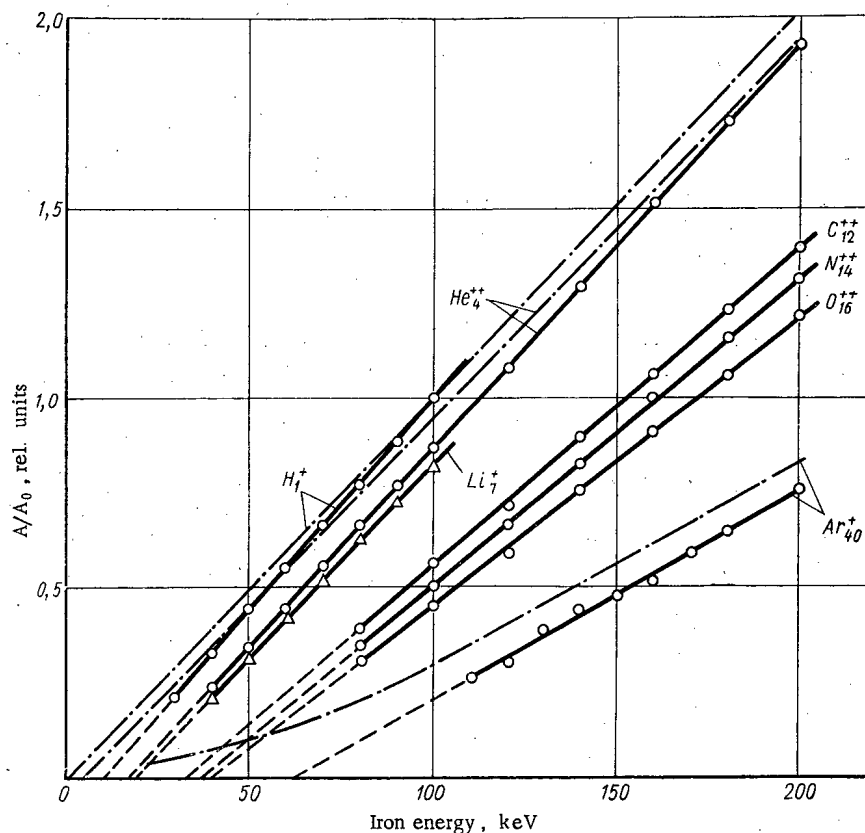


Fig. 1. Height of detector pulse as function of ion energy. The dot-dash lines show the calculated curves.  $A_0$  is the pulse height for 100 keV  $\text{H}_1^+$  ions.  $A$  is the pulse height of the various ions.

Translated from *Atomnaya Energiya*, Vol. 32, No. 1, pp. 66-68, January, 1972. Original article submitted December 17, 1970.

© 1972 Consultants Bureau, a division of Plenum Publishing Corporation, 227 West 17th Street, New York, N. Y. 10011. All rights reserved. This article cannot be reproduced for any purpose whatsoever without permission of the publisher. A copy of this article is available from the publisher for \$15.00.



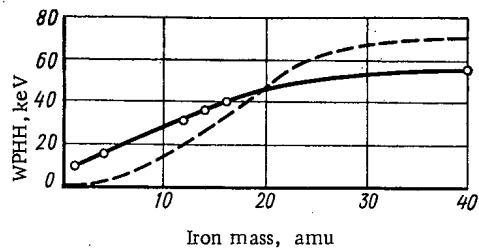


Fig. 2

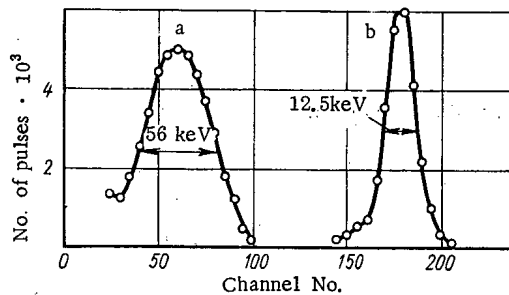


Fig. 3

Fig. 2. Dependence of WPHH on ion mass for an ion energy of 140 keV. The dashed line shows the calculated curve.

Fig. 3. Detector pulse height distribution for 140 keV  $\text{Ar}_{40}^{++}$  and  $\text{He}_4^{++}$  (a and b respectively).

separator fed with multienergetic beams of the above ions. The energy dispersion of the ions in the beam at the separator output was not more than 1%.

Figure 1 shows the pulse height characteristics of the detector for the various ions. The theoretical characteristics calculated with loss of energy of the ions by atomic scattering taken into account are shown by the dot-dash lines. In the calculations we utilized the data given in [1, 2] (for  $\text{H}_1^+$  and  $\text{He}_4^{++}$ ) and in [3] (for  $\text{Ar}_{40}^{++}$ ). Energy losses of ions in the dead band of the window were ignored. It can be seen that for all ions the detector has linear pulse height characteristics, the slope of which decreases and the "cutoff" (distance from the origin to the point where the extrapolated characteristic intersects the axis of abscissas) of which increases with increasing ion mass. Increasing the ion mass is accompanied by a marked rise in the WPHH (Fig. 2). Below  $0_{16}^{++}$  the measured value is greater than calculation, while above  $0_{16}^{++}$  the opposite is the case. Figure 3 shows the pulse height distribution for the ions  $\text{Ar}_{40}^{++}$  and  $\text{He}_{16}^{++}$  at an energy of 140 keV.

The measured pulse height characteristics are in good agreement with the results cited in [4] for the ions  $\text{H}_1^+$ ,  $\text{He}_4^+$ ,  $\text{N}_{14}^+$  and  $\text{Ne}_{20}^+$ , which were obtained ( $t = 18^\circ\text{C}$ ) with a detector of comparatively low-resistivity silicon ( $\sim 150 \Omega \cdot \text{cm}$ ). For example, for  $\text{N}_{14}^+$  cutoff and WPHH were found in [4] to be 35 and 34 keV respectively. Our values are 37 and 36 keV respectively. Our detectors have a better resolution and smaller cutoff values than the cooled ( $t = -100^\circ\text{C}$ ) detectors of higher-resistivity silicon ( $\sim 10\text{-}20 \text{ k}\Omega \cdot \text{cm}$ ) utilized in [5] for the spectrometry of  $\text{H}_1^+$ ,  $\text{He}_4^+$ ,  $\text{N}_{14}^+$ ,  $\text{Ne}_{20}^+$ , and  $\text{Ar}_{40}^+$ . For  $\text{Ar}_{40}^+$ , for example, cutoff and WPHH in [5] amount respectively to 24 and 6.5 keV, whereas in our case the values are 64 and 56 keV. It is significant that the reduction in the WPHH by a factor of 8.6 cannot be due to cooling alone.

The feature of a sizable pulse height defect in the recording of heavy ions suggests that surface-barrier silicon detectors can be used for a rough mass analysis, for example, of two-component multienergetic beams consisting of light and heavy ions.

In conclusion we wish to thank G. M. Novikov for presenting the detectors and V. V. Strulev and B. G. D'yakonov for their help with the measurements.

#### LITERATURE CITED

1. J. Lindhard et al., Kgl. danske vid. selskab. Mat.-fus. medd., 33, No. 10 (1963).
2. H. Schiott, *ibid.*, 35, No. 9 (1966).
3. E. Haines and A. Whitehead, Rev. Scient. Instrum., 37, 190 (1966).
4. G. Forcinal, P. Siffert, and A. Coche, IEEE Trans., NS-15, 475 (1968).
5. J. Ray and C. Barnett, *ibid.*, NS-16, 82 (1969).

## MEASUREMENT OF NEUTRON SPECTRA WITH THRESHOLD DETECTORS

K. K. Koshaeva, S. N. Kraitor,  
and L. B. Pikel'ner

UDC 539.12.08

Neutron spectra are measured with a set of threshold detectors whose operation depends on the fission of heavy nuclei by neutrons. The most widely used is the Hurst set consisting of  $U^{238}$ ,  $Np^{237}$ , and  $Pu^{239}$  behind a filter of  $2.2 \text{ g/cm}^2$  of  $B^{10}$  and supplemented by  $S^{32}$  [1]. We consider in detail the characteristics of a set of detectors as applied to actual neutron spectra and take as an example of an alternative  $U^{235}$ ,  $U^{235} + Cd$  and  $U^{235}$ ,  $Np^{237}$ ,  $U^{238}$ , and  $S^{32}$  behind a filter of  $1 \text{ g/cm}^2$  of  $B^{10}$ ; we propose a new interpretation of the data below the  $Np^{237}$  fission threshold which enables the accuracy of spectrometric measurements to be increased.

In recording neutrons with threshold detectors the energy dependence of the fission cross section  $\sigma(E)$  is replaced by an effective cross section which is assumed constant above the energy threshold and zero below. The effective cross section is related to the energy threshold  $E_{thr}$  by the expression

$$\sigma_{eff} \int_{E_{thr}}^{\infty} \Phi(E) dE = \int_0^{\infty} \sigma(E) \Phi(E) dE,$$

where  $\Phi(E)$  is the differential neutron flux. Since  $\sigma_{eff}$  and  $E_{thr}$  depend on the form of the function  $\Phi(E)$ ,  $\sigma_{eff}$  can be computed as a function of  $E_{thr}$  for various actual neutron spectra. The necessary data on the  $Np^{237}$  and  $U^{238}$  fission cross sections and the  $S^{32}(n, p)P^{32}$  cross section were obtained from [2, 3]. Since we consider an arrangement in which  $Np^{237}$  is behind a  $1 \text{ g/cm}^2$  filter of  $B^{10}$ , its subthreshold fission is not taken into account [4].

Data have been obtained on calculated and experimental spectra of various critical assemblies and reactors [5, 6]. The results for  $U^{238}$  are shown in Fig. 1. The figure shows the maximum deviation of the effective cross section  $\eta$  from the mean for various threshold energies. The figure indicates the value of the threshold energy for which the spread of the effective cross section is minimum. Henceforth the cross section and energy are taken as  $1.55 \text{ b} (\pm 2\%)$  and  $0.56 \text{ MeV}$  for  $Np^{237}$ ,  $0.525 \text{ b} (\pm 4\%)$  and  $1.4 \text{ MeV}$  for  $U^{238}$ , and  $0.28 \text{ b} (\pm 5\%)$  and  $2.8 \text{ MeV}$  for  $S^{32}$ .

Since the energy dependence of the  $U^{235}$  fission cross section with a  $1 \text{ g/cm}^2$   $B^{10}$  filter is far from that of an ideal threshold detector [7], the whole energy range from  $10^2$  to  $10^7$  eV was divided into two parts, one below a few hundred keV and the other above. The characteristics of the system were investigated separately in these energy ranges. The boundary between them was taken as the  $Np^{237}$  threshold

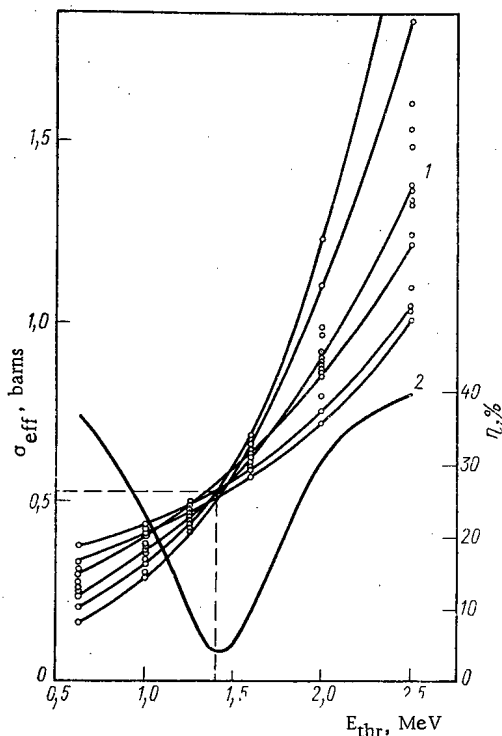


Fig. 1. Effective  $U^{238}$  fission cross section (curve 1) and its maximum deviation from the mean  $\eta$  (curve 2) for various neutron spectra as functions of the threshold energy.

Translated from *Atomnaya Energiya*, Vol. 32, No. 1, pp. 68-70, January, 1972. Original article submitted December 14, 1970.

© 1972 Consultants Bureau, a division of Plenum Publishing Corporation, 227 West 17th Street, New York, N. Y. 10011. All rights reserved. This article cannot be reproduced for any purpose whatsoever without permission of the publisher. A copy of this article is available from the publisher for \$15.00.

TABLE 1. Maximum Errors in Determining the Neutron Flux in Particular Energy Ranges for Various Spectra

Energy range	Maximum error, %			
	fission spectrum	uranium-graphite reactor	water-cooled reactor	outside Rachel reactor shield
2,8-10,0 MeV	5	5	5	5
1,4-2,8 MeV	8	6,2	4,8	5,4
0,56-1,4 MeV	11	9,3	3,6	5,6
400 eV-0,56 MeV	14	10,4	10,4	10,3
0,4-400 eV	—	5,3	5,0	5,1
Integrated neutron flux with energies above 0.4 eV	3,2	5,1	6,8	6,9

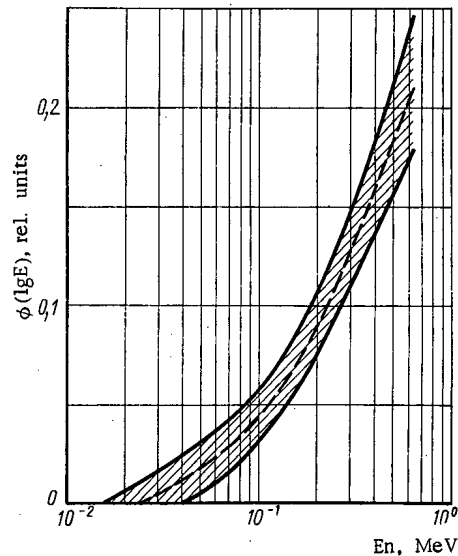


Fig. 2. Differential neutron spectra in the 0.04-0.56 MeV range minus the  $1/E$  part, and the average spectrum (broken curve).

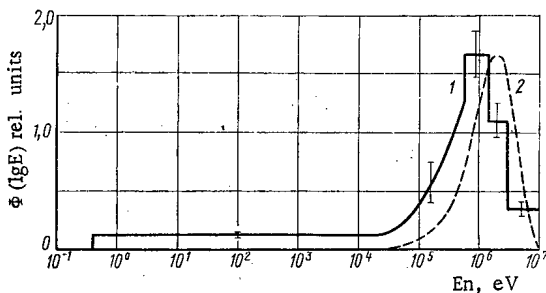


Fig. 3. 1) Neutron spectrum of OIYaI IBR reactor with a 4 cm water moderator; 2) fission spectrum.

energy 0.56 MeV. For energies above 0.56 MeV the calculated  $U^{235}$  fission cross section is  $1.21 \pm 0.02$  b, and below it is  $2.05 \pm 0.20$  b for  $E_{thr} = 400$  eV.

The average value of the  $U^{235}$  fission cross section, which is needed to determine the neutron flux below 400 eV, is calculated from the set of spectra to be  $33.4 \pm 1.5$  b. The  $U^{235}$  fission cross section for thermal neutrons is given in [8].

Thus the set of threshold detectors considered permits a sufficiently accurate determination of the neutron flux in the following energy ranges: 0.01-0.4, 0.4-400 eV, 400 eV-0.56 MeV, 0.56-1.4, 1.4-2.8, 2.8-10 MeV. Dividing these by the size of the energy range gives the average differential flux in each range. However, determining such neutron characteristics in the 400 eV-0.56 MeV range by using average fluxes can lead to appreciable errors. Therefore instead of the usual assumption on a uniform neutron distribution on a logarithmic energy scale in this range we propose another interpretation of the results.

An analysis of various neutron spectra indicates that the spectrum in the 400 eV-0.56 MeV range can be represented as the sum of a  $1/E$  part continued from the 0.4-400 eV range and a contribution in the 0.04-0.56 MeV range from neutrons undergoing moderation. Figure 2 shows the differential neutron spectra [5, 6] with the  $1/E$  contribution subtracted off and normalized to the same total flux in the 0.04-0.56 MeV range. It is clear from the figure that all the spectra lie in a rather narrow region between the solid curve and clearly admit the introduction of an average neutron spectrum (broken curve). A unit neutron flux with energies in the 0.04-0.56 MeV range can be represented to within 3 to 5% by the empirical relation

$$\Phi(\lg E) = 2.8 \cdot 10^{-6} (E - 10)(2000 - E),$$

where  $\Phi(\lg E)$  is the neutron flux per unit of the logarithm of the energy, neutrons/cm<sup>2</sup> log E, and E is the neutron energy in keV.

This method of determining the differential neutron flux has an accuracy of 28% at 100 keV and 14% at 400 keV.

The accuracy with which the average differential flux in other energy ranges, and the integrated flux can be measured depends on the spectrum. Calculations were made for the fission spectrum, spectra in uranium-graphite [9] and water-cooled water-moderated reactors [10], and the spectrum outside the shield of the Rachel reactor [10]. The results of the calculations are listed in Table 1.

The set of detectors considered was used to determine the neutron spectrum of the OIYaI IBR pulsed reactor [11]. The measurements were made at a distance of 10 m from the core with a 4 cm water moderator. The set of threshold detectors was constructed by placing inside a spherical shell of  $B^{10}$  1 g/cm<sup>2</sup> in thickness a cadmium liner containing an  $S^{32}$  pellet and the  $U^{238}$ ,  $Np^{237}$ , and  $U^{238}$  targets attached to silica glass plates for the detection of fission fragments. In order to compare readings in the low-energy range gold foils and thermoluminescent  $Li^6$  glasses [6] were irradiated simultaneously with the set of detectors.

The results of the measurement of the filtered neutron spectrum of the OIYaI IBR pulsed reactor are shown in Fig. 3. The figure also shows the undistorted fission spectrum (dashed curve) for comparison. As should be expected the IBR neutron spectrum is softer than the fission spectrum because of the energy drop in the core and the moderator.

The average differential flux of slow neutrons in the 0.4-400 eV range as measured by  $U^{235}$  detectors, thermoluminescent lithium glasses, and gold foils were respectively  $1.01 \pm 0.09$ ,  $1.02 \pm 0.12$ , and  $0.97 \pm 0.06$ , with the arithmetic mean of the three values being taken as unity. They agree within the limits of experimental error.

The authors thank I. B. Keirim-Markus for his interest in the work and for helpful discussion, I. A. Bochvar and T. I. Gimadovaya for supplying and measuring the thermoluminescent lithium glasses, I. I. Denisov and G. I. Sokolovaya for determining the activity of the gold foils, and N. T. Khot'ko for help with the measurements.

#### LITERATURE CITED

1. G. Hurst et al., *Rev. Sci. Instrum.*, 27, 153 (1956).
2. W. Hart, UK-USSR Seminar, Paper UK-10 (1968).
3. BNL-325, Sec. Ed. Supp. 2 (1965).
4. K. A. Gavrilov et al., *Atomnaya Énergiya*, 28, 362 (1970).
5. I. B. Keirim-Markus et al., *Handling of Nuclear Accident Dosimetry Systems*, Proc. IAEA Panel, Vienna (1969), p. 84.
6. I. A. Bochvar et al., *Neutron Monitoring*, Proc. Symp. IAEA, Vienna (1967), p. 459.
7. L. Anderson et al., *Personal Dosimetry for Radiation Accidents*, Proc. Symp. IAEA, Vienna (1965), p. 645.
8. I. V. Gordeev, D. A. Kardashev, and A. V. Malyshev, *Nuclear Physics Constants Handbook* [in Russian], Gosatomizdat, Moscow (1963).
9. S. Wright, *Calculation of High Energy Neutron Spectra*, AERE, R 4080.
10. Yu. A. Egorov, V. I. Zharkov, and Yu. V. Orlov, *Atomnaya Énergiya*, 28, 170 (1970).
11. G. Benezech and H. Zaborowsky, *Cf.* [7], p. 349.
12. G. E. Blokhin et al., *Atomnaya Énergiya*, 10, 437 (1961).

## THE EFFECT OF NEUTRON IRRADIATION ON THE OPERATION OF SURFACE BARRIER FISSION FRAGMENT DETECTORS

E. A. Seregina, N. N. Semenova,  
and B. D. Kuz'minov

UDC 539.1.074.88

In the study of fast-neutron reactions the radiation detectors frequently receive the same neutron flux as the target [1, 2]. Elastic and inelastic scattering of neutrons from silicon nuclei produces radiation damage in the crystal lattice, mainly in the form of irreversible defects. Most of these have levels in the forbidden zone of the semiconductor and are electrically active. If the atoms displaced from their equilibrium positions have kinetic energies above the threshold for defect formation  $E_d$  they can displace secondary atoms. In such a case the total number of structural defects can be considerably larger than the number of primary nuclear interactions.

The effect of neutrons on the operation of silicon surface barrier counters has been studied before [3-5], but quantitative information on the effect of neutrons on semiconductor detectors is required to determine the possibility of performing certain experiments. The present work was undertaken to determine the maximum admissible doses of 1.5, 2.8, and 15 MeV neutrons to which silicon surface barrier detectors can be subjected and still be sufficiently accurate for fission fragment studies.

Surface barrier counters of n-type silicon with resistivities of 300 and 3000  $\Omega \cdot \text{cm}$  but identical sensitive areas of 3  $\text{cm}^2$  were irradiated with 1.5, 2.8, and 15 MeV neutrons. The counters were constructed as described in [6]. The effect of irradiation was determined by measuring the fission fragment spectrum after subjecting the detector to various neutron doses. The integrated neutron flux was estimated from the number of fissions in a  $\text{U}^{238}$  target of known weight. The equipment was provided with an automatic device eliminating the effect of amplification factor instability or detector capacitance on the magnitude of the recorded pulse.

The effect of neutrons on the operation of a silicon detector depends on its resistivity. Low-resistivity silicon counters exhibited a greater resistance to 1.5 and 2.8 MeV neutron irradiation. For a neutron dose of  $6 \cdot 10^{12}$  neutrons/ $\text{cm}^2$  there were no changes in the spectra of the fission fragments. High-resistivity counters subjected to this same dose show significant changes in fission fragment spectra.

Figure 1 shows the relative losses of charges produced by fragments as functions of the total neutron dose. Low-resistivity detectors show practically no charge losses due to defect formation for doses of up to  $10^{13}$  neutrons/ $\text{cm}^2$  ( $E_n = 1.5$  and 2.8 MeV). Low resistivity detectors are more sensitive to 15 MeV neutrons because these neutrons produce more than twice as many elementary structural defects as 1.5 or 2.8 MeV neutrons for the same integrated flux [7].

The time characteristics of the counters were studied before and after neutron irradiation. A schematic diagram of the measuring apparatus is shown in Fig. 2. The variable resistance  $R_0$  is used to determine the collection time of the charge

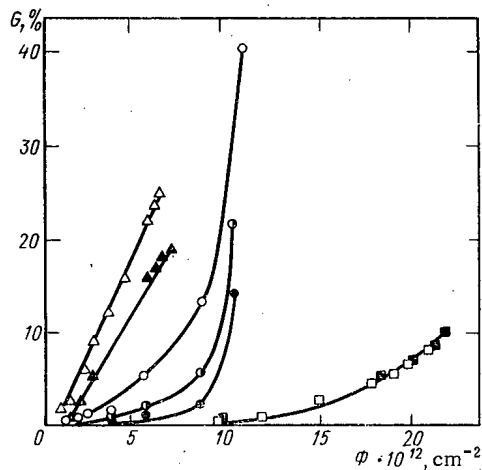


Fig. 1. Relative losses of charges produced by fragments as functions of neutron dose at energy  $E_n$ .

Translated from *Atomnaya Energiya*, Vol. 32, No. 1, pp. 70-72, January, 1972. Original article submitted January 11, 1971; revision submitted February 2, 1971.

© 1972 Consultants Bureau, a division of Plenum Publishing Corporation, 227 West 17th Street, New York, N. Y. 10011. All rights reserved. This article cannot be reproduced for any purpose whatsoever without permission of the publisher. A copy of this article is available from the publisher for \$15.00.

TABLE 1

Parameter	△	▲	○	⊙	●	□	■
$\rho$ , $\Omega \cdot \text{cm}$	3000	3000	300	300	300	300	300
$E_n$ , MeV	1,5	2,8	15	15	15	1,5	2,8
V, volts	30	70	25	50	75	30	70

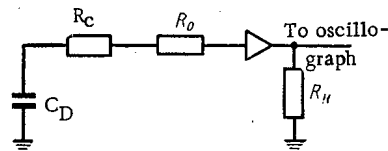


Fig. 2. Schematic diagram of apparatus for measuring charge collection time.

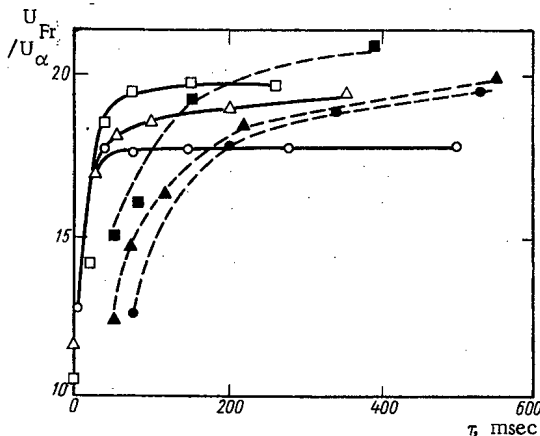


Fig. 3. Ratio of  $\text{Cf}^{252}$  fission fragment and alpha particle pulse heights as a function of the time constant of the circuit  $\tau = C_D(R_0 + R_C)$  for low-resistivity silicon detectors with biases of 25 ( $\circ$ ,  $\bullet$ ), 50 ( $\Delta$ ,  $\blacktriangle$ ), and 100 V ( $\square$ ,  $\blacksquare$ ) before irradiation (open points) and after irradiation (black points) by a dose of  $2.3 \cdot 10^{13}$  neutrons/cm<sup>2</sup>.

produced by fragments. A dense plasma is formed as the fission fragments slow down in the detector. Therefore the collection time for the charge produced by fragments is the sum of the time for the dissipation of the plasma and the time for charges to drift to the collecting electrodes. The plasma density is appreciably lower for alpha particles, and if other conditions remain the same the charge is collected more rapidly than for fragments. We use this fact in our work. As  $R_0$  is increased the time constant of the circuit  $\tau = C_D(R_0 + R_C)$  increases;  $C_D$  is the capacitance of the detector and  $R_C$  is its contact resistance. The ratio of the fragment and alpha particle pulse heights  $u_{Fr}/u_\alpha$  will increase and gradually approach a maximum. Figure 3 shows the ratio of the fission fragment and alpha particle pulse heights as a function of the time constant of the circuit  $\tau$ . The collection time for charges produced by fragments can be determined from the curves. For unirradiated counters this time is about 20 nsec. After irradiation by an integrated flux of  $10^{13}$  neutrons/cm<sup>2</sup> the collection time is increased to 150-200 nsec. The bias voltage has an appreciable effect on the collection time only for irradiated counters.

The following conclusions can be drawn from our investigations.

1. Low-resistivity ( $\rho = 200\text{--}300 \Omega \cdot \text{cm}$ ) silicon surface barrier detectors can be used for spectrometric studies when irradiated by integrated fluxes of up to  $10^{13}$  1.5 or 2.8 MeV neutrons/cm<sup>2</sup>, and by a flux of  $5 \cdot 10^{12}$  15 MeV neutrons/cm<sup>2</sup>. Larger fluxes lead to a loss of collected charge and to considerable distortions of spectra.
2. High resistivity ( $\rho = 2000\text{--}3000 \Omega \cdot \text{cm}$ ) silicon detectors cannot be used for practical fission fragment spectroscopy in the presence of a neutron flux.
3. The collection time of charges produced by fission fragments is about 20 nsec for unirradiated detectors.
4. When irradiated by integrated fluxes of  $2 \cdot 10^{13}$  neutrons/cm<sup>2</sup> counters experience considerable changes in their time characteristics; the charge collection time is increased to 150-200 nsec.

The authors thank P. P. D'yachenko and A. I. Sergachev for help in the work.

#### LITERATURE CITED

1. V. G. Vorob'eva, B. D. Kuz'minov, and A. I. Sergachev, *Yadernaya Fizika*, **9**, 296 (1969).
2. P. P. D'yachenko, B. D. Kuz'minov, and M. Z. Tarasko, *Yadernaya Fizika*, **8**, 286 (1968).
3. R. Klingersmith, *IRE Trans. Nucl. Sci.*, **8**, No. 1 (1961); *Semiconductor Radiation Counters* [in Russian], Gosatomizdat, Moscow (1962).
4. I. A. Baranov and N. M. Kazarinov, *Atomnaya Énergiya*, **16**, 60 (1964).

5. G. George and E. Gunnerson, Nucl. Instrum. and Meth., 25, 253 (1964).
6. P. P. D'yachenko, B. D. Kuz'minov, and M. V. Chukichev, Pribory i Tekh. Éksperim., No. 5, 85 (1965).
7. E. Smith et al., IEEE Trans. Nucl. Sci., 13, No. 6, 11 (1966).

THE EFFECT OF THE ANGULAR DIMENSIONS OF A DETECTOR ON  
THE ERROR IN THE DETERMINATION OF CERTAIN KINEMATIC  
CHARACTERISTICS

G. N. Potetyunko

UDC 539.17:518.3

Analytic expressions have been obtained in [1, 2] for calculating the error in the determination of the energy of a reaction product in a two-body nuclear collision as a function of the angular dimensions of the detector in both the nonrelativistic and relativistic cases. This is called kinematic broadening in [2]. Unfortunately these expressions are very cumbersome and of little use in practical calculations.

We present nomograms for finding the relative error in the energy  $E_1$  of a product of a nuclear reaction of the type  $I + II = 1 + 2$  (Fig. 1) and the differential effective cross section in the center-of-mass system  $\sigma_{C.M.}$  (Fig. 2) as a function of the angle of emission  $\vartheta_1$  of particle 1 in the laboratory system and the dimensionless parameter  $\rho_1$  given by [3]

$$\rho_1 = \sqrt{\frac{A_1 E_I}{E_I - E_{It}}}; \quad A_1 = \frac{m_1 m_I}{m_2 m_{II}}; \quad (1)$$

$$E_{It} = -\frac{M}{m_2} Q,$$

where  $E_I$  is the energy of the beam in the laboratory system and  $M = m_I + m_{II}$ , or is found from the nomogram in [4]. Our nomograms are constructed for  $\Delta\vartheta_1 = \pm 1^\circ$  and  $0 \leq \rho_1 \leq 1$ . For  $\Delta\vartheta_1 = \pm k^\circ$  the error obtained from our nomogram must be multiplied by  $k$ .

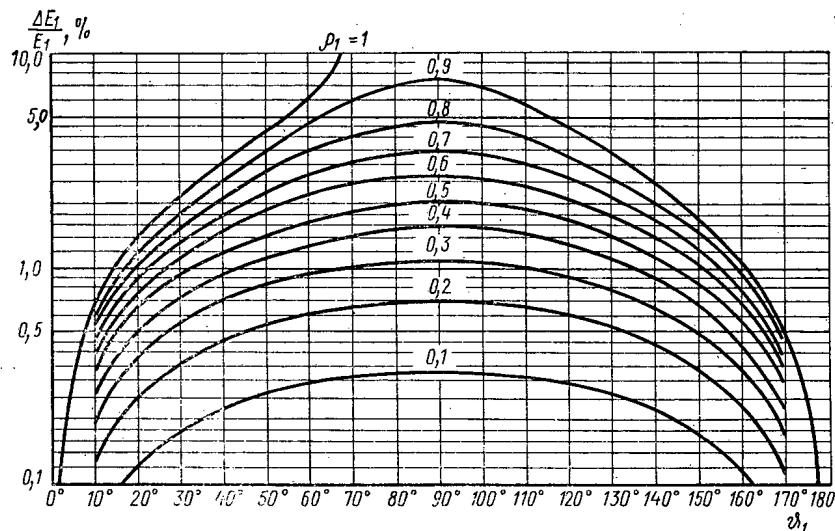


Fig. 1. Nomogram for determining the relative error in the energy of a reaction product in a two-body nuclear collision for  $\Delta\vartheta_1 = \pm 1^\circ$ .

Translated from *Atomnaya Énergiya*, Vol. 32, No. 1, pp. 72-73, January, 1972. Original article submitted December 8, 1970; revision submitted June 8, 1971.

© 1972 Consultants Bureau, a division of Plenum Publishing Corporation, 227 West 17th Street, New York, N. Y. 10011. All rights reserved. This article cannot be reproduced for any purpose whatsoever without permission of the publisher. A copy of this article is available from the publisher for \$15.00.



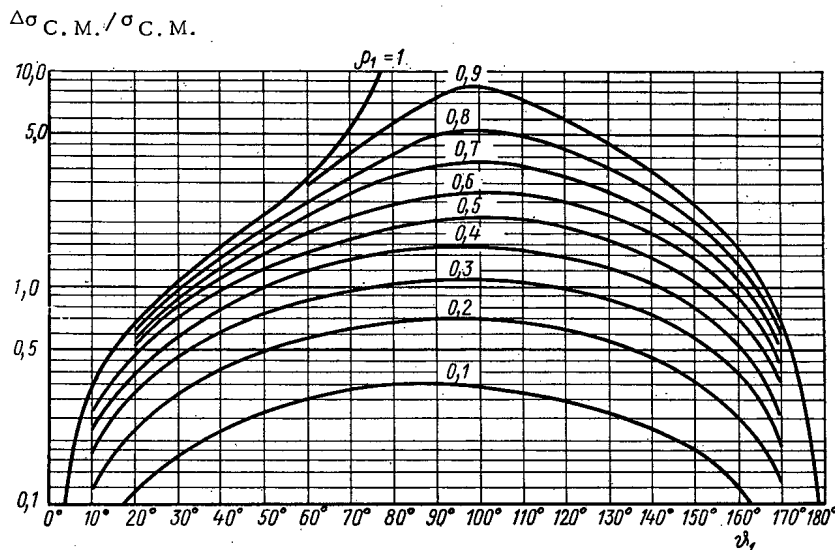


Fig. 2. Nomogram for determining the relative error in the differential effective cross section in the center-of-mass system for a two-body nuclear collision for  $\Delta\psi_1 = \pm 1^\circ$ .

Our nomograms are based on the equations

$$E_1 = \frac{m_1 m_1}{M^2} \frac{E_I}{\rho_1^2} (\sqrt{1 - \rho_1^2 \sin^2 \theta_1} \pm \rho_1 \cos \theta_1)^2; \quad (2)$$

$$\frac{\sigma_{C.M.}}{\sigma_{lab}} = \frac{\sqrt{1 - \rho_1^2 \sin^2 \theta_1}}{(\sqrt{1 - \rho_1^2 \sin^2 \theta_1} \pm \rho_1 \cos \theta_1)^2}. \quad (3)$$

In these expressions the plus sign holds when  $\rho_1 < 1$ , but both solutions must be considered when  $\rho_1 > 1$ .

Equation (3) is cited in practically all handbooks on the kinematics of nuclear reactions (e.g., [3]). Equation (2) has not been previously cited anywhere. Equation (2) is convenient since it expresses  $E_1$  in terms of quantities defined in the laboratory system ( $E_I$  and  $\psi_1$ ) and the parameter  $\rho_1$  which appears in all the other kinematic equations, and can be used together with the other expressions for  $E_1$  [3, 5] to calculate the energy of a product of a two-body nuclear collision.

#### LITERATURE CITED

1. D. Smith, Nucl. Instrum. and Methods, 58, No. 2, 315 (1968).
2. D. Smith, Nucl. Instrum. and Methods, 63, No. 1, 23 (1968).
3. A. M. Baldin et al., Kinematics of Nuclear Reactions [in Russian], Atomizdat, Moscow (1968).
4. G. N. Potetyunko, Preprint OIYaI 4-4109 [in Russian], Dubna (1968).
5. J. Winter and H. Schmid, EUR 3908e, Brussels (1968); J. Winter, Nucl. Instrum. and Methods, 59, No. 1, 167 (1968).

## VISUALIZATION OF SPATIAL DOSE DISTRIBUTION IN A FAST ELECTRON BEAM

Yu. P. Vagin, G. L. Kabanov,  
Yu. A. Medvedev, and B. M. Stepanov

UDC 539.12.08

When using high intensity electron beams, it is often necessary to measure the spatial characteristics of dose fields created by electron interactions in a target, by electron scattering in various media, by the action of electromagnetic fields on the electron beam, etc.

It was shown experimentally [1] that the intensity of fluorescence excited in air by a pulse of fast electrons was proportional to absorbed dose rate. Obviously, the phenomenon of fluorescence can be used for visualization of spatial dose distribution. To demonstrate this fact, the fast-electron scattering field and the luminosity field in air were investigated by photoelectron and photographic methods; the characteristics of the luminosity field were also compared with results from a crude theory of electron multiple scattering. An electron beam with electron energies of 4 and 1 MeV was used in the experiments. The respective electron currents per pulse were 0.1 and 3 A, the pulse durations, 2 and 1.2  $\mu$ sec, and the repetition rates 400 and 25 Hz. The electron beam was scattered in air, forming a typical luminous cone.

A photoelectron detector (photomultiplier and Faraday cup) recorded luminous intensity and electron current simultaneously. In this case, air luminosity was observed from a small volume ( $\sim 1 \text{ cm}^3$ ) located inside the cavity of the Faraday cup and limited by the entrance diaphragm ( $\sim 1 \text{ cm}$ ). The luminous intensity was produced by electrons moving along the axis of the measuring volume. Photographic recording of the luminous zone was obtained with "Zenite-3M" equipment on "Foto-250" isopanchromatic film (limit of resolution, 680 nm) having a uniform spectral sensitivity in the visible portion of the spectrum.

Typical photographs of the luminous region in air excited by electron beams with energies of 1 and 4 MeV are shown in Fig. 1. The photographs show a bright central region of luminosity and a faint luminous cone which is formed by electrons scattered by a titanium foil (see Fig. 1a). The boundary of the luminous cone becomes indistinguishable at distances of the order of 8-10 cm from the foil because of additional electron scattering by air.



Fig. 1. Luminous regions in air excited by electron beams with energies of 1 (a) and 4 MeV (b).

Translated from *Atomnaya Énergiya*, Vol. 32, No. 1, pp. 73-75, January 1972. Original article submitted February 1, 1971.

© 1972 Consultants Bureau, a division of Plenum Publishing Corporation, 227 West 17th Street, New York, N. Y. 10011. All rights reserved. This article cannot be reproduced for any purpose whatsoever without permission of the publisher. A copy of this article is available from the publisher for \$15.00.

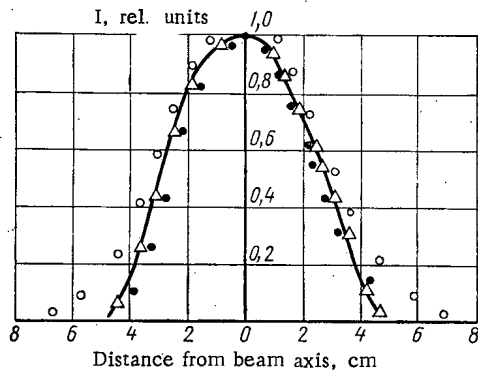


Fig. 2. Transverse distribution of intensity  $I$  of air luminosity (●) by photoelectron method; (○) by photographic method) and of 1-MeV electron current (Δ).

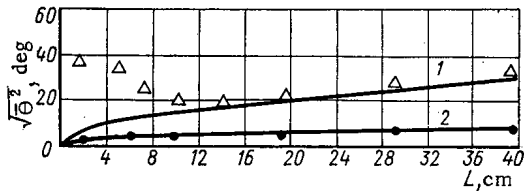


Fig. 3. Dependence of electron scattering angle in air on distance  $L$  along the beam axis: 1, 2) theoretical curves for 1- and 4-MeV electrons; Δ, ● experimental points for 1- and 4-MeV electrons.

Negatives obtained at different exposures were photometrized perpendicularly to the beam axis in a region of normal blackening. The transverse distribution of luminous intensity, which was in the form of a Gaussian, was plotted from the density distribution curve with corrections for film contrast and inertia.

Measurements of luminous intensity by photoelectron and photographic methods and of electron current over the cross section of the electron beam at 3 cm from the exit window of the accelerator are plotted in Fig. 2. It is evident that the results obtained with the three methods are in good agreement with one another, and deviate by no more than  $\pm 10\%$  from a mean Gaussian curve for the distribution. The results lead one to conclude that there is a correspondence between the distributions of luminous intensity and electron current and, consequently, that there is a possibility of measuring dose fields in electron beams [1] by recording the luminosity field by one means or another (photographically, for example).

The result of a study of the longitudinal characteristics of the luminous field by a photographic method is a further verification of this conclusion. The average contour of the luminosity field was graphically plotted from the measured halfwidths of the transverse luminosity distribution at various distances from the exit window of the accelerator. The scattering angle was determined from the slope of the tangent to the contour at several points; it was compared to the mean angle calculated from a formula given by a crude theory for multiple scattering of electrons [2]:

$$\sqrt{\theta^2} = \sqrt{\frac{7000L}{E^2}},$$

where  $L$  is the electron path length in air along the beam axis in cm and  $E$  is the electron energy in keV.

The theoretical (curves 1, 2) and experimental data are given in Fig. 3. At 4 MeV, it is clear that good agreement between experimental and theoretical data is observed; at 1 MeV, satisfactory agreement is observed starting at a distance of the order of 10 cm where one can neglect the electrons scattered by the titanium foil and consider only the air scattering of the central portion of the electron beam (see Fig. 1). The experimental points characterizing the scattering cone near the exit window of the accelerator (1.5 and 5 cm) are in good agreement with the theoretical electron scattering angle for a titanium foil.

Thus visualization and measurement of dose fields from high-intensity pulsed electron beams can be reduced to photographic recording of the luminosity field and photometric analysis of the negatives.

#### LITERATURE CITED

1. Yu. P. Vagin et al., *At. Énerg.*, 28, 177 (1970).
2. G. Hine and G. Brownell, *Radiation Dosimetry* [Russian translation], Izd-vo Inostr. Lit., Moscow (1958).

SPECTRA OF ELECTRONS EJECTED IN THE PASSAGE OF  $\text{Co}^{60}$   
GAMMA RAYS THROUGH A TWO-COMPONENT MEDIUM

L. V. Popova and L. B. Chegodaeva

UDC 539.172.3

We have used the Monte Carlo method to find the spectra of primary electrons produced in the gamma irradiation of two-component finely divided systems. As model systems we investigated aluminum-water, copper-water, and platinum-water. For comparison with the two-component systems we studied the electron spectrum in a one-component system - water.

A point source of  $\text{Co}^{60}$  gamma rays was placed in an infinite uniformly mixed medium. Multiply scattered gamma photons were traced through the medium until they were completely degraded.

The Monte Carlo method assumes a mock-up of the process under study - in the present case the simulation of the penetration of gamma rays through matter. Since the medium is assumed homogeneous and isotropic it is sufficient to consider the trajectory of a gamma photon in energy space.\* At  $\text{Co}^{60}$  photon energies ( $\sim 1.25$  MeV) only two processes occur with appreciable probability: inelastic scattering from free electrons (Compton scattering) and photoelectric absorption. The cross section for Compton scattering is

\*The homogeneity of the two-component systems considered follows from the fact that the sizes of the metal particles are assumed to be two to three orders of magnitude smaller than the mean free path of the gamma photons.

TABLE 1. Spectrum of Recoil Electrons in Water and in the Components of Mixtures

Energy range, MeV	Water			Aluminum-water						Copper-water						Platinum-water					
	$\Phi$	K	$\Phi + K$	Al			$\text{H}_2\text{O}$			Cu			$\text{H}_2\text{O}$			Pt			$\text{H}_2\text{O}$		
				$\Phi$	K	$\Phi + K$	$\Phi$	K	$\Phi + K$	$\Phi$	K	$\Phi + K$	$\Phi$	K	$\Phi + K$	$\Phi$	K	$\Phi + K$	$\Phi$	K	$\Phi + K$
0-0.01	0	45.5	45.5	0	14.8	14.8	0	17.0	17.0	0	6.6	6.6	0	7.9	7.9	0	1.8	1.8	0	3.6	3.6
0.01-0.02	0	12.7	12.7	0	6.4	6.4	0	7.3	7.3	0	3.2	3.2	0	3.9	3.9	0	1.1	1.1	0	1.6	1.6
0.02-0.03	0.7	6.1	6.8	0	3.6	3.6	0	4.0	4.0	0	2.7	2.7	0	3.2	3.2	0.1	0.9	1.0	0	1.3	1.3
0.03-0.04	2.4	3.8	6.2	0.8	2.2	3.0	0.1	2.5	2.6	0	2.2	2.2	0	2.7	2.7	0.3	0.8	1.1	0	1.1	1.1
0.04-0.05	1.7	2.6	4.3	1.9	1.6	3.5	0.3	1.7	2.0	0.2	1.9	2.1	0	2.2	2.2	0.5	0.7	1.2	0	1.0	1.0
0.05-0.06	0.9	2.0	2.9	1.7	1.2	2.9	0.3	1.3	1.6	0.5	1.5	2.0	0	1.9	1.9	0.5	0.7	1.2	0	0.8	0.8
0.06-0.07	0.5	1.5	2.0	1.2	1.0	2.2	0.2	1.1	1.3	1.1	1.4	2.5	0	1.6	1.6	0.6	0.6	1.2	0	0.8	0.8
0.07-0.08	0.2	1.3	1.5	0.7	0.8	1.5	0.1	0.9	1.0	1.5	1.1	2.6	0	1.4	1.4	0.7	0.6	1.3	0	0.9	0.9
0.08-0.09	0.1	1.1	1.2	0.4	0.7	1.1	0.1	0.8	0.9	1.7	1.0	2.7	0	1.2	1.2	0.8	0.6	1.4	0	0.8	0.8
0.09-0.1	0.1	1.0	1.1	0.3	0.6	0.9	0	0.7	0.7	1.6	0.9	2.5	0	1.1	1.1	0.8	0.5	1.3	0	0.8	0.8
0-0.1	6.6	77.6	84.2	7.1	32.9	40.0	1.0	37.4	38.4	6.6	22.5	29.1	0	27.1	27.1	4.4	8.3	12.7	0	12.7	12.7
0.1-0.2	0.1	4.8	4.9	0.6	2.9	3.5	0.1	3.4	3.5	7.2	4.6	11.8	0.1	5.7	5.8	11.0	4.0	15.0	0	5.6	5.6
0.2-0.3	0	2.3	2.3	0	1.4	1.4	0	1.7	1.7	1.1	2.4	3.5	0	2.9	2.9	4.8	2.9	7.7	0	3.9	3.9
0.3-0.4	0	1.6	1.6	0	1.0	1.0	0	1.1	1.1	0.2	1.6	1.8	0	2.0	2.0	2.4	2.1	4.5	0	2.9	2.9
0.4-0.5	0	1.3	1.3	0	0.8	0.8	0	0.9	0.9	0.1	1.3	1.4	0	1.6	1.6	1.4	1.8	3.2	0	2.5	2.5
0.5-0.6	0	1.0	1.0	0	0.7	0.7	0	0.7	0.7	0	1.1	1.1	0	1.3	1.3	1.0	1.6	2.6	0	2.2	2.2
0.6-0.7	0	1.0	1.0	0	0.6	0.6	0	0.6	0.6	0	1.0	1.0	0	1.1	1.1	0.7	1.4	2.1	0	2.1	2.1
0.7-0.8	0	0.9	0.9	0	0.5	0.5	0	0.6	0.6	0	0.9	0.9	0	1.1	1.1	0.5	1.5	2.0	0	2.0	2.0
0.8-0.9	0	0.9	0.9	0	0.5	0.5	0	0.6	0.6	0	0.9	0.9	0	1.1	1.1	0.4	1.4	1.8	0	1.9	1.9
0.9-1.0	0	1.1	1.1	0	0.6	0.6	0	0.7	0.7	0	1.1	1.1	0	1.3	1.3	0.4	1.7	2.1	0	2.3	2.3
1.0-1.1	0	0.9	0.9	0	0.6	0.6	0	0.7	0.7	0	1.0	1.0	0	1.1	1.1	0.4	1.6	2.0	0	2.2	2.2
1.1-1.2	0	0	0	0	0	0	0	0	0	0	0	0	0	0	0	3.5	0	3.5	0	0	0
1.2-1.25	0	0	0	0	0	0	0	0	0	0	0	0	0	0	0	0.4	0	0.4	0	0	0

Note:  $\Phi$ ) Photoelectrons; K) Compton electrons.

Translated from *Atomnaya Énergiya*, Vol. 32, No. 1, pp. 75-77, January, 1972. Original article submitted February 23, 1971; revision submitted July 12, 1971.

© 1972 Consultants Bureau, a division of Plenum Publishing Corporation, 227 West 17th Street, New York, N. Y. 10011. All rights reserved. This article cannot be reproduced for any purpose whatsoever without permission of the publisher. A copy of this article is available from the publisher for \$15.00.

TABLE 2. Relative Number of Electrons and Fraction of the Energy Carried by Them in the Ranges 0-0.1 and 0.5-1.25 MeV

System	Energy range MeV	Ratio of number of electrons to total number of primary electrons in mixture, %	Energy in range to total energy of all electrons in mixture
Water	0-0,1	84	0,19
	0,5-1,25	5,7	0,53
Aluminum -water	0-0,1	78	0,19
	0,5-1,25	7,6	0,58
Copper-water	0-0,1	56	0,11
	0,5-1,25	13	0,53
Platinum-water	0-0,1	25	0,03
	0,5-1,25	29	0,67

found from the Klein-Nishina formula [1] by integrating over all scattering angles. The photoabsorption cross section is determined from experimental data. Since analytic expressions for the cross sections are more convenient than tables in Monte Carlo calculations we approximate the experimental values of the photoabsorption cross sections by expressions of the form

$$\sigma_{\varphi} = A + B\alpha^{-c}, \quad (1)$$

where  $\alpha$  is the energy of a gamma photon in units of the rest energy of an electron  $m_0c^2$ ; A, B, and C are coefficients given in [2]. The total cross section for the interaction of a gamma photon with a given component is the sum of the cross sections of both processes.

Since a two-component mixture is considered, the probability of an interaction with the individual components must be found. Knowledge of the probability of an interaction with atoms or molecules of individual components

of the mixture permits a lottery with a set of random numbers to determine the component with which the interaction occurred and whether it was Compton scattering or photoabsorption. If Compton scattering occurred, the energy of the scattered photon must be found from the Klein-Nishina formula. A lottery to draw the energy directly from the Klein-Nishina formula is difficult, however, since this requires solving a transcendental equation [6]. A number of algorithms [7-9] have been developed for drawing the energy of a gamma photon after Compton scattering without using the Klein-Nishina formula. We used the algorithm proposed in [6] as the simplest and the one requiring the minimum expenditure of machine time.

The energy of a primary electron ejected in Compton scattering is equal to the difference of the incident and scattered photon energies; this is the energy recorded in the calculation. The energy of an electron ejected in a photoelectric absorption is equal to the energy of the absorbed photon minus the ionization energy. The electron spectrum obtained from the calculation is in the form of the numbers of primary electrons ejected from atoms and molecules of each material.

The calculation was performed on a Minsk-22 computer. Up to twenty thousand histories were traced in each case. The maximum calculational error is 15% and the average is 5%.

## RESULTS AND DISCUSSION

The results of the calculation are shown in Table 1. The number of ejected electrons with energies in a given range is given as a percentage of the total number of electrons ejected in a given mixture. Since most of the electrons are created with energies below 0.01 MeV, the 0-0.1 MeV range was subdivided into 10 subintervals for the calculation. The weight ratio of the components in the two-component mixtures was 1:1.

It is clear from Table 1 that most of the Compton electrons have energies below 0.1 MeV. There is a particularly large number of such electrons in water and in mixtures of light materials.

Table 1 shows that the total spectrum of ejected electrons has a maximum in the 0-0.1 MeV range for all the systems studied. However, in spite of the fact that electrons with such energies are in the overwhelming majority, their total energy is relatively small. Table 2 lists the relative number of electrons and the energy carried by them as fractions of the total energy of all primary electrons in the mixture for the low-energy range 0-0.1 MeV and the high-energy range 0.5-1.25 MeV.

The average number of electrons ejected per gamma photon was also found in the calculation. This number is smaller the larger the photoabsorption in the elements of the mixture. It is equal to 15, 11-12, 6-7, and 3 for water and for the aluminum-water, copper-water, and platinum-water mixtures respectively.

In conclusion the authors thank I. G. Kaplan for helpful discussions.

LITERATURE CITED

1. O. I. Leipunskii, B. V. Novozhilov, and V. I. Sakharov, The Propagation of Gamma Rays in Matter [in Russian], Fizmatizdat, Moscow (1960).
2. L. V. Popova and L. A. Sholokhova, Atomnaya Énergiya, 30, 384 (1971).
3. G. V. Gorshkov, Penetrating Radiations of Radioactive Bodies [in Russian], Izd-vo AN SSSR (1967).
4. H. Kahn, USAEC Report R-1237, 19 (1954).
5. B. Carlson, AECU-2857 (1953).
6. I. G. Dyad'kin, Zh. Vychisl. Matem. i Matem. Fiz., 6, 384 (1966).

ANGULAR DISTRIBUTIONS OF BREMSSTRAHLUNG FROM 12-22 MeV  
ELECTRONS AS A FUNCTION OF TARGET THICKNESS

V. P. Kovalev, V. P. Kharin,  
and V. V. Gordeev

UDC 539.163:539.124

Most of the available reports of experimental and theoretical studies of bremsstrahlung from electrons involve thin targets [1].

We have measured the angular distributions of bremsstrahlung for targets of Al, Ti, Cu, Mo, Ta, and W having thicknesses from  $0.01 X_0$  to  $2.2 X_0$ , where  $X_0$  is the radiation length.

The target dimensions, the detectors, and the geometry of the experiment are similar to those used in [2] except that in measuring the angular distributions the collimator in front of the detector was removed. A  $25 \text{ cm}^3$  ionization chamber with a 10 mm thick Plexiglas cap was placed 100 cm from the target.

The experimental results are shown in Fig. 1 and 2. The results not shown in the figures are given in Table 1 as bremsstrahlung yields at various angles with the direction of the electron beam. The last

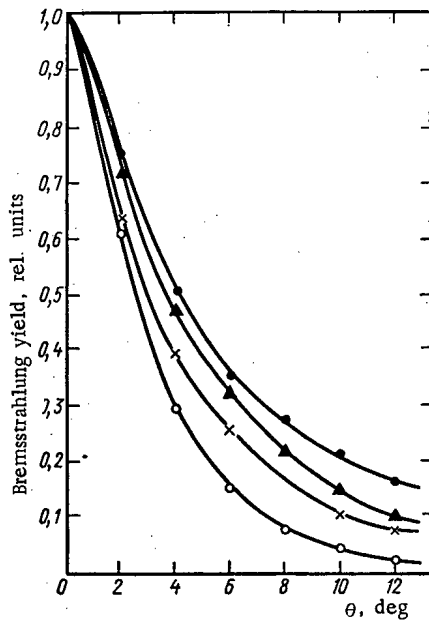


Fig. 1

Fig. 1. Angular distributions of bremsstrahlung as functions of thickness of a tungsten target. Electron energy 22 MeV, copper detector: ○)  $0.036 X_0$ ; ×)  $0.108 X_0$ ; ▲)  $0.18 X_0$ ; ●)  $2.17 X_0$ .

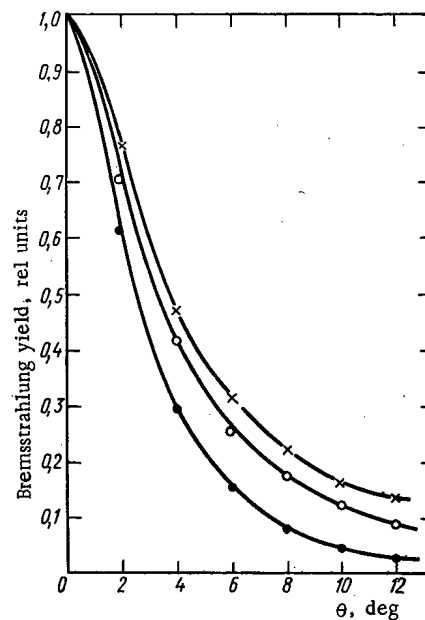


Fig. 2

Fig. 2. Angular distribution of bremsstrahlung as functions of electron energy. Copper detector, tungsten target of thickness  $0.036 X_0$ : ●) 22 MeV; ○) 16 MeV; ×) 12.8 MeV.

Translated from *Atomnaya Énergiya*, Vol. 32, No. 1, pp. 77-79, January, 1972. Original article submitted February 8, 1971; revision submitted March 15, 1971.

© 1972 Consultants Bureau, a division of Plenum Publishing Corporation, 227 West 17th Street, New York, N. Y. 10011. All rights reserved. This article cannot be reproduced for any purpose whatsoever without permission of the publisher. A copy of this article is available from the publisher for \$15.00.

TABLE 1. Relative Bremsstrahlung Yields.

Angle, deg	Aluminum												Titanium																																		
	MeV						MeV						MeV	MeV						MeV																											
	Cu <sup>63</sup>			chamber			Cu <sup>63</sup>			chamber				Cu <sup>63</sup>			chamber																														
	C12	Cu <sup>63</sup>		chamber		Cu <sup>63</sup>		chamber		C12	Cu <sup>63</sup>		chamber		Cu <sup>63</sup>		chamber		C12	Cu <sup>63</sup>		chamber		C12	Cu <sup>63</sup>		chamber																				
0,0347	0,0116	0,0347	0,104	1,5	0,0116	0,347	0,104	1,5	0,0347	1,5	1,5	0,03	0,01	0,03	0,068	1,09	0,01	0,03	1,09	0,01	1,09	1,09	0,03	0,01	0,03	0,068	1,09	0,01	0,03	1,09	0,01	1,09	1,09														
0	1,0	1,0	1,0	1,0	1,0	1,0	1,0	1,0	1,0	1,0	1,0	1,0	1,0	1,0	1,0	1,0	1,0	1,0	1,0	1,0	1,0	1,0	1,0	1,0	1,0	1,0	1,0	1,0	1,0	1,0	1,0	1,0															
2	0,522	0,506	0,646	0,663	0,695	0,628	0,68	0,69	0,70	0,65	0,68	0,8	0,594	0,516	0,657	0,684	0,72	0,564	0,718	0,738	0,594	0,69	0,79	0,25	0,207	0,331	0,355	0,38	0,307	0,38	0,40	0,42	0,452	0,50	0,545	0,26	0,218	0,339	0,362	0,44	0,316	0,41	0,482	0,40	0,490	0,545	
4	0,123	0,080	0,154	0,210	0,222	0,126	0,211	0,256	0,265	0,36	0,395	0,40	0,114	0,11	0,17	0,213	0,277	0,178	0,257	0,326	0,292	0,345	0,37	0,045	0,034	0,082	0,135	0,155	0,073	0,119	0,143	0,165	—	—	0,310	0,057	0,058	0,102	0,133	0,179	0,102	0,179	0,233	—	0,264	0,26	
6	0,022	0,016	0,044	0,090	0,114	0,047	0,085	0,094	0,107	—	—	—	—	—	—	—	—	—	—	—	—	—	—	10	0,041	0,010	0,025	0,065	0,083	0,020	0,045	0,067	0,075	—	—	—	0,014	0,026	0,046	0,058	0,102	0,059	0,104	0,152	—	0,184	0,18
8	0,011	0,008	0,021	0,051	0,065	0,018	0,035	0,045	0,051	—	—	—	—	—	—	—	—	—	—	—	—	—	12	0,011	0,008	0,021	0,051	0,065	0,018	0,035	0,045	0,051	—	—	—	0,014	0,026	0,046	0,058	0,102	0,059	0,104	0,152	—	0,184	0,18	
10	0,006	0,004	0,011	0,028	0,036	0,009	0,018	0,023	0,026	—	—	—	—	—	—	—	—	—	—	—	—	—	12	0,006	0,004	0,011	0,028	0,036	0,009	0,018	0,023	0,026	—	—	—	0,014	0,026	0,046	0,058	0,102	0,059	0,104	0,152	—	0,184	0,18	
12	0,003	0,002	0,005	0,013	0,017	0,004	0,008	0,011	0,012	—	—	—	—	—	—	—	—	—	—	—	—	—	12	0,003	0,002	0,005	0,013	0,017	0,004	0,008	0,011	0,012	—	—	—	0,014	0,026	0,046	0,058	0,102	0,059	0,104	0,152	—	0,184	0,18	
14	0,002	0,001	0,003	0,007	0,010	0,002	0,004	0,006	0,007	—	—	—	—	—	—	—	—	—	—	—	—	—	14	0,002	0,001	0,003	0,007	0,010	0,002	0,004	0,006	0,007	—	—	—	0,014	0,026	0,046	0,058	0,102	0,059	0,104	0,152	—	0,184	0,18	
16	0,001	0,000	0,001	0,003	0,004	0,001	0,002	0,003	0,004	—	—	—	—	—	—	—	—	—	—	—	—	—	16	0,001	0,000	0,001	0,003	0,004	0,001	0,002	0,003	0,004	—	—	—	0,014	0,026	0,046	0,058	0,102	0,059	0,104	0,152	—	0,184	0,18	
18	0,000	0,000	0,000	0,001	0,001	0,000	0,001	0,001	0,001	—	—	—	—	—	—	—	—	—	—	—	—	—	18	0,000	0,000	0,000	0,001	0,001	0,000	0,001	0,001	0,001	—	—	—	0,014	0,026	0,046	0,058	0,102	0,059	0,104	0,152	—	0,184	0,18	
20	0,000	0,000	0,000	0,000	0,000	0,000	0,000	0,000	0,000	—	—	—	—	—	—	—	—	—	—	—	—	—	20	0,000	0,000	0,000	0,000	0,000	0,000	0,000	0,000	0,000	—	—	—	0,014	0,026	0,046	0,058	0,102	0,059	0,104	0,152	—	0,184	0,18	

Note: Cu<sup>12</sup>, Cu<sup>63</sup> chamber-detectors: boldface figures indicate thicknesses in X<sub>0</sub>.

line of the table lists the widths of the distributions at half maximum  $\bar{\theta}$ . The statistical errors of the measurements are less than 1% at 0° and 3% at 12°.

The following conclusions can be drawn from the experimental results:

1. A very pronounced increase in the width of the angular distribution with increasing target thickness is observed up to thickness corresponding approximately to the maximum bremsstrahlung yield (Fig. 1).
2. The widths of the angular distributions  $\bar{\theta}$  for targets of the same thickness but different atomic numbers Z are the same within 3% for thicknesses up to 0.1 X<sub>0</sub>, in agreement with theory [3]. The width of the angular distribution increases with increasing Z for thicknesses greater than 0.1 X<sub>0</sub>.
3. For constant target thickness t in the range t > 0.1 X<sub>0</sub> the slope of the curve for  $\bar{\theta}$  as a function of the electron energy increases with increasing Z.
4. The width tends to increase with a lowering of the threshold for recording bremsstrahlung. With an increase in the angle the difference in the angular distributions measured by detectors with different thresholds becomes more noticeable as predicted theoretically by Hisdal [4].

The dependence of the width of the angular distributions on electron energy, thickness, and atomic number of the target in the range of target thicknesses and energies examined can be described by the semi-empirical expression

$$\bar{\theta} = 2\theta_0 + a(E, Z) e^{-\frac{b(Z)}{t}} \text{ deg.} \tag{1}$$



where  $\theta_0 = 57.28 m_0 c^2 / E$ ;  $m_0 c^2 = 0.511$  MeV;  $E$  is the electron energy in MeV;  $t$  is the target thickness in radiation lengths; and  $a(E, Z)$  and  $b(Z)$  are functions of the electron energy and the atomic number of the target material.

The functions  $a(E, Z)$  and  $b(Z)$ , determined from the experimental data, have the form:

$$a(E, Z) = (5.17 - 1.32 \lg E + 2.28 \cdot 10^{-2} Z)$$

for the  $\text{Cu}^{63}$  detector:

$$a(E, Z) = (4.72 - 1.826 \lg E + 7.62 \cdot 10^{-2} Z)$$

for the ionization chamber;

$$b(Z) = (5.1 \cdot 10^{-3} + 3.1 \cdot 10^{-4} Z).$$

The widths of the angular distributions of bremsstrahlung calculated by Eq. (1) do not differ from the experimental values by more than 10%.

A comparison of the experimental angular distributions of bremsstrahlung with theory confirms the conclusion of Lanzl and Hanson [5] that the use of the Moliere formula [6] for the angular distribution of electrons gives better agreement with experiment than does the Schiffer and Lawson [3, 7] theory in which the Williams [8] and Rossi and Griesen [9] formulas are used for the angular distributions of electrons. The calculations were compared with measurements made with a copper detector. The Lanzl and Hanson calculations give good agreement with experiment for small angles ( $\theta \leq 50$ ) and target thicknesses less than  $0.1 X_0$ .

#### LITERATURE CITED

1. H. Koch and J. Motz, *Rev. Mod. Phys.*, 31, 4 (1959).
2. V. P. Kovalev et al., *Atomnaya Energiya*, 31, 289 (1971).
3. J. Lawson, *Proc. Phys. Soc.*, A63, 653 (1950).
4. E. Hisdal, *Phys. Rev.*, 105, 1821 (1957).
5. L. Lanzl and A. Hanson, *Phys. Rev.*, 83, 959 (1951).
6. G. Moliere, *Z. Naturforsch.*, 3a, 78 (1948).
7. L. Schiff, *Phys. Rev.*, 83, 252 (1951); E. Muirhead et al., *Proc. Phys. Soc.*, A65, 59 (1952).
8. J. Williams, *Phys. Rev.*, 58, 292 (1940).
9. B. Rossi and K. Griesen, *Rev. Mod. Phys.*, 13, 240 (1941).

## MATCHING OF ACCELERATING CHANNELS IN A HIGH ENERGY PROTON LINEAR ACCELERATOR

B. I. Bondarev and L. Yu. Solov'ev

UDC 621.384.64

To achieve particle energies of the order of 100–200 MeV in a linear proton accelerator, a transition is made to an accelerating field of shorter wavelength. With a wavelength reduction by a factor  $n$ , the phase width of a bunch becomes  $n$  times larger, as measured in the phase scale of the shortwave section, while the phase capture area of the shortwave section remains the same as the capture areas of the longwave section.

At the same time, the momentum width of a bunch remains practically unchanged during the transition into the second section; it is less than the momentum capture area. Therefore the phase width of a bunch can be decreased at the entrance to the shortwave section by virtue of an increase in the momentum spread of the particles.

Known devices for matching accelerating channels\* require the introduction of a third, intermediate wave. The construction of such devices requires rf oscillators, accelerating systems, and other equipment operating at the intermediate wavelength. The two matching devices described below operate at the wavelength of the first, longwave section of an accelerator.

The first of the devices is a cavity installed between the two sections of the accelerator and operating at the frequency of the longwave section. The frequency of the longitudinal oscillations in this cavity is greater than the frequency of the longitudinal oscillations in the other cavities of the longwave section of the accelerator. The cavity length is equal to an odd number of quarter wavelengths of the longitudinal oscillations.

Increases in the frequency of longitudinal oscillations in the matching cavity is achieved by an increase in synchronous phase (to 60–70°) and amplitude of the rf field (to maximum permissible values). This cavity also accelerates particles but with lower efficiency.

The operating principle of the matching device is shown in Fig. 1. We consider the phase plane ( $\psi, h$ ), where  $\psi = \varphi - \varphi_c$ ,  $h = (p - p_c)/p_c$ ,  $Q$  and  $p$  are the phase momenta of the accelerated particles, and  $\varphi_c$  and  $p_c$  are the phase and momentum of the center of the bunch.

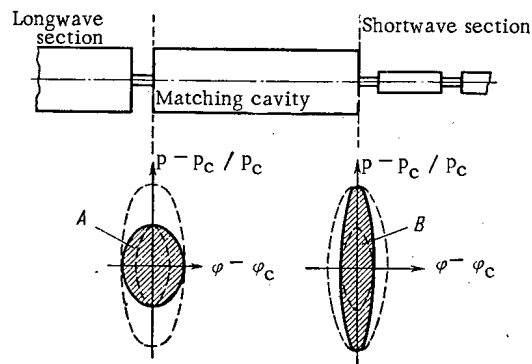


Fig. 1. Matching accelerating channels with a quarter-wave cavity.

We assume that the particle coordinates in this plane at the entrance to the matching cavity of the longwave section lie within the shaded ellipse A. In proportion to the acceleration in the matching cavity, the particle image points in the phase plane are shifted into an ellipse which is more elongated along the ordinate when compared with the ellipse which is the envelope of the bunch because of the higher frequency of longitudinal oscillations in the cavity. After a quarter cycle of the longitudinal oscillations, i.e., at the exit of the last cavity of the longwave section, the bunch will have the shape of the shaded ellipse B. The phase

\*A. D. Vlasov, Theory of Linear Acceleration [in Russian], Atomizdat, Moscow (1965), p. 75.

Translated from *Atomnaya Energiya*, Vol. 32, No. 1, pp. 79–81, January, 1972. Original article submitted December 18, 1970.

© 1972 Consultants Bureau, a division of Plenum Publishing Corporation, 227 West 17th Street, New York, N. Y. 10011. All rights reserved. This article cannot be reproduced for any purpose whatsoever without permission of the publisher. A copy of this article is available from the publisher for \$15.00.

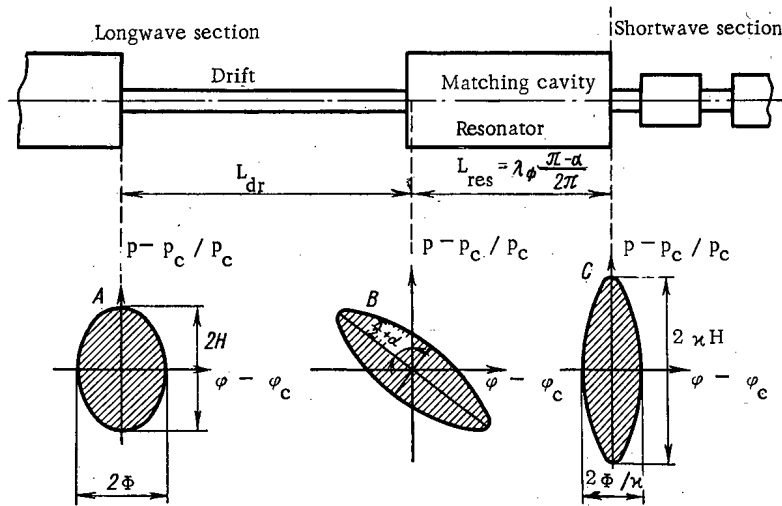


Fig. 2. Matching of accelerator channels by using a drift space and matching cavity.

dimension of the bunch is reduced and the momentum spread increased while the area of the image ellipse is preserved. Such an ellipse better fits in the capture area of the shortwave section. Optimum matching can be achieved by choosing the synchrotron phase and amplitude of the accelerating field in the matching cavity.

The second device consists of a drift space and matching cavity at the end of the longwave section. The wavelength, synchronous phase, and field intensity in the matching cavity are chosen to be the same as in the other cavities of the longwave section, and the cavity length is selected such that the longitudinal dimension of a bunch at the exit from this section of the accelerator is minimal.

Consider the operation of such a matching device. Let  $\Omega$  be the frequency of the longitudinal oscillations at the exit of the next to last cavity and in the last, matching cavity of the longwave section (we neglect adiabatic variation of parameters in it). As before, we assume the particle coordinates in the  $(\psi, h)$  plane at the exit of the next to last cavity lie within the ellipse A (Fig. 2), which satisfies the equation

$$\frac{\psi^2}{\Phi^2} + \frac{h^2}{H^2} = 1, \quad (1)$$

with  $\Phi$  and  $H$  the semi-axes of the ellipse A, which are related by the expression  $H = (\Omega\gamma^2/\omega)\Phi$ , where  $\omega$  is the frequency of the accelerating rf field;  $\gamma = (1 - \beta^2)^{-1/2}$ ;  $\beta = v/c$ ;  $v$  is the particle velocity; and  $c$  is the velocity of light. After passing through a drift space of length  $L_{dr}$ , the particle representative points are displaced parallel to the abscissa by an amount  $-kh$ , where  $k = 2\pi L_{dr}/\beta\lambda\gamma^2$  and  $\lambda$  is the wavelength of the accelerating field. The ellipse A transforms into the ellipse B, the equation for which is

$$\frac{(\psi + kh)^2}{\Phi^2} + \frac{h^2}{H^2} = 1. \quad (2)$$

After drifting, the particles arrive at the matching cavity and the ellipse B is rotated by an angle  $\pi/2 + \alpha$  in proportion to the acceleration in the cavity, and is transformed into the ellipse C, the axes of which coincide with the coordinate axes. The matrix  $M$  which describes the transformation of coordinates at the cavity entrance into the coordinates at the exit is

$$M = \begin{pmatrix} -\sin \alpha, & \frac{\omega}{\Omega\gamma^2} \cos \alpha \\ \frac{\Omega\gamma^2}{\omega} \cos \alpha, & -\sin \alpha \end{pmatrix}. \quad (3)$$

Subjecting the coordinates  $\psi$  and  $h$  in Eq. (2) to the transformation (3), we obtain an equation for the ellipse C at the exit of the longwave section. To make the axes of the ellipse C coincide with the coordinate axes, we set the coefficient of the  $\psi h$  term equal to zero in the equation for this ellipse. Then

$$\alpha = \frac{1}{2} \operatorname{arctg} \frac{2}{m}, \quad (4)$$

where  $m = (\Omega\gamma^2/\omega)k$ . Substituting the resultant value of  $\alpha$  in the equation for the ellipse C, we find that its phase spread is reduced by a factor  $\kappa$  in comparison with ellipse A:

$$\kappa = \sqrt{1 + \frac{m^2}{2}} + m \sqrt{1 + \frac{m^2}{4}}, \quad (5)$$

and the momentum spread of the particles is increased by the same factor.

By selecting  $L_{dr}$ , the shape of the ellipse can be optimally matched to the capture area of the short-wave section.

It is easy to show that nonlinearity and nonconservation of longitudinal motion, as well as random perturbations of it, do not reduce the practical efficiency of the matching devices discussed.

In principle, the matching devices discussed above can be used where there is a need for linear transformation of bunch phase space.

In high-energy and high-current linear proton accelerators (meson factories, neutron generators), matching devices can be used for matching the accelerating channels of the longwave and shortwave sections of the accelerator, making it possible to prevent particle loss and to increase operational reliability and acceleration efficiency. In linear accelerators used as injectors for proton synchrotrons, matching of accelerating channels helps to decrease particle momentum spread at the accelerator exit along with an increase in acceleration efficiency.

EFFECT OF NONLINEAR RESONANCES ON BEAM DIMENSIONS  
IN THE 70-GeV ACCELERATOR

V. I. Gridasov, K. P. Myznikov,  
and V. N. Chepegin

UDC 621.384.6

The emittance of an accelerated proton beam is one of the most important parameters determining the operating efficiency of an accelerator extraction system. However, the very first measurements made at the IHEP (Institute of High-Energy Physics) showed that beam emittance at the end of acceleration differed considerably from the calculated value [1]. Our present purpose is the clarification of the reasons for this effect and an experimental study of the possibilities for suppressing it.

The dependence of horizontal and vertical dimensions of the beam on the magnitude of the magnetic field in the accelerator is shown in Fig. 1. In this case, acceleration was produced at the central radius beginning at 4000 Oe. The beam dimensions were determined by means of internal targets. A target was introduced into the beam at a given time in the acceleration cycle. Its position could be changed both

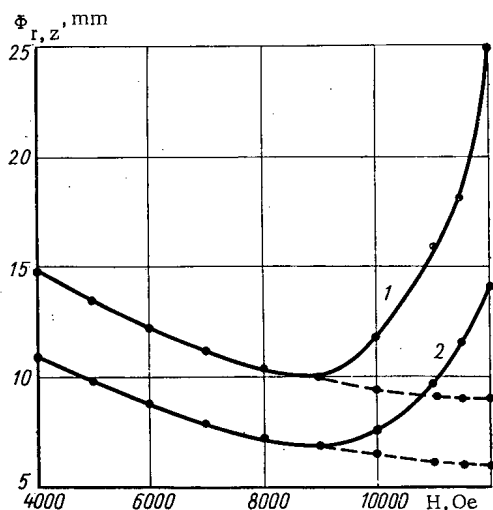


Fig. 1

Fig. 1. Dependence of horizontal (1) and vertical (2) beam dimensions in a radially focusing section on the magnetic field in the accelerator during acceleration at the central radius. ----) The same dependence when a correction was introduced into the magnetic field gradient in the accelerator.

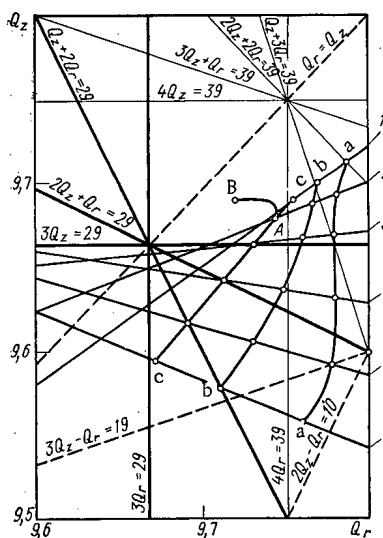


Fig. 2

Fig. 2. Operating region for the frequencies  $Q_{r,z}$  with linear resonances to fourth order. 1-6) Operating point trajectories for radial beam displacement at various inductions; 1) 4000, 2) 9000, 3) 10,000, 4) 11,000, 5) 11,500, 6) 12,000; aa, bb, cc) operating point trajectories corresponding to acceleration at radii  $\langle \Delta R \rangle$  equalling  $-10$ ,  $-5$ , and  $0$  mm; AB) operating point trajectory with gradient correction.

Translated from *Atomnaya Energiya*, Vol. 32, No. 1, pp. 81-82, January, 1972. Original article submitted January 6, 1971; revision submitted May 10, 1971.

© 1972 Consultants Bureau, a division of Plenum Publishing Corporation, 227 West 17th Street, New York, N. Y. 10011. All rights reserved. This article cannot be reproduced for any purpose whatsoever without permission of the publisher. A copy of this article is available from the publisher for \$15.00.

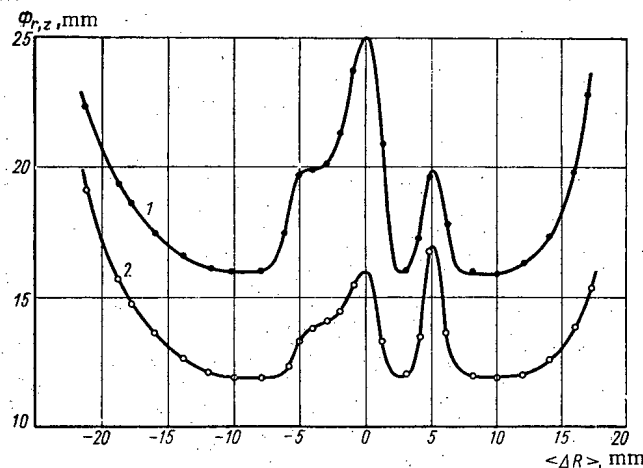


Fig. 3. Dependence of the horizontal (1) and vertical (2) dimensions of the accelerated beam in a radially focusing section on its motion at various radii during the flat portion of the magnetic field for  $H = 12$  kOe.

vertically and horizontally with an accuracy of 0.5 mm. The edge of the beam corresponded to that target position for which no limitation on the accelerated beam intensity was observed as measured by signal electrodes with an accuracy of a few percent. Figure 1 indicates beam dimensions in both planes increase starting at a field of 9 kOe when the effects of iron saturation become noticeable. Furthermore, the nature of the dependence is determined by the mean radius of the accelerated beam orbit. In order to explain this effect, the dependence of betatron oscillation frequencies on radial position of the beam [2] was measured for various values of the magnetic field in the accelerator. The frequency cell  $Q_{r,z}$  is shown in Fig. 2; it shows how the frequencies change with radial beam displacement for various magnetic field inductions in the accelerator. The lines aa, bb, and cc correspond to trajectories of operating point motion for acceleration at various radii. By analyzing Fig. 2, one can explain the increase in beam dimensions occurring above 9 kOe by the effect of the third order resonances  $3Q_z = 29$ ,  $2Q_z + Q_r = 29$ , and  $3Q_r = 29$ . The beam dimensions during the flat portion of the magnetic cycle were studied as a function of radial position. The results are shown in Fig. 3. They can also be explained on the basis of Fig. 2.

In order to eliminate the effect of the resonances, conditions were created for which the operating point was in a resonance-free region. For this purpose, the beam was accelerated with an accuracy better than  $\pm 1$  mm on the central radius starting at 4 kOe by choosing a rigorously defined law for the variation of the accelerating voltage frequency. For this beam position, a current variation in the pole windings for gradient correction was selected for which the trajectory of operating point motion corresponded to the curve AB (see Fig. 2). The measurements of beam dimensions in this case are shown in Fig. 1 by the dashed lines. It is clear that there are practically no effects from nonlinear resonances, and beam dimensions decrease up to the end of acceleration as a result.

On the basis of these studies, one can conclude that an increase in beam dimensions resulting from the effects of nonlinear resonances occurs at the end of the acceleration cycle for acceleration at any of the possible radii. By selecting the necessary law for correction of the magnetic field gradient for a given radius of acceleration, one can avoid this effect and reduce the horizontal and vertical emittance of the accelerated beam to values no more than  $\pi$  mm  $\cdot$  mrad. The correction mode studied also makes it possible to improve the time structure of secondary particle beams generated at internal targets; this structure arises because resonances appear while the accelerated beam is being directed onto the target [3]. The correction mode studied makes possible an increase in extraction efficiency for both fast and slow extraction. In slow extraction, the correction method discussed can be combined successfully with the required correction for quadratic nonlinearity of the magnetic field [4]. The authors are grateful to A. A. Kardash, V. V. Lapin, and V. G. Sinenko who provided operation of the gradient correction system during the experiments.

#### LITERATURE CITED

1. V. I. Gridasov et al., in: Proceedings of the VII International Accelerator Conference [in Russian], Vol. 2, Erevan (1970), p. 509.

2. K. F. Gertsev et al., IHEP Preprint SKU 70-86, Serpukhov (1970).
3. V. I. Gridasov et al., IHEP Preprint SKU 70-57, Serpukhov (1970).
4. K. P. Myznikov, V. M. Tatarenko, and Yu. S. Fedotov, IHEP Preprint SKU 70-51, Serpukhov (1970).

VALUE OF  $\bar{\nu}$  FROM ENERGY BALANCE IN  $U^{233}$  AND  $Pu^{239}$  FISSION

N. P. Kolosov, B. D. Kuz'minov,  
A. I. Sergachev, and V. M. Surin

UDC 621.039.512.23

The set of known experimental data characterizing the energy dependence of  $\bar{\nu}$  is comprehensively presented and systematized in [1]. However, the divergent results of different authors or the lack of sufficiently detailed information about values of  $\bar{\nu}$  hinder to a considerable extent a detailed understanding of the dependence of  $\bar{\nu}$  on neutron energy  $E_n$ . Because of this, it is advisable to use indirect data also to clarify the energy dependence of  $\bar{\nu}$ . The dependence of  $\bar{\nu}$  on  $E_n$  was analyzed [2-4] on the basis of energy balance including the results of measurements on mass and kinetic energy distributions of fragments during the fission of  $Th^{232}$ ,  $U^{235}$ ,  $U^{238}$ , and  $Pu^{239}$  by neutrons with energies to  $E_n = 6$  MeV.

In this paper, a similar analysis was made for  $U^{233}$  and  $Pu^{239}$  in the neutron energy range 0-1.6 MeV. For this purpose, the yields and kinetic energies of fragments were measured for fission of  $U^{233}$  and  $Pu^{239}$  by neutrons in the energy ranges 0-1.6 and 0-0.8 MeV respectively. The neutron energy resolution was  $\pm 50$  keV. The method of measuring mass and kinetic energy distributions of the fragments has been described [5]. The present results for  $Pu^{239}$  and those in [5] agree within the limits of statistical error ( $\pm 100$  keV). The average value of the results in these two papers was used in the energy balance analysis.

The dependence of  $\bar{\nu}$  on neutron energy  $E_n$  can be represented in the following form [3, 4]

$$\bar{\nu}(E_n) = \bar{\nu}(E_n^0) + \alpha(\Delta E_n - \Delta \bar{E}_K + \Delta \bar{E}_f^Z) + \Delta \bar{\nu}_Y, \quad (1)$$

where

$$\Delta E_n = E_n - E_n^0; \quad \Delta \bar{E}_K = \int \Delta E_K(M) Y(M) dM;$$

$$\Delta E_K(M) = E_K(M, E_n) - E_K(M, E_n^0);$$

$$\Delta \bar{\nu}_Y = \int \nu_0(M) \Delta Y(M) dM;$$

$$\Delta Y(M) = Y(M, E_n) - Y(M, E_n^0);$$

$M$  is the fragment mass;  $\Delta \bar{E}_f^Z$  is the change in the mean fission energy because of redistribution of charges between fragments;  $Y(M)$  is the yield of fragments with mass  $M$ ;  $E_K$  is the kinetic energy of the fission fragments; and  $\alpha^{-1}$  is the energy expended in the ejection of a neutron. In the analysis, it was assumed  $\Delta \bar{E}_f^Z = 0$ . The value of  $\alpha$  for  $Pu^{239}$  was 0.104 [4]. In evaluating the magnitude of  $\alpha$  for  $U^{233}$ , the same method was used as in [4], using the results for fragment yields and kinetic energy when  $E_n = 4.5$  and 5.3 MeV. The value  $\alpha = 0.102$  was obtained for  $U^{233}$ . The values of  $\bar{\nu}$  for thermal neutron fission of  $U^{233}$  and  $Pu^{239}$  - 2.48 and 2.8738 respectively - served as the reference values  $\bar{\nu}[E_n^0]$ . The results of the analysis are shown in Fig. 1. All the  $\bar{\nu}$  values were taken from [1] in accordance with the calibration used there. The data for  $U^{233}$  in [6] is an exception. These results were calibrated with respect to the reference value for  $\bar{\nu}$  at  $E_n = 400$  keV. The reference value was selected by analysis of the fission energy including the dependence of  $E_K$  on  $E_n$  obtained in [7]. Since the present experimental results and the results in [7] do not agree, the reference value of  $\bar{\nu}$  at  $E_n = 400$  keV was renormalized with allowance for the present results. The solid line in Figs. 1a and 1b shows the energy dependence of  $\bar{\nu}$  obtained by analysis of fission energy balance. The same figure shows the results of measurements of the dependence of  $E_K$  on  $E_n$ .

Translated from *Atomnaya Energiya*, Vol. 32, No. 1, pp. 83-84, January, 1972. Original article submitted February 25, 1971.

© 1972 Consultants Bureau, a division of Plenum Publishing Corporation, 227 West 17th Street, New York, N. Y. 10011. All rights reserved. This article cannot be reproduced for any purpose whatsoever without permission of the publisher. A copy of this article is available from the publisher for \$15.00.



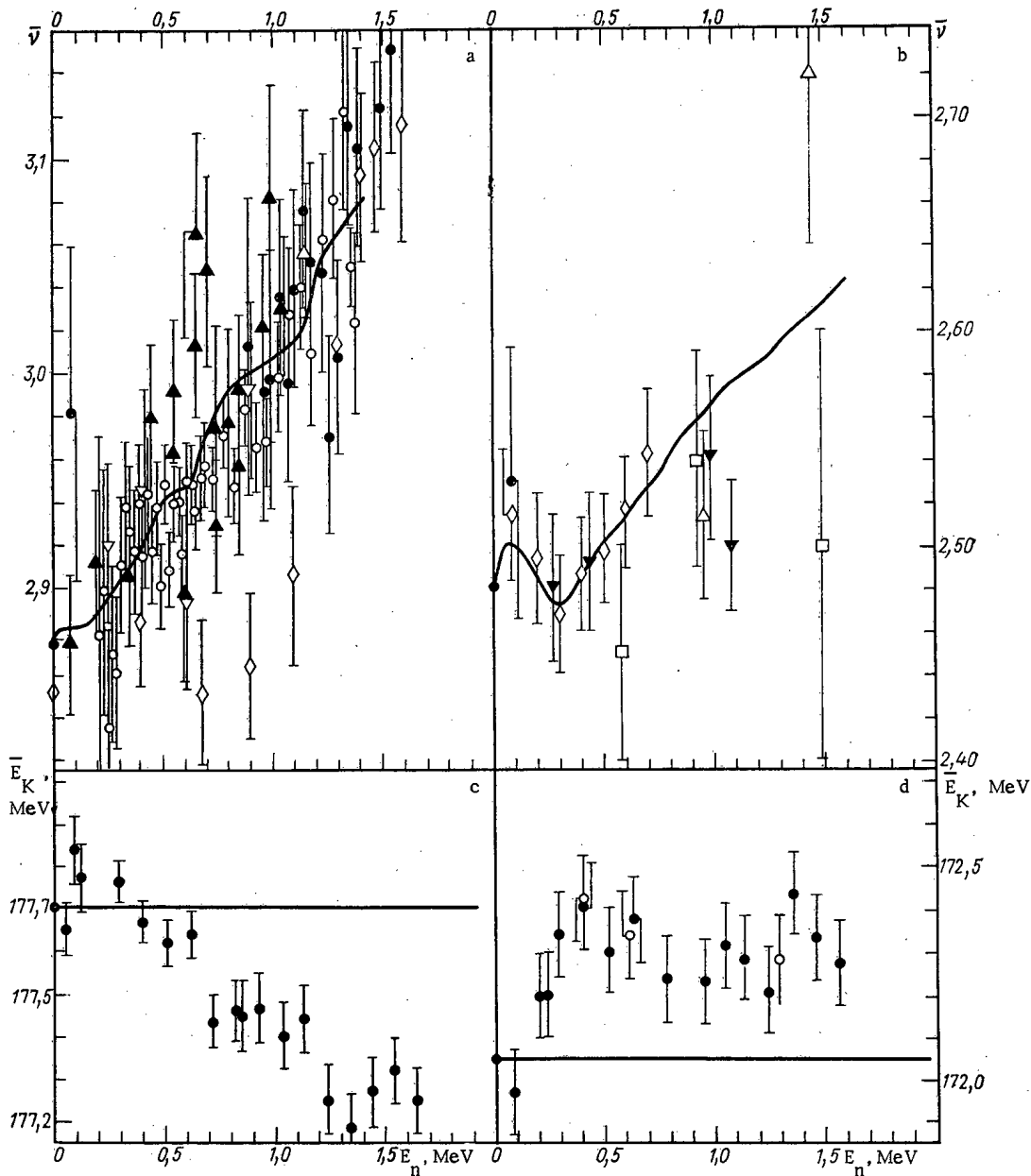


Fig. 1. Energy dependence of  $\bar{\nu}$  for  $\text{Pu}^{239}$  (a) and  $\text{U}^{233}$  (b). Experimental data taken from [1]; —) our recommendations. Average kinetic energy of fission fragments for  $\text{Pu}^{239}$  (c) and  $\text{U}^{233}$  (d): ●) present work; ○) results of [8].

It should be remembered that the reliability of the results for the energy dependence of  $\bar{\nu}$  is determined in many respects by the validity of the assumptions used in the calculations. The small value of  $\alpha$  for  $\text{Pu}^{239}$  and  $\text{U}^{233}$  is obviously associated with the presence of some process which reduces the average fission energy. In particular, the redistribution of charges between fragments or the broadening of the charge distribution [3, 4] can be related to such phenomenon. However, the value of the parameter  $\alpha$  is not critical for the neutron energy region under consideration, and if the effects not considered in the computation of  $\alpha$  occur mainly at higher neutron energies, this has only a slight effect on the results of the calculation to determine the energy dependence of  $\bar{\nu}$ .

The authors are grateful to N. P. D'yachenko and V. F. Mitrofanov for help with the measurements.

#### LITERATURE CITED

1. V. Konshin and F. Manero, INDC(NDS)-19/N, International Atomic Energy Agency, Vienna (June, 1970).

2. P. Djachenko et al., Phys. Letters, 31B, 122 (1970).
3. V. G. Vorob'eva et al., At. Énerg., 29, 130 (1970).
4. V. G. Vorob'eva et al., Paper No. 26/88 at the Second International Conference on Nuclear Data for Reactors, Helsinki (June, 1970).
5. A. I. Akimov et al., Yadernaya Fizika, No. 3 (1971).
6. V. F. Kuznetsov and G. N. Smirenkin, Nuclear Data for Reactors, International Atomic Energy Agency, Vienna (1967).
7. Yu. Blimkina et al., Nucl. Phys., 52, 648 (1968).
8. P. P. D'yachenko et al., Yadernaya Fizika, 6, 1167 (1967).

ABSOLUTE MEASUREMENTS OF THE QUANTITY  $\alpha$  FOR  $U^{235}$  AND  
 $Pu^{239}$  IN THE NEUTRON ENERGY REGION OF 10 keV-1 MeV

V. N. Kononov, E. D. Poletaev,  
 Yu. S. Prokopets, A. A. Metlev,  
 and Yu. Ya. Stavisskii

UDC 539.172.4

The aim of this experiment was to obtain new experimental data on the quantity  $\alpha$  for  $U^{235}$  and  $Pu^{239}$  in the most important neutron energy interval for fast reactor calculations, 10 keV-1 MeV. The experiment was performed with a time-of-flight spectrometer on a pulsed electrostatic accelerator. The method of measuring the quantity  $\alpha$  was based on the use of a large liquid scintillation detector (scintillation tank) charged with cadmium [1-3], which served for the detection of radiative capture and fission events by prompt  $\gamma$ -rays and for the identification of capture and fission events by detecting fission neutrons after their moderation and absorption in the cadmium. By this method the value of  $\alpha$  may be obtained from the relation

$$\alpha = \frac{\varepsilon_{\gamma f} N_1/N_2 [1 - C(1-P)] - C(1-P)}{\varepsilon_{\gamma c} (1-P) - N_1 P/N_2}, \quad (1)$$

where  $N_1$  and  $N_2$  are the two types of detected events: single events (primarily capture), and events accompanied by the detection, during a certain required time interval, of supplementary pulses from the fission neutrons (primarily fission);  $\varepsilon_{\gamma c}$  and  $\varepsilon_{\gamma f}$  are the efficiencies for the detection of capture and fission events by prompt  $\gamma$ -rays;  $C$  is the probability that the fission event will not be accompanied by the detection of fission neutrons in the required time interval;  $P$  is the probability that the event is accompanied by random background pulses.

The experiment to measure the quantity  $\alpha$  for  $U^{235}$  and  $Pu^{239}$  was performed on a pulsed electrostatic van de Graaf accelerator. The parameters of the proton beam on the accelerator target were: length of current pulses, 20 nsec; size of pulse current, 1 mA; pulse repetition rate, 300 kc. The measurements were conducted on a 1.125 m base with 18 nsec/m resolution using a continuous spectrum of neutrons from "thick" targets for an energy range of 10-80 keV and in an experiment on monoenergetic neutrons with a resolution of 10-30 keV in the neutron energy region of 100 keV-1 MeV. The  $Li^7(p, n)Be^7$  and  $T(p, n)He^3$  reactions served as the neutron source. Metallic lithium targets and standard T-Ti targets were used.

The detector was a scintillation tank with a 400 liter volume, with a cylindrical cavity in the center of it filled with an aqueous solution of cadmium nitrate, which is a convertor for the detection of fission neutrons. This type of detector construction permitted us to obtain a high concentration of cadmium nuclei (H: Cd = 100:1) and thereby to decrease the life time of neutrons in the detector. The length of the required time interval was taken to be 6  $\mu$ sec on the basis of the measurement of the distribution of fission neutron life times in the detector with a fast-acting fission  $Cf^{252}$  chamber [4]. The electronic apparatus used in the experiment permitted the measurement of the neutron energy by the time-of-flight method, the identification of neutron radiative capture and fission events, the measurement of the pulse-height spectra for the detector in the detection of capture and fission events, and also the measurement of the fission probability  $C$  using ionization chambers and, in the course of the experiment, of the probability  $P$ . To determine the value of  $\alpha$  a sample of metallic  $Pu^{239}$  with a diameter of 40 mm, thickness of  $2.9 \cdot 10^{21}$  nuclei/cm<sup>2</sup>, and  $Pu^{240}$  content of 0.2%, and a  $4.1 \cdot 10^{21}$  nuclei/cm<sup>2</sup> thick  $U_3O_8$  sample enriched with up to 90%  $U^{235}$  were used. Moreover, to measure the dependence of the background level on the time-of-flight, equivalent scattering samples of carbon and lead were used. The quantity  $C$  was determined using fast fission ionization chambers

Translated from *Atomnaya Energiya*, Vol. 32, No. 1, pp. 85-87, January, 1972. Original article submitted April 29, 1971.

© 1972 Consultants Bureau, a division of Plenum Publishing Corporation, 227 West 17th Street, New York, N. Y. 10011. All rights reserved. This article cannot be reproduced for any purpose whatsoever without permission of the publisher. A copy of this article is available from the publisher for \$15.00.

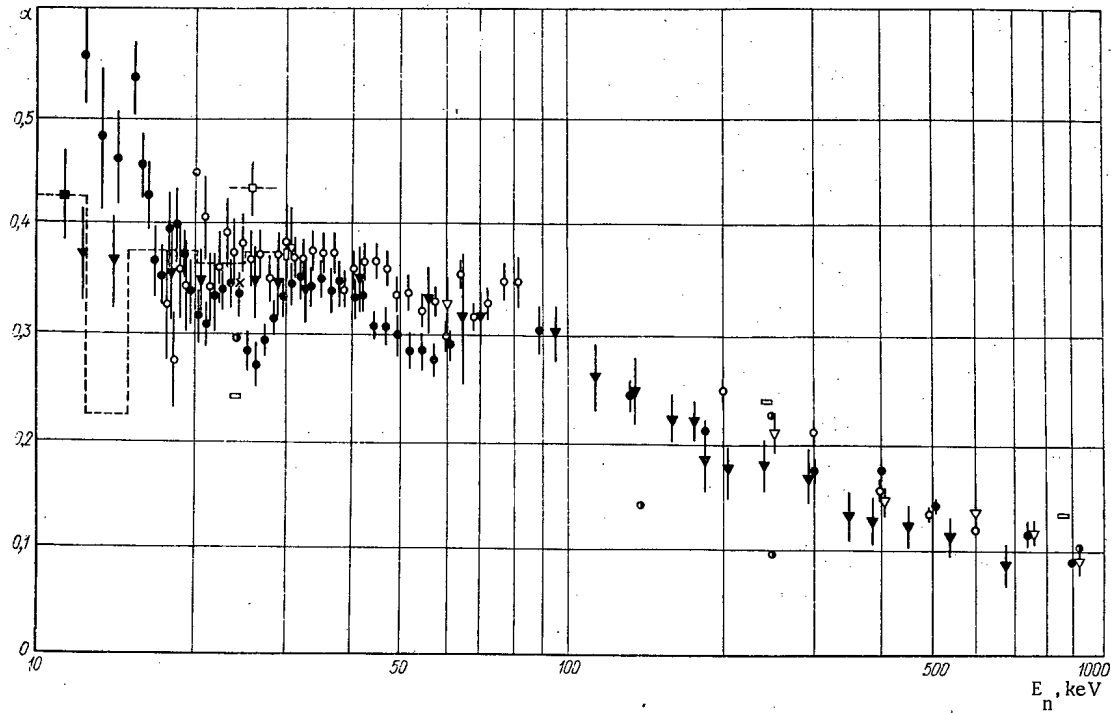


Fig. 1. Dependence of the quantity  $\alpha$  for  $U^{235}$  on neutron energy: ●) FÉI, 1970, present study; ▽) LASL, 1962, [1]; ▼) ORNL, 1964, [2]; ○) ORNL, 1967, [3]; ⊙) IAE, 1956, [5]; □) FÉI, 1958, [6]; ×) FEI, 1965, [7]; --□-- UCRL, 1970, [9]; --■-- OIYaI, 1965, [10].

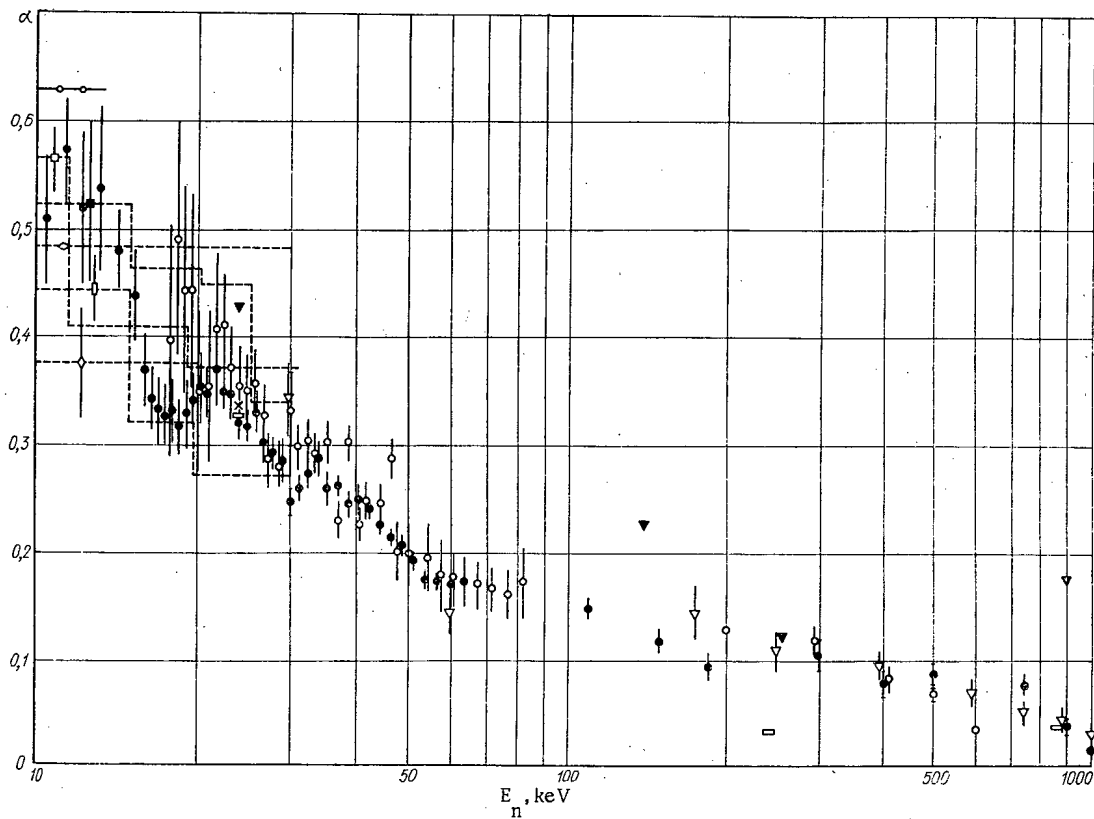


Fig. 2. Dependence of the quantity  $\alpha$  for  $Pu^{239}$  on neutron energy: ●) FÉI, 1970, present study; ▽) LASL, 1962, [1]; ○) ORNL, 1967, [3]; ▼) IAE, 1956, [5]; ⊙) FÉI, 1958, [6]; ×) FEI, 1965, [7]; --□-- UCRL, 1970, [9]; --◇-- OIYaI, 1970, [14]; --□-- ORNL - RPI, 1970, [11]; --■-- Harw, 1970, [12]; --◇-- OIYaI - FÉI, 1970, [13].

[4] with coatings of  $U^{235}$  and  $Pu^{239}$ . In experiments with plutonium this quantity for our detector was  $C_{Pu^{239}} = 0.2955 \pm 0.0073$ , and in experiments with uranium,  $C_{U^{235}} = 0.2962 \pm 0.0053$ . Moreover, to control the conditions of the experiment the quantity  $C$  was periodically determined in the process of the experiment through the detection of spontaneous  $Pu^{240}$  and  $Cf^{252}$  fission events. During the analysis of the experimental results for high neutron energies a small correction for the dependence of the probability  $C$  on the average number of fission neutrons  $\bar{\nu}$  was introduced.

The values of the quantity  $\alpha$  obtained in the experiment for  $U^{235}$  and  $Pu^{239}$  are presented in Figs. 1 and 2. They are the result of averaging five independent series of measurements for  $U^{235}$  and nine for  $Pu^{239}$ . The error indicated in the figures is root-mean-square error obtained as a result of averaging and does not include the indeterminacy of the constants of the experimental apparatus  $\varepsilon_{\gamma f}/\varepsilon_{\gamma c}$  and  $C$ , characterizing thereby the indeterminacy in the relative energy dependence of the quantity  $\alpha$ . The total absolute error of the quantity  $\alpha$ , including the indeterminacy of all quantities in (1), is 10-15%. The majority of experimental data available at present on the quantity  $\alpha$  in the region of neutron energies 10 keV-1 MeV is also presented in the figures.

It is possible to note a substantial agreement of all experimental data on  $Pu^{239}$  obtained on van de Graaf accelerators by the analogous method. For  $U^{235}$  our data in the region of neutron energies 20-100 keV lies systematically lower by 15% than the results of [1-3]. However, it must be observed that in these studies significantly thicker ( $\sim 6$  times) samples were used, and a detailed comparison evidently requires consideration of the different effects of resonance blocking. The marked structure in the dependence of the quantity  $\alpha$  on the neutron energy obtained by us both for  $U^{235}$  and for  $Pu^{239}$  is worthy of attention. This structure may be the cause of significant discrepancies in the case of  $U^{235}$  in the results of measurements of  $\alpha$  by the transmission method in the spherical geometry on photoneutron sources Sb-Be [5-7]. The presence of such a structure in the quantity  $\alpha$  is not surprising and may be linked with the strong structure in the fission cross section, which for  $U^{235}$  in this region of neutron energies was recently discovered [8].

In conclusion the authors express their gratitude to A. I. Leipunskii, L. N. Usachev, A. I. Abramov, and V. A. Romanov for their constant attention and cooperation in the completion of the present study and also to V. S. Shorin, M. V. Bokhovko, N. S. Kosulin, V. I. Volodin, and V. N. Kanaki for their participation in the preparation and conducting of the experiments.

#### LITERATURE CITED

1. J. Hopkins and B. Diven, Nucl. Sci. Eng., 12, 169 (1962).
2. L. Weston, G. de Saussure, and R. Gwin, Nucl. Sci. Eng., 20, 80 (1964).
3. G. de Saussure et al., Nucl. Data Reactors, Vol. II, Vienna, IAEA (1967), p. 233.
4. V. N. Kononov et al., Pribory i Tekh. Eksperim., No. 6, 51 (1969).
5. P. E. Spivak et al., At. Énerg., No. 3, 21 (1956).
6. V. N. Andreev, At. Énerg., 4, 185 (1958).
7. A. A. Van'kov and Yu. Ya. Stavisskii, At. Énerg., 19, 41 (1965).
8. B. Patrick et al., AERE-R 6350 (1970).
9. Y. Czirr and J. Lindsey, Nucl. Data Reactors, Vol. I, Vienna, IAEA (1970), p. 331.
10. Van-Shi-Di et al., Phys. Chem. Fission, Vol. I, Vienna, IAEA (1965), p. 287.
11. R. Gwin et al., Nucl. Sci. Eng., 40, 306 (1970).
12. M. Schomberg et al., Nucl. Data Reactors, Vol. I, Vienna, IAEA (1970), p. 315.
13. V. N. Kononov et al., Preprint P-3-5112, Dubna (1970).
14. Yu. V. Ryabov et al., Preprint P-3-5113, Dubna (1970).

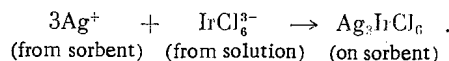
CHILL-CASTING METHOD OF BITUMINIZING NATURAL  
SORBENTS FOR Ir<sup>192</sup>\*

Kh. Daiev, G. Delchev,  
G. Gradev, S. Simov,  
and V. Zhelyazkov

UDC 546.93

The chill-casting method of bituminizing the isotopes Cs<sup>137</sup>, Ag<sup>110</sup>, Tl<sup>204</sup>, Sr<sup>90</sup>, and Ca<sup>45</sup> retained on natural sorbents (zeolite with clinoptilolite and vermiculite) has been described in the literature [1-3]. This article reports a study of Ir<sup>192</sup> sorption by several naturally occurring sorbents, and the fixing of those sorbents in bitumen by a method which we developed.

In contrast to the above elements, iridium ions in aqueous solutions tend to form various complexes [4, 5] which have the effect of complicating iridium sorption processes. Data are available on sorption of iridium only on synthetic resins [6], none being available on sorption of iridium on naturally occurring sorbents. It seems that the complicated relationship between the different forms in which iridium occurs adds difficulties to sorption of iridium on a specific cation or anion exchange resin. On the other hand, the literature contains descriptions [4, 7] of sparingly soluble iridium compounds with silver, mercury, lead, thallium, etc., of the type M<sub>3</sub>IrA<sub>6</sub>, where M stands for silver, mercury, lead, or thallium, and the IrA<sub>6</sub> denotes complexes of iridium in which A stands for Cl<sup>-</sup>, OH<sup>-</sup>, NO<sub>2</sub><sup>-</sup>, and so on. Sorbents of that type exhibit high sorption power with respect to silver, mercury, lead, and thallium. We therefore undertook an investigation of the iridium sorption conditions via precipitation reactions, i.e., we converted an appropriate sample of sorbent to the silver, mercury, lead, or thallium form suitable for precipitation reactions, and passed a solution of iridium through the bed of sorbent. For example, in the case of the silver form of the sorbent, a reaction of that type can be represented as follows:



Sorption of Ir<sup>192</sup> on natural sorbents (zeolite and vermiculite) and bituminization of sorbents retaining the isotope in question were investigated.

\*This research was done at Vienna under IAEA contract.

TABLE 1. Chemical Composition of Sorbents (%)

Sorbent	SiO <sub>2</sub>	Fe <sub>2</sub> O <sub>3</sub>	Al <sub>2</sub> O <sub>3</sub>	CaO	MgO	Na <sub>2</sub> O	K <sub>2</sub> O	TiO <sub>2</sub>	SO <sub>3</sub>	P <sub>2</sub> O <sub>5</sub>
Zeolite with clinoptilolite	65,90	0,45	12,97	2,30	0,43	2,12	4,93	0,08	—	—
Vermiculite	41,92	5,46	5,41	4,03	23,84	0,61	0,28	0,82	5,93	1,31

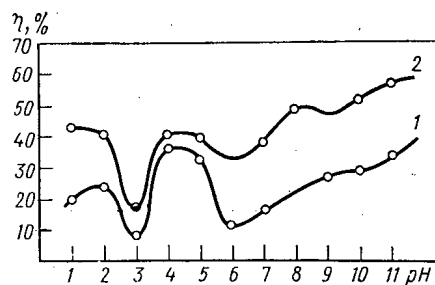


Fig. 1. Dependence of sorption coefficient  $\eta$  of Ir<sup>192</sup> on pH: 1) zeolite; 2) vermiculite.

Physics Institute of the Bulgarian Academy of Sciences, Sofia. Translated from Atomnaya Energiya, Vol. 32, No. 1, pp. 87-89, January, 1972. Original article submitted May 20, 1971.

© 1972 Consultants Bureau, a division of Plenum Publishing Corporation, 227 West 17th Street, New York, N. Y. 10011. All rights reserved. This article cannot be reproduced for any purpose whatsoever without permission of the publisher. A copy of this article is available from the publisher for \$15.00.

TABLE 2. Results of Experiments on Sorbents with Presorbed Cations

Cation	Zeolite with clinoptilolite			Vermiculite		
	specific activity, pulses/min-ml		sorption coefficient, %	specific activity, pulses/min-ml		sorption coefficient, %
	initial solution	solution passed through bed		initial solution	solution passed through bed	
Silver	2040	202	90,1	2040	118	94,2
Mercury	2040	135	93,4	2040	33	98,4
Lead	2040	235	88,5	2040	299	85,3
Thallium	2040	1032	49,4	2040	857	58,0

TABLE 3. Specific Activity of Natural Waters and of Waters Washing Bitumen Block

Water analyzed	Specific radioactivity, nCi/liter					
	1970			1971		
	October	November	December	January	February	March
Water washing bitumen block with embedded $\text{Ir}^{192}$	0,045	0,012	0,025	0,018	0,028	0,170
Radioactive fallout	0,044	0,013	0,020	0,017	0,021	0,170

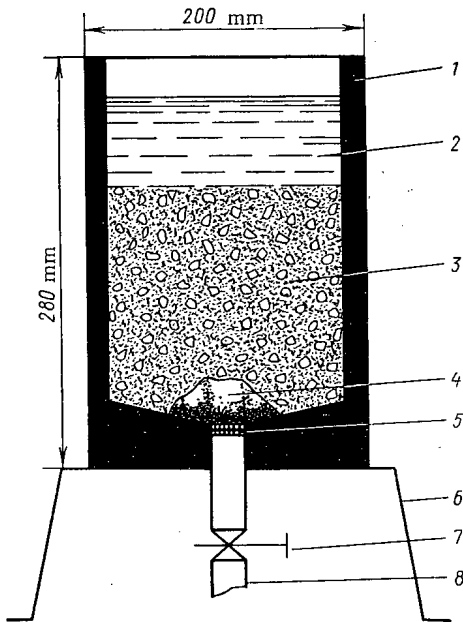


Fig. 2. Layout of bitumen fixing unit: 1) bitumen bowl; 2) radioactive solution of  $\text{Ir}^{192}$ ; 3) sorbent treated with silver nitrate; 4) fiber glass (glass wool); 5) metallic gauze; 6) support stand; 7) control valve; 8) discharge tube.

were laid down in the bowl (Fig. 2): a lower layer of vermiculite and a top layer of zeolite. A solution of silver nitrate was passed through the sorbents, and after washing with distilled water, a solution of  $\text{Ir}^{192}$  with total activity of  $10^{-3}$  Ci was passed at a flowrate of 15 to 20 ml/min. After that, the activity of the  $\text{Ir}^{192}$  solution did not differ from the activity of the naturally occurring sample due to radioactive fallout.

The sorbents were washed with distilled water (silver and iridium were not detected in the wash water), and after drying in air the bowl was sealed with molten bitumen.

The bitumen block with sorbent "loaded" with the radioactive isotope was left to stand in the open. Measurements were taken on a monthly basis to monitor the radioactivity of the water (rain or snow) washing the block, and the status of the surface of the block was observed visually.\* The results, listed in Table 3, show that the eluted radioactivity is of the order of magnitude of the amount due to radioactive fallout.

\*The method of retention and the results of monitoring observations checking on the state of the bituminous block and on the radioactivity of the collected atmospheric precipitation washing the block are described in detail in [1].

The chemical composition of the sorbents used in the naturally occurring state appear in Table 1; the grain size belongs to the class (-3.0; +0.3 mm).

The initial solution containing the iridium in the form of ammonium chloroiridite  $(\text{NH}_4)_3\text{IrCl}_6$  has a specific activity of 2040 pulses/min-ml. A specified volume of a solution whose pH is controlled by buffers was passed through a sample of sorbent at a specified flowspeed. The specific activity of the initial solution and of the solution passed through the sorbent was measured, and the sorption coefficient of iridium was calculated. The results, plotted in Fig. 1, lay bare the complicated dependence of the iridium sorption on pH, and the possibility of retaining as much as 50% (roughly) of the iridium on the sorbents referred to.

In the experiments staged with sorbents that had first been converted to their silver, mercury, lead, or thallium form, a solution of silver, mercury, lead, or thallium in nitrate form was passed through the sample. After washing with distilled water till a negative reaction was obtained for the corresponding ion, a solution containing iridium was passed through the sorbent. The results (Table 2) attest to the possibility of sorption of  $\text{Ir}^{192}$  by natural sorbents in amounts of 98-99%, upon prior sorption of silver, mercury, or lead.

Bituminization of sorbents retaining  $\text{Ir}^{192}$  was carried out according to a procedure developed by the authors [1]. Storage-battern bitumen was used to make the bitumen bowl, which was cast in a special metal chill mold. Two layers of sorbent

The investigations of Ir<sup>192</sup> on natural sorbents (zeolite with clinoptilolite and vermiculite) established the favorable effect of the presorbed cations: silver, mercury, or lead, on sorption of iridium through the formation of precipitated compounds on the sorbents. The sorbents retaining Ir<sup>192</sup> were bituminized by the chill-casting method.

The method proposed here expands the range of applications of the chill-casting method for processing low-level and medium-level liquid radioactive wastes.

#### LITERATURE CITED

1. Kh. Daiev et al., in: Management of Low- and Intermediate-Level Radioactive Wastes, IAEA, Vienna (1970), p. 739.
2. Kh. Daiev et al., Izv. Inst. Fiziki s ANEB Bolgar. Akad. Nauk, 22 (1971).
3. Kh. Daiev et al., Izv. Inst. Fiziki s ANEB Bolgar. Akad. Nauk (in press).
4. A. Werner and O. Vzies, Ann. Chemie, 364, 87 (1909).
5. F. Bimish, Analytical Chemistry of Noble Metals, Part 1 [in Russian], Mir, Moscow (1969).
6. O. Samuel'son, Ion Exchange Separations in Analytical Chemistry [in Russian], Khimiya, Moscow (1966), p. 347.
7. M. Delepine, Comptes Rendus, 149, 1073 (1909).



## INFORMATION

ALL-UNION IZOTOP AGENCY SERVING THE NATIONAL ECONOMY  
EXHIBIT AT EXPOSITION OF ACHIEVEMENTS OF THE  
NATIONAL ECONOMY

V. A. Dolinin

A topical exhibit designated as "All-Union Izotop Agency Serving the National Economy" was inaugurated in September, 1971 at the Atomic Energy pavilion of the Exposition of Achievements of the National Economy. This is the first time that an exhibit of that type has been set up at the Exposition. It constitutes a sort of report on the ten years of activities of the V/O Izotop agency.

This agency, set up in 1961, has been called upon to serve various branches of industry, agriculture, science, and medicine in providing them with sources of ionizing radiations, radioactive and stable isotopes, labeled compounds and rare earths, radioisotope process monitoring instrumentation, radiation techniques and equipment, personnel shielding equipment, equipment for handling radioactive materials, electron physics equipment, dosimetric and radiometric equipment.

The problems highlighted by various sections of the exhibit are timely ones. The displays clearly indicate how the problem of utilizing nuclear and radiation processes in science and in industrial practice, posed in the resolutions of the XXIV Congress of the Communist Party of the Soviet Union, is being met.

There are seven sections in the exhibit.

The introductory section is devoted to the activities of the V/O Izotop agency and of its subdivisions. The beautifully conceived display stands graphically illustrate the increased volume of V/O Izotop deliveries in 1970 over the 1965 level, in percentages:

Isotope production .....	206
Radioisotope process monitoring devices .....	180
Electron physics, dosimetric, and radiometric equipment.....	350
Shielding and personnel protection.....	250
Radiation equipment .....	150
Total volume of deliveries.....	278
Volume of export deliveries.....	676

It is also clear that the production of isotope equipment in 1970 increased by 318 items over the 1965 level, while the production of electron physics equipment, and of dosimetric and radiometric equipment, was increased by 175 items.

The "Personnel protection and equipment for handling radioactive materials" division of the exhibit informs visitors of measures taken in the USSR to ensure labor safety in work with radioactive materials. Specimens of special plastic laminate protective clothing, as well as equipment for handling radioactive materials, such as: various types of glove boxes, hoods and dry boxes, remote-control manipulating equipment, protective devices, and conveying equipment, are on display in that section.

Several types of gamma-ray nondestructive testing instruments were on display in the "Radiation equipment" section. At the present time, gamma-ray inspection and nondestructive testing is one of the

---

Translated from Atomnaya Energiya, Vol. 32, No. 1, pp. 91-93, January, 1972.

© 1972 Consultants Bureau, a division of Plenum Publishing Corporation, 227 West 17th Street, New York, N. Y. 10011. All rights reserved. This article cannot be reproduced for any purpose whatsoever without permission of the publisher. A copy of this article is available from the publisher for \$15.00.

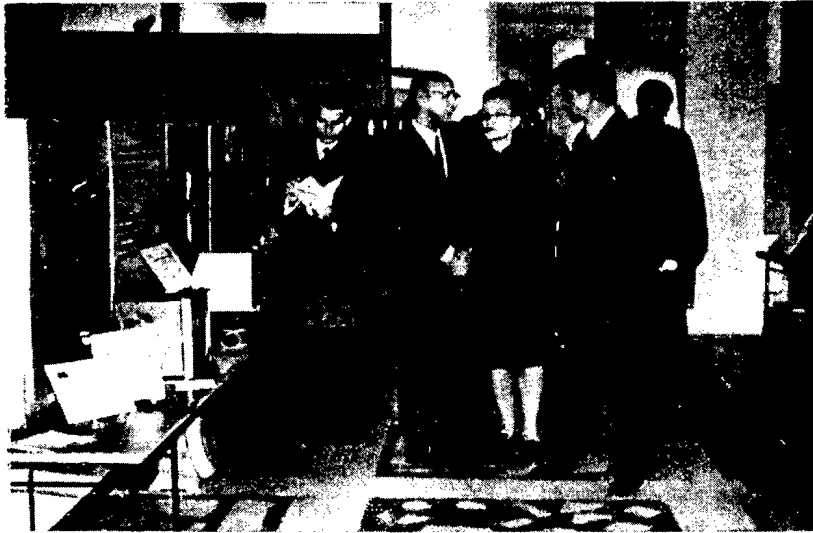


Fig. 1. In the exhibit halls.



Fig. 2. In the exhibit halls.

efficient methods available in quality control of materials, parts, and equipment (with no need to destroy or dismantle the equipment inspected), laying the basis for great strides forward in improving the characteristics of goods manufactured, improving the reliability of machine parts performance, and preventing damage to equipment, mechanisms, and parts. Visitors have the opportunity to become familiarized with the RD-11, RD-21, Gazprom, and other gamma-ray nondestructive testing instruments, as well as accessories for gamma-ray nondestructive testing instruments.

The radiation processing outfits designed for radiation research and radiation processes in biology, medicine, chemistry, and agriculture, were presented at the exhibit in the form of diagrams, photographs, and working mockups.

The neutron activation analysis section deals with one of the most sensitive and up-to-date methods of ultimate analysis of the composition of materials, and displays a full-size K-1 neutron activation analysis set for oxygen determinations and a diagram of the SO-1 neutron activation analysis system.

The "Radioisotope process monitoring instrumentation" section is the most representative one at the exhibit. Automated measurements of forgings and automatic control of 2000-ton and 3000-ton hydraulic drop forge presses with the aid of the RTP2-1S dual-channel radioisotope relay instrument have been instituted at the V. I. Lenin Neva Machinery Factory, with improved forging precision, increases in the

number of press strokes, better forging quality, and better working conditions resulting. Annual savings of 59,000 rubles are reported.

Nine UR-8 radioisotope level gauges and 32 gamma relay units are in use at the Slavgorod chemical plant, for monitoring flowrate and fill level of liquefied gases and corrosive fluids. Savings of 200,000 rubles annually are reported.

The installation of three radioisotope liquid density gauges at the Nikopol'marganets trust ore processing mill in Grushevka has resulted in annual savings of 60,000 rubles.

Use of an ITShch-496 radioisotope thickness gauge on a coil cut-up line at the Novolipetsk metallurgical plant, with automatic sorting and grading of steel plate, made it possible to free 30 workers for other assignments, and resulted in annual savings of 42,500 rubles.

The RRV-64 radioisotope gauges and weight controllers for paper and cardboard sheet, installed on four machines at the Sloka paper and pulp combine, have constituted an efficient means of raising labor productivity, achieving savings in raw materials and finished materials, and in improving product quality. Savings resulting from the installation of RRV-64 devices on production lines have totalled 30-40 thousand rubles per year per device.

The use of 120 radioisotope instruments on automatic process lines for interlocking in the event of cutting tool breakage has yielded savings of 500 rubles annually per instrument, through curtailment of scrap and turnover of tools.

The display stand of the Karaganda metallurgical plant, showing 172 radioisotope instruments in effective service for automated monitoring and control of the fill level of materials in tanks, for measuring moisture content and weight of sinter burdens, ash content of coals, thicknesses of hot-rolled plate, and analysis of raw materials and finished products, is of great interest. The use of 82 gamma relay units in the sintering department of that plant, for automatic monitoring of the fill level of materials in hoppers, has yielded 90,000 rubles yearly in savings. The display of the Krasnoe Sormovo plant gave an account of automatic control of metals casting on a continuous steel casting machine. Savings have amounted to 160,000 rubles a year.

The "Electronic nuclear physics equipment" section presented full-size specimens of various types of equipment, including: PP-9-2M, BP-100, and PP-15 scaling circuits, the Protoka proportional-flow  $4\pi$ -counter, and many others.

Dosimetric and radiometric instrumentation for monitoring the radiation environment and ensuring radiation safety of personnel in handling of radioactive materials is on display: a pocket set of direct-indicating DK-02 dosimeters with the ZD-5 charging device, the KID-20 set of personnel dosimeters, the IFK-2, 3 set of personnel film badges, the IZV-1 portable dosimeter for monitoring the dust load in the local air and the content of radon daughters in dust, the Ol'kha-1 aerosol radiometer, and the Araks dosimetering device.

The "Stable and radioactive isotopes" section is set up in an interesting and attractive way, informing visitors that the V/O Isotop agency is the general delivery agent for all isotope products in the USSR.

Many of the display stands present accounts of the applications of stable isotopes in chemistry, biology, biochemistry, physics, and also applications of radioactive isotopes as labeled atoms in scientific and industrial research, as sources of ionizing radiations in automatic process control and monitoring instrumentation.

The exhibit came to constitute a large educational forum for hundreds of specialists in the national economy. Seminars were held for the benefit of specialists from various regions of the country on special passes issued by the Exposition of Achievements of the National Economy of the USSR, to promote more widespread utilization of the atom for peaceful purposes.

## SEMINARS AND CONFERENCES AT V/O IZOTOP

While the topical exhibit "All-Union Izotop agency in the service of the national economy" was being held at the "Atomic Energy" pavilion of the Exposition of Achievements of the National Economy of the USSR, the All-Union Izotop agency was holding five seminars. The agenda of these seminars consisted of presentation of reports on the agency's activities. The seminar participants were familiarized with the list of devices, dosimetric and electron physics equipment, supplied to industry by the agency for research and industrial use, and the new types of instruments planned for delivery in 1972. The seminars attracted a total of 250-odd specialists: representatives of ministries, representatives of management boards, scientific-research and planning institutes, grass-roots level isotope laboratories, organizations and industrial plants in the various cities and districts of the country.

The seminars will contribute to more widespread acceptance and utilization of radioisotope techniques and equipment in the various branches of industry, agriculture, and in scientific and medical institutions throughout the nation.

The three day seminar on the topic "Isotopes and isotope instruments in the national economy" was held at the Scientific-Research Institute for Nuclear Physics, Electronics, and Automatic Control attached to the S. M. Kirov Tomsk Polytechnic Institute, in July, 1971. About 300 engineering and technical personnel from plants, scientific-research personnel, and party leaders took part in this seminar.

An "Isotopes in the service of humanity" exhibit was running concurrently with the seminar. This exhibit displayed 250 items in isotope products, nuclear instrumentation, and personnel protection.

The seminar and the exhibit stimulated a good deal of interest on the part of specialists in the city and nearby localities.

A conference on "Radiation techniques in the automation of mines and ore processing plants" was held at Donetsk on September 22-24, 1971. Specialists from power and machinery management bodies of mining and ore combines dealing with automation, mine automation mechanics, and technology, and other specialists, were attracted to the conference. The implementation and perspective applications of radioisotope equipment in the coal industry were discussed at the conference. The conference participants heard reports on experience in the introduction of radioisotope equipment and practice at the Donetskugol', Artemugol', Makeevugol', Voroshilovgradugol', and Pavlogradugol' combines.

After hearing and discussing the papers and reports, the conference participants pointed out that a lot of work has been done in recent years on applications of radioisotope equipment at plants and enterprises in the coal industry.

The conference participants were afforded the opportunity of familiarizing themselves with the operation of automation instruments in the mines of the Krasnoarmeiskugol' mining and ore combine.

A seminar on "Applications of radioisotope methods and instruments in the chemical process industry" was held in the "Atomic Energy" pavillion of the Exposition of Achievements of the National Economy of the USSR in September, 1971. The seminar attracted 112 representatives of 40 chemical and petrochemical plants, scientific-research institutes, organizations, and design agencies. The purpose of the seminar was to promote exchanges of experience and information on the development of new radioisotope hardware, and on the implementation of radioisotope techniques and instruments in various branches of the chemical process industry.

The reporters drew attention to the increased number of studies and projects in applications of radioisotope instruments in the design of automatic process control systems, as well as the development of

---

Translated from Atomnaya Energiya, Vol. 32, No. 1, pp. 93-94, January, 1972.

© 1972 Consultants Bureau, a division of Plenum Publishing Corporation, 227 West 17th Street, New York, N. Y. 10011. All rights reserved. This article cannot be reproduced for any purpose whatsoever without permission of the publisher. A copy of this article is available from the publisher for \$15.00.

nuclear physics techniques for monitoring the composition and properties of chemical products, and implementation of full-scale industrial methods for monitoring chemical processes with the aid of radioactive tracers. Several chemical process plants and combines are already making use of a hundred or more radioisotope instruments each, with appreciable savings and improvements in working conditions as a result.

The seminar participants acknowledged the need for more widespread acceptance of radioisotope instruments in chemical production processes, in order to facilitate further expansion of the utilization of the achievements of applied nuclear physics in the chemical process industry, with emphasis on their use in the production of mineral fertilizers, in the plastics industry, in synthetic fiber production, in the production of ore processing raw materials, and in chlorine industry, where they be used to maximum economic effect.

On the initiative of the Ministry of Public Health of the USSR and the Moscow Scientific-Research Institute for X-Radiology, a seminar on "Modern techniques and equipment for radiation therapy of malignant neoplasms and clinical dosimetry" was held in September, 1971 at the "Atomic Energy" pavilion of the Exposition of Achievements of the National Economy of the USSR. Participating in this seminar were 130 radiologist-physicians (radiation therapists). Of these, 80 were representatives of therapeutic-prophylactic and scientific-research institutes in the republics of the Union.

The seminar participants heard reports in which the present state of the art and the developmental outlook of radiation therapy and clinical dosimetry were examined.

The seminar participants recommended holding of future seminars on medical radiology. The feasibility of scheduling a symposium on diagnostics and treatment of lymphogranulomatosis was pointed out.

A scientific-technical conference on "Applications of radioisotope instruments in the national economy" in October, 1971, was held in the city of Dushanbe. There were four panel sessions at the conference. The conference participants heard over 40 papers and reports discussing applications of radioisotope techniques and instruments in the ore and mining industry, in the building materials industry, cotton growing, medicine, and other fields.

The reporters noted that the Dushanbe reinforced concrete structures and structural parts plant is making successful use of radioisotope equipment and techniques, with appreciable gains in the engineering costs picture. Methods of nuclear geophysics are being used effectively in expeditions and laboratories of the Geology Board of the Council of Ministers of the Tadzhik SSR. The Institute of Plant Physiology and Biophysics of the Academy of Sciences of the Tadzhik SSR worked out a method for autoradiography of cotton plants, and completed work on control of the transport of plant assimilants. Radioactive isotopes and sources of ionizing radiations are being used effectively in some medical institutions in Central Asia for diagnostics and treatment of various illnesses.

The conference contributed to exchange of experience on the applications of radioisotope equipment in the national economy, and more widespread implementation of scientific-research developments in industry.

## CONFERENCES

SIXTH ALL-UNION CONFERENCE ON SYNTHESIS, PRODUCTION,  
AND APPLICATIONS OF SCINTILLATORS

L. Ya. Zhil'tsova, E. N. Matveeva,  
and I. M. Stoletova

The regular VI All-Union conference on the synthesis, production, and applications of scintillators was held in May, 1971, in Khar'kov.

A large number of the papers submitted to the conference dealt with research and development work in the physics of the scintillation process in alkali halide crystals. A paper by L. M. Shamovskii and colleagues dealt with the nature of light diffusion centers and the conditions governing their formation in the process of growing ionic crystals from a melt. The nature of light-scattering inclusions was studied in the case of melt-grown fluorite crystals produced under a variety of melt conditions. It was shown that elimination of light-diffusing inclusions brings about improved scintillator quality.

A report by E. M. Arm et al. dealt with the outlook for utilization of scintillation detectors with a base of CsI(Na) single crystals at elevated temperatures. They established the advantage of these scintillators over CsI(Tl) scintillators. The scintillators investigated display a plateau in their counting characteristic at temperatures 140-150°C. A large number of papers were devoted to investigation of the properties of these crystals. In line with the expanding opportunities for applications of CsI(Na) crystals, we note an interesting paper submitted by I. I. Kisel' and N. I. Krainikov on growing CsI(Na) single crystals in a horizontally rotating ampule. It was demonstrated that the growth rate of the single crystals can be increased above five times over the rates used in growing single crystals by the Stockbarger method. Single crystals grown at a rate of 11 mm/h are not inferior in their scintillation characteristics to the best single crystals grown by the Stockbarger method at a rate of 2 mm/h.

B. K. Damitov et al. proposed a new method for determining the intrinsic resolution of small-size NaI(Tl) crystals by using a photomultiplier with a large photocathode diameter.

A report on an improvement in the technological process in mass production of polystyrene scintillators was submitted by a team working at the VII Monokristallov (All-Union Scientific-Research Institute of Single-Crystals) (O. A. Gunder, A. L. Lifshits, others), covering investigations of the technological factors influencing the polymerization process and the scintillation properties of plastic scintillators, and presenting recommendations on how to best fabricate them.

G. P. Volosyuk et al. gave an account of the effect of such secondary solvents as naphthalene on the optical and scintillation properties of element-containing (heteroorganic) plastic scintillators, which are capable of raising the light yield of plastic scintillators by 30-35% when secondary solvents are used and luminescence additives are selected.

O. A. Gunder and colleagues studied the effect of vinylxylene synthesis technology on the light yield of plastic scintillators. It was demonstrated that an isomer of 2,4-dimethylstyrene exhibits the best scintillation properties.

Research on polymethylmethacrylate base plastic scintillators has been continued (S. A. Malinovskaya et al.). Shortening of the fluorescence decay time and simultaneous increase in the amplitude of the light pulse with increasing concentration of luminescent additives have been detected.

---

Translated from *Atomnaya Énergiya*, Vol. 32, No. 1, pp. 94-95, January, 1972.

© 1972 Consultants Bureau, a division of Plenum Publishing Corporation, 227 West 17th Street, New York, N. Y. 10011. All rights reserved. This article cannot be reproduced for any purpose whatsoever without permission of the publisher. A copy of this article is available from the publisher for \$15.00.

A. E. Buklei et al. developed and investigated a  $1000 \times 1000 \times 20$  mm counter based on such a plastic scintillator of enhanced transparency. The counter efficiency was measured with a beam of relativistic  $\pi^-$ -mesons, and found to be close to 100% over its entire area.

Many of the reports presented were read at the panel on applications of scintillators and detectors based on scintillator crystals.

A report by V. V. Chernikov (in the name of a team of colleagues at VNIIMonokristallov) was devoted to a slow-neutron activation detector using plastic and liquid scintillators containing chlorine, bromine, iodine, and zinc. Introduction of iodine into plastic scintillators proved most successful. Neutron recording efficiency was 0.61 when plastic scintillators with a base of styrene and 10% diiodobenzene copolymer was used. A liquid neutron detector with an efficiency  $\geq 0.66$  was obtained by the authors upon introducing a tributylphosphate solution of  $\text{InCl}_3$  into  $\alpha$ -methylnaphthalene.

E. M. Burymov reported on applications of platelet type deuterated scintillators in fast-neutron spectrometry. Deuterated anthracene or naphthalene can be used as the platelet material. This scintillator, in the form of a stack of alternately sandwiched deuterated (0.05 mm) and glass (0.1 mm) wafers, can provide an amplitude resolution of 1.3% and a peak-to-valley ratio of 30.

During the conference discussion, investigations of scintillators as detectors of long-wavelength x-ray emission and of new scintillation detector units for x-ray equipment came under discussion (V. R. Al'perovich et al.), as well as enhanced sensitivity in recording of ultraweak bioluminescence of living tissues (E. V. Buyanov et al.), utilization of a low-background scintillation  $\gamma$ -ray spectrometer for investigating radiation purity of several materials (V. D. Gorin), investigations of the characteristics of scintillation detectors with the aid of light generators (Yu. N. Kuzin et al.), and so forth. Topics relating to the solutions of those problems received a prominent place in the discussion. A report by E. I. Minsker on optical adhesives with a polyorganosiloxane base was considered of great practical interest.

The conference proceedings will be published in the next collection of articles in the series "Single Crystals, Scintillators, and Organic Phosphors" issued by VNIIMonokristallov, Khar'kov. The next conference, the seventh, is scheduled for 1974.

FOURTH CONFERENCE OF THE INTERNATIONAL NUCLEAR  
DATA COMMITTEE

M. F. Troyanov

The regularly scheduled IV conference of the IAEA International Nuclear Data Committee (INDC) was held in July, 1971, at the Homi Bhabha Atomic Research Center in Trombay (India). The conference was attended by 14 INDC members, 13 representatives of various countries plus one IAEA representative, in addition to six scientific advisors and observers.

The conference was opened with welcoming remarks by the director of the Center, H. Setna, who emphasized the importance of nuclear data in the development of atomic science, particularly for India. An isochronous cyclotron is being built in India (at Calcutta) to aid nuclear physics research there, and a pulsed fast reactor is also under construction (near Madras).

The INDC conference agenda began with communications from the representatives of the several countries, dealing with work on nuclear data measurements made and reported over the past year. The basic findings on new measurements were reported at the conference on neutron cross sections held in the USA (Knoxville, State of Tennessee, March, 1971), and at a neutron physics conference held in Kiev (May, 1971). Written reports of the activities on nuclear data studies in various countries are on file at the Obninsk nuclear data center.

Neutron standard data came under discussion at the INDC conference. Current "standards" for this work are the nuclides  $H^1$ ,  $He^3$ ,  $Li^6$ ,  $B^{10}$ ,  $C^{12}$ ,  $U^{235}$ . The importance of working out a system of recommended data on standards was stressed, and agreement was reached on the free exchange of estimated data on nuclear standards. This means that the estimated data on the nuclides mentioned, obtained in various laboratories throughout the world, will be made available for general use.

The committee reviewed the status of the most important nuclear data, and discussed the principal discrepancies found in the fund of data. It was reported that recent measurements of fission spectra at Argonne and Karlsruhe have confirmed the Los Alamos data. An opinion was expressed on the need to conduct additional integrated experiments to secure information on fission spectra. In that connection, IAEA scheduled its August, 1971 conference of specialists to discuss the findings of fission spectrum measurements.

Disparities in the determination of the number of secondary neutrons emitted in spontaneous fission of  $Cf^{252}$ , which still eludes explanation, were discussed. The measurements will have to be continued, using a variety of methods.

A suggestion was advanced to measure the energy dependence of the ratio of the capture cross section of gold to the fission cross section of plutonium, with the object of clearing up some discrepancies in the fission cross sections of  $Pu^{239}$  and  $U^{235}$ .

A review paper authored by M. Sowerby (Britain) and V. Kon'shin (USSR) dealt with analysis of a set of experimental values of the ratio of the radiative capture cross section to the fission cross section ( $\alpha$ ) of the nuclide  $Pu^{239}$ . This review paper analyzes results reported by various authors, and suggests the recommended data.

A protracted discussion followed the presentation of reports on neutron data, particularly in the light of the interaction between INDC and the Working Team on nuclear structures and reactions organized under

---

Translated from *Atomnaya Énergiya*, Vol. 32, No. 1, pp. 95-96, January, 1972.

© 1972 Consultants Bureau, a division of Plenum Publishing Corporation, 227 West 17th Street, New York, N. Y. 10011. All rights reserved. This article cannot be reproduced for any purpose whatsoever without permission of the publisher. A copy of this article is available from the publisher for \$15.00.



IAEA sponsorship. The committee stressed the fact that neutron data retain unquestioned priority in any nuclear data work, and that the entire activities of the team must be directed primarily toward the solution of applied problems, with the team working under the supervision of INDC.

The conference heard reports on the work of nuclear data centers and on exchange of experimental information between four such data centers. A conference of the four centers was held in October, 1971 at Brookhaven, facilitating thorough discussion of their activities.

The INDC IV conference discussed compiling a list of inquiries on nuclear data. At the present time several inquiry formats, including some developed in the USSR, have been submitted to IAEA. In the coming months all of these inquiries will be incorporated in a general list broken down by sections: reactors, thermonuclear fusion reactors, system of guarantees. These lists will be revised on a basis of roughly once every two years.

The INDC conference heard reports on nuclear data estimates activities. The agreement reached on free exchange of estimated data based on "standards" is a first step on the path to free exchange of all estimated data based on "standards" is a first step on the path to free exchange of all estimated data. To smooth the free exchange of these data and reach agreement on approaches to estimating techniques, IAEA prepared and scheduled a conference of specialists on the subject for August-September, 1971. A seminar on estimates of nuclear data was called in Rumania for the summer of 1972. In 1972, IAEA will be holding a conference on neutron "standards," and in 1973 a symposium on the acquisition, compilation, estimates, and dissemination of applied nuclear data, to be followed by the III general nuclear data conference scheduled for 1974.

## INTERNATIONAL CONFERENCE ON ELEMENTARY PARTICLES

I. A. Savin

The International Conference on Elementary Particles was held in Amsterdam (Holland) from June 30 to July 6, 1971 under the auspices of the Dutch Ministry of Education and Science and the University of Amsterdam, with the support of the European and Dutch Physical Societies, and the active participation of CERN.

The work of the Conference was centered on plenary meetings with rapporteur's talks on broad topics preceded by parallel section sessions where reports of original work or mini-rapporteur's talks on original works were heard.

The Conference was attended by 590 scientists from many countries. About 440 original experimental and theoretical papers were discussed.

The plenary sessions were concerned with the following topics: high energy hadron physics (G. Giacomelli, H. Zats), medium energy hadron dynamics (R. Barluto, M. Deutchman, and R. Phillips), low energy hadron physics (R. Dalitz, K. Schmid), weak interactions (K. Winter), electromagnetic interactions (E. Drell), and hadron symmetry (K. Kallan). Two invited talks were heard: on the status of the CERN proton-proton colliding beams (ISR) (K. Johnson) and on electron-muon universality (V. Telegdi).

The rapporteur and invited talks will be published. The more interesting experimental results reported at the conference are outlined below.

High energy hadron physics was represented, in the main, by work done at IFVÉ (Serpukhov) on the 70 BeV accelerator and by preliminary results from the ISR.

The results of measurement of the  $\pi^+$ ,  $K^+$  and proton total cross sections on protons and deuterons was at the center of attention of the conference, particularly the discovery at Serpukhov that the  $K^+p$  total cross sections grow at high energies. Much interest was aroused by the relatively slow decrease in the  $\pi^\pm p$  interaction cross section difference [ $\Delta\sigma_t(\pi^\pm p) \sim p^{-1.2}$ ]. According to other data from IFVÉ the total charge-exchange cross section decreases with increasing energy at much faster rate ( $\sigma_{ex} \sim p^{-1.2}$ ) up to 50 BeV. It was pointed out in discussions that there must be a change in the energy dependence in the  $\geq 200$  BeV energy range or the well-known inequality  $(\Delta\sigma_t)^2 \leq \text{const } \sigma_{ex}$  would be violated.

Thus, the results of measurement of positive particle total cross sections together with the previously verified results on negative particles imply that the total cross section differences for  $\pi^\pm p$ ,  $K^\mp p$ , and  $p^\pm p$  continue to decrease with increasing energy. It follows that speculations about the possible violation of the Pomeranchuk theorem were premature.

Another direct method of verifying theories of the behavior of scattering amplitudes, and in particular of measuring the behavior of the difference of total cross sections was used in an experiment performed at IFVÉ by a group from Dubna in conjunction with groups from countries participating in OIYaI (HPR and ChSSR). This consisted in measuring  $f_{21}^0$ , the amplitude for transmission regeneration of  $K_L^0 - K_S^0$  on hydrogen, whose imaginary part is proportional to  $\Delta\sigma_t(\bar{K}_p^0 - K_p^0)$ , the difference of the  $K_p^0$  and  $\bar{K}_p^0$  total cross sections (or through isotopic spin invariance  $K_p^+n$  and  $K_p^-n$ ). The results indicate that the modulus of the regeneration amplitude  $|f_{21}^0|/K \sim p^{-0.5}$  while its phase ( $\varphi_{21}^0$ ) is constant in agreement with Regge model calculations and dispersion relations. It follows from these results that  $\Delta\sigma_t(K_p^0 - \bar{K}_p^0)$  decreases with

---

Translated from Atomnaya Énergiya, Vol. 32, No. 1, pp. 96-97, January, 1972.

© 1972 Consultants Bureau, a division of Plenum Publishing Corporation, 227 West 17th Street, New York, N. Y. 10011. All rights reserved. This article cannot be reproduced for any purpose whatsoever without permission of the publisher. A copy of this article is available from the publisher for \$15.00.

increasing energy in agreement with requirements of the Pomeranchuk theorem. More accurate data will be available in the near future on the energy behavior of  $|f_{21}^0|$  and  $\arg(\varphi_{21}^0)$  from American (3-10 BeV/C) and Dubna (10-42 BeV/C) groups.

Much time was given at the conference to the presentation of preliminary results from the ISR. The greatest interest was aroused by the announcement that the slope parameter ( $b$ ) of the pp diffraction cone has different values at a given center of mass energy  $S$  for different momentum transfer intervals (for instance, for  $S = 2800 \text{ BeV}^2$ ,  $b$  equals  $12.8 \pm 0.2$  and  $11.6 \pm 0.15$ ). This apparently reflects a decrease in the growth of  $b$  as compared with extrapolations of the results of the Dubna group at the IFVÉ accelerator to ISR energies. This fact implies that the effective proton radius ceases to grow at very high energies.

Many papers were devoted to medium energy hadron dynamics. First of all, we consider papers on elastic scattering. The combined data shows that the pp and  $K^+p$  diffraction cones shrink with increasing energy up to  $\sim 25 \text{ BeV/C}$ ,  $\pi^+p$  shrinks slowly, pp shrinks and then reaches a plateau, while  $K^-p$  does not shrink at all. At large momentum transfers the cross sections have a complex behavior with minimums and maximums. Some of these were observed for the first time.

For backward scattering there are peaks for all reactions except pp. Elastic  $\pi p$  scattering is identical to pp scattering up to momentum transfers of  $6(\text{BeV/C})^2$ . The polarization of  $p^\pm$ ,  $\pi^\pm$ , and  $K^\pm$  scattering on protons has been studied in detail.

Among papers on inelastic two-body scattering, we note the first results on  $pp \rightarrow \Sigma^-\bar{\Sigma}^+$ ,  $\Sigma^+\bar{\Sigma}^+$ ,  $2\pi$ , and  $2K$  reactions. The first reaction exhibits a forward peak in the angular distribution, while the second has a forward peak and a break in the angular distribution for  $t = -1.2 (\text{BeV/C})^2$  together with a break in the polarization in the same region.

Quasi two-body reactions were represented by papers on the angular distributions and exchange dynamics of definite strange and nonstrange states for processes of the type  $K^-p \rightarrow \Delta^+K^{*-}$ ,  $PK^{*-}$ ,  $nK^{*0}$  ( $890 \text{ MeV/C}^2$ ),  $PK^{*-}$ ,  $nK^{*0}$  ( $1420 \text{ MeV/C}^2$ ),  $K^-p \rightarrow \Lambda p$ ,  $\Lambda\omega$ ,  $\Sigma p$ ,  $\Sigma\varphi$ ,  $K^+p \rightarrow \Delta^{++}K^0$ ,  $\pi^+p \rightarrow \Delta^{++}\omega$ , etc. for which information was obtained regarding the angular distributions and dynamics of exchange through specific singular and nonsingular states.

The study of many-particle reactions was represented by two methods: exclusive reactions, i.e., experiments where the parameters of all particles are fully determined, and inclusive reactions, where the characteristics of one (or two) particles are studied and the parameters of the remaining finite system are summed over (missing-mass type experiments).

Definite success has been achieved in the study of exclusive reactions due to the use of van Hove's LPS procedure (decreasing the number of variables by summing over the perpendicular momenta). An exchange hierarchy  $\sigma(P) > \sigma(M) > \sigma(S) > \sigma(E)$  has been established for both total and differential cross sections where P, M, S, and E indicate vacuum, mesonic, strange, and exotic poles. All the cross sections except for those proceeding through P exchange diminish with increasing energy.

Inclusive reactions were analyzed in terms of the hypothesis of scale invariance according to which cross sections at high energies depend only on  $P_\perp$  and the ratio  $X = P_\parallel/P_{\text{max}}$ . This hypothesis was tested in a large energy region including ISR energies. Scaling invariance holds for certain reactions ( $pp \rightarrow \pi^+ + \dots$ ;  $pp \rightarrow p + \dots$ ) while it is obviously broken for others ( $K^+p \rightarrow K^0 + \dots$ ,  $K^-p \rightarrow \lambda + \dots$ ,  $K^-p \rightarrow K^0 + \dots$ ) or holds in a limited region of  $X$  ( $\pi^+p \rightarrow \pi^- + \dots$ ,  $\pi^+p \rightarrow \pi^+ + \dots$ ).

Low energy hadron physics was represented at the Conference by papers studying the characteristics of resonances. Reports were heard on the systematic study of baryon resonances in  $K^+N$  interactions. Resonances have been observed in the  $\Lambda\omega^-$ ,  $\Sigma\pi^-$ ,  $\Sigma^*$  ( $1385 \text{ MeV/C}^2$ ),  $\pi^-$ , and  $\Xi\pi$  systems. There are indications of the existence of a strangeness +1 resonance in the reaction  $K^+d \rightarrow K^0pp$  with  $M = 1760 \text{ MeV/C}^2$  and  $\Gamma = 300 \text{ MeV/C}^2$ . The existence of a  $\Lambda\gamma$  resonance with a mass of  $1327 \text{ MeV/C}^2$  in the reaction  $K^-p \rightarrow \pi^0\Lambda\gamma$  has not been substantiated. Two groups, ITÉF and CERN, have also reported observation of a resonance in the  $p\pi^+\pi^-$  system ( $1700 \text{ MeV/C}^2$ ).

New information on boson resonances has been found. One of the most important results is the absence of splitting in the  $A_2$  meson as determined by high-statistics experiments at CERN and Brookhaven.

Also of interest is the joint IFVÉ and CERN work on the energy dependence of boson production cross sections. The  $A_2$  meson production cross section is constant over a wide momentum range (25-40 BeV/C) while the R meson either disappears completely from 10 to 25 BeV/C or has a factor of ten decrease in its production cross section.

Weak interactions, which have been intensively studied by experimentalists and theorists since 1964, when CP-invariance was found to be violated in  $K_L^0 \rightarrow \pi^+ + \pi^-$  decays, were again generating broad interest.

The effort of many years by physicists to measure the modulus and phase of the parameters  $\eta_{+-}$  and  $\eta_{00}$ , which are the branching ratios for the  $K_L^0$  and  $K_S^0$  neutral and charged two pion decay, would seem to have ended in 1970 when ITÉF and OIYaI groups established reliably that  $|\eta_{00}| \approx |\eta_{+-}|$ . This result was confirmed at the Conference by a CERN group whose results were  $|\eta_{00}/\eta_{+-}| = 1.00 \pm 0.06$ . Taken together with the mean weighed values of the phases  $\varphi_{00}/\varphi_{+-} = 0.99 \pm 0.25$ , this means that the superweak interaction theory which explains the mechanism of CP-invariance violation is correct. It follows from this theory that there should be no CP-violation effects except in  $K_L^0$  decays. This has held true up to the present despite the vigorous efforts of experimentalists to find other CP-violating decays.

An experiment recently performed at Berkeley which established the upper limit for  $K_L^0 \rightarrow \mu^+\mu^-$  ( $\leq 1.8 \cdot 10^{-9}$ ) decays was discussed at the Conference. This limit is several times lower than the possible theoretical limit which is estimated using electromagnetic interactions on the basis of the previously shown decay probability  $K_L^0 \rightarrow \gamma\gamma$ , confirmed at the Conference by an ITÉF group.

If one assumes both results to be correct, then one can expect that the new result is tied to another manifestation of CP-violation.

From the remaining data on the properties of weak interactions, the work of a CERN group concluding the long effort to verify the  $\Delta S = \Delta Q$  rule in leptonic decays of  $K^0$  mesons should be noted. It has been shown experimentally that this rule holds to an accuracy of a percent in  $K_{e3}^0$  decays.

FOURTH INTERNATIONAL CONFERENCE ON PLASMA PHYSICS AND  
CONTROLLED NUCLEAR FUSION

B. B. Kadomtsev and V. D. Shafranov

The Fourth International Conference on Nuclear Fusion of the IAEA was held in June, 1971, at the University of Wisconsin at Madison. About 600 scientists from about 30 countries participated in the conference, and about 140 reports were heard. Most of the reports were delivered by the rapporteur system. The conference dealt with the results of work in controlled thermonuclear fusion over the last three years. As in previous conferences, most of the work has been experimental.

The conference opened with a session on studies of plasma behavior in toroidal traps having inner conductors – levitrons and multipoles; reports on an astron were also heard. At one time it appeared that devices having internal conductors would significantly simplify studies of physical properties of plasmas in a toroidal geometry, since a deep magnetic well, which should lead to a prolonged stable confinement of the plasma, can be easily produced in such devices. Unfortunately, this turned out not to be so. The quite complicated behavior of the plasma in multipoles has necessitated a prolonged and persistent study which has not yet led to a common point of view regarding the mechanisms for plasma escape.

Nor was a common point of view reached at this conference. For example, in studies carried out at the University of Wisconsin with two octupoles – a small one with supports and a larger levitating octupole, it has been shown that the plasma is subject to an anomalously rapid escape at a rate of the order of the Bohm rate. This anomalously rapid plasma escape may be associated with small perturbations from inhomogeneous external fields. It was reported in other studies that the plasma confinement time in an octupole reaches 300 Bohm times; collisional diffusion approximately three times as rapid as classical diffusion is observed at a high plasma density, and only at low densities do the additional losses associated with the imperfections in the magnetic field and the plasma loss at the supports become apparent.

Preliminary data indicate that the imposition of a toroidal magnetic field does not reduce the collisional diffusion of the plasma as is expected on the basis of "neoclassical" theory; in other words, so-called pseudoclassical diffusion is observed. This expression is now used for the semiempirical dependence of the transport coefficients proposed first by L. A. Artsimovich (USSR) for the electronic thermal conductivity, which is proportional to the collision frequency and the square of the Larmor radius corresponding to the "poloidal" (azimuthal) magnetic field. S. Yoshikawa et al. (USA) have observed in a levitated spherator that the plasma decays after emission at decay times approximately equal to the classical values, but they observe increased diffusion during the plasma heating.

Other studies of traps having internal conductors have been concerned with such topics as the isolation of supports by current flow within them, plasma stabilization by freezing of lines of force at the plasma boundary, oscillations in the stable-confinement regions, the formation of convective cells associated with inhomogeneities in the neutral-gas flow, etc.

Reports on the astron device dealt with electron accumulation in a E layer, the equilibrium of this layer, and its stability along with that of the plasma. Theory shows that the flute instability cannot be avoided in the ordinary astron, so the astron modification having an additional toroidal magnetic field is to be preferred. The resulting system is actually similar to a tokamak operating in the escaping-electron mode. One astron version having a toroidal magnetic field is an astron spherator, proposed in a report by S. Yoshikawa and N. Christophilos (USA). It has been found possible to invert the magnetic field within a ring formed by relativistic electrons in a small model at Cornell University.

---

Translated from *Atomnaya Énergiya*, Vol. 32, No. 1, pp. 98-101, January, 1972.

© 1972 Consultants Bureau, a division of Plenum Publishing Corporation, 227 West 17th Street, New York, N. Y. 10011. All rights reserved. This article cannot be reproduced for any purpose whatsoever without permission of the publisher. A copy of this article is available from the publisher for \$15.00.

There was much interest in tokomaks (two complete sessions were devoted to these devices). Experimental results found in studies of plasma behavior at the new T-4 and T-6 tokomaks (I. V. Kurchatov Institute of Atomic Energy) and the TS tokomak (Princeton University), were reported and there was a discussion of the theory of plasma properties in tokomaks.

The experimental results reported demonstrated progress in the study of plasma parameters and of the mechanisms operating in plasmas. For example, the achievement of an electron temperature of 3 keV and an ion temperature above 0.6 keV was reported by L. A. Artsimovich, V. S. Strelkov, et al. (USSR) in studies with the T-4 device, which is based on the T-3. This became possible because of a significant current increase achieved by overcoming the barrier at  $q = 3$  ( $q = rB_z/RB_\theta$  is the so-called stability reserve, where  $r$  and  $R$  are the minor and major axes of the torus, and  $B_z$  and  $B_\theta$  are the toroidal and azimuthal magnetic fields) and by converting to smaller  $q$  values, as low as  $q = 2$  (according to preliminary data, values as low as  $q = 1$  have sometimes been achieved).

The physical bases of the possible change to lower  $q$  values were clarified in a report by S. V. Mirnov and I. B. Semenov (USSR), who reported correlation measurements of corkscrew instabilities in plasmas. It was shown that instabilities of mode  $m$  arise in a plasma when the  $q$  value at the plasma boundary approaches integral values of  $m$ . Between these values there are wide stability regions, so that by rapidly changing the current and going by the critical  $q$  values, one can reach stability regions having smaller  $q$ . These results correspond well to theoretical ideas about the resistive nature of corkscrew instabilities of modes having  $m > 1$  (V. D. Shafranov). These results also show why it is possible to pass the critical  $q$  values only at a high plasma conductivity. Interestingly, precisely these same results regarding the development of the corkscrew instabilities at the edge of a plasma were found in studies with the Princeton TS tokomak.

Identical results were obtained with these two devices on another subtle effect – the kink or disruptive instability: a series of sharp negative spikes in the time dependence of the loop voltage, accompanied by plasma expansion. This instability, observed in all tokomaks, is initiated as the current channel is contracted (e.g., due to corkscrew perturbations or neutral-gas cooling of the plasma periphery, and when the plasma is displaced along the major radius). However, the nature of the instability has not yet been resolved. H. Furth and P. Rutherford (USA), e.g., analyzed the natural assumption that the  $m = 1$  mode develops within the plasma, but it turns out that the negative voltage spikes cannot be explained in this manner. It should be kept in mind, incidentally, that the quasilinear approximation was used in this study, while according to the experimental data of Mirnov and Semenov (USSR) there is a random, turbulent spectrum of magnetic perturbations at the instant of the disruptive-instability outburst.

As was mentioned above, experimental results obtained with the T-3 and T-4 devices, on the one hand, and the TS device, on the other, display an agreement which is rare in plasma studies. However, there are some discrepancies. One concerns the radial dependence of the electron temperature: in the TS device this temperature has a sharper maximum at the center of the plasma than in the T-3 and T-4 devices. Furth reported that this discrepancy could be caused by a temperature instability: the radial temperature distribution turns out to be extremely sensitive to slight perturbations, e.g., in the neutral-gas flux from the chamber walls. Another discrepancy is in the conclusions regarding the diffusive flux. In the T-3 and T-4 devices, the diffusive flux is reported to be much less than the thermal flux, while in the TS device these fluxes are comparable. This discrepancy will probably require refinement of the calculation of the diffusive flux in the T-3 and T-4.

In regard to the magnitude of the plasma escape we find for the ionic thermal conductivity a good agreement with the neoclassical value (except perhaps for the "banana" region of very low collision frequencies), while the electronic thermal conductivity (and, in the TS device, diffusion) is much greater than neoclassical, while the thermal-conductivity coefficient is roughly proportional to the collision frequency and independent of the toroidal magnetic field. A special term was even introduced for this dependence, which was proposed previously by Artsimovich on the basis of an analysis of experimental data: "pseudoclassical diffusion (or thermal conductivity)." Yoshikawa showed that a slight random inhomogeneity of the plasma, due, e.g., to drift instabilities, can lead to pseudoclassical diffusion. He also reviewed many experiments in toroidal devices, including some in stellarators, in which diffusion may be interpreted as pseudoclassical.

The conference heard some results of studies carried out at the recently completed TO-1 and T-6 tokomaks in the Institute of Atomic Energy (USSR); these devices differ structurally from the "traditional"

tokomaks. Instead of a conducting sheath to maintain the plasma at equilibrium in the TO-1, there is a system which automatically regulates the transverse confining field. In the T-6 the conducting sheath is within the evacuated chamber. The spectrum of neutral charge-exchange atoms escaping tangent to the wall of the torus has been measured in this device, and it has thus been possible to prove the isotropy of the ion temperature. Interferometric measurements have shown that the plasma density profile is accentuated in the discharge, and the density increases at the axis. This new effect may be due to the pinching of toroidally trapped particles discussed in a report by A. Ware (USA).

The conference heard theoretical reports on the equilibrium and stability of a toroidal plasma and the recent developments in neoclassical theory. A. A. Galeev and R. Z. Sagdeev (USSR) carried out a detailed study of the role of impurities in neoclassical theory. M. Rosenbluth (USA), L. M. Kovrizhnykh (USSR), and T. Stringer et al. (Great Britain) have derived a systematic theory for plasma revolution in a toroidal magnetic field and have studied its role in the diffusion. In particular, they have shown that revolution along the minor, rather than the major, azimuth along the torus plays the more important role when longitudinal viscosity is taken into account. The theoretical reports took up certain effects described by neoclassical theory: the plasma pinching, the related additional heating, the temporal evolution of the plasma, etc.

Working on the basis of neoclassical theory, B. B. Kadomtsev and Shafranov (USSR) showed that the diffusive expansion of a low-density plasma results in movement of a poloidal magnetic field toward the periphery. As a result, when a sufficiently large ratio of the plasma pressure to the pressure of the poloidal magnetic field is reached, it becomes possible to maintain a longitudinal current in a tokamak by a single diffusive flux, without an external vortex electric field. In this manner a steady-state (instead of pulsed) tokamak becomes possible, differing little in this regard from a stellarator. An analogous idea was advanced by R. Bickerton, J. Taylor, and O. Connor (Great Britain).

Although the tokamak data found in various laboratories were found to be similar, the stellarator data remained extremely contradictory. Several years back in conference discussions, one frequently heard the expression "Munich mystery" for the sharp contradiction between classical plasma confinement at the Wandelstein stellarator at Munich and the anomalously rapid plasma decay with a Bohm time at stellarator S. Today, not only has this "mystery" not been resolved: the number of contradictions has even increased. One gets the impression that stellarators can be classified into a group in which classical confinement is observed and into a group in which there is an anomalously rapid decay.

A very nearly classical confinement (within a factor of two to four) has been observed in the Proto-Cleo device, in which the collisionality parameter, i.e., the ratio of the loop length to the mean free path, was varied over five orders of magnitude. Classical confinement has also been observed in Saturn 1, in which the dependence of the confinement time on the neutral-gas pressure has been measured. In a study carried out under similar conditions and in the presence of a neutral gas, V. I. Volosov observed anomalously rapid plasma leakage governed by the development of instabilities of the drift type. Japanese physicists have also observed anomalously rapid decay of plasma accompanied by the excitation of drift-type fluctuations. Diffusion an order of magnitude more rapid than classical has been observed in a heliotron. These contradictory results on confinement have not yet been resolved. Presumably plasma confinement, at least at a very low density, is very sensitive to small changes in the field geometry and the parameters of the device, so that it can easily enter a region of unstable confinement. It is satisfying in this connection to note that in the transition to higher densities and temperatures in the Uragan device the behavior being observed has much in common with that of the plasma in tokomaks. Specifically, although the confinement time is much less than classical, the results have been in qualitative correspondence with those found in tokomaks: the energetic lifetime is governed by the anomalous electronic thermal conductivity (almost two orders of magnitude greater than the classical thermal conductivity), while the diffusion time has been much greater than the energetic time.

The lack of agreement on the basic question of mechanisms for plasma leakage has not stopped stellarator studies of subtler physical phenomena. Soviet reports dealt in detail with the increase in the plasma decay rate near values of the rotational-transformation angle corresponding to closing of the lines of force. It was shown that the increased leakage is due to the development of convection in the plasma. An experimental study has been made in the Liven-1 stellarator of the development of a quasistationary ion flow in the plasma, apparently due to the formation of departure cones in the ion distribution function. A detailed study of turbulent plasma heating in a stellarator was also reported.

Thirteen reports were delivered to the session on open traps, covering the most recent and deeper studies of leakage mechanisms and physical properties of the plasmas in adiabatic traps. Successful studies have been made of plasma parameters [a temperature of up to  $10^6$  eV at a density of  $10^{12}$   $\text{cm}^{-3}$  in a hot-electron plasma (R. Dandl et al., USA) and an ion temperature of up to 8 keV at a density of  $5 \cdot 10^{13}$   $\text{cm}^{-3}$  in a hot-ion plasma in the 2X device] and the processes in plasmas.

Some studies were devoted to plasma instabilities. D. Sweetman et al. (Great Britain) showed that the threshold for cyclotron instability in a hot-ion plasma is governed by Landau electron damping. They have observed capture of an injected neutral beam in a confined plasma. The cyclotron instability of a low-density plasma was also studied by M. K. Romanovskii, N. N. Brevnov et al. (USSR). M. S. Ioffe (USSR) reported that the plasma in the PR-6 device, having a density of  $10^{11}$   $\text{cm}^{-3}$  and an ion energy of about 1 keV, decays anomalously rapidly because of an instability of the cone type, which turns out to be extremely sensitive to the plasma potential (this instability is excited when the potential is increased). As yet no adequate theoretical description of this effect has been reported.

Studies of z-pinchs were discussed. Dutch and British physicists have succeeded in improving the z-pinch stability with a longitudinal magnetic field. Theoretical stability studies by D. Robinson have shown that magnetic field configurations exist in which the plasma is hydrodynamically stable at currents much larger than those attainable in tokomaks. The essential question here is whether the conditions necessary for stability can be arranged. According to the classification proposed by H. Bodin et al. (Culham, England), pinchs stabilized by longitudinal magnetic fields can be divided into three groups according to stabilization method: the screw pinch, in which the stabilizing longitudinal field increases at the same time as the current in the plasma does; the "stabilized pinch," in which there is a paramagnetic distribution of the longitudinal magnetic field; and a pinch with an inverted (outside the plasma) longitudinal magnetic field. Unfortunately, the experiments which have been carried out so far by Bodin and colleagues have been devoted only to the stability itself, which sets in under the conditions predicted by theory. The maximum plasma temperature, of the order of 100 eV, according to data from experiments carried out both at Culham and at Julich and Garching (West Germany), is found in the screw-pinch mode. The high temperature is retained for only a short time, however, because of the rapid decay (in  $\sim 20$   $\mu\text{sec}$ ) of the discharge current. Van der Lane et al. discussed the reasons for this rapid current decay.

In recent years there has been much interest in  $\theta$ -pinches, in which quite high plasma parameters have been achieved. Numerous results found with linear  $\theta$ -pinches were reported at the 1968 Novosibirsk conference. However, these results were flawed because of the presence of end losses and the hydromagnetic instability of a  $\theta$ -pinch of finite length. The  $\theta$ -pinch configuration has now been changed: the linear systems have given way to toroidal systems, which are similar to stellarator or tokomak systems.

The first experimental results were reported on  $\theta$ -pinches of toroidal geometry – in a spatially periodic magnetic field with protective annular conductors (Nagoya University, Japan), in a tokomak configuration with an elongated elliptical cross section (Julich), and in a corkscrew configuration corresponding to a single-turn stellarator (Garching). F. Ribe reported experimental heating and confinement of a plasma in the 5-m toroidal sector of the Scyllac device at Los Alamos. The first experiments have shown the validity of the theoretical prediction of a possible counterbalancing of the toroidal extension of the plasma through the combined use of a spatially periodic field and a single-turn corkscrew field. Freiberg showed that the experimental absence of the second and higher perturbation modes predicted on the basis of MHD theory was due to the finite size of the Larmor ion radius.

Definite progress in the study of plasma-focus physics was demonstrated at the conference. Rayleigh–Taylor instability of the focus has been observed, the ion energy has been measured on the basis of light scattering, the temporal dependence of the soft x-radiation has been studied, and the angular distribution of the neutron radiation has been studied. Calculations by Potter and Haines have shown that the ion velocity distribution at the focus axis may become highly anisotropic. This result is apparently a key to the explanation for the observed anisotropy in the neutron emission from a plasma focus.

Several reports were devoted to the possible creation of a thermonuclear plasma by means of intense electron beams (Babykin et al., USSR) and laser beams. Calculations and some first experimental results on laser heating of a solid target were reported by others. J. Dawson et al. (USA) proposed a thermonuclear reactor with magnetic thermal insulation based on a long-wave  $\text{N}_2$ – $\text{CO}_2$  gas laser.



A long session (22 reports) was devoted to theoretical and experimental studies of collective turbulent phenomena in plasmas. A detailed review of turbulent plasma heating incorporating new results found from noise measurement in plasmas was given by K. E. Zavoiskii et al. (USSR). Other reports dealt with the results of a detailed study of turbulent plasma heating under various conditions. These results are generally in agreement and lead to the conclusion that ion-acoustic oscillations play the leading role in producing the anomalously high plasma resistance. However, electron beams appear in the plasma, either simultaneously with the ion sound or at alternate times, and the beam-plasma interaction which arises complicates the pattern of turbulent processes. The interaction of electron beams (including relativistic beams) with plasmas have been studied at Khar'kov, Prague, Oak Ridge, and Novosibirsk, where many interesting results have been found on the physics of this beam-plasma interaction and on energy transfer from the beam to the plasma. In particular, it has been shown that in the interaction of an intense beam with a plasma the heating is achieved by a reverse current induced in the plasma. Several reports were devoted to the theory of anomalous plasma resistivity [L. I. Rudakov and D. D. Ryutov (USSR) and W. Drummond (USA)].

Some new experimental results were reported on rf heating of a plasma during propagation of electromagnetic waves in it, and new ideas regarding the use of rf fields in plasma heating were reported.

One aspect of the conference which reflected the clear progress in controlled-fusion research was the session on reactor systems. In the corresponding reports, hypothetical reactors were discussed on the basis of existing plasma-confinement systems: tokomaks, stellarators, open traps, etc. Analysis of the engineering problems involved in thermonuclear reactors is already necessary, to furnish a basis for better evaluation of the outlook for various research directions.

## BRIEF COMMUNICATIONS

The State Committee for Utilization of Atomic Energy of the USSR organized a "scientific familiarization visit" to the Soviet Union from August 5 to September 7, 1971 for groups of specialists from member countries of the International Atomic Energy Agency with the theme, "Use of isotopes and irradiation in agriculture." Representatives from Cuba, Rumania, Poland, Chile, the UAR, Cyprus, India, Ceylon, Iran, Iraq, Ethopia, Burma, Uruguay, and other countries took part in the visit. This arrangement was made through facilities granted voluntarily by the USSR from the technical aid funds of the International Atomic Energy Agency.

One-day seminars were organized for the participants during the visit on the problem of use of isotope tracers in studying the fertility of soil at different levels, use of stable  $N^{15}$  and radioactive  $P^{32}$  isotopes, and the adoption of radiation technology in agriculture.

The specialists from abroad visited and learned about the research works of the V. I. Lenin All-Union Academy of Agricultural Science, the V. V. Dokuchaev Soil Institute, the Timiryazev Agricultural Academy, the All-Union Research Institute for Electrification in Agriculture, the All-Union Research Institute for Fertilizers and Agronomic Soil Science, the Department of Soil Biology of the Moscow State University, the Leningrad Agrophysical Research Institute, the Ukrainian Research Institute for Plant Physiology at Kiev, and the Institute of Cytology and Genetics of the Ural Branch of the Academy of Sciences of the USSR at Novosibirsk.

\* \* \*

A return delegation of Canadian specialists on reactor materials, headed by Dr. Hart, was received in September, 1971 in the Soviet Union.

The Canadian specialists visited the I. V. Kurchatov Institute of Atomic Energy, the Khar'kov Physical-Power Institute at Obninsk, the Atomic Reactor Institute at Melekess, the Beloyarsk nuclear electric power station and the "First Nuclear Power Station in the World." They became acquainted with the work of Soviet scientists and specialists on vacuum extrusion of uranium, zirconium, niobium, and tantalum; with findings on the properties of zirconium alloys working in boiling liquid conditions; with the technology for extrusion of cladding materials from zirconium alloys and their inspection; with the particular features of the structure of zirconium alloy with 1% niobium; with problems on hydrogen absorption and corrosion in a neutron field in a boiling medium. The Canadian delegation were interested in work on structural materials for fast reactors and for low-power reactors for use in the far-North.

At the concluding meeting with the State Committee for Use of Atomic Energy in the USSR, opinions were exchanged between the Soviet and Canadian specialists on the problems examined. A recommendation was expressed regarding the provision of scientific seminars on a defined range of problems.

\* \* \*

An International School on High Energy Physics for Experimental Workers was held from 13 to 27 June, 1971 and the Joint Institute for Nuclear Research together with the Bulgarian Academy of Sciences and with participation from the European Organization for Nuclear Research (CERN), not far from Varna, Bulgaria. The object was to acquaint young experimental physicists with the contemporary state of theoretical physics.

---

Translated from *Atomnaya Énergiya*, Vol. 32, No. 1, pp. 101-102, January, 1972.

© 1972 Consultants Bureau, a division of Plenum Publishing Corporation, 227 West 17th Street, New York, N. Y. 10011. All rights reserved. This article cannot be reproduced for any purpose whatsoever without permission of the publisher. A copy of this article is available from the publisher for \$15.00.

The scientific program was in three parts: 1) a basic course of lectures devoted to the theory of strong interactions and multiple production and also problems of extreme nonelastic electron-proton interactions; 2) specific problems in the theory of relativistic equations, duality and Venetsiano's model; 3) the scientific work of the Joint Institute for Nuclear Research, the high-energy laboratory of the Joint Institute for Nuclear Research, the Institute for High-Energy Physics at Serpukhov, and work at CERN. Seminar tasks were set on the basis of the lectures.

The main course of lectures was given by D. V. Shirkov (JINR), Zh. Préntki (CERN), V. S. Barashnikov (JINR), A. Byalas (Poland), Nguen Van Quey (Vietnam) (in a lecture written jointly with A. A. Logunov), O. Kofed-Khansen (CERN), and V. A. Matveev (Dubna).

Prominent in the program of scientific research were: the Vice-Director of JINR, A. Mikhul and the Director of the High-Energy Laboratory at JINR, A. M. Baldin; the Corresponding Secretary of Institute of High-Energy Physics, V. A. Yabra (with a report written jointly with the Director of the Institute, A. A. Logunov) and the Director of CERN, V. Entchke.

The total number of participants was 109 from 21 countries. Their training was not all alike - more than half those who took part had virtually no experience in research work and approximately 1/3 of the participants had been occupied in research work for three years or more.

The school succeeded in the main task of acquainting young experimental physicists with contemporary aspects of theoretical physics. In the opinion of Soviet participants the school was of great value. Mention should be made of the excellent organization of the school and the warm welcome extended by our Bulgarian friends to all those who attended.

The proceedings of the school are being published by the Joint Institute for Nuclear Research in two volumes.





# A New Bimonthly Journal Covering Man-Made Fibers **FIBRE CHEMISTRY**

*A cover-to-cover translation of Khimicheskie volokna,  
a periodical organ of the Ministry of the Chemical Process Industry of the USSR*

Editor-in-chief: **G. I. Kudryavtsev**

Editorial Board:

**N. Ya. Alekhin, A. G. Bol'shakov, A. L. Borisov, A. G. Borik, A. G. Grigor'yants, V. A. Gruzdev** (Deputy Chief Editor), **S. L. Dich, A. A. Konkin, A. P. Krainov, R. V. Kupinskii, B. A. Mukhin, N. V. Mikhailov, E. M. Mogil-evskii, B. V. Petukhov, A. B. Pakshver, Z. A. Rogovin,** and **A. T. Serkov** (Deputy Chief Editor).

Translated from the Russian

This bimonthly journal, devoted to furthering the growth of artificial fibre production, will provide access to Soviet and non-Soviet advances in the science and technology of fibre synthesis. The journal describes the present state of the industry and its future prospects, discusses theoretical and practical progress in the production of all types of artificial fibres, and presents the most important advances in research on macromolecular compounds suitable for the manufacture of fibres. It deals with the development of new processes, the mechanization and automation of individual operations, the designs of new equipment, the planning and modernization of plants, the economics and organization of production, and quality control. All those concerned with the science and technology of man-made fibre production will find this English language edition a valuable reference source.

Selection of articles from issues 1-5, 1968

**CONTENTS:** Polymerization of acrylonitrile in presence of the potassium persulphatesodium metabisulphite system, **N. M. Beder** and **V. A. Meglitskii**. Influence of the molecular weight of polythene on fiber formation and properties, **A. A. Aver'yanov, D. V. Fil'bert,** and **A. A. Konkin**. Supermolecular structure of graft-modified cellulose fibers, **T. S. Sydykov, L. S. Antonyuk,** **R. M. Livshits,** and **Z. A. Rogovin**. Prevention of foam-

ing in the spinning and finishing baths in manufacture of high-strength viscose cord, **V. K. Tavetkov**. Influence of chemically bound azo dyes on the thermal stability of Kapron fiber, **M. N. Bogdanov** and **W. U. Leshchiner**. Interaction of certain vat dyes with polycapromide., **L. N. Mizerovskii, A. N. Bykov, V. K. Gusev, G. A. Pythova,** and **E. G. Koroleva**. Structure of hydrate cellulose cord fibres, **G. V. Nikonovich, S. A. Leont'eva,** and **Kh. U. Usmanov**. Flow of viscose in cylindrical channels, **P. A. Shankin**. Single-sorbent method for removing hydrogen sulphide and carbon disulphide from waste gases in the viscose industry, **V. I. Kostrikov, N. V. Kel'tsev,** and **P. I. Nivin**. Changes in the properties of acetate yarn under the influence of repeated tensile stresses, **B. Ya. Kharimov**. High-speed spindle for final twisting of Kapron yarn, **Ya. I. Koritysskii, I. V. Kornev, N. N. Lebedeva, V. S. Kuznetsov, E. I. Belyaev,** and **T. Pi. Tereshchenko**. New fiber-forming polyamides, **O. Ya. Fedotova, M. I. Shtil'man,** and **G. S. Kolesnikov**. Electron microscope study of viscose gelling, **M. M. Iovela, S. I. Banduryan,** and **S. P. Papkov**. Structure of chemically cross-linked Kapron fibers, **E. Z. Fainberg, E. A. Vasil'eva-Sokolova, L. A. Kalinina,** and **N. V. Mikhailov**. Advances in colloidal methods for production of fibres and films, **N. V. Mikhailov, T. A. Sharai,** and **A. N. Arsen'ev**.

Annual subscription (6 issues)	1969	\$90.00
Single issue		\$30.00
Single article		\$15.00

Examination copies available upon request.

**PLENUM PUBLISHING CORPORATION**

New York and London

Consultants Bureau • Plenum Press • IFI/Plenum Data Corporation

227 WEST 17th STREET, NEW YORK, N. Y. 10011

# OXIDATION OF METALS

An International Journal of the Science of Gas-Solid Reactions

Edited by **D. L. Douglass**  
Professor of Materials Division  
University of California, Los Angeles, California

Associate Editors:  
**G. C. Wood**  
Corrosion Science Division, University of Manchester  
Institute of Science and Technology  
Manchester, England  
and **J. B. Wagner, Jr.**  
Professor of Material Science,  
Northwestern University, Evanston, Illinois

**Advisory Board:**

**J. Bardolle**, Université d'Orléans-Tours  
**J. Bernard**, Laboratoire de Chimie Minérale de  
l'Université de Paris  
**C. E. Birchenall**, University of Delaware  
**J. V. Cathcart**, Oak Ridge National Laboratory  
**B. Cox**, Chalk River Nuclear Laboratories  
**E. A. Gulbransen**, Westinghouse Research  
Laboratories

**K. Hauffe**, Institut für Physikalische Chemie  
der Universität Göttingen  
**P. Kofstad**, Central Institute for Industrial  
Research, Blindern-Oslo  
**K. R. Lawless**, University of Virginia  
**S. Mrowec**, Katedra Chemii Nieorganicznej,  
Akademii Gorniczo-Hutniczej, Krakow  
**W. W. Smeltzer**, McMaster University  
**J. Stringer**, University of Liverpool  
**G. R. Wallwork**, University of New South Wales

This new international journal, to be published quarterly beginning 1969, will answer the need for a central forum for high quality scientific papers dealing with all aspects of gas-solid reactions. The journal will provide for the first time a specific medium for the rapid dissemination of research in gaseous oxidation — work which has previously been scattered and often lost in a myriad of publications. Topics considered will include kinetics, mechanisms, studies of scales from the structural as well as morphological viewpoints, transport properties in scales, and phase boundary reactions. Both experimental and theoretical papers will be in-

cluded as well as occasional reviews and short technical notes. Care will be taken to publish articles within six months of receipt. Prospective contributors may submit articles to Professor Douglass, Materials Division, University of California, Los Angeles, California. Subscribers are requested to contact the publisher for further information:

Annual subscription (4 issues) 1969 \$22.00  
Individual Subscription \$14.00\*

Outside U.S.A. add \$1.80 for postage.

\*Available to individual subscribers certifying that the journal is for their personal use.

(Circle OXM on order form).

## PLENUM PUBLISHING CORPORATION

New York and London

Consultants Bureau • Plenum Press • IFI/Plenum Data Corporation

227 WEST 17th STREET, NEW YORK, N. Y. 10011